A mass balance across the rapidly growing Mediterranean Ridge accretionary complex

Achim Kopf, SCRIPPS Institution of Oceanography, UCSD, 9500 Gilman Drive, La Jolla, CA 92093-0244, USA
e-mail: akopf@ucsd.edu
Jean Mascle, Géosciences Azur, BP 48, 06235 Villefranche-sur-Mer Cédex, France
e-mail: mascle@obs-vlfr.fr
Dirk Klaeschen, GEOMAR, Marine Geodynamics, Wischhofstrasse 1-3, 24148 Kiel, Germany
e-mail: dklaeschen@geomar.de

Abstract

Depth migration of seismic reflection profiles across the Mediterranean Ridge accretionary complex between the African and Eurasian blocks illustrate profound variations in the geometry and internal structure along strike. Structural interpretations of four cross sections, together with bathymetric and acoustic surface information and drilling data, are used to volumetrically balance the amount of subduction versus accretion with time. Results infer the existence of three distinct scenarios, with a jump in décollement in the west, intense backthrusting in the central part between Libya and Crete, and transcurrent tectonism in the east. The onset of accretion coincides with exhumation of thrust sheets approximately 19 Ma before present. Thereafter, rapid sediment accretion is inferred for either scenario, with thick, evaporite-bearing incoming successions facilitating outward growth of the wedge. The minimum rate of accretion (20-25% of the total sediment supply) is observed where the ridge suffers maximum deformation. Here, the indenting leading edge of the African Plate apparently forces the sediment into subduction, or local underplating. In contrast, an estimated 40-60% of the available sedimentary input got accreted in the western domain where collision is less accentuated. The results support the hypothesis that highly destructive forearc collisional events, like the slab breakoff and exhumation of thrust sheets, are followed by periods of accretion and continuous growth of accretionary wedges.

Introduction and Geological Setting

Parts of the Eastern Mediterranean Sea represent remnants of Tethyan oceanic seafloor which have been preserved despite collision of the Arabian Plate with Eurasia, or more generally spoken, Alpine orogenesis. This seafloor is presently subducted along the Hellenic subduction south of mainland Greece and the island of Crete, while the volcanic arc is represented by small islands (e.g., Santorini) in the southern Aegean Sea. The Mediterranean Ridge accretionary complex is a more than 300 km-wide and approximately 2000 km long accretionary prism south of Greece. It has been demonstrated to be the fastest outward growing wedge in most recent Earth history, with a rate of up to 10 km/Ma (Kastens, 1991). Owing to numerous geophysical surveys during the previous decade (see Chaumillon et al., 1996; Harjes et al., 1997; Mascle et al., 1999), the geometry of the area down to levels of several 10's of km is well imaged.

In this paper, we present a first balance of subducted versus accreted solid rock volume along four cross sections over the entire up to 340 km long prism. Models for the sedimentary input into the Ionian and Herodotus basins are compared to the wedge geometry varying along strike. The hypothesis to be tested include (i) the possible influence of rapidly deposited, overpressured sediment (Ionian Basin, Nile deep sea fan) on style of deformation, (ii) the role of salt (Messinian evaporites) on the décollement level and rate of outward growth of the wedge, (iii) the effect of accentuated deformation the impact of the Libyan margin south of Crete on rate of accretion, and (iv) the long-term growth of accretionary wedges after strong changes in the regional tectonic framework (after HP/LT metamorphism and exhumation of parts of the Greek forearc).

Methods

Seismic data

96-Channel MCS (Multi-Channel Seismic) data collected in the study area reveal important structural insights. Data acquisition is outlined in Chaumillon et al. (1996). Onshore pre-processing included trace editing, CDP sorting, spherical divergence correction, deconvolution, fk filtering, and frequency domain filtering, all carried out with

GLOBE Claritas processing software. Pre-stack depth migration was then used to image and analyse reflective boundaries, using the commercial Kirchhoff migration package KirPack (SIRIUS® from GX Technology). Migration velocities are updated iteratively in a process called depth-focusing analysis on a "one layer at the time" basis, as the overburden velocities affect those determined for deeper level [MacKay and Abma, 1992]. After several iterations, 2D velocity models were created downsection, as are shown in the illustrations underlying the interpretative line drawing of each seismic profile.

Seismic profiles across the Mediterranean Ridge attest profound changes in the geometry of the accretionary wedge along strike. In the western part (Line 3), a wide prism is observed, which is hardly affected by the overall shortening in the area. Further east, both Line 6, and to a much largerextent Line 18/19 show considerable shortening, with the wedge being pushed frontally over the Libyan margin (with no abyssal plain remaining at the toe) and backwards over the deformable backstop, namely the Inner Ridge. This intense deformation in the main collision zone between Africa and Eurasia results in higher p-wave velocities and an only 145 km wide wedge along Line 18/19. By comparison, the wedge along Line 3 is more than twice this length, i.e. approximately 340 km wide. In the east, where subduction is olique and collision is less pronounced, a gently folded, 200 km wide wedge is offscraped from the Herodotus abyssal plain.

Mass balance calculations

Each migrated true-depth cross section was interpreted as too which portion of the forearc had been offscraped and accreted to the frontal upper plate. Then, these areas were calculated along each of the four profiles (Lines 3, 6, 18/19, and 30). This accreted material was then divided into a solid and a fluid portion on the basis on seismic velocity as a function of depth, and on porosity derived from drillcore data from holes by the Ocean Drilling Program Leg 160 into the accretionary prism (Emeis et al., 1996). The same data were used to decompress the deeper portion of these accreted sediments to account for burial which had already taken place as a function of time.

As for the sedimentary input, basin models along each of the seismic traverses were created as restored wedges in a coordinate system with age (i.e. time) versus thickness. The only complication to this 2D model is the necessity of to account for the changes in plate convergence rate on the x-axis. In general, age (or time) is marked using the convergence rates of the incoming plate (Africa) relative to Eurasia. Hence, the x-axis of the basin model also defines the position of the deformation front at any given time, while the absolute length of the model gives the corresponding width (i.e., how much sediment of the input wedge has already passed the deformation front). A change in net convergence rate occurred 13 Ma bp due to onset of Aegean spreading (Le Pichon and Angelier, 1979), which has been accounted for. Similarly, the changes in sedimentation rates (taken from DSDP and ODP drilling results from numerous cruises) define the relative growth in thickness of the input wedge on the y-axis. As a result of the influence of the Nile deep sea fan on sediment accumulation on the Herodotus abyssal plain (Line 30 in the east), we reconstructed models for two scenarios. One model with moderate Messinian and PlioQuaternary rates was used for the balance estimates along Lines 3, 6, and 18/19 in the western and central part of the Mediterranean Ridge. A second input model with enhanced sedimentation during most recent Earth history was used when balancing along Line 30 in the very east of the accretionary wedge. The models' limits are chosen to be 19 Ma bp, when after slab break-off the uplift of the Hellenic forearc started (Thomson et al., 1998), to allow accretion as a consequence. The calculated areas of the sediment wedge were divided into solid and fluid fractions similar to the accreted areas.

Both sets of data, i.e. areas of solid and fluid material of the input basin wdge and accreted forearc wedge were then used to determine
a) the rate of accretion (the percentage of solid material from the lower, subducting plate added to the upper, overriding plate);
b) the total volume flux into the mantle (i.e. the subducted portion of the solids which did not get added to the leading edge of the overriding Eurasian Plate); and
c) the outward growth of the wedge as a function of initiation of accretion 19 Ma ago, present width of the prism along each line studied, and time.

Results

For the balance calculation, only the solid portion of the basin model and accreted wedge along each line is used. The relative rate of accretion is obtained by dividing the solid area of the wedge through that of the total sediment input. The rate is

hence the percentage of the total input which was transferred from the incoming plate to the upper plate forearc. Vice versa, the relative amount of subducted material can be obtained as the ratio of subducted material (i.e., $area_{sed.\ input}$ - $area_{accr.\ wedge}$) relative to the total input. As to be expected from the considerable variation of the accretionary wedge from west to east, the rate of sediment accretion changes from approximately 60% (Line 3) and 40% (Line 6) in the west to 20% (Line 18/19) in the main collision zone, before increasing again to approximately 25% in the east (Line 30). Abundant mud volcanism (Kopf, 1999) in the area would equal only approximately 1 % of the sedimentary input in this solid rock balance.

Concerning the absolute amount of material being subducted and recycled into the mantle (the subduction flux), a systematic increase from west to east is obeserved. In the west, where the accretionary rate is very high (Line 3), only 17.7 km^3 of solid rock per km trench length and Million year are subducted. A stepwise increase in the subducted volume occurs over Lines 6 (26 km^3) and 18/19 (34.5 km^3) to reach 47.5 km^3 of solid rock per km trench length and Ma. The latter value plots in the upper range of subduction fluxes on a global scale (von Huene and Scholl, 1991).

When estimating the outward growth of the wedge since the formation of a backstop some 19 Ma ago, we find the published rate of 10 km/Ma by Kastens (1991) well within our results. Maximum growth of the wedge occurs at its western branch where consumption of abyssal seafloor takes place. Here, the prism grows 18 (Line 3) and 12 (Line 6) km per million year. In the collision zone (Line 18/19), where no abyssal plain is left and the wedge is squeezed between the continental plates, the growth rate drops to approximately 7 km/Ma, before it increases again in the east (Line 30) to a value of 11 km/Ma. The minimum in the central part indicates that between Libya and Crete, some material of the accreted wedge may have already been eroded or underplated, the latter being supported by its elevation to about 2 km below sealevel.

Discussion and Conclusion

The two main observations to be made from this balance study are
1) the elevated rates of accretion and amounts of outward growth of the accretionary wedge, which represent global maxima when compared to mass balances (von Huene and Scholl, 1991) and dynamic studies (Kastens, 1991); and
2) the minima in accretion and wedge growth in the central collision zone (Line 18/19).

The first phenomenon seems to be linked to the catastrophic event of slab break-off and exhumation of HP-LT units, which now form parts of Crete and Greece (Thomson et al., 1998). The uplift caused formation of an abutment, or backstop, to facilitate offscraping of considerable amounts of sediment from the Neo-Tethyan seafloor. Similar catastrophic processes have been observed off Southern Chile recently, where a spreading centre disaggregtes the forearc. Post-collisional accretion and growth rates there are extremely enhanced (Behrmann and Kopf, 2001), suggesting a self-controlling mechanism of forearc growth after highly destructive events (at least on a several Ma scale).

The second aspect has to be viewed as a consequence of the initial stages of continental collsion between Libya and Crete (Mascle et al., 1999). Given that all abyssal seafloor was consumed as a result of plate convergence some 4-5 Ma ago, no sediment accretion and outward growth was possible. On the contrary, ongoing compression possibly forced some accreted material down into the mantle, with the wedge decreasing in size in the process (Kopf et al., under review).

Acknowledgments

The authors thank the European Union for financial support for data processing at GEOMAR, Kiel, Germany through the large scale facility programme.

References

Behrmann, J.H., and Kopf, A., Balance of tectonically accreted and subducted sediment at the Chile Triple Junction (Ocean Drilling Program Leg 141). Geol. Rundschau, 2001 (in press)

Chaumillon, E., Mascle, J., and Hofmann, H.J., Deformation of the western Mediterranean Ridge: Importance of Messinian evaporitic formations. Tectonophysics, 263, 162-190, 1996.

Emeis, K.-C., Robertson, A.H.F., Richter, C., and Shipboard Scientific Party ODP Leg 160, Proc. ODP, Initial Reports, v. 160, College Station, TX (Ocean Drilling Program), 972 p., 1996.

Harjes, H.-P., Janik, M., Büsselberg, T., Knapmayer, M., Schmidt, H., Schweitzer, J., and Vafidis, A. Structure and dynamics of the Hellenic subduction zone under Crete from seismic array measurements. Abstract IASPEI 97, Thessaloniki, 18, 1997.

Hatzfeld, D., Besnard, M., Makropoulos, K., and Hatzidimitriou, P., Microearthquake seismicity and fault-plane solutions in the southern Aegean and its geodynamic implications. Geophys. J. Int., 115: 799-818, 1993.

Huguen, C., Volcanisme boueux et déformation récente à actuelle au sein de la Ride Méditerranéenne, d'après les données de la campagne PRISMED II. DEA thesis, Univ. Pierre et Marie Curie, Paris, 37pp., 1998.

Kastens, K.A., Rate of outward growth of the Mediterranean Ridge accretionary complex. Tectonophysics, 199: 25-50, 1991.

Kopf A., Fate of sediment during plate convergence at the Mediterranean Ridge accretionary complex: volume balance of mud extrusion versus subduction-accretion. Geology, 27, 87-90, 1999.

Kopf A., Mascle, J., and Klaeschen, D., The Mediterranean Ridge: A mass balance across the fastest growing accretionary prism on Earth. Journal of Geophysical Research, under review.

Le Pichon, X., and Angelier, J., The Hellenic Arc and trench system: a key to the neotectonic evolution of the eastern Mediterranean area. Tectonophysics 60: 1-42, 1979.

Mascle, J., Huguen, C., Benkhelil, J., Chamot-Rooke, N. Chaumillon, E., Foucher, J.-P., Griboulard, R., Kopf, A., Lamarche, G., Volkonskaia, A., Woodside, J., and Zitter, T., Images may show start of European-African Plate collision. EOS Trans. AGU, 80/37: 421-428, 1999.

Thomson, S.N., Stöckhert, B., and Brix, M.R., Thermochronology of the high-pressure metamorphic rocks of Crete, Greece: Implications for the speed of tectonic processes. Geology 26: 259-262, 1998

von Huene R, and Scholl DW, Observations at convergent margins concerning sediment subduction, subduction erosion, and the growth of continental crust. Rev. of Geophysics, 29/3, 279-316, 1991.

Avaliação da ameaça sísmica na região SE do Brasil através do método probabilístico

Jesus Berrocal (Berrocal@iag.usp.br) e Celia Fernades (celia@iag.usp.br),
Instituto de Astronomia, Geofísica e Ciências Atmosféricas (IAG/USP), São Paulo Brasil
Andréia A . Diniz de Almeida (adiniz@civ.puc-rio.br) e João Luis Pascal Roehl (roehl@civ.puc-rio.br)
Pontifica Universidade Católica do Rio de Janeiro (PUC-RIO), Rio de Janeiro, Brasil

Abstract

Geological and seismological data from the region between 15°S to 32°S and 35°W to 52°W are being used to assess the seismic hazard in the SE region of Brazil, by using the probabilistic method. The main centers of Brazilian socio-economic development are located in that region; consequently large engineering works need to be constructed, some of them having potential risk for the population living in or around those centers, in the case that their structure be affected by large earthquakes that may occur in the region.

Aspectos geotectônicos

De acordo com a divisão do território brasileiro, em províncias estruturais, proposta por Almeida et al. (1977), a região Sudeste do Brasil abrange porções das Províncias Mantiqueira, São Francisco, Tocantins, Paraná e Margem Continental. Nos terrenos mais antigos das três primeiras províncias, constituídas de rochas pré-cambrianas, podem ser destacadas as falhas transcorrentes, associadas a faixas cataclásticas, ultramilonitos e protomilonitos com larguras de até 2 km, denominadas faixas de cisalhamento ou Região de Dobramentos Sudeste.

Além das falhas de cisalhamento, existem outras de caráter normal, principalmente nas serras do Mar e Mantiqueira, menores em tamanho e geologicamente mais jovens. Estudos recentes (Salvador & Riccomini, 1995) mostram evidências de movimentos quaternários recorrentes, na forma de falhas ativas até tempos recentes, principalmente no Alto Estrutural de Queluz.

Existe uma certa correlação entre as características tectônicas da região central-leste dos Estados Unidos, com o território brasileiro. São regiões continentais intraplaca, compostas por escudos estáveis, com níveis relativamente baixos de sismicidade, e nas que predominam rochas pré-cambrianas e paleozóicas. Por este motivo, as recomendações efetuadas por Budnitz et al. (1997) para essa região podem ser adotadas para sua utilização na região de estudo.

Sismicidade histórica e recente

Os dados sismológicos para este trabalho foram extraídos do catálogo apresentado por Berrocal et al. (l984), que contem informações sobre eventos sísmicos ocorridos no Brasil no intervalo 1560-1981, e os dados mais recentes, do Boletim Sísmico Brasileiro, que é publicado na Revista Brasileira de Geofísica e na página WEB do IAG/USP, contando com dados de sismos sísmicos ocorridos até 2000. Foi revisado, para o presente trabalho, as magnitudes de alguns sismos desse boletim, ocorridos depois de 1981.

A região SE apresenta um nível de atividade sísmica relativamente baixo (Fig. 1), típico de regiões intraplaca, embora quando, comparado com o de outras regiões do Brasil, seja significativo. Nela ocorreram alguns sismos de magnitude pouco maior que m_b>5,0 e um com m_b=6,3.

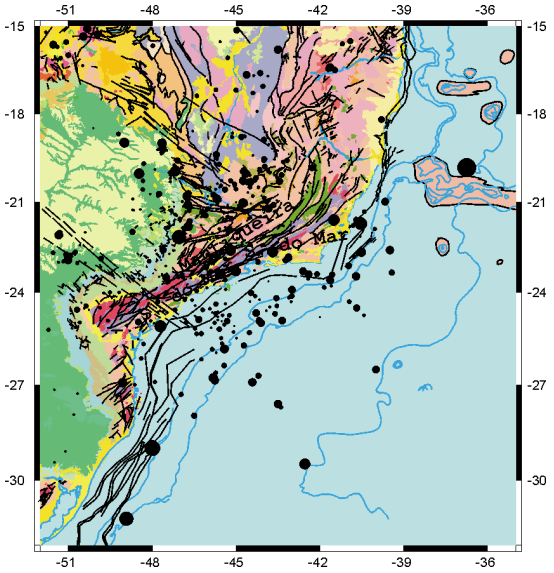

Figura 1 – Mapa Sismotectônico da região de estudo

Parâmetros de sismicidade

Caracterização da fonte sismogênica

Devido à rede sismográfica na região não ser muito densa as determinações hipocentrais da maioria dos sismos ocorridos na região de estudo não tem a precisão desejada, por isso não é possível efetuar correlações seguras entre a distribuição espacial da atividade sísmica e as feições tectônicas potencialmente sísmicas. A caracterização da fonte sismogênica é um parâmetro importante para efetuar uma análise probabilística da ameaça sísmica (APAS).

A distribuição da sismicidade na região de estudo se apresenta como uma atividade sísmica difusa, sem concentrações claras em torno de feições tectônicas, o

que caracteriza uma província sismotectônica. A porção dessa região onde estão concentrados os epicentros do mapa da Fig. 1, será definida como ***a Província Sismotectônica do Sudeste (PSS).*** Essa província está delimitada pelo polígono apresentado na Fig. 2.

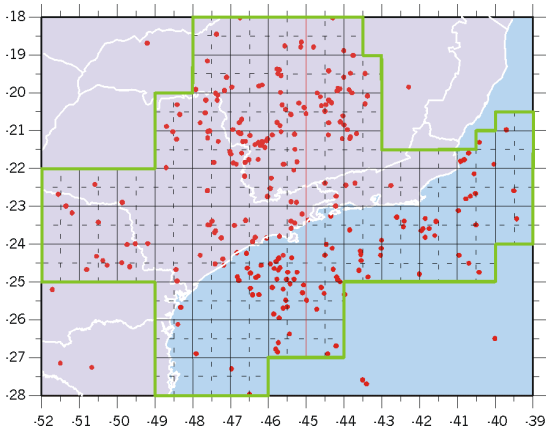

Figura 2- A Província Sismotectônica do Sudeste

O sismo de magnitude máxima possível

Um parâmetro importante para efetuar a APAS, é o sismo de magnitude máxima possível (SMMP) da fonte sismogênica em estudo que fixa seu limite superior da relação freqüência/recorrência.

De acordo com (Budnitz et al. 1997), a avaliação do SMMP numa área-fonte, como a PSS, é uma tarefa difícil já que não se conhece a dimensão das falhas provocadas pelos sismos dessa província, que é o dado principal para estimar o SMMP. Neste caso, a alternativa para estimar o SMMP considera: a) a sismicidade histórica dessa província; b) a sismicidade de outras fontes sismogênicas próximas; e c) a sismicidade de outras fontes com características sismotectônicas semelhantes.

Pela primeira alternativa o SMMP para a PSS seria de m_b=5,1, correspondente ao sismo de Pinhal-SP , ocorrido em 1922. Pela segunda alternativa o SMMP seria m_b=6,5, correspondente ao sismo da Serra do Tombador–MT, ocorrido em 1955 ou entre $6,5 \leq m_b \geq 7.0$, se aceita a possibilidade de que um sismo ocorrido em 1767 e que afetou severamente a cidade de Vitória-ES, tivesse o seu epicentro na mesma fonte, Alto Vitória–Trindade, como o sismo de m_b=6,3 ocorrido em fevereiro de 1955. Pela terceira alternativa o SMMP para a PSS seria m_b=7,0, utilizando um valor um pouco menor que o utilizado para a região leste dos Estados Unidos (M_W 7,5, que corresponde a m_b=7,1), por ser essa região de um índice de sismicidade maior que o SE do Brasil.

De acordo com as considerações acima, será adotado m_b 7,0 para o SMMP na PSS.

O intervalo de recorrência sísmica

Outro parâmetro necessário para efetuar a APAS é o intervalo de recorrência de sismos de determinada magnitude na província sismotectônica definida neste trabalho.

O intervalo de recorrência sísmica de uma fonte sísmica é determinado com base na distribuição temporal da sismicidade dessa fonte. Para isso é necessário contar com um catálogo de eventos sísmicos históricos e recentes, que permita inferir os intervalos nos quais o catálogo é completo, para diferentes níveis de magnitudes.

Segundo Budnitz et al. (1997), nas regiões de baixo nível de sismicidade como a PSS, as curvas freqüência/recorrência sísmica são obtidas quase que exclusivamente com dados instrumentais, que normalmente são sismos de pequena magnitude, ocorridos num intervalo relativamente pequeno. Como alternativa complementar esses autores recomendam a utilização de dados históricos, que permitam incluir sismos com grandes magnitudes, próximas da magnitude máxima possível.

Neste trabalho, é utilizado o método da relação freqüência/magnitude de Gutemberg & Richter, para determinar a distribuição temporal da sismicidade na PSS. Com base nos dados recentes da auscultação instrumental com a rede sismográfica regional, entre 1975-1998, foram obtidas as seguintes relações, com o limiar de detectabilidade em m_b=3,5:

$$\log N = 3{,}18\ (\pm 0{,}03) - 1{,}06\ (\pm 0{,}04)\ m_b \qquad (1)$$

$$\log \Sigma N = 6{,}54\ (\pm 0{,}08) - 1{,}81\ (\pm 0{,}12)\ m_b \qquad (2)$$

para a distribuição de magnitudes simples e acumulativas, respectivamente.

Incluindo a distribuição dos dados históricos, por faixas de magnitude, a relação da Eq. (2) é:

$$\log \Sigma N = 4{,}44\ (\pm 0{,}02) - 1{,}28\ (\pm 0{,}02)\ m_b \qquad (3)$$

Essas relações são mostradas no gráfico da Fig. 3. A reta da relação (2), não representa de forma apropriada a distribuição acumulativa de magnitudes da PSS, que teria que ser uma curva exponencial. No caso da relação (3), visto que o intervalo do catálogo é muito maior que os 24 anos utilizados para obter a relação (2), essa distribuição pode ser linear. Por esse motivo,

a relação (3) será utilizada neste trabalho para calcular os intervalos de recorrência na PSS.

Atenuação da Energia Sísmica

Na APAS é necessário determinar a atenuação da energia sísmica, existente na região de interesse, em função da distância até o local de interesse e do valor dentro da faixa de magnitudes considerada. Este parâmetro se determina, nas regiões com alto índice de sismicidade, analisando os registros de aceleração das partículas do solo, registrados a diferentes distâncias.

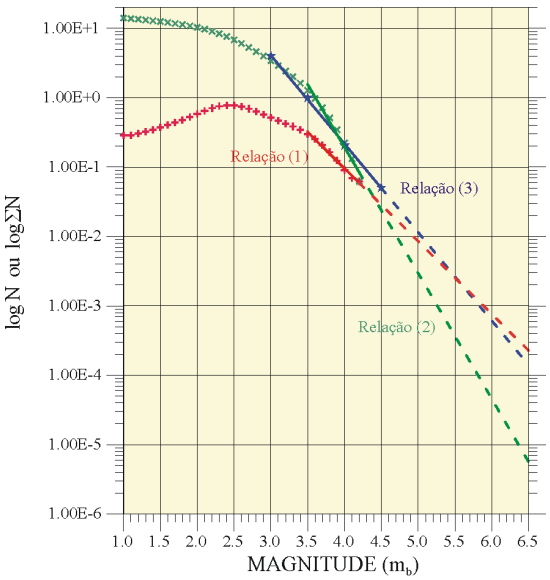

Figura 3- Relações freqüência/magnitude na PSS

No caso do território brasileiro, não foi possível, até o presente, efetuar medições desse tipo. Uma alternativa neste caso é utilizar funções de atenuação determinadas para outras regiões da Terra, que tenham semelhança com as características tectônicas da região de estudo, como a função de atenuação desenvolvida por Toro et al. (1997), para região Centro-Leste dos Estados Unidos.

Eles desenvolveram funções de atenuação tanto para acelerações de um espectro de freqüências como para a aceleração horizontal máxima do terreno, com base em um modelo estocástico de excitação da fonte e um modelo de efeitos da trajetória que considera raios múltiplos em uma crosta composta de camadas horizontais. Esses modelos e os valores de seus parâmetros foram desenvolvidos através de uma análise exaustiva de dados reais de movimento do terreno e outros dados relevantes.

A relação de atenuação para acelerações horizontais máximas em rocha, é a seguinte:

$$\ln(Y)=2,07 + 1,2(M-6) - 1,28[\ln(R_M)] + 0,05\max[\ln(R_M/100), 0] - 0,0018(R_M) \quad (4)$$

onde Y = aceleração horizontal máxima (em g)

$R_M = (R^2 + 86,49)^{1/2}$

onde R = distância epicentral em km.

M=magnitude m_b, do limiar até o SMMP.

No cálculo da relação (4) o desvio padrão $\sigma_{\ln(Y)}$ representa o efeito combinado no valor de ln(Y), das incertezas associadas à (M), à distância epicentral (R) e aos modelos utilizados, que podem ser estimadas através de:

$$\sigma_{\ln(Y)} = [(\sigma_M)^2 + (\sigma_R)^2]^{1/2} \quad (5) \quad \text{onde,}$$

$\sigma_M = 0,34 + 0,07(M - 6)$ M varia até SMMP

$\sigma_R = 0,54$ ou $[0,54 - 0,0227(R-5)]$ ou 0,20

para R=<5 km ou 5≤R≤20 km ou R>20 km

Análise Probabilística

A metodologia para executar a APAS é detalhada por Diniz de Almeida (2001), sob a forma de uma sistemática analítica que estima a probabilidade de vários níveis de vibrações do terreno, causadas por sismos, serem excedidos para um determinado local em um dado período de tempo. Os resultados da APAS são expressos em uma curva de ameaça.

A utilização dos conceitos de análise probabilística permite que sejam explicitamente consideradas na avaliação da ameaça sísmica, as incertezas existentes no cálculo da magnitude, na localização dos hipocentros e na determinação da razão de recorrência sísmica, assim como nas variações das características do movimento do terreno com a magnitude e localização dos sismos.

A APAS pode ser descrita como um procedimento que se executa em quatro etapas: a) identificação e caracterização das fontes sísmicas; b) determinação da recorrência da atividade sísmica, tendo como limite o SMMP; c) determinação do nível de vibrações causada por sismos de qualquer magnitude, inclusive o SMMP, e que ocorram em qualquer ponto da fonte, através das relações de predictividade; e d) combinação das incertezas na localização e no cálculo da magnitude dos sismos com a predição dos parâmetros do movimento do terreno, para obter a probabilidade de que o parâmetro desse movimento seja excedido durante um período particular de tempo.

Pela definição de província sismotectônica reconhece-se que tem uma sismicidade uniforme (a mesma função de freqüência/ recorrência e uma magnitude máxima possível) e admite-se a hipótese de sismicidade homogênea (qualquer ponto dentro da província sismotectônica tem a mesma probabilidade de ser o

epicentro dos sismos que ocorram na mesma, inclusive o SMMP).

A probabilidade resultante da distribuição de magnitude é dada pela função de distribuição acumulativa e pela função de densidade de probabilidade (das magnitudes dos sismos utilizados) respectivamente, as quais são determinadas a partir da lei de recorrência e dos limites extremos de magnitude. Com b=1,28, a função $f_M(m)$ para a PSS é dada por:

$$f_M(m) = \frac{2{,}948 \cdot \exp[-2{,}948 \cdot (m - 3{,}5)]}{1 - \exp[-2{,}948 \cdot (7{,}0 - 3{,}5)]} \qquad (6)$$

A incerteza referente à localização dos sismos dentro da província $[P_R(r)]$ é representada pela distribuição de probabilidade das distâncias entre o sítio e os possíveis epicentros, ou seja, distribuição da distância epicentral. No caso, a província é dividida em uma malha densa de elementos de igual tamanho (Fig. 2), e obtém-se um histograma que descreve a freqüência relativa das diferentes distâncias entre o centro de cada elemento da malha e o sítio

$$P_R(r) = [\text{Pontos com } R=r] / \text{ Total de pontos} \qquad (7)$$

Para calcular a probabilidade da ameaça sísmica ocorrer num dado período de tempo, a distribuição da ocorrência sísmica com relação ao tempo, deve ser considerada. Admite-se que os sismos ocorrem aleatoriamente com o tempo, e de fato, observações em catálogos sismológicos têm revelado poucas evidências de um padrão temporal na recorrência dos fenômenos sísmicos.

A característica de ocorrência aleatória dos sismos permite utilizar modelos de probabilidade simples para representar a distribuição da ocorrência temporal da atividade sísmica como, por exemplo, o modelo de Poisson. Nesse modelo, a probabilidade da ocorrência de pelo menos um evento com parâmetro do movimento do terreno maior do que y* em (t) anos é dada por:

$$P\left[Y > y^* \text{ em } t \text{ anos}\right] = 1 - \exp\left[\sum_{i=1}^{S}\sum_{k=1}^{N_M}\sum_{l=1}^{N_R} -t \cdot \nu_i \cdot P\left[Y > y^* \mid m_k, r_l\right] \cdot P_R(r_l) \cdot (f_M(m) \cdot dm)\right] \qquad (8)$$

Resultados da análise probabilística

A Eq. (8) é a equação final da curva de ameaça sísmica, que inclui as incertezas e as características da sismicidade que devem ser utilizadas na APAS da PSS. Aplicou-se a APAS, neste trabalho, para as principais capitais localizadas dentro da PSS: Belo Horizonte - MG, Rio de Janeiro - RJ e São Paulo - SP, e foram obtidos os resultados apresentados na Fig. 4 (Diniz de Almeida, 2001). Nesses casos, a Eq. 8 foi aplicada com uma malha de 1/8 de grau por célula na poligonal da Fig. 2.

A Tabela 1 exibe valores de aceleração máxima horizontal (a), nas três capitais, para uma faixa de probabilidade anual máxima de ultrapassagem variando entre 10^{-5} e 10^{-3}.

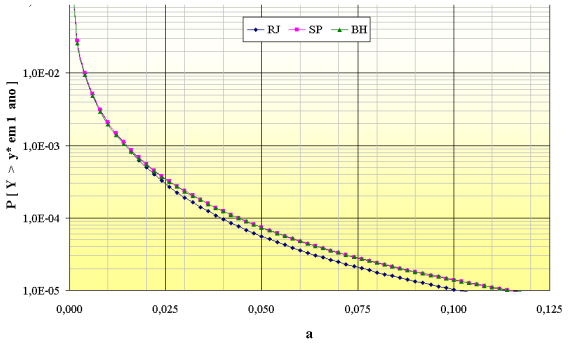

Figura 4- Curvas de ameaça para as principais capitais do Sudeste.

Discussão

Os resultados da Fig. 4 apresentam à quantificação da ameaça sísmica para fixação da aceleração máxima referida a locais em rocha, nessas capitais, com diferentes níveis de probabilidade anual de ocorrência. Aparentemente, as acelerações máximas no Rio de Janeiro são ligeiramente menores que nas outras capitais.

Tabela 1: Aceleração horizontal máxima (a), medida em *g* (aceleração da gravidade) para as principais capitais do Sudeste.

Probabilidade	**RJ**	**SP**	**BH**
$\mathbf{10^{-5}}$	0,100	0,114	0,114
$\mathbf{10^{-4}}$	0,038	0,043	0,042
$\mathbf{10^{-3}}$	0,015	0,015	0,015

Referências

Almeida, F.F.M., 1978. Cronotectonic boundaries for Precambrian time divisions in South America. An. Acad. Bras. Ciên. **50** (4):527-535. Rio de Janeiro.

Berrocal, J., Assumpção, M., Antezana, R., Dias Neto, C.M., Ortega, R., França, H. & Veloso, J.A.V., l984. Sismicidade do Brasil. Inst. Astronôm. e Geofis., 320p. São Paulo.

Budnitz ,R.J., .Apostolakis, G., Boore, D.M., Cluff, L.S., Coppersmith, K.J., Cornell, C.A & Morris, P.A. 1997. Recomendations for Probabilistic Seismic Hazard Analysis. NUREG/CR-6372, UCRL-ID-122160, Vol. 1

Diniz de Almeida, A. A., 2001. Análise probabilística de estruturas submetidas à ameaça sísmica no Brasil., Tese de Doutorado (em desenvolvimento), PUC-RJ

Salvador, E.D. & Riccomini, C., 1995. Neotectônica da região do Alto Estrutural de Queluz (SP-RJ, Brasil)

Brasilia (DF) Earthquake of Nov. 20, 2000: In Quest of Unravelling

Vasile MARZA[*)]*, Lucas BARROS, Cristiano CHIMPLIGANOND and Daniel CAIXETA,*
All at Seismological Obs.,Univ. of Brasilia, CP 04598, Campus Univ., Brasília, Brazil,<obsis@unb.br>; [*)] *On leave from Seismological Laboratory, National Institute (R&D) for Earth Physics, Bucharest, Romania*

Abstract

At 07h36m AM Brasilia Local Time, November 20, 2000 the Federal District (Districto Federal – DF) and neighbourhoods experienced the effects of the first ever reportedly local earthquake. This seismic event exhibited a handful of uncommon features, as: (*i*) it is the first ever-detected earthquake in an area previously supposed, by many, as essentially aseismic; (*ii*) it lacked the usual aftershock activity (in spite of an enhanced seismographic monitoring deployed shortly after the 'mainshock' in the epicentral area); (*iii*) it excited very strong short period surface waves (Lg); (*iv*) it did not exhibit the habitual quadrantal first motion polarity distribution of tectonic faulting; (*v*) it has a particular (quasi-circular) macroseismic field; etc. The paper is reporting the relevant source parameters: origin time, location and depth, size and nature of the source (bearing in mind its particular traits). The macroseismic effects are investigated and the consequences discussed. The main effort of the analysis was the elucidation of the causative mechanism of the source process by sorting out and validating the most likely of the following carried hypotheses: (*a*) a (fanciful) underground nuclear test ("divulged" through some e-media); (*b*) a reservoir triggered seismic event (note that the epicenter is laying in the proximity area of the Paranoa artificial lake); (*c*) a fluid extraction induced event (there are a lot of deep water wells in use for water extraction); (*d*) a tectonic earthquake; and (*e*) a collapse shock (hence a roof fall could be the causative mechanism), although this last hypothesis is quite compelling it must be checked. The first three hypotheses, of anthropogenetic origin and exotic character, were discarded for obvious or conceptual reasons. The remaining two competing mechanisms were evaluated based on observational and modelling evidences in order to provide some constraints on the nature of the source. The outcome points out (more likely) a collapse parentage.

Introduction

The epicentral area of the Brasilia (DF) event lays in the southern outskirts of Brasilia's satellite town São Sebastião. During the available observation span, i.e., around a century, of which the instrumental period began by end of the '60s of 20th century no earthquake was observed or detected in an area with a radius of about 150 km around Brasilia (DF). Figure 1 presents an epicentral map for the period 1901-2000 showing all known events in a radius of 300 km around Brasilia (DF), i.e., 78 events spanning a magnitude range from less than 2 up to 3.7 (m_R). The data contained in the seismicity map of Fig. 1 are the result of a 'search' made in SISBRA – the *Seismic Data Base* of the Seismological Observatory of the University of Brasilia – which is built on the master earthquake catalog of Berrocal et al. (1984) for the period until 1981. Afterwards it is compiled based on Brazilian Seismic Bulletins (published periodically in *Brazilian Journal of Geophysics*) and Observatory's own data collected from its seismographic network, routinely processed and analysed (NB: as of March 18, 2001 SISBRA contains 6.254 events)

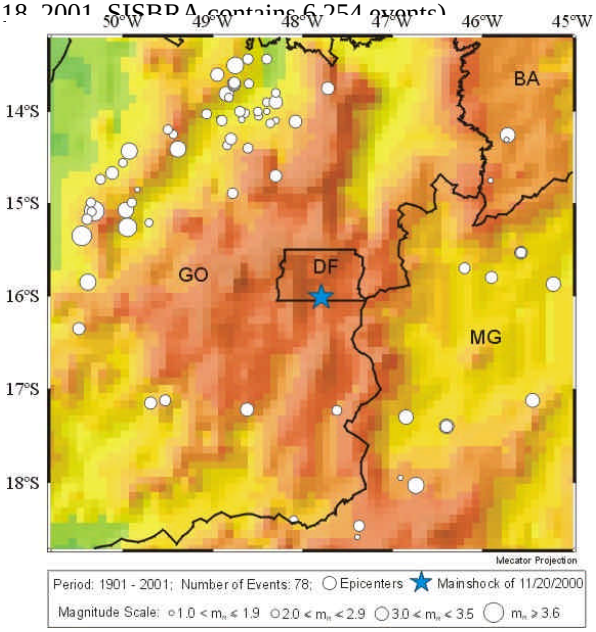

Fig.1 – Seismicity around Brasilia during 20th century [only epicentres within a radius of 300 km around the analysed event (marked with a star) were considered].

The Brasilia (DF) earthquake was widely felt and it was recorded by as many as 37 seismic stations whose distribution is shown in Figure 2. The network in Figure 2 is rather hybrid and inhomogeneous, being composed by analogic or digital instruments, uni- or tri-axial stations, local monitoring micro-networks, one array (BSA – Brasilia Seismic Array, a T-shape array, with 2.5 km spacing), SP or BB receivers etc. Although combining information from such an heterogeneous net may introduce some biases, for sake of achieving most complete description we are using all available pieces of information.

Brasilia (DF) Earthquake of Nov. 20, 2000

Data, Analysis and Source Parameters

The closest recording stations (some 40 km) were the stations making up the BSA, while the most distant was RCBR (an IMS secondary stations) (NB: close to CP station of the BSA is operating an IMS/GTSN primary station, BDFB – a BB borehole tri-axial station).

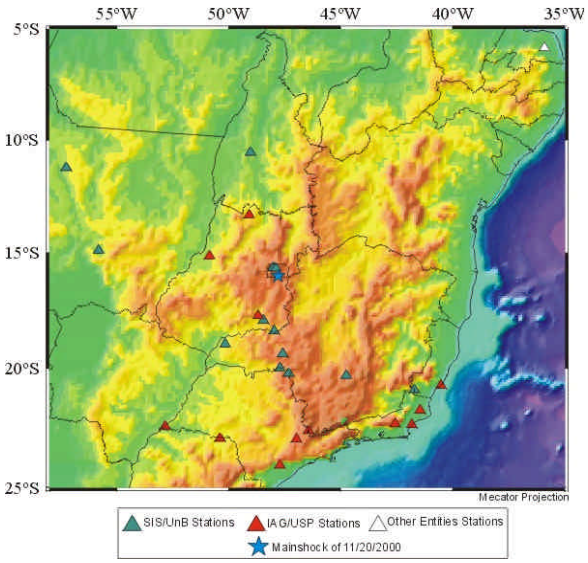

Fig.2 – General map of the area depicting the epicentre (star) and the seismograph network used in this study.

Although BSA has only 1-comp. vertical stations, incidentally, during the event at the station E4 (called also as "Casamata" that is "the vault") were operating (for testing purpose) on the same pier a set of tri-axial SP and/or BB receivers (models S-3000EQ, S-13, CMG-40T or L4C) linked at digital data loggers, luckily supplying richer information than the common uni-axial records of the BSA usual instruments. Figures 3 and 4 show a selection of representative waveforms.

Table 1 – Velocity model used in this study

Layer Depth (km)	Vp (km/s)	Vs (km/s)	Vp/Vs
0.00	5.50	3.16	1.740
3.00	6.00	3.45	1.739
15.02	6.78	3.90	1.738
40.00	8.22	4.73	1.738
60.00	8.30	4.77	1.740
80.00	8.38	4.82	1.739
100.00	8.45	4.86	1.739

First, we picked the arrival times of P and S waves and first motion polarity on vertical components (for digital data we used the SAC code and for analogic data the traditional procedure), with these data we have done the location using the HYPOCENTER code and a slightly modified "regional velocity model", to take into account the effects of shallow geology (see Table 1).

Second, for magnitude determination we used the routine procedure applied in Brazil, that is the *regional magnitude scale* (viz. Assumpção, 1983) m_R, which use the maximum amplitude in the P-wave train [NB: the regional magnitude scale is calibrated in terms of teleseismic *body wave scale* (m_b)].

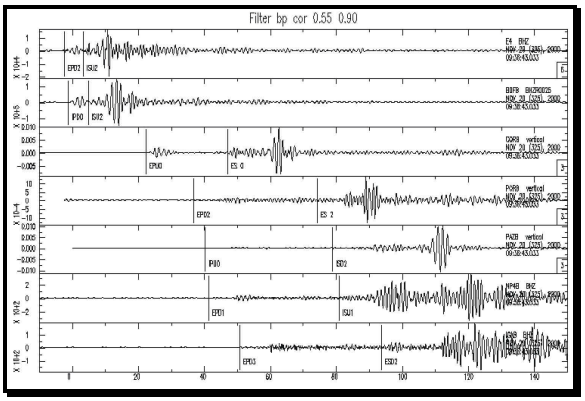

Fig.3 – Filtered waveforms (to enhance Rayleigh waves) of vertical components at various stations (depicted at the right side of traces), showing very well developed SP surface waves (Lg).

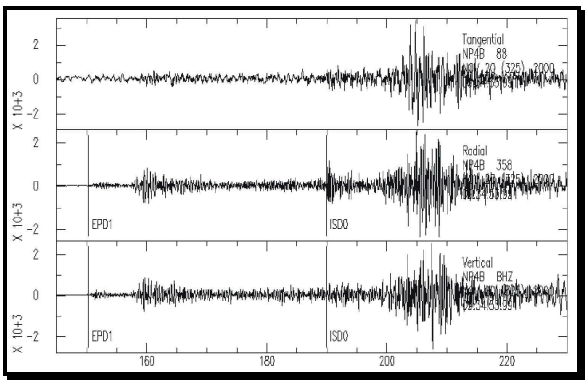

Fig.4 – NP4B broadband station rotated records, showing rather weak SH (on tangential component).

Third, we made a field survey in order to map the macroseismic effects. A summary of source and additional parameters is as it follows:

Date: 2000 NOV 20; *Origin Time*: 09:36:33.4 (UTC);
Epicenter: 16.01°S, 47.79°W; Depth: 0.5 km (fixed);
Magnitude: m_R= 3.7;
Statistics of location: r.m.s. of time residuals = 0.13 s;
Maximum intensity: I_o= VI (MM);
Elastic energy released: E_S= 4.0×10^9 J.

Macroseismic Field

Based on the interpretation of a Macroseismic Questionary, filled by people who experienced the quake, it was drawn up the macroseismic field map

presented in Figure 5. The available sampling of the territory allowed to seize only intensities down to III (MM) and the last ones only a few in number and azimuthal distribution. However, the amount of available sites with higher intensities left us to draw the isoseismals of intensities IV, V and VI (MM). In spite of some sites with incongruous values, nevertheless the resulted geometry of the isolines is very particular in respect of their shape, i.e., the macroseismic filed has a quite regular circular form, which may be a result of the causative mechanism of the source (see discussion in the next section).

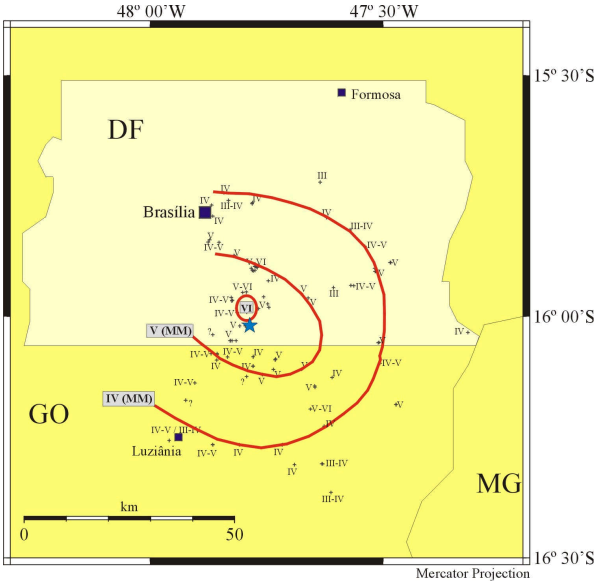

Fig.5 – Macroseismic field of the Brasilia (DF) earthquake of Nov. 20, 2000. The roman numerals show intensity values and the isolines for intensities VI, V and IV (MM) are displayed, as well.

Genetic Characterization of the Source

Brasilia (DF) earthquake has a series of traits which make it pretty unusual. These unusual features are as it follows:

(i) total lack of aftershock activity, despite the high detection level provided by nearby BSA and the temporary deployed high sensitive tri-axial stations just above the hypocentral region;

(ii) overwhelmingly, the first polarities are 'negative' or 'down' (see Figure 5 for first polarity distribution diagram);

(iii) the short period surface waves (see Fig. 3 and 4) are very strong, suggesting a very shallow source; and

(iv) a quite regular macroseismic field.

Under such circumstances we had to choose from all possible generic source mechanism the one which should best match the observational and heuristic available evidences.

We first discarded a whimsical hypothesis that the event was a nuclear testing, bizarrely circulating on e-media, as extravagant and without technical, logistic or conceivable support. Next, an artificial (man-made triggered) event was at hand because the epicenter of the event lies relatively close (roughly 20 km from nearest reservoir branch) to an artificial reservoir (Paranoa lake, volume 1.9 km^3 and dam height 48 m, filled in 1962) or because the epicenter is placed, as well, in an area rich in rather deep holes for water extraction. It is well known that both two above human engineering works (reservoir impoundment and operation and fluid extraction from crust) may trigger earthquakes and such phenomena are quite frequently observed in Brasil (Berrocal et al. 1984, p. 245-274; Assumpção et al. 2000; etc). However, both artificial hypotheses [the reservoir induced event (RIEq) and fluid extraction triggered event (FEEq)] were abandoned, as well. As a RIEq occurrence is hard to happen such a long time after the initiation of the reservoir and moreover the event occurred during a stage of low water lever of the reservoir, also the distance from lake is at the limit of the area of influence of it. As regards the FIEq hypothesis it also does not meet the features of manifestation typical for such kind of phenomena.

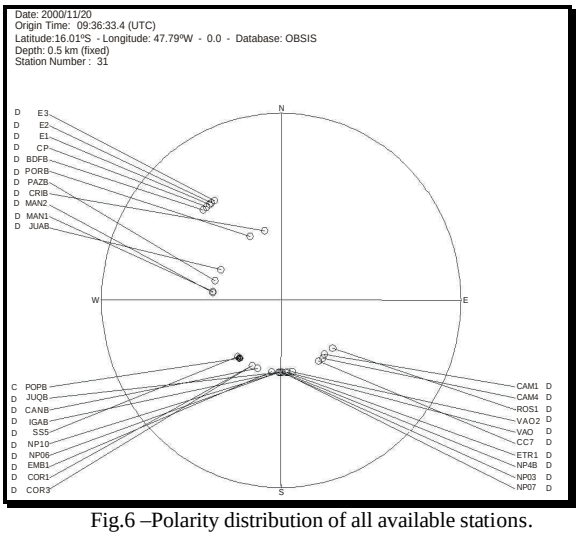

Fig.6 –Polarity distribution of all available stations.

The remaining two possibilities, tectonic earthquake or collapse event have to be antithetically analyzed. The collapse events are a very tiny fraction (much less than 1%) of the total of seismic events, whose huge majority is composed by tectonic events (accounting for more than 97%), between these to extreme genetic classes of earthquakes are placed the volcanic ones (less than 3%); cf. Båth (1979), with percentage estimations cf. Marza, (2000, Undergraduate Course Notes *'Basic Seismology'*). The possibility that the earthquake of Nov. 20, 2000 was produced by a collapse event is fairly attractive hy-

pothesis what must be checked against the prevalent tectonic (i.e., faulting) occurrence.

To check the feasibility of the collapse hypothesis we have tested it through simple work-energy physics relations, constrained by the seismic energy of the event. Considering that elastic (seismic) energy (E_s) is supplied by the kinetic energy (E_k) of the impact of the falling roof rock through seismic efficiency (h), $E_s = E_k * h$, literature gives for h a range from 10^{-4} to 5×10^{-2} (e.g., Scholz, 1990; Morrissey et al. 1999), here we adopted a value of 5×10^{-3} which is in the midrange of quoted values. Taking the event magnitude m_R ($\equiv m_b$) = 3.7, it results [using Duda's (1989) energy-magnitude relation: $log_{10} E_s$ (J) = 2.57 m_b –2.22] that $E_s \cong 2\times10^7$ J, which in turn (with the adopted value of h) gives an impact kinetic energy, $E_k \cong 4\times10^9$ J. Using elementary standard physics we may write: $E_k = V*r*h*g$, where: V is the volume of falling rock, r (= 2540 kg m^{-3}) is the density of rock (supposed to be limestone), h is the height of the fall and g is the acceleration due to Earth's gravity (taken as 10 m s^{-2}). The last relation does allow to infer the size of the falling rock, considering a simple geometry of the falling body (i.e., a disc shape of radius r and thickness/height H), whose volume would write: $V = p*r^2*H$. Now considering the kinetic energy (4×10^9 J) needed to match the radiated seismic energy (2×10^7 J) via the above geometrical-energetic relationships combined: $p*r^2*H = E_k / r*h*g$, it is required [for a discoidal body of thickness H = 10 m falling h = 25 m (a distance matching an average cave height)] a radius $r \approx 15$ m (hence a diameter ≈ 30 m) necessary to account for the energy budget (NB: the corresponding rock mass is 16×10^6 kg).

Other check regarding the causative mechanism is made (as suggested by Assumpção M., 2001, personal communication) analyzing the efficiency in generation of SH-waves, a strong and clear SH-wave is indicative of faulting rupture (i.e., tectonic event), while a weak one is compatible with a collapse/impact source which theoretically should be a less efficient generator of such waves. To do this check we rotated the horizontal components of tri-axial records in Radial (R) and Tangential (T) components and compared the T-comp. (carrying SH-wave) with the R-comp. (carrying SV-wave). A typical example is depicted in Fig. 4, which shows poor SH-wave (upper trace) comparing with SV-wave. Other tri-axial records in different azimuths show, more or less, similar features.

Discussions and Conclusions

The Brasilia (DF) event of November 20, 2000 is unusual in a series of features: it had a macroseismic field (Fig. 5) pretty circular (as a rule the isoseismals for tectonic events are elongated), it missed the (usual) aftershock activity, it was very shallow as suggested by location solution and very strong L_g waves generated (see Fig.3 and 4), all but one of the available first motion polarities show a negative (down) onset, fact that is hard to explain for a faulting radiation [for the sake of fairness we have to note that we lack data in the first quadrant (see Fig. 6), but this does not hamper too much our hereinafter conclusions], last but not least, the presence of an underground cave in the area where the event eventuated it is not inconceivable. Under such compelling and synergic context we find that the Brasilia seism is more likely to be a collapse event than the prevalent (at global scale) tectonic manifestation of seismicity. The natural portent of the occurrence of the Brasilia (DF) earthquake directs to the issue of earthquake hazard and risk of the area. The issue deserves a closer look as the earthquake potential may be greater than it is commonly perceived, a habitual attitude in low seismicity areas.

References

Assumpção, M. (1983) A regional magnitude scale for Brazil, *Bull. Seis. Soc. Am.* **73**: 237-246.

Assumpção, M., Marza, V., Barros, L. et al. (2000) Reservoir induced seismicity in Brazil, *PA-GEOPH* (in print).

Båth, M. (1979) *Introduction to Seismology,*2nd Revised Ed., Birkhäuser Verlag, Basel, 428 pp.

Berrocal, J., Assumpção M., Antezana R. et al. (1984) Seismicity of Brazil, *IAG/USP and CNEN*, São Paulo, 320 pp. plus 4 plates (in Portuguese).

Morrissey, M.M, Savage, W.Z. and Wieczorek, G.F. (1999) Air blasts generated by rockfall impacts: Analysis of the 1996 Happy Isles event in Yosemite National Park, *J. Geophys. Res.***104**: 23,189-23,198.

Scholz, C.H. (1990) *The Mechanics of Earthquakes and Faulting*, Cambridge Univ. Press, Cambridge, 439 pp.

Acknowledgments

We are grateful to M. Assumpçao for advice and seismograms of USP stations. Our colleagues J. Soares, Monica Von Huelsen, D. Fontenele, E. Neves, I. Gomes, R. Macedo are acknowledged for support in various stages of the work. The maps were drawn using the GMT software package.

Consequences of the fractal dimension of data distribution on the gravity mapping of the Parnaíba Basin

Jeferson de Souza and Mauro Andrade de Sousa, MCT/Observatório Nacional, Brazil. E-mail: jeferson@dge1.on.br *and* mauro@on.br

Abstract

We present a method to estimate the optimum interpolation interval of gravity data based on the evaluation of fractal dimension of the data distribution. Results for the whole Parnaíba Basin showed that gravity anomalies of large wavelengths (> 144km) can be appropriately represented allowing realistic interpretations of their origins to be proposed. The need of gravity interpretation being supported by data distribution with good spatial resolution, but also with enough dimensional resolution has been confirmed.

Introduction

The quality of the representation through maps, of geophysical data and, specifically, of gravity anomalies has been object of concern of many researchers. The production of a map of gravity anomalies involves an interpolation onto a regular grid, starting from a, generally, irregular and heterogeneous distribution of gravity stations. The low sampling and/or the heterogeneity of the data distribution introduces spurious anomalies in the resulting maps. Moreover, the interpolation process itself can generate false anomalies due to the phenomenon known as aliasing. The size of the interpolation grid to be used is a critical decision to be taken in the process of map production. In this work, the optimum interpolation interval is estimated directly from the calculation of the correlation dimension – an approach for the estimate of fractal dimension – of the gravity data distribution. The Parnaíba Basin was chosen as the study area for this work since a regional gravity interpretation of this basin demands the evaluation of the truthfulness of gravity anomalies maps. The data distribution is quite heterogeneous, due to logistics and ease of access, and some times due to interest in specific subareas for mineral and hydrocarbon prospecting.

Fractals

The simplest definition of fractal is a set of objects generated by a power law relationship $N(d) = a \cdot d^{-D}$, where N is the number of objects, D is named the fractal dimension, d is a characteristic of the objects (length, area, mass, etc.) and a is a constant. The fractal concept was introduced by Mandelbrot (1967), analyzing measurements of the perimeter of the British coastline. Measurements of the coastline length increased with increasing resolution, and the slope of the $\log(L(d))$ x $\log(d)$ plot defines the fractal dimension. Many geophysical phenomena present fractal geometry, *e.g.* the frequency and intensity distribution of fractures, earthquakes and volcanic eruptions (Turcotte, 1989); topography, gravimetric and magnetic surfaces (Turcotte, 1989); and the distribution geophysical data sets (Lovejoy *et alli*, 1986).

The study area

The Parnaíba Basin is a huge intracratonic basin situated in north/northeast Brazil (Figure 1). It is roughly ellipsoidal in shape and covers an area of approximately 600,000 km^2. The Parnaíba Basin is mainly Paleozoic in age and filled with siliciclastics of mostly continental origin deposited in five great depositional cycles from Upper Ordovician to the Cretaceous. Regional uncomformities due to slow epeirogenic crustal movements have been recognized and the sedimentary cover has been intruded by volcanic rocks of Lower Jurassic and Lower Cretaceous ages. Palaeozoic sediments reach up to 2,900 m and are mainly sandstones with subordinate siltstones and shales. These rocks define broad and regionally distributed lithostratigraphic units with small facies variations (Cunha, 1986). Mesozoic and Cenozoic sediments do not exceed about 600 m and are of lesser importance than in the neighboring coastal basins, where they reach up to 9,000 meters.

Gravity data distribution

The gravity database of the Parnaíba Basin is made up of 21,432 stations in the continental area and 19,438 measurements offshore (Figure 2). Different sampling patterns are exhibited in different sub-areas of the basin and this heterogeneity is quite appropriate for the present investigation. A regional gravity study of this basin was earlier accomplished by De Sousa (1996).

Fractal analysis

It is generally assumed is that mapping algorithms are capable of a realistic exhibition of the observed quantity. Also, input parameters defining the gravity anomaly, *e.g.* the mean upper crust density in the Bouguer anomalies, are correctly estimated. Both assumptions have been object of concern, either focusing on the precision reached by different interpolation algorithms (Eckstein,1989; El Abass *et alli*,

1990), or terrain density estimates Thorarinsson & Magnusson (1990), Chapin (1995). Imprecision in gravity mapping lead to residual anomalies of doubtful quality and unrealistic mass estimates.

Lovejoy *et alli* (1986) studied the degree of heterogeneity of geophysical datasets through use of the fractal dimension. Korvin *et alli* (1990) and Keating (1993, 1998) investigated the consequences of the distribution of gravity stations on maps of different tectonic provinces in Australia and Canada, respectively. Keating (1993) used the box method, earlier proposed by Mandelbrot (1982) and Feder (1988), to compute the fractal dimension of the Canadian gravity data distribution. The box method consists of dividing the area into small squares of various sizes *d,* and counting the number $N(d)$ of squares containing data. When the scale regime is constant,

$$N(d) \alpha d^{-D_f}, \quad 0 < \mathrm{D_f} < 2,$$

and at any given interval the distribution is looked at, data density is constant. Then, the fractal dimension instead of the Euclidian dimension scales information. When the scale regime is constant, the sampling rate, *i.e.* the number of observations per unit area is also constant and follows Shannon´s theorem: $N = pX^2 / \lambda_{\min}^2$, where N is the number of necessary samples to restore the original observable; X is the size of the square and λ_{min} is the smallest detectable wavelength. If the data distribution is uniform, the Euclidian 2D dimension – $D_f = 2$ is found. A more computationally efficient technique to evaluate the fractal dimension of geophysical data distributions has been proposed by Grassberger & Procaccia (1983). This method calculates the cumulative frequency distribution of interstation distances – named the correlation function – $N(r)$, for increasing radii r. The scale regime occurs when

$$\langle N(r) \rangle \propto r^{-D_c}, \qquad 0 < D_c < 2,$$

where $\langle N(r) \rangle$ is the average number of stations within the disk of radius r. This technique was adopted in this study and is similar to the box method. However, the parameter recovered is the correlation dimension D_c, very similar to the fractal dimension for most geophysical applications (Lovejoy *et alli*, 1986).

Results

Five areas (1 to 5) were selected in the continental Parnaíba Basin and one area offshore within the study area. The entire continental area was also studied (Figure 2). Selection was based on the conspicuous variety of patterns of data distribution and densities. Matlab® and Fortran programs were developed for the calculation of the correlation function. The geographical coordinates of the stations were orthogonally projected according to a Lambert conical projection. Graphs and linear regression estimates were prepared with ORIGIN® software. Graph 1 shows the linear fit for the continental area as a whole.

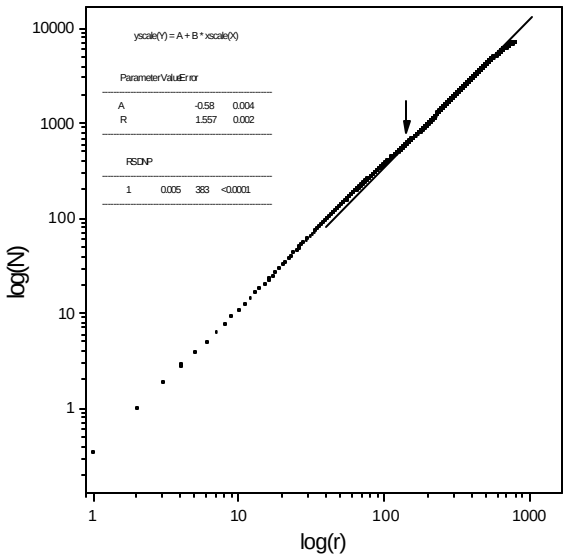

Graph 1 – Evaluation of the correlation dimension for the entire continental area. The arrow indicates the onset of the scaling regime.

Table 1 – Correlation dimension and the onset of the scaling regime for selected areas and the entire continental area.

area	correlation dimension	scaling regime beginning (km)
1	1.393±0.002	45
2	1.840±0,003	9
3	1.602±0,002	20
4	1.878±0,005	3
5	1.798±0,005	33
6	1.507±0,022	22
continental	1.557±0,002	144

Results of the linear fits are tabulated in Table 1.
Area 1 shows a low dimension and the scaling regime also begins at a relatively low value. This is an expected result, because the data are poorly distributed and their density is also low. Areas 2, 3 and 4 are similar regarding the distribution pattern, the only important difference among them being the density of gravity stations. Our results show that data density affects the correlation dimension and the scaling regime. Area 5 presents a high correlation dimension but the scale regime begins at 33 km. This result has

been interpreted as a rather homogeneous data distribution producing a correlation dimension close to the Euclidian dimension. As the data density is low, the onset of the scaling regime is affected. Results for Area 6 are also expected, due to the already known aliasing affecting oceanic gravity data acquisition. The scale regime begins at 22 km, which is approximately the spacing between navigation cruises. For the entire continental area, the scale regime begins at 144 km, indicating that only wavelengths larger than this value can be realistically detected.

Conclusions

Our results indicate that, when considering the entire area of the Parnaíba Basin, only a large interpolation grid produces a realistic gravity map. It is quite obvious that the many and large data gaps seen in data distribution are to be blamed. The low fractal dimension found leads to the conclusion that only a regional gravity interpretation is supported by the current dataset. Filling these gaps with new data is the only solution to this dilemma. On the other hand, the same criterion shows that some sub-areas possess good data sampling and distribution patterns, thus allowing a more detailed analysis. This indicates that in some cases, it is preferable to integrate the maps generated in several sub-areas. Interpolation schemes based on the fractal dimension criterion does not introduce any new physical information to the interpolated values. It simply minimizes the chance of introducing numeric artifacts which may lead to biased map interpretation

References

BANKS, R. (1992), "Contouring algorithms", *Geobyte*, **6**(5): 15-123

BRAILLE, L.W. (1978), "Comparison of four random to grid methods", *Computers & Geosciences*, **4**: 341-349.

CHAPIN, D.A. (1995), "A deterministic approach toward gravity residuals – A case study from South America", *Geophysics*, **61**(4): 1022-1033.

DE SOUSA, M.A. (1996), "Regional gravity modeling and geohistory of the Parnaíba Basin (NE Brazil)", *Ph.D. Thesis,* University of Newcastle upon Tyne, 127 pp.

DE SOUSA, M.A. & Oliveira, M.F.B (1995), "Geophysical evidence of the Transbrasiliano Lineament in the Parnaíba Basin", *Annals of III Simpósio Nacional de Estudos Tectônicos*, Gramado, 260-263.

ECKSTEIN, B.A. (1989), "Evaluation of spline and weighted average interpolation algorithms", *Computers & Geosciences*, **15**(1): 79-94.

EL ABASS, T., Jalloili, C., Albouy, Y. e Diament, M. (1990), "A comparison of different surface fitting algorithms for geophysical data", *Terra Nova*, **2**: 467-475.

FEDER, J. (1988), "Fractals", *Plenum Press*.

GRASSBERGER, P. & Procaccia, I. (1983), "Measuring the strangeness of strange attractors, *Physica*, **9D**: 189-208.

KEATING, P.B. (1998), "Weighted Euler deconvolution of gravity data", *Geophysics*, **63**(5): 1595-1603.

KEATING, P.B. (1993), "The fractal dimension of gravity data sets and its implications for gridding", Geophysical prospecting, **41**: 983-993.

KORVIN, G. Boyd, D.M. & O'Dowd, R. (1990), "Fractal characterization of the South Australian gravity station network", *Geophysical Journal International*, **100**: 535-539.

LOVEJOY, S. Schertzer, D. & Ladoy, P. (1996), "Fractal characterization of inhomogeneous geophysical measuring network", *Nature*, **319**: 43-44.

MANDELBROT, B.B. (1982), "The fractal geometry of nature", *W.H. Freeman and Company*, New York.

THORARINSSON, F. & Magnusson, S. (1990), "Bouguer density determination by fractal analysis", *Geophysics*, **55**(7): 932-1935.

TURCOTTE. D.L. (1993), "Fractals and Chaos in Geology end Geophysics", *Cambridge University Press*.

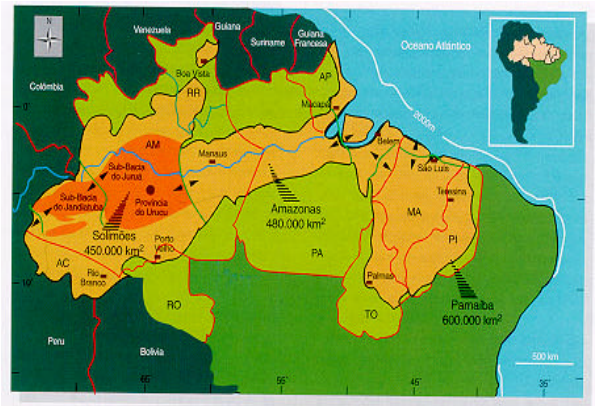

Figure 1 - Location of the study area.

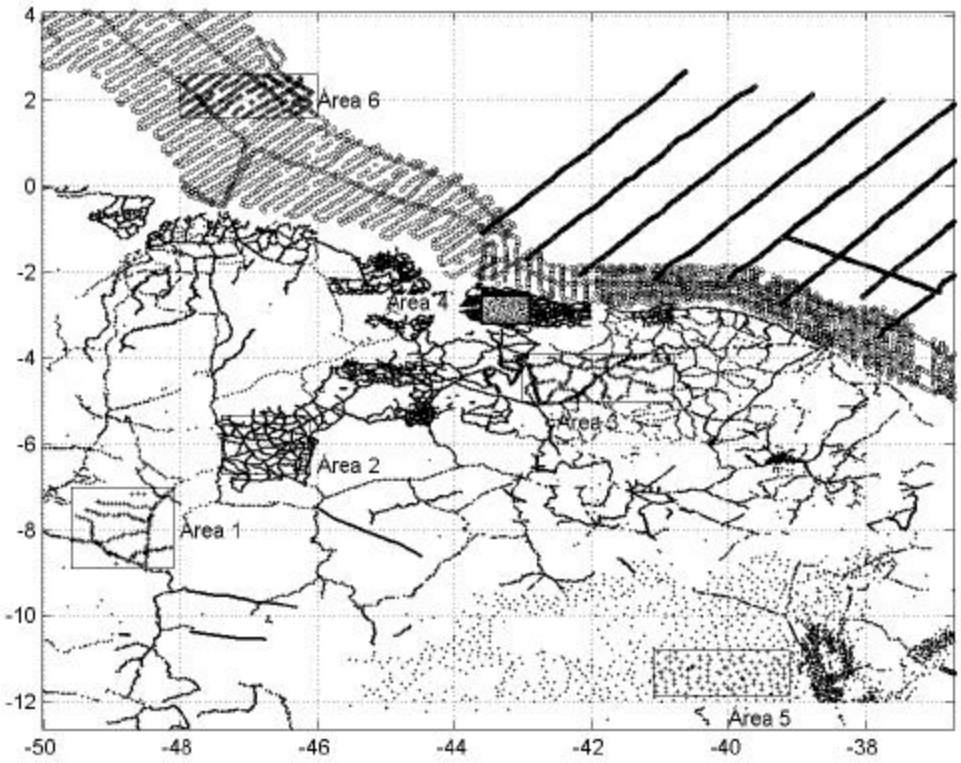

Figure 2 – Distribution of stations and selected areas in the Parnaíba Basin.

Deformación tectónica cuaternaria y migración del frente de empuje del Cerro La Cal : Implicancias paleosísmicas

Francisco A. Mingorance, U.N.Cuyo, Argentina

Abstract

The overall pattern of surface deformation in the vecinity of the migrated Cerro La Cal Thrust Front is explained as the effects of fault-plane bending. The Frontal Fault had been active until early Pleistocene time. This reverse fault thrusts the Cerro La Cal over a pile of basin-fill sediments, and a sedimentary wedge was formed on its down-thrown side. In middle Pleistocene time (?), a low-angle thrust was formed in the sedimentary wedge presumably as a bedding slip. As a result, the Frontal Fault became inactive and the location of the surface faulting advanced 0.6 km basin-ward. Coseismic deformation associated with the 1861 earthquake occurred entirely along the migrated La Cal thrust fault. This seismogenic fault advanced east-ward at a migration rate of 0.75 mm/yr.

Introducción

La migración hacia el valle de fallas inversas que bordean frentes montañosos, es un rasgo bastante común en ambientes tectónicos compresivos.

Un frente de empuje migrado en tiempos cuaternarios presenta generalmente una Falla Maestra que empuja a la sierra sobre los sedimentos de relleno y una Falla Activa Frontal migrada hacia el valle, cuya iniciación es aproximadamente contemporánea con la cesación de la actividad de la Falla Maestra (Ikeda, 1983).

El patrón de deformación superficial en la vecindad de un frente de empuje migrado, es el resultado de la curvatura del plano de falla, en el sentido de que la porción más superficial de la falla buza con un ángulo significativamente menor que la porción más profunda. A medida que la Falla Maestra se mueve, sedimentos de relleno son acumulados sobre su bloque hundido, favoreciendo la formación de una Cuña Sedimentaria. Una vez que esta pila de sedimentos de relleno en forma de cuña se ha desarrollado completamente, y debido a la marcada diferencia en rigidez entre la cuña sedimentaria y el basamento, el fallamiento original produce la concentración de esfuerzos de cizalla en la cuña (interface cuña – basamento) y a lo largo de la extensión hacia arriba de la Falla Maestra. La anisotropía mecánica de la cuña sedimentaria, por su naturaleza estratificada, favorece la propagación de la falla a lo largo de una interface subhorizontal, en lugar de su propagación hacia arriba a lo largo de la Falla Maestra. En consecuencia, un Corrimiento de Estratificación (Bedding Thrust) es formado en la cuña, y el frente de empuje avanza hacia el valle. Ambas, la Falla Maestra y la Falla Activa Frontal, convergen en profundidad en un mismo plano (Ikeda, 1983).

En este proceso de migración del frente de empuje, el cual no requiere cambios en el régimen tectónico regional, la dimensión de la cuña sedimentaria sería un factor dominante en el control de la cantidad de migración (Ikeda, 1983).

Generalmente, la Falla Maestra no es activa, tal como lo demuestran las evidencias de deformación cosísmica asociadas a los terremotos compresivos de 1861 (Mendoza, Argentina), 1896 (Rikuu, Japón) y 1971 (San Fernando, California), las cuales aparecieron exclusivamente a lo largo de la Falla Activa Frontal (Ikeda and Yonekura, 1979; Ikeda, 1983; Mingorance, 2000; 2001).

En base a las consideraciones anteriores, y teniendo en cuenta que la deformación cosísmica primaria asociada al terremoto de 1861 ocurrió a lo largo de la falla activa La Cal, y que el bloque estructural del Cerro La Cal ejerce un evidente control sobre la geometría del trazo de aquella fuente sismogénica (Figura 2); el sector central de esta zona de falla fue analizado con el objeto de comprender las relaciones geométricas, espaciales y temporales de la deformación tectónica cuaternaria, y establecer un posible mecanismo de migración para el frente de empuje del Cerro La Cal. La Zona de Falla La Cal se localiza en el extremo sur del Cinturón de Empuje de la Precordillera (Provincia de Mendoza – Figura 1), sobre el segmento de subducción subhorizontal de los Andes Centrales.

Deformación tectónica cuaternaria

El frente orogénico actual (Frente Diaguítico: 2 Ma), localizado sobre el borde oriental de la Precordillera y del Cerro La Cal (Figuras 2 y 3), es todavía activo (Ramos, 1988). Evidencias de deformación cosísmica histórica y prehistórica almacenadas en el registro geológico cercano a la superficie (Mingorance, 2000; 2001), confirman la actividad del frente de empuje analizado en el actual régimen sismotectónico.

La principal estructura de esta zona de deformación cuaternaria, está representada por la falla activa La Cal, un corrimiento de bajo ángulo de 30.7 km de longitud, que se prolonga dentro del populoso Gran Mendoza.

Esta fuente sismogénica deforma y desplaza superficies aluviales de edad Pleistocena Superior – Holocena (Tabla I), con la mayor cantidad de desplazamiento vertical para las superficies más antiguas. Esto indica que la falla activa La Cal se ha movido progresivamente durante dichas épocas.

Información proveniente de una trinchera exploratoria excavada a través del trazo de la falla activa La Cal (T en Figura 3), indica que su mecanismo de deformación superficial está controlado por

Migración del Frente de Empuje del Cerro La Cal – Implicancias paleosísmicas

Figura 1 – Localización de la provincia de Mendoza.

Plegamiento de Propagación de Falla, y que la estructura interna de la escarpa se resuelve mediante un plano de falla principal (16º a 25º O) y dos planos de falla secundarios (30º O y 35º O) localizados en el bloque levantado (Mingorance, 2001).

El grado de actividad tectónica cuaternaria del Frente de Empuje del Cerro La Cal (Falla Frontal), fue clasificado mediante la aplicación de una técnica específica basada en análisis geomorfológicos cuantitativos. Esta técnica es particularmente útil, ya que los frentes montañosos limitados por fallas presentan un arreglo característico de geoformas que registran las interacciones entre levantamiento y erosión (Bull, 1987). La identificación y cuantificación de geoformas diagnósticas presentes en el frente montañoso y en el piedemonte local del cerro (Tabla I), permitieron asignar la Clase 2 (Rápida) a los sectores 2, 3b y 4, mientras que la Clase 3 (Lenta) fue asignada a los sectores 1 y 3a (Figura 3). Las variaciones estructurales y topográficas observadas a lo largo del frente montañoso analizado, indican preliminarmente que el frente podría estar segmentado en dos bloques (Bloque Norte: 3b y 4 – Bloque Sur: 1, 2 y 3a).

Evidencias estratigráficas expuestas como resultado de la explotación minera intensiva del Bloque Sur, permitieron confirmar el carácter y sincronización temporal (deformación Plio-Pleistocena) de las fallas presentes en los sectores 1, 2 y 3a. De especial significancia es la exposición del plano de la Falla Frontal (Figura 4), el cual coloca a las calizas de la Fm. San Juan (Ordovícico) sobre estratos de la Fm. Mogotes (?). La edad asignada a esta formación varía entre alrededor de 3 Ma y 1 Ma (Irigoyen et al., 1999).

Un rasgo saliente en la evolución geomorfológica del piedemonte local del cerro, está dado por la presencia y profunda incisión de la superficie geomórfica Q_0 (Pleistoceno Inferior), la cual forma un contacto recto Piedemonte - Frente Montañoso (sectores 1, 2 y 3b). Esta evidencia, sumada al hecho de que la falla La Cal no afecta a la superficie Q_0 en ningún sector a lo largo de su trazo (30.7 km), indicaría que la Falla Frontal fue activa durante el Plioceno Superior – Pleistoceno Inferior. La cuña sedimentaria iniciada en dicha época, y desarrollada completamente hacia el Pleistoceno Medio (?), habría favorecido la formación de un Corrimiento de Estratificación de bajo ángulo, el cual sería responsable de la migración hacia el Este del frente de empuje (Figuras 3 y 5). La expresión superficial de esta migración subhorizontal, está representada por la escarpa principal de la falla La Cal.

El Ritmo de Migración estimado para el Frente de Empuje del Cerro La Cal, desde el Pleistoceno Medio, es de 0.75 mm/año. Asumiendo que el Ritmo de Migración es equivalente al Ritmo Medio de Deformación (Slip Rate), el valor obtenido es consistente con aquel estimado para el sistema de fallamiento compresivo cuaternario de la Precordillera Oriental (0.6 mm/año - Bastías y Bastías, 1987).

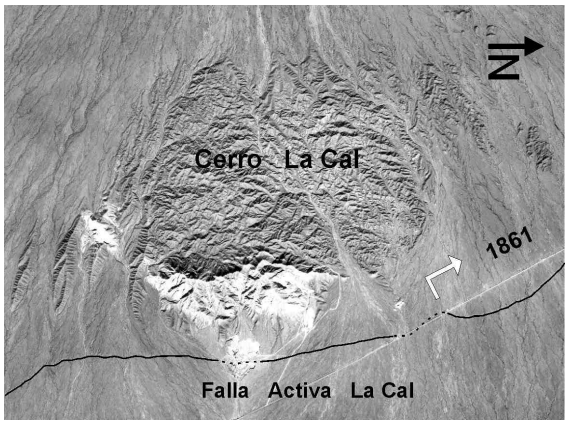

Figura 2 – Vista en planta del Cerro La Cal en el piedemonte oriental de la Precordillera. Este bloque estructural (3.8 km por 3.5 km) ejerce un evidente control sobre la geometría de la falla activa La Cal (FALC). La posición del trazo de la FALC, a 0.6 km del frente montañoso, pone en evidencia la migración hacia el Este del frente de empuje. 1861 indica el tramo de falla que experimentó deformación cosísmica primaria asociada al terremoto de 1861 (Ms: 7.0).

La cantidad total de migración del frente de empuje analizado (0.6 km), estaría relacionada al desarrollo de una cuña sedimentaria de relativamente poco espesor.

Implicancias paleosísmicas

Modelos de dislocación simples demuestran que la cantidad de deformación superficial (1.5 m) asociada al terremoto de 1971, estuvo relacionada a una cantidad mayor de deformación subsuperficial (5.5 m), a lo largo de un corrimiento de estratificación (13º) de bajo ángulo (Ikeda and Yonekura, 1979).

Información proporcionada por una trinchera exploratoria excavada a través de la FALC (T en Figura 3), indica que el evento prehistórico más reciente produjo un rechazo estratigráfico múltiple de 1.5 m,

Migración del Frente de Empuje del Cerro La Cal – Implicancias paleosísmicas

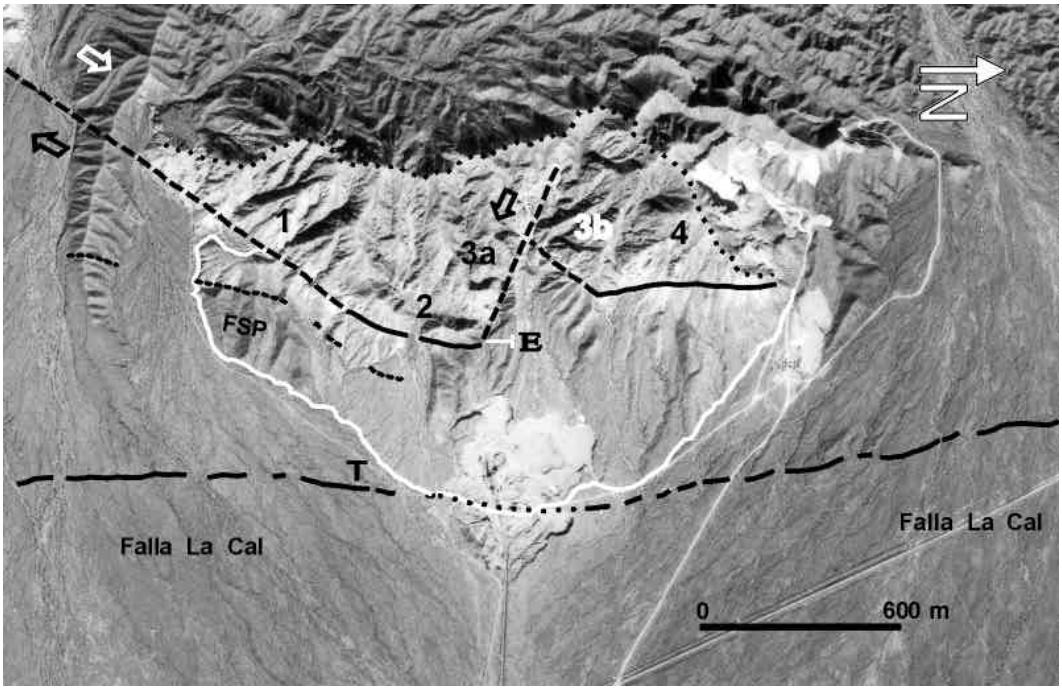

Figura 3 – Distribución espacial y geometría de las fallas Cuaternarias localizadas en el frente de empuje del Cerro La Cal (Borde oriental). Falla Inversa Frontal (Sectores 2 y 4), Falla Inversa con posible componente de rumbo (Sectores 1, 3 a y 3b). **E**: Exposición del plano de la Falla Frontal. **T**: Trinchera exploratoria a través de la Falla Activa La Cal. **FSP**: Falla secundaria probable. Línea blanca: Piedemonte Local del Cerro La Cal. La fotografía aérea muestra al frente montañoso y al piedemonte local del cerro, con anterioridad al inicio de la explotación minera intensiva.

PARÁMETROS	**FALLA ACTIVA LA CAL**	**FALLA FRONTAL**
TIPO DE FALLA	Corrimiento de Bajo Angulo	Inversa
LONGITUD	30.7 km	1 km (sectores 2 y 4 solamente
RUMBO DEL TRAZO	Norte	Norte
BUZAMIENTO DEL PLANO (superficie)	16º - 25º O (Trinchera)	47º O (Exposición)
GEOMETRÍA DEL TRAZO	Curva	Rectilínea
GEOFORMAS CARACTERÍSTICAS		
Frente Montañoso (FM)		Facetas triangulares – Perfiles en V
Piedemonte Local (PL		Contacto recto FM - PL (sectores 2, 3b y 4) Abanicos incididos (Q_0 profundamente) Ballenas deformadas (sectores 1 y 3b)
Piedemonte Regional (PR)	Escarpa de falla (compuesta)	Ballenas deformadas (sector 1)
Superficie Marcadora	Q_2 - Q_3 - Q_4	Q_0
Edad (relativa)	Pleistoceno Superior - Holocen	Pleistoceno Inferio
Formación Involucrada	Innominada	San juan - Mogotes - Innominada
Edad (relativa - absoluta)	Pleistoceno Superior - Holoceno	Ordovícico - Plioceno (S) - Pleistoceno (I)
Mecanismo de Deformación Superficia	Pliegue de propagación de fall	Fallamiento invers
ACTIVIDAD CUATERNARIA		
Grado o Clase	Activa (actividad Holocena)	Clase 2 (sectores 2, 3b y 4) - Clase 3 (1 y 3a)
DEFORMACIÓN COSISMICA	1861 (Ms: 7.0)	

Tabla I – Parámetros geológicos y geomorfológicos de las fallas cuaternarias presentes en el frente de empuje del Cerro La Cal.

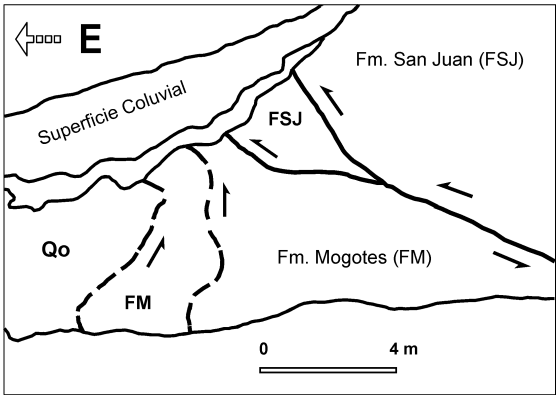

Figura 4 – Exposición del plano de la Falla Frontal. Esta falla inversa coloca a las calizas de la Fm. San Juan (Ordovícico) sobre los estratos de la Fm. Mogotes (?) (Plioceno Superior). Un posible contacto por falla existe entre la Fm. Mogotes y las gravas Cuaternarias (**Q_0**). La ubicación del sitio está indicada en la Figura 3 (**E**).

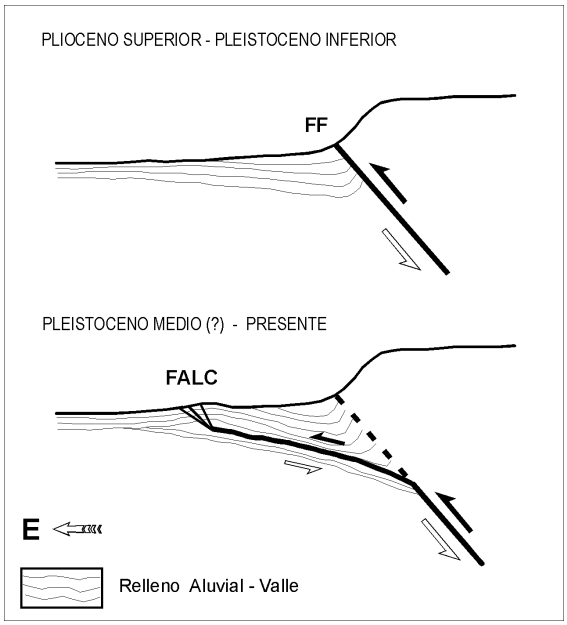

Figura 5 – Posible mecanismo de migración del Frente de Empuje del Cerro La Cal durante el Cuaternario. FF: Falla Frontal (Inversa), FALC: Falla Activa La Cal. El incremento de espesor hacia el Oeste de una Cuña Sedimentaria compuesta fundamentalmente por estratos de la Fm. Mogotes (?) y relleno aluvial cuaternario, habría favorecido la migración hacia el Este del Frente de Empuje, mediante el desarrollo de un Corrimiento de Estratificación de bajo ángulo. La expresión superficial de esta migración subhorizontal está representada por la escarpa de la FALC.

controlado por Plegamiento de Propagación de Falla. La estructura interna de la escarpa (FALC en Figura 5), por otro lado, se resuelve mediante un plano de falla principal (16º a 25º O) y dos planos de falla secundarios (30º y 35º O). Estas evidencias sugieren que el Corrimiento de Estratificación subsuperficial responsable de la migración del frente (Figura 5), tendría un ángulo bastante menor (posiblemente 10º - 12º), con una gran componente horizontal de desplazamiento.

En zonas de fallamiento compresivo activo, la determinación del Ritmo Medio de Deformación basado en la información proporcionada directamente por la escarpa de falla (componente vertical), podría conducir a un verdadero subdimensionamiento del parámetro.

Conclusiones

El Frente de Empuje del Cerro La Cal evidentemente migró hacia el Este en tiempos cuaternarios, a un ritmo de 0.75 mm/año. El mecanismo de migración propuesto es el que mejor se ajusta a las evidencias geológicas, geométricas y sismotectónicas existentes.

Referencias

Bastías, H y Bastías, J., **1987**. Análisis de desplazamientos y velocidades en el área diferencial de Precordillera, provincia de San Juan. Asociación Geológica Argentina, Revista XLII (3-4): 261-266.

Bull, W., **1987**. Relative rates of long-term uplift of mountain fronts. U.S.G.S, Open – File Report 87-673: 192-202.

Ikeda, Y., **1983**. Thrust-front migration and its mechanisms – Evolution of intraplate fault systems. Bulletin of the Dept. of Geography, University of Tokyo, Vol. 15: 125-159.

Ikeda, Y and Yonekura, N., **1979**. Dislocation fault models of the San Fernando, California, earthquake of 1971-Bending of fault plane and its tectonic significance. J. Seism. Soc. Japan, 32: 477-488 (en Japonés).

Irigoyen, M., Brown, R. and Buchan, K., **1999**. Cronología neogénica de los depósitos sinorogénicos aflorantes en la región de Cacheuta-Tupungato, norte de Mendoza. XIV Congreso Geológico Argentino, Salta, Actas I: 63-64.

Mingorance, F., **2000**. Caracterización de la geometría de la zona de fallamiento activo La Cal, Mendoza, Argentina. IX Congreso Geológico Chileno, Actas, Vol. 1: 800-804.

Mingorance, F., **2001**. Parámetros geológicos de la deformación superficial cosísmica asociada al terremoto de Mendoza de 1861 (Ms: 7.0), Argentina. 7th International Congress of the Brazilian Geophysical Society (*in press*).

Ramos, V., **1988**. The tectonics of the Central Andes, 30º to 33º S latitude. Geological Society of America, Special Paper 218: 31-54.

ESTRUTURAÇÃO DA CROSTA SUPERIOR NA REGIÃO DE MINAÇU (GO) UTILIZANDO O MÉTODO DA REFRAÇÃO SÍSMICA – Resultados Preliminares

Juliana Alencar Antunes, IAG/USP (juliana@iag.usp.br); Jesus Berrocal, IAG/USP (berrocal@iag.usp.br)

Abstract

This study is a part of a deep seismic refraction experiment belonging to the Thematic Project "Geophysical Studies and Tectonic Model of the Tocantins Province Central and Southeast Sectors, Central Brazil". The main objective of this work is to analyze part of the data of the Porangatu Deep Seismic Refraction Line (shots 5, 6 and 7), located in the central sector of the Tocantins Province, called Minaçú Line in this work. The final objective is to obtain a seismic velocity model, showing the physical features of the main discontinuities in the upper crust and correlate these results with the main tectonic features in the studied area.

Introdução

O presente trabalho está inserido nos estudos de refração sísmica profunda do Projeto Temático "Estudos Geofísicos e Modelo Tectônico dos Setores Central e Sudeste da Província Tocantins, Brasil Central", finaciado pela FAPESP. Nesses estudos foram levantadas três linhas de refração de aproximadamente 300 km de extensão (Soares et al., 2001; Perosi et al., 2001). O trabalho aqui proposto tem por objetivo a análise de uma porção dos dados da Linha de Refração Sísmica Profunda de Porangatu (Tiros 5, 6 e 7), localizada na porção oeste do setor central da Província Tocantins e denominada aqui de Linha Minaçú. Será elaborado um modelo de velocidades sísmicas, contendo as características físicas das principais descontinuidades na parte superior da crosta terrestre existentes na região, além de efetuar uma tentativa de correlação com as principais feições tectônicas da área estudada.

Aspectos Geológicos

A região de Minaçú está inserida dentro do domínio geotectônico da Província Estrutural Tocantins (Almeida et al., 1968), a qual abrange quase totalmente os estados de Goiás, Tocantins e o Distrito Federal, parte de Minas Gerais e Mato Grosso do Sul, além de uma estreita área do extremo leste do Pará. É delimitada a noroeste pelo Craton Amazônico, a sudeste pelo Craton São Francisco/Congo, a norte pela Bacia do Parnaíba e a sul pela Bacia do Paraná.

A Província Tocantins engloba os metassedimentos das faixas de dobramentos Brasília, Paraguai e Araguaia, assentadas sobre um embasamento de alto grau metamórfico, essencialmente granito-gnáisssico, e envolvendo um segmento central geologicamente complexo que apresenta características de porções continentais e de arcos de ilha (Maciço de Goiás). Esta província teria sido formada pela convergência e colisão de blocos continentais, representando um sistema de inversão de bacia oceânica de margem passiva (Fuck et al., 1994).

A Faixa Brasília constitui, provavelmente, o melhor cinturão orogênico neoproterozóico preservado no Brasil. Mostra feições tais como *melange*-ofiolítica, arco de rochas calcialcalinas, granitos colisionais tipo-S e *nappes* estruturais de escala regional indicando transporte tectônico em direção a E (Pimentel et al., 2000). É comparável, em dimensões e provavelmente em feições, a cadeias de montanhas atuais como o Himalaia e os Alpes (Berrocal et. al., 1996).

A Faixa Brasília é dividida, segundo Dardenne (1978, 1981), Fuck (1990), Fuck et al. (1993), Fuck (1994) e Fuck et al. (1994) em três zonas distintas, que se diferenciam pela litologia, taxa de deformação e metamorfismo: 1) zona cratônica que compreende as rochas metassedimentares dos grupos Bambuí e Paranoá, e exposições do embasamento; 2) zona externa formada por ortognaisses e *greenstone belts* e por metassedimentos de margem passiva estruturados em um cinturão de dobras e cavalgamentos de ante-país; e 3) zona interna formada por exposições de ortognaisses, granulitos e um complexo de rochas metamórficas que em alguns lugares reúne características de *mélange* ofiolítica (Strieder e Nilson, 1992).

O Maciço de Goiás é uma grande área, geologicamente complexa, onde ortognaisses, granitóides, seqüências vulcano-sedimentares, complexos acamadados e corpos granulíticos de várias idades e naturezas estão expostos. Estudos atuais envolvendo petrologia, geocronologia e geoquímica levaram Pimentel & Fuck (1992) e Pimentel et al. (2000) a redefinirem o Maciço de Goiás, reconhecendo na sua estruturação diversos domínios geológico/tectônicos com diferentes idades e significados tectônicos. Os terrenos neoproterozóicos, formados por ortognaisses e metavulcânicas, apresentam assinatura geoquímica e isotópica própria de arcos de ilha e seus limites geográficos ainda são pouco conhecidos (Pimentel et al., 1994).

A descoberta de rochas de arco juvenil, assim como intrusões graníticas peraluminosas colisionais associadas a unidades de rochas metassedimentares na parte sul da Faixa Brasília, foram fundamentais para contestar os modelos ensiálicos anteriores que considerava essa região como uma grande exposição do embasamento (Pimentel et al., 2000).

A área de estudo deste trabalho localiza-se na porção norte do Estado de Goiás, no limite entre a Faixa Brasília (Zona Interna) e os terrenos do Maciço de Goiás (Figura 1).

Metodologia

A seção sísmica a ser estudada, denominada Linha Minaçú, possui aproximadamente 100 km de extensão, com direção geral W-E, perpendicular as principais estruturas tectônicas. Possui três pontos de tiro distanciados entre si de 50 km e 40 sensores localizados a cada 2.5 km, aproximadamente.

O perfil inicia-se próximo a cidade de Trombas, passa pela cidade de Minaçú e estende-se até a Mineração Toniolo Busnello, localizada próxima ao lugarejo do Araí, município de Cavalcante. Os registradores utilizados foram, em sua maioria, registradores SGRs (*Seismograph Group Recorders*), três registradores KINEMETRICS (modelo SSR1), cada um com dois enlaces telemétricos e um sensor ligado direto por cabo, e quatro registradores PRAGMÁTICA, montados no Brasil e pertencentes ao IAG/USP. Todos os registradores são digitais: os SGRs trabalham com registro em fita magnética e os registradores SSR1 e PRAGMÁTICA com memória em disco rígido. Todos utilizam um sistema de janelas de registro, que são habilitadas no momento programado e possuem um relógio interno que é ajustado antes e após as explosões, para o cálculo da deriva. Foram utilizados sismômetros verticais de período curto (T_0= 0,5 s) modelo L4-C da MARK PRODUCTS.

As fontes de energia foram explosões realizadas com explosivo IBEMUX, de alta velocidade de detonação (5.2 km/s) e densidade de 1.25 g/cm^3, acomodados em poços de 6 polegadas de diâmetro e em torno de 50 m de profundidade. As cargas utilizadas nas explosões foram de 600 kg no extremo oeste da linha, 800 kg no centro e 1000 kg no extremo leste, considerando que esses tiros foram programados para uma linha de 300 km de extensão e correspondem aos três tiros finais.

Os dados obtidos estão sendo processados utilizando o programa Seismic Unix (Stockwell & Cohen, 1998). A partir das seções sísmicas será elaborado um modelo preliminar, tentando definir o número de camadas e a velocidade aproximada da onda P em cada uma delas. Esses dados serão testados através de alguns métodos de interpretação de dados de refração sísmica, tais como o método dos retardos (*delay-time*) e de tempo de interseção (*intercept-time*), entre outros (Sheriff & Geldart, 1982).

Posteriormente, serão elaborados modelos teóricos utilizando o pacote de programas SEIS88 (Cervený & Psencik, 2000), através do método de propagação de raios sísmicos e da construção de sismogramas sintéticos. O pacote também permite a elaboração de sismogramas sintéticos que possibilitam a obtenção de modelos bastante complexos, com variações de velocidades 2D e estruturas como *pinch-outs*, lentes e falhas, além de permitir verificar a eficiência de outros métodos de interpretação de dados de refração sísmica.

Resultados Preliminares

Os dados das seções sísmicas de Minaçú (tiros direto, central e reverso) estão apresentados nas figuras 2, 3 e 4, respectivamente. A figura 5 mostra o gráfico tempo-distância para as primeiras chegadas. Pode-se notar nesse gráfico que as variações, além de refletir a topografia da região, podem estar refletindo, principalmente, possíveis estruturas em sub-superfície, que serão melhor estudadas durante o projeto.

Conclusões

Observa-se que a qualidade dos dados, de forma geral, é muito boa, principalmente para as primeiras chegadas da fase P. A geologia desta área é bastante complexa, conforme exposto acima. Pretende-se neste estudo de refração sísmica atingir profundidades até 15 km, que ajudarão a entender melhor a estruturação da crosta superior sob a região de Minaçú.

Referências Bibliográficas

Almeida de, F.F.M. (**1968)**. An. Acad. Brasil. Ciências, v. 40, p.285-295.

Berrocal et al. (**1996)**. Estudos Geofísicos e Modelo Tectônico dos Setores Central e Sudeste da Província Tocantins, Brasil Central. Projeto temático de pesquisa financiado pela FAPESP a partir de janeiro/98.

Cervený, V. and Psencik, I. (**2000)**. Pacote do programa modelagem de raio e cálculo de sismograma sintético Seis88.
http://seis.karlov.mff.cuni.cz/software/seis/ .

Dardenne, M.A. (**1978)**. In: Congresso Brasileiro de Geologia, 30, Anais, Recife, SBG, v. 2, p.597-600.

Fuck, R.A. (**1990)** In: Congresso Brasileiro de Geologia, 36, Bol. Resumos. Natal, SBG, p.288-9.

Fuck, R.A. (**1994)** A Faixa Brasília e a Compartimentação Tectônica na Província Tocantins. In: Simpósio de Geologia do Centro-Oeste, 4, Anais, Brasília, SBG, p 184-187.

Fuck *et al*. (**1993**). In: Domingues, J.M.L., Misi, A. (eds.). O Craton do São Francisco. Salvador, SBG/SGM/CNPq, p. 161-185.

Fuck *et al*. (**1994**). Anais do IV Simpósio de Geologia do Centro-Oeste, p 215-216.

Pimentel, M.M. & **Fuck.** R.A. (**1992**). Neoproterozoic crustal accretion in central Brazil, Geology, 20, p. 375-379.

Pimentel *et al*. (**2000**). The basement of the Brasília Fold Belt and the Goiás Mgmatic Arc. In: Tectonic evolution of South America, Rio de Janeiro: 31st International Geological Congress, p 195-229.

Perosi, F.A. **(2000)**. Refração sísmica profunda no setor sudeste da Província Tocantins, Dissertação de Mestrado. IAG/USP.

Sheriff, R.E., **Geldart**, l.P (**1982**). Exploration Seismology, History, Theory, and Data Acquisition. Vol. 1. Cambridge. Ed. Cambridge Univ. Press.

Soares, *et al*. **(2000)**. Deep Refraction Experiment in the Central Portion of the Tocantins Province, State of Goiás, Central Brazil. Anais do 31º Congresso Internacional de Geologia, Rio de Janeiro (RJ).

Stockwell, J.W. & Cohen, J..K. (**1998**). CWP/SU: Seismic Unix Release 32: a free package for seismic research and processing, Center for Wave Phenomena. Colorado School of Mines.

Strieder, A.J. & **Nilson**, A.A. (**1992**). Melange ofiolítica nos metassedimentos Araxá de Abadiânia (GO) e implicações tectônicas regionais. RBG, 22(2), 204-215.

Agradecimentos

Agradeço a Fapesp pela concessão da bolsa de mestrado, processo 00/06242-6 e ao Departamento de Geofísica do Instituto de Astronomia, Geofísica e Ciências Atmosféricas (IAG/USP).

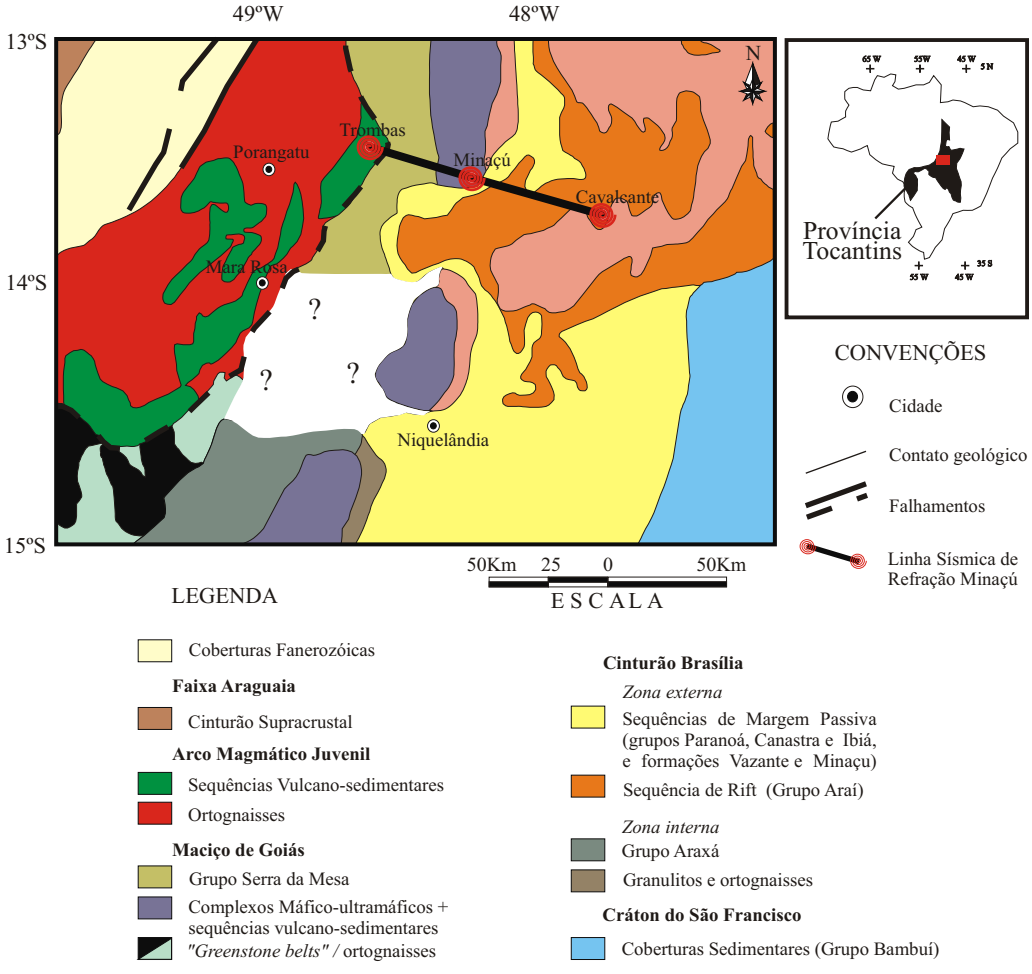

FIGURA 1 - Mapa geológico da região de Minaçú (modificado de Pimentel *et al*., 2000).

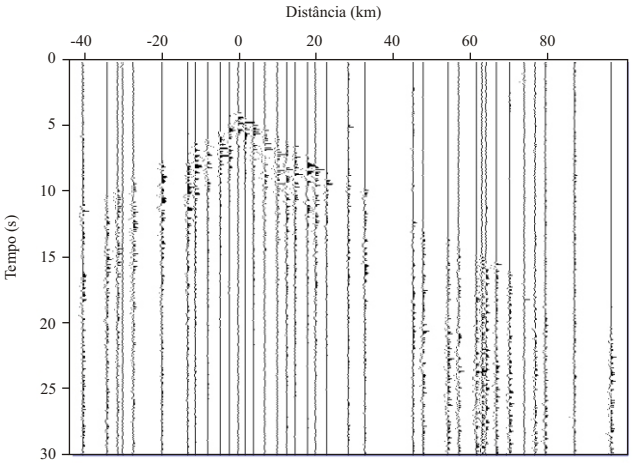

FIGURA 2 - Seção Sísmica do Tiro Direto da Linha Minaçú (sunormalize norm=max; sugain; sufilter 15-25 Hz).

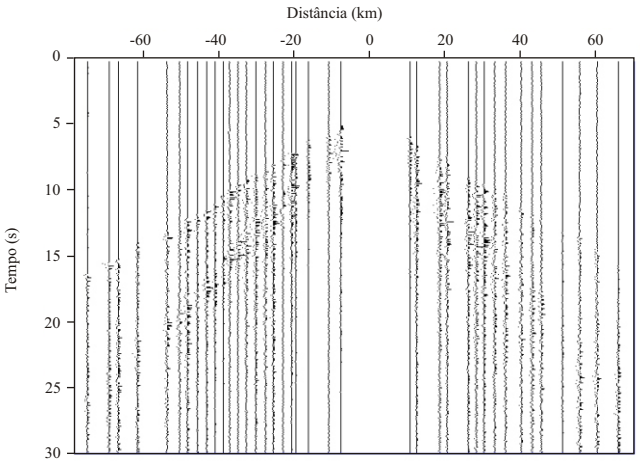

FIGURA 3 - Seção Sísmica do Tiro Central da Linha Minaçú (sunormalize norm=max; sugain; sufilter 15-25 Hz).

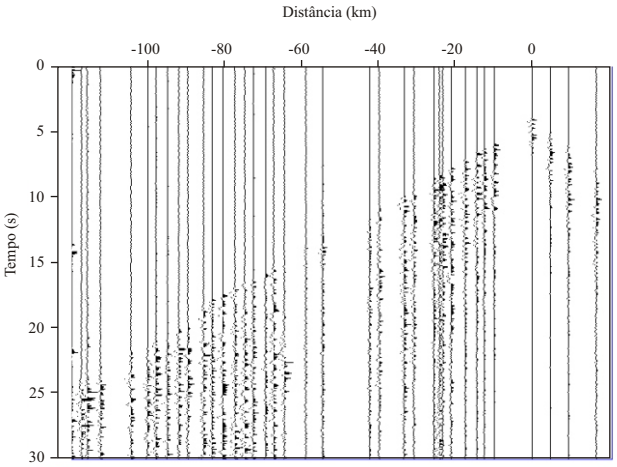

FIGURA 4 - Seção Sísmica do TiroReverso da Linha Minaçú (sunormalize norm=max; sugain; sufilter 15-25 Hz).

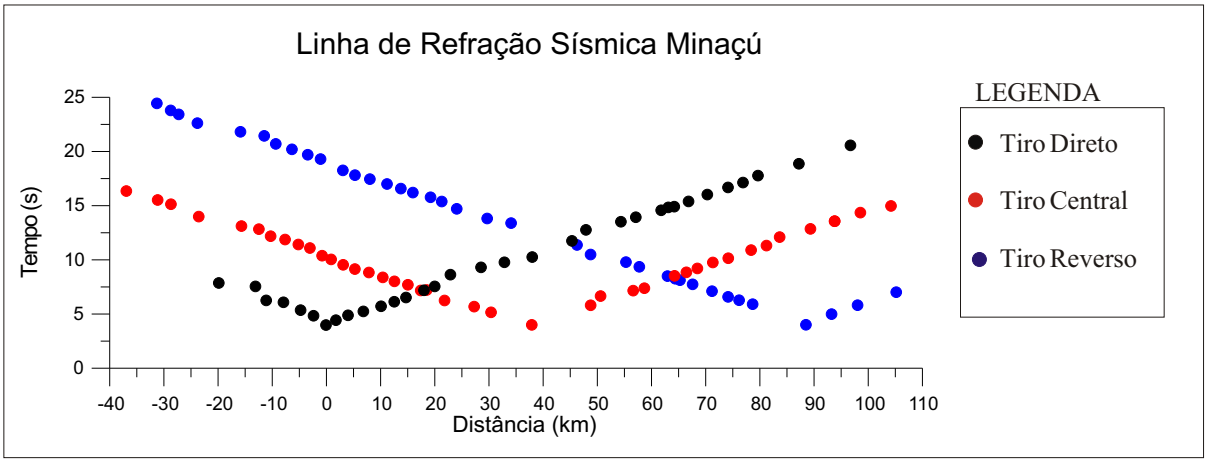

FIGURA 5 - Gráfico tempo-distância das primeiras chegadas da fase P.

Estudos de sismicidade induzida nos reservatórios da CHESF, na região Nordeste do Brasil

Celia Fernades, Jesus Berrocal e Michele Domingues Martins.

Instituto de Astronomia, Geofísica e Ciências Atmosféricas-Universidade de São Paulo(IAG/USP), São Paulo Brasil

celia@iag.usp.br, berrocal@iag.usp.br, michele@iag.usp.br

Abstract

In this paper we present the results of seismographic monitoring of provable induced seismic activity at three hydro-electrical reservoirs of the Companhia Hidro Elétrica do São Francisco (CHESF), located at the Northeastern region of Brazil. A local network of portable seismographs with up to six stations was deployed in Oct. 1978 around the Sobradinho reservoir that started to be filled up during the first months of that year. Since its installation, the network recorded some micro-earthquakes with magnitude about 1.0, with the largest magnitude (m_b =1.9) event in July 1979. Since then, the number of events and their magnitude has diminished down to insignificant levels. During the first years of the 1990-decade, the network was moved to monitor the Itapararica reservoir. After around four years of instrumental monitoring in this reservoir no one, local seismic event was recorded at the network. It was observed that small earthquakes that use to occur before the impoundment of the reservoir stopped to occur when the lake was filled. Since the beginning of the 1990s we started to monitor the Xingo reservoir. It is located in a region were occur small tectonic earthquakes. Immediately after the beginning of impoundment of the lake in May 1994, began to occur small micro tremors with the highest activity in July 20th of that year. After that the activity diminished to insignificant levels after three or four years.

Introdução

Atualmente, a ocorrência de fenômenos sísmicos associados ao enchimento de grandes reservatórios, ou sismicidade induzida por reservatório (SIR), é um fato comprovado e tem sido observado em diversas regiões da Terra, independentemente de seus respectivos níveis de sismicidade natural. Em alguns casos, esses sismos induzidos podem ser de proporções notáveis, a ponto de colocar em risco vidas humanas e comprometer a estrutura da própria barragem. Por esta razão e devido ao aumento do número de grandes reservatórios nas últimas décadas, a comunidade sismológica e diversos organismos internacionais recomendam a execução de estudos e monitoração sismológicos, que possam permitir uma compreensão adequada sobre o mecanismo de indução de atividade sísmica pelo enchimento de reservatório.

De acordo com Berrocal et al., (1984) o primeiro caso de SIR no Brasil, e sentido pela população, ocorreu em dezembro de 1970 no reservatório do Carmo do Cajurú-MG, que teve seu maior evento (m_b = 3,7 e intensidade VI MM) em janeiro de 1972. Desde então, outros reservatórios têm apresentado casos de SIR no território nacional como os de Capivari/Cachoeira-PR em 1971 (VI MM), Volta Grande/Porto Colômbia-MG/SP em 1974, onde ocorreu o maior sismo induzido (m_b = 4,2, VI-VII MM) no território brasileiro, Capivara-SP/PR em 1976 (VI MM) e em 1979 (m_b = 3,7, V-VI MM) e Paraibuna/ Paraitinga-SP em 1977 (M_L = 3,4, IV MM), caso que ainda apresenta atividade sísmica na atualidade (agosto/88)

Neste trabalho apresentamos e analisamos a atividade sísmica provavelmente induzida pelos reservatórios de Sobradinho (BA), Itaparica (BA/PE/ SE) e Xingo (SE/AL), que são de propriedade da Companhia Hidro-Elétrica do São Francisco..

SIR no Reservatório de Sobradinho

O reservatório de Sobradinho está localizado na porção noroeste do Estado da Bahia, no curso médio do rio São Francisco, próximo das cidades de Juazeiro-BA e Petrolina-PE (ver Fig. 1). Tem uma capacidade de armazenamento de $34{,}1 \times 10^6 m^3$, embora a barragem tenha uma altura de somente 41m. A crista da barragem tem um comprimento de 3.600m. O lago tem uma extensão de aproximadamente 300 km, com uma área na cota de 392,5m de aproximadamente $4.200 km^2$.

O início do enchimento do reservatório de Sobradinho foi em dezembro de 1977 e concluído no final do primeiro semestre de 1978. A Rede Sismográfica de Sobradinho (RSS) foi instalada em setembro-novembro de 1978, com 6 estações, conforme mostra o mapa da Fig. 1. Cada estação da RSS está constituída de um conjunto sismográfico de período curto operando na componente vertical, e um registrador portátil com papel e tinta. A RSS operou até março/1986, quando foram desativadas todas as estações

exceto SER que continua operando até o presente com um sismômetro Willmore MK III.

A localização de epicentros foi efetuada automaticamente utilizando o programa HYPO71 (Lee et al., 1975), para sismos com um número suficiente de leituras confiáveis de P e S.

O nível de sismicidade da região que circunda o reservatório de Sobradinho, correspondente a uma área estável do ponto de vista tectônico, justificado pela presença dominante do Craton do São Francisco nessa região.

No período compreendido entre outubro de 1978 até março de 1986 foram registrados pela RSS 185 microtremores ($m_b < 2,0$) com epicentro na área coberta pelo reservatório de Sobradinho ou nas bordas do mesmo. Todos estes eventos, cujos epicentros estão projetados no mapa da Fig. 1, foram considerados como sismos provavelmente induzidos por esse reservatório. Esses eventos nunca foram sentidos pelos moradores próximos as áreas epicentrais.

A porção do reservatório, onde se concentra a quase totalidade dos eventos provavelmente induzidos, corresponde a uma das porções mais profundas do reservatório, onde se encontra o maior volume de água. Essa parte também corresponde às últimas dobras de 90° do antigo leito do rio São Francisco, antes da barragem. Esta característica fisiográfica normalmente está relacionada a falhamento, logo existem condições para associar os eventos sísmicos com a reativação da provável falha, pela presença do reservatório.

Esse tipo de distribuição temporal de atividade sísmica é típico de SIR. Ou seja, um início crescente até atingir um pico máximo de atividade para depois decair com o passar do tempo até a atividade cessar completamente. Esse fato, juntamente com a polaridade invertida dos primeiros impulsos do evento de 05 de julho de 1979 nas estações SAG e GRO sugerem que a atividade local registrada pela RSS é induzida pelo reservatório de Sobradinho.

O decaimento da energia liberada pelos sismos induzidos é constante a partir do 3° trimestre de 1979. A curva de decaimento indica que a partir de 1986 a atividade sísmica induzida estará representada somente por eventos com $m_b < 0$.

SIR no Reservatório de Itaparica

A auscultação sísmica na área do reservatório de Itaparica foi efetuada no período pré e pós-enchimento. A Rede Sismográfica de Itaparica (RSI) começou a operar com uma estação em fevereiro de 1983 e foi ampliada para cinco estações em dezembro de 1986. A partir de julho de 1989 a RSI passou a operar com 3 estações. Em todo o período em que operou a RSI, não foi registrado nenhum evento sísmico que possa ser qualificado como evento sísmico induzido.

Pelo contrário, o preenchimento do reservatório de Itaparica provocou o desaparecimento de um nível de atividade baixo que ocorria antes disso perto de Floresta, PE, atividade essa associada provavelmente ao lineamento Recife-Patos, onde ocorre algum tipo de atividade sísmica em vários locais.

SIR no Reservatório de Xingo

A auscultação do Reservatório de Xingo iniciou vários anos antes de seu enchimento. A Rede Sismográfica de Xingo (RSX) com 5 estações telemétricas e com registro digital, começou em julho de 1995. Entretanto o inicio do enchimento foi em junho de 1994. Nessa época a RSX operou com três estações telemétricas e registro digital.

.Após o início do enchimento do reservatório de Xingo em 07 de junho, a atividade sísmica na área desse reservatório, começou em 12 de junho e aumentou significativamente, de sismos com magnitudes oscilando entre m_b -1,0 e 1,0 em junho, até sismos com m_b da ordem de 1,7 em 20 de julho de 1994.

Os epicentros dos eventos ocorridos entre julho e setembro 1994, registrados em duas ou três estações da RSX, são mostrados no mapa da Fig. 2. A maior parte da atividade sísmica está concentrada ao redor dos 40km iniciais do reservatório de Xingo, principalmente nas proximidades da barragem e no outro extremo dessa zona sísmica, ao sul de Delmiro Gouvêa. Nesta última porção da zona sísmica é que ocorreram os sismos de maior magnitude durante esse intervalo.

O maior sismo da série ocorreu em 20 de julho 1994 (m_b=1,7), três dias antes da cota do reservatório chegar a 134m. Em 28 de julho ocorreu um outro sismo de magnitude significativa (m_b=1,6). Após esses dias de maior atividade, aparentemente houve uma diminuição de liberação de energia.

Esse sismo de maior magnitude, de acordo com relações empíricas entre magnitude e intensidade sísmica deve ter gerado uma intensidade de III MM ou no máximo de IV MM. Agora podemos calcular a aceleração horizontal máxima (a_h) que esse sismo provocou no terreno, próximo ao epicentro, utilizando a seguinte equação sugerida por Campbell (1982):

$$Ln(a_h) = 1,05 - 0,158m_D + 0,63\ I_{MM}$$

Com os valores de magnitude (1,7) e intensidade (III ou IV MM, ou melhor 3 ou 4 para efetuar os cálculos), obtém-se valores de 14,5 e 27,2 $cm.s^{-2}$ para a_h, ou seja entre 0,01 e 0,03 g no máximo.

CONCLUSÕES

A análise efetuada neste trabalho para Sobradinho está baseada exclusivamente nos dados auscultados pela RSS. Eles indicam que o ciclo de atividade sísmica se iniciou provavelmente com o enchimento do reservatório, teve seu auge em julho de 1979 e desde então está diminuindo gradualmente, com a tendência de alcançar o limite inferior de observação, em 1989. Evidentemente que esta conclusão, baseada nas observações dos último 8 anos, pode sofrer alterações no futuro, devido a fenômenos não detectáveis no período de observação ou por outra índole, como por exemplo, fenômenos geológicos de geodinâmica externa que possa mudar as características sismotectônicas da área do reservatório de Sobradinho.

No mês de junho de 1994, após o início do enchimento, começou a atividade sísmica na área do reservatório de Xingo. Ocorreram aproximadamente 58 micro-tremores com magnitudes m_b entre -1,0 e 1,0, que provavelmente tenham sido induzidos pelo enchimento do reservatório. Esses eventos podem corresponder a possíveis acomodações das camadas superficiais, causadas pela sobrecarga, ou a prováveis liberações de pequenas quantidades de energia acumulada nas proximidades da superfície, provocadas pela percolação d'água.

BIBLIOGRAFIA

Berrocal, J., Assumpção, M., Antezana, R., Dias Neto, C.M., Ortega, R., França, H. & Veloso, J.A.V., 1984 – Sismicidade do Brasil, 320 pp.

Campbell, K.W., (1982). A ground motion model for the central United States based on near-source acceleration data. In: Earthquakes and Earthquake Engineering-Eastern United States, Beavers, J.E., Editor. Ann Arbor Science, **1**: 213-232.

Lee, P. & Lahr, J.C., 1975 – HYPO71 (Revised): a computer program for determining hypocenter, magnitude and first motion pattern of local earthquakes. U.S. Geol. Surv., Open File Rep., 114 pp.

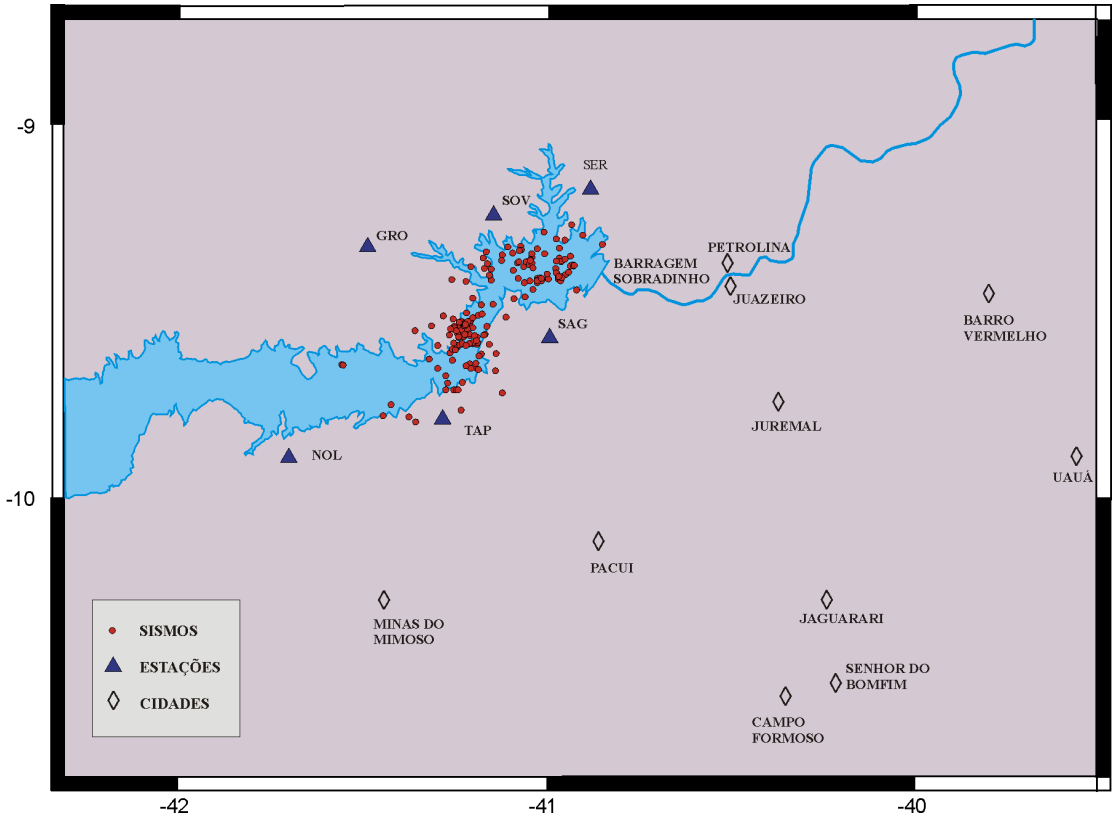

Figura 1 – Mapa de epicentros registrados na Rede Sismográfica de Sobradinho

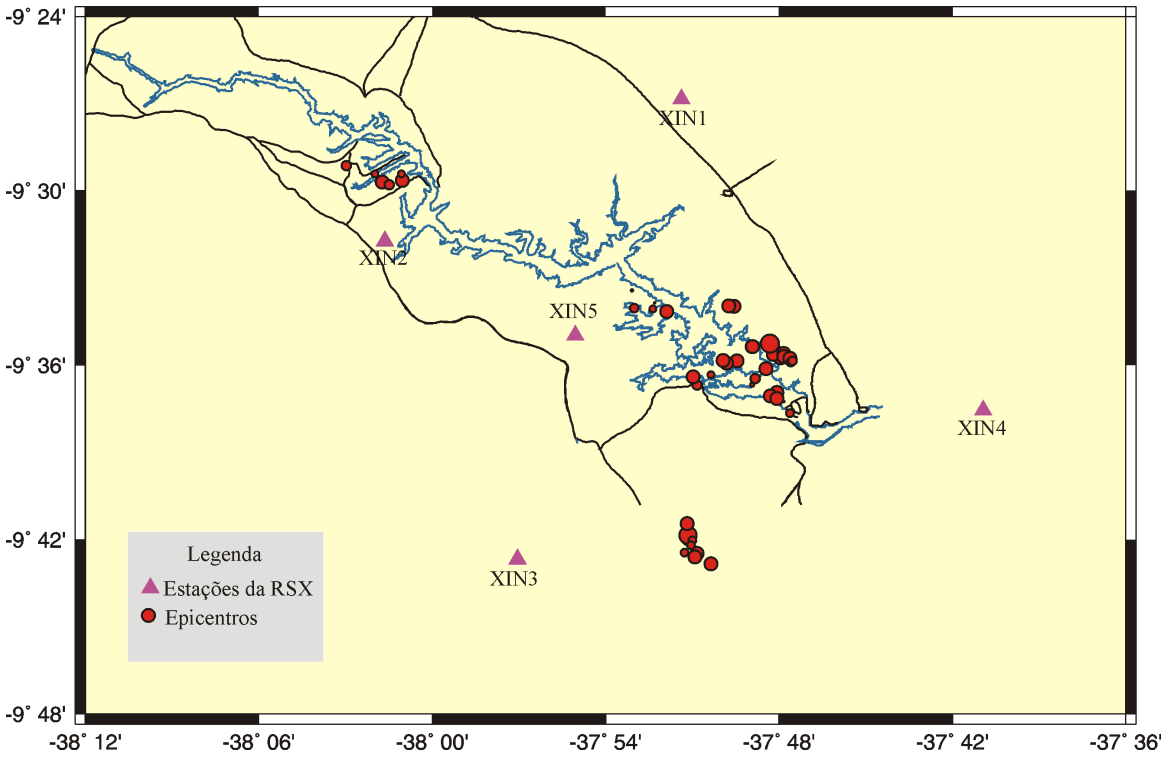

Figura 2 – Mapa de epicentros registrados na Rede Sismográfica de Xingo

Geothermal Gradient and Heat Flow in the State of Rio de Janeiro

Marcelo Perrota Raymundo and Valiya M. Hamza, Observatório Nacional, Rio de Janeiro, Brazil

Abstract

Measurements of geothermal gradients and heat flow have been carried out in the state of Rio de Janeiro over the past two years as part of a geothermal resource assessment program. The results obtained at more than 50 localities indicate that the geothermal regime is characterized by two narrow east–west trending belts of high heat flow (> 80 mW/m^2) superimposed on a regional pattern of low to normal values (30 – 70 mW/m^2). One of the high heat flow belt is located in the southern part, parallel to the coast and close to the zone affected by alkaline magmatism of the tertiary period. The second one is situated on the northern part and is roughly parallel to the Além Paraiba fault system. No significant manifestations of geothermal activity have been found in near surface layers, but there are indications that geothermal aquifers of limited aerial extent may be present at depths of 1-3 km.

Introduction

Availability of geothermal data in southeastern parts of Brazil is limited to a few isolated measurements in the highlands, there being hardly any measurements at all, along the coastal areas. Lack of geothermal data has been an obstacle in understanding the subsurface thermal regime of this region, which is contiguous with the major oil producing platform areas. In this context, a project was proposed in to carry out experimental determination of geothermal gradients and heat flow and provide a preliminary evaluation of geothermal resources in the state of Rio de Janeiro. Results obtained during the initial stages of this project are reported in the present work.

Outline of Geology and Tectonics

A number of regional geologic studies of the state of Rio de Janeiro and neighboring areas has been carried out (Hasui et al, 1982; Riccomini, 1997; among others) and geologic maps are available in the scale 1:400.000 (Oliveira et al, 1977; Fonseca, 1998). The main local geologic units are metamorphic rocks of the Fluminense complex, Paraíba do Sul Group and Serra dos Órgãos complex, all of Precambrian in age. The structural setting is characterized by large fault systems in the northeast – southwest direction. The basement rocks of coastal regions in the southeastern parts of Brazil have undergone tectonic reactivation during Meso-Cenozoic times. Alkaline magmatism and volcanic activity has been prevalent during Tertiary times along a narrow belt extending from Cabo Frio to Poços de Caldas. There are indications that morphology and uplifted mountain ranges in the Fluminense lowlands are related to subsurface intrusive activity associated with alkaline magmatism. There is a moderate level of micro-seismic activity not only along the coastal regions but also along the platform areas.

Geothermal Investigations

The geothermal investigations carried out so far include determination of heat flow based on measurements of geothermal gradients and thermal conductivity and estimates of deep aquifer temperatures using geochemical methods. Summaries of the main results of these investigations are presented below.

Determination of Geothermal Gradients*:* The geothermal gradients were determined based on results of temperature logs carried out in boreholes and wells. A manually operated logging system, equipped with thermistor sensors capable of having relative precision of 0.001^0C was setup for this purpose. Measurements were carried out at intervals of 2 meters, while the probe was being lowered into the borehole. Most of the measurements in the present work were carried out in abandoned water wells, drilled during the last few decades. Information about well locations was obtained in collaboration with the Groundwater sector of CPRM (Companhia Pesquisa de Recursos Minerais) and also through direct contacts with drilling companies. Data concerning drilling and production of a total of 537 wells, distributed in 21 municipalities, were examined during the first stage of the project. Lack of suitable deep boreholes and wells has been a major obstacle in obtaining reliable data on geothermal gradients. Most of the wells had depths less than 150 meters. Because of technical problems logs were attempted only in wells without submersible pumps.

The geothermal gradients were calculated by linear fits to data for the selected depth intervals. In wells with significant groundwater flows, the gradient was calculated based on the difference between temperature at the bottom of the well and the mean annual temperature. This is in fact a variant of the BHT method, employed extensively for analysis of thermal data from oil wells (Carvalho and Vacquier, 1977). In a few cases gradient was estimated temperature of water pumped water, following procedures discussed by Santos et al (1986).

Values of geothermal gradients calculated using this procedure are given in table (1). Most of the values fall in the interval of 10 to 30 ^{0}C/km, a range typical of normal gradients in tectonically stable areas.

Table (1) Geothermal gradients in the state of Rio de Janeiro

***Municipality/* Locality**	**Depth (m)**	**Thermal Gradient (^{0}C/km)**
Angra dos Reis	32 - 66	22 - 88
Cambuci	0 - 84	26,32
Campos		
Campus UENF	50 - 76	19,75
Cons. Josino	44 - 100	10,97
Boa Vista	60 - 100	26,90
Baixo Grande	0 - 108	19,00
Carapebús	0 - 90	26,25
Duas Barras	80 - 122	15 - 17
Itaocara		
Jaguarembé	0 - 100	11,83
Cor. Teixeira	0 - 76	24,79
Itatiaia	46 - 90	3,5 – 12,3
Laje de Muriaé	0 - 100	33,58
Maricá	40 - 98	7,3 – 9,8
Vassouras	56 - 80	3,3 – 11,4
Miguel Perreira	52 - 78	5,1 – 12,0
Miracema	40 - 100	19,5 - 25,9
Niteroi	0 - 18	> 100
Paraíba do Sul	68 - 100	5,8 – 11,4
Porciúncula	0 - 80	13,53
Rio Bonito	75 - 108	7,07
Rio Claro	50 - 66	4,4 – 10,0
São Seb. Alto	90 -116	3,1 - 7,5
Sapucaia	50 - 78	8,8
Teresópolis		
Água Quente	18	> 100
Meudon	55 - 148	12,9 – 21,0
Volta Redonda	56 - 70	8,9

Because of the limitations of the data set, the values given in this table should be considered as estimates of geothermal gradients at shallow depths. The possibility that the gradients at deeper levels are significantly different from the values given here cannot entirely be ruled out. Thus the anomalously high values of gradients indicated for three localities should be viewed with caution.

Thermal Conductivity Measurements: The thermal conductivity measurements were carried out using ISOMET 104, a portable thermal property-measuring device. The principle of operation of this equipment is based on the plane source method (Carslaw and Jaeger, 1959). The main advantage of this device, in relation to the commonly used needle probe method (Von Herzen e Maxwell, 1959), is that the effective sampling area for thermal property estimates is large. Thus problems arising from conductivity variations associated with small-scale heterogeneities, grain sizes and pore geometry can be minimized. The calibration setup of this equipment was verified using primary standards of known thermal conductivity, such as fused silica. To minimize problems arising from large-scale heterogeneities measurements were repeated at three different positions for each sample.

Samples used for thermal conductivity measurements included drill cuttings from wells as well as fresh unweathered samples from outcrops. In the case of drill cuttings the measured values were corrected incorporating appropriate data on volumetric proportions of mineral grains and porosities. The outcrop samples were collected by Department of Geology of the State University of Rio de Janeiro (UERJ), as part of routine geologic mapping of the state of Rio de Janeiro. These samples are considered as representative of the main rock formations in near surface layers. Though the litholgy is rather complex on local scales within the study area the available data may be considered as indicative of the general pattern of thermal conductivity distribution of the main rock formations in the state of Rio de Janeiro. A summary of thermal conductivity data is presented in table (2).

Table (2) Thermal conductivity values of the main rock types in the state of Rio de Janeiro

Tectonic Unit	**Rock Type**	**Condutivity (W/m^{0}C)**
Bacia de Campos	Argila Areia	2,2 – 2,6 2,4 – 3,8
Complexo Costeiro	Granito Gnaisse Diabásio	3,6 4,1 2,8
Juiz de Fora	Granulito	2,9
Complexo Rio Negro	Tonalito Leuco Granito Granada Gneisse	2,7 4,1 3,3
Serra dos Orgãos	Granodiorito	3,1
Paraíba do Sul	Gnaisse	4,1

Distribution of Heat Flow: Heat flow values were calculated using conventional, BHT and aquifer temperature methods. The choice of the method was based on the nature of available data. Hamza and Muñoz (1996) discussed reliability criteria for these methods.

The results of heat flow calculations are presented in table (3). In most of the localities heat flow values are in the range of 30 to 80 mW/m^2. This range

is usually considered as representative of the thermal regime of tectonically stable platform and shield áreas. In some localities heat flow is estimated to be in excess of 100 mW/m^2. Thus Angra dos Reis, Niterói and Carapebus in the south and Água Quente (eastern part of Teresópolis) and Laje de Muriaé in the north may be considered as localities of anomalously high heat flow. However, because of the uncertainties in original data these high heat flow values may only be considered as tentative estimates.

Table (3) Heat flow values based on Gradient and Conductivity measurements

Region	Locality	Heat Flow (mW/m^2)
Coastal	Maricá	30 - 45
	Rio Bonito	25 – 35
	Carapebús	90 - 120
Flminense	Campus UENF	45 – 65
	Cons. Josino	25 - 35
	Boa Vista	60 – 85
	Baixo Grande	40 – 60
	São Sebastião	
Northeast	Miracema	55 – 65
	Paraíso Tobias	70 – 90
	Santa Clara	35 - 45
	Jaguarembé	30 - 40
	Cor. Teixiera	65 - 85
	Laje de Muriaé	90 - 115
	Monte Verde	70 - 90
Teresópolis	Água Quente	> 100
	Meudon	45 - 70
	Fazenda Texas	75 - 95
N. Central	Sapucaia	25 - 30
	Duas Barras	25 - 60
	Valão do Barro	10 - 25

Inferences based on Geochemical Methods: A number of mineral springs occur mainly in the southern parts of the state of Rio de Janeiro. The outflow temperatures of these springs are in the range of 25 to 30^{0}C, but these are believed to rise from thermal aquifers at several kilometers deep. The mineral contents of these springs may be used to estimate the temperatures of these deep-seated aquifers, based on well-known methods in geochemical thermometry (see for example Fournier, 1981). In the present work results of calculations based on Sílica, Na-K and Na-K-Ca thermometers are presented in table (4) along with estimates of heat flow according to the method Swanberg and Morgan (1979).

Table (4) Estimates of Temperatures and Heat flow based on Geochemical methods.

Locality	Temperature (^{0}C)	Heat Flow (mW/m^2)
São Gonçalo	117	> 100
Rio de Janeiro	109-140	> 100
Niterói	134	> 100
Rio Bonito	150	> 100
Sto. Ant. Pádua	106-121	> 100
Paraíba do Sul	107	< 100
Campos	85	< 100

Conclusions

The available experimental data on geothermal gradients and estimates based geochemical methods indicate that heat flow is highly variable in the state of Rio de Janeiro. The general pattern is indicative of low to normal heat flow, with values in the range of 30 to 80 mW/m^2. This is typical of the thermal regime of tectonically stable platform and shield areas.

There are however indications of at least two east–west trending belts where heat flow may have values higher than 100 mW/m^2. The locations of the geothermally anomalous areas are indicated in the map of figure (1). One of these belts is located in the south just to the north of the coastal area, between Angra dos Reis and Cabo Frio. This belt is thus practically coincident with the zone of alkaline magmatism of Tertiary age. The other belt is located in the northern part, between Teresópolis and Laje de Muriaé. It appears to be roughly parallel to the Além Paraíba fault. Areas falling within these belts have been chosen as targets for a detailed study of the geothermal energy resources.

Acknowledgments

The geothermal measurements were carried out as part of project No. E–26/150.954/99, funded by Fundação Amapro à Pesquisa do Estado do Rio de Janeiro – FAPERJ. The first author of this paper is recipient of a PIBIC scholarship

References

Hasui, Y., Almeida, F.F.M. de, Mioto, J.A. e Melo, M.S. de, 1982, Geologia tectônica, geomorfologia e sismologia regionais de interesse às usinas nucleares da praia de Itaorna. Publicação IPT No. 1225.

Riccomini, C., Peloggia, A.U.G., Saloni, J.C.L., Kohnke, M.W. and Figueira, R.M., 1989, Neotectonic activity in the Serra do Mar rift system (southeastern Brazil). J. of South American Earth Scinces, 2, 191-197.

Fonseca, M.J.G., 1998, Mapa Geológico do Estado do Rio de Janeiro, Escala 1:400.000, Publica-

ção Departamento Nacional da Produção Mineral (DNPM), Brasília (DF).

Oliveira, J.A.D., Machado Filho, L., Ribeiro, M.W., Liu, C.C. e Meneses, P.R., 1977, Mapa geológico do Estado do Rio de Janeiro, Escala 1:400.000. Departamento de Recursos Minerais – DRM, Rio de Janeiro.

Carvalho, H.S. and Vacquier, V., 1977, Method for determining terrestrial heat flow in oil fields. Geophysics, 42, 584-593.

Santos, J., Hamza, V.M. and Shen, P.Y., 1986, A method for measurement of terrestrial heat flow density in water wells. Rev. Bras. Geofisica, 4, 45-53.

Carslaw, H.S. and Jaeger, J.C., 1959, Conduction of heat in solids. Clarendon Press, 2nd edn., 510pp.

Von Herzen, R. and Maxwell, A.E., 1959, The measurement of thermal conductivity of deep-sea sediments by a needle-probe method. J. Geophys. Res., 64, 1557-1563.

Hamza, V.M. and Muñoz, M., 1996, Heat flow map of South America. Geothermics, 25, 599-646.

Swanberg, C.A. and Morgan, P., 1978, The linear relation between temperature based on the silica content of groundwater and regional heat flow: a new heat flow map of the United States. Pure Appl. Geophys., 117, 227-241.

Fournier, R.O., 1981, Application of water chemistry to geothermal exploration and reservoir engineering. In Geothermal Systems: Principles and Case Histories. L. Rybach and L.J.P. Muffler (Eds.), 109- 143.

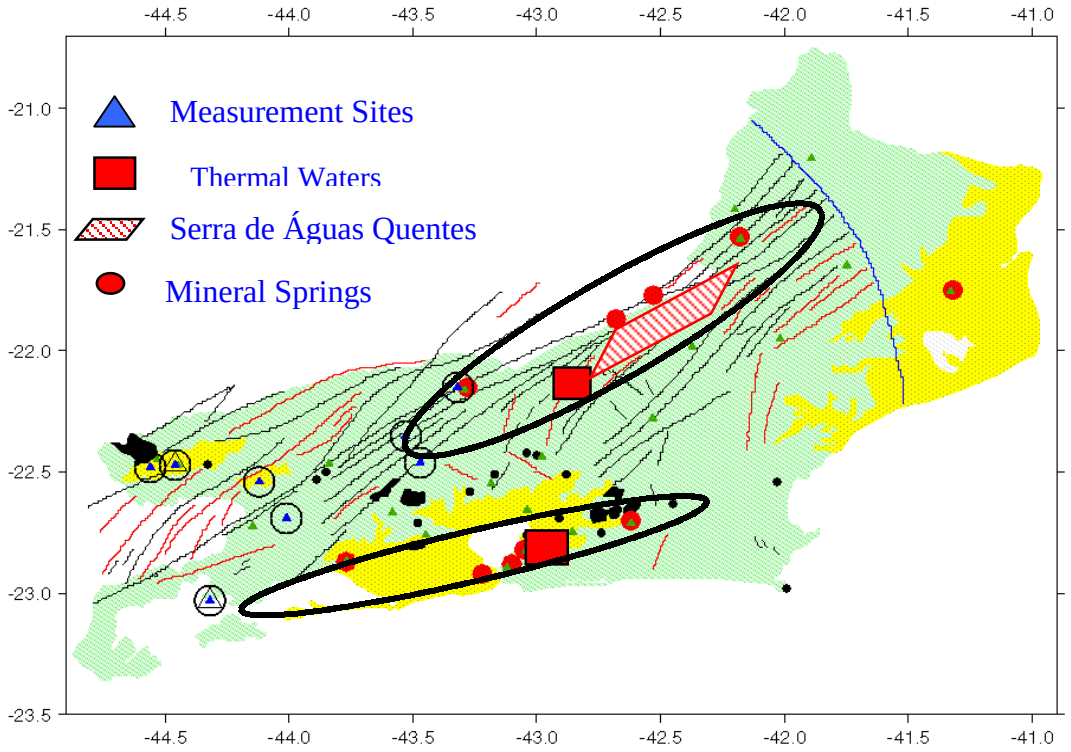

Figure (1) Map indicating locations of geothermal measurements and thermal manifestations. The oval shaped zones are areas where deep heat flow is tentatively estimated to be higher than 100 mW/m^2.

In-situ stress and wellbore stability in a Brazilian basin

Aline Theophilo Silva, Fundação Gorceix/CENPES, alinet@cenpes.petrobras.com.br
Claudio Lima, CENPES/PETROBRAS, claudioc@cenpes.petrobras.com.br
Luis Antonio Canelas Palermo, palermo@cenpes.petrobras.com.br

Abstract

The knowledge of the in-situ stress has been recognized as a fundamental parameter in planning exploitation activities in the oil industry. Wellbore projects, hydraulic fracturing, prevention of sand production and other activities are highly influenced by the in-situ stress state.

In Brazil exploitation projects are usually done considering the paradigm that the Brazilian basins are tectonically relaxed. Nevertheless, a number of evidences indicates that such idea should be reconsidered.

Here we show a study prepared for a given oil field to determine the in-situ stress using breakouts analysis, leak-off inversion technique and available information from density logs. The results indicated that the oil field is submitted to a normal stress regime, the horizontal principal stresses are unequal and the maximum horizontal stress (SHmax) is oriented parallel to NNE-SSW.

To demonstrate how the in-situ stress could impact wellbore projects, a wellbore stability simulator was used. The input data to the simulator were: breakout information; values of mud weight, pore pressure and leak-off test data; rock mechanics properties; directional characteristics of wells. The program's visualization tools have shown how important is to determine as precisely as possible the in-situ stress.

Introduction

Assuming that the Brazilian basins are tectonically relaxed, the exploitation activities in Brazil are planned considering that the maximum and minimum horizontal principal stresses are equal and given as a function of the overburden (SHmax = Shmin = *f*(Sv)). However, there is a number of evidences that in intraplate areas compressional regimes prevail, meaning, the maximum principal stress is horizontal (σ_1 = SHmax).

Compilation of stress state around the world, carried out in the World Stress Map context (Zoback, 1992), has shown that in a global scale the maximum stress is horizontal. In Brazil, studies based on seismology and breakout analyses (Assumpção, 1992, 1997 and 1998; Lima *et al*., 1997) and on stress magnitude analyses estimated using available information from hydraulic fracturing and leak-off tests (Lima Neto & Beneduzi, 1998; Lima Neto, 1999) have been indicating that the maximum stress is horizontal.

A few methods are used by the industry to define the stress regime in an area. Those methods are based on information from tests and well logs, associated with some deformation on the wellbore wall. Such deformation is induced by stress redistribution around the wellbore and as so it is used to evaluate the in-situ stress. To define the stress redistribution around the wellbore and predict the potential rupture zones (by shear or tensile stresses) most authors make use of the Kirsch equations combined with some rupture criteria (Bell, 1990, Silva, 2001).

Here we show the results of a study concerning how the stresses acting on a given oil field could impact wellbore projects. To achieve the stress tensor we used: breakout analyses to determine the orientation of the maximum and minimum horizontal stresses (SHmax and Shmin); leak-off inversion technique to calculate the orientation and the magnitudes of the horizontal stresses; density logs to calculate the vertical stress magnitude (assumed as perpendicular to the surface and equivalent to overburden). To demonstrate how the in-situ stress could impact well design we used the wellbore stability simulator SFIB (**S**tress and **F**ailure of **I**nclined **B**orehole; Peska & Zoback, 1996)

Breakouts Analysis

Breakouts are abrupt wellbore diameter ovalizations, continuously oriented through thick depth intervals, independently of lithology. The ovalization is produced by wellbore collapses induced parallel to the minimum stress (Shmin) (fig. 1). This is the result of the tangential stress concentration around the borehole described by the Kirsch equations. The maximum stress orientation (SHmax) is found at 90^o from Shmin (Plumb & Hickmann, 1985; Bell, 1990; Lima & Nascimento, 1994; Fejerskov & Bratli, 1998).

Whenever the mud weight overcomes the rock's tensile strength and the minimum compressive stress concentration (fig.1), a hydraulic fracturing will be induced oriented parallel to SHmax (Plumb & Hickmann, 1985;Bell, 1990;Lima & Nasci mento, 1994; Fejerskov & Bratli, 1998).

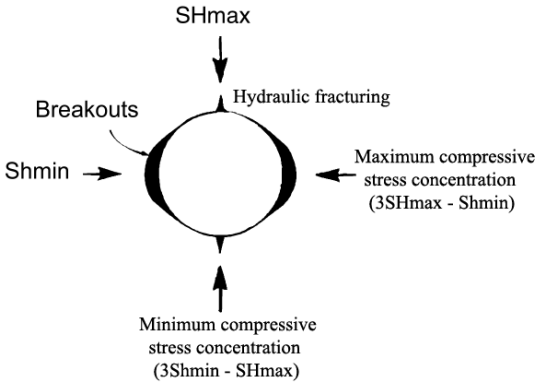

Figure 1. Stress redistribution and deformation around a wellbore (modified from Lima, 1999).

In the oil field studied there are 5 wellbores from which 26 ovalized intervals were identified, representing 50.6 m of continuous breakouts. From such intervals we determined the mean orientation of Shmin (N101.1^o ± 12^o) and SHmax (N11.1^o± 12^o) in the field (Silva, 2001).

The leak-off inversion technique

This method uses stress transformation equations to calculate the orientation and the magnitudes of the two horizontal in-situ stresses (SHmax and Shmin), taking advantage of the directional characteristics of deviated wells (Aadnoy, 1988). The model results in an overdetermined equations system (eq. 1) in which any numbers of leak-off values (over than three) can be used.

$$[\sigma]=\{[A]^T[A]\}^{-1}*[A]^T[P'] \quad (1).$$

- $[\sigma]$ – a matrix containing the two horizontal in-situ stresses;
- $[P']$ – a matrix containing measured data (leak-off tests values, pore pressure, mud weight, tensile strength and the directional characteristics of wells);
- $[A]$ – a matrix containing the values calculated using the Kirsch equations.

An *n* number of $[\sigma]$ is calculated for which leak-off value, varying the parameter β from 0^o to 90^o (β represents the possible SHmax orientation). The difference between the calculated and the measured values defines the error $[e]$ (eq. 2) for each number *n* of $[\sigma]$ and than this error will be minimized by a least squares method (e^2, square error; eq. 3).

$$[e]=[A][\sigma]-[P'] \quad (2);$$

$$e^2=[e]^T[e] \quad (3).$$

The least value of square error determine the best result of $[\sigma]$ (Aadnoy, 1988; Silva, 2001).

Using that method the obtained SHmax orientation for the oil field is N7^{o}E. This is in good accordance with the breakouts analysis result (N11.1^{o}E). The calculated horizontal stresses magnitudes were: $\sigma_H/\sigma_v = 0{,}8667$ and $\sigma_h/\sigma_v = 0{,}7368$ (equivalent to SHmax=42MPa and Shmin=36MPa, for a vertical stress Sv=48MPa).

Wellbore stability simulation

The software used to simulate wellbore stability was the SFIB (**S**tress and **F**ailure of **I**nclined **B**orehole; Peska & Zoback, 1996). This program calculate the in-situ stress redistribution around a wellbore with any directional characteristic and indicates potential zones to failure by shear or tensile stresses. The program assumes a linear-elastic model, which is a conservative one. In spite of this limitation, the visualization tools of software have furnished a good illustration for how well design can be affected by the in-situ stresses. Following the simulation, even though the horizontal stresses anisotropy is little it is sufficient to impact the stability of deviated wellbore

Figure 2 illustrates wellbore tendency to failure under shear stresses (breakout formation). The simulation tells us that drilling towards N120E or N60W would allow more inclined wells than drilling towards N30E or S30W.

Figure 3 illustrates wellbore tendency to failure under tensile stresses (hydraulic fracture formation). In this case, the simulation tells us that drilling towards N30E or S30W would imply using lighter mud to prevent the formation of hydraulic fractures, a consideration that would be particularly relevant for highly deviated wells.

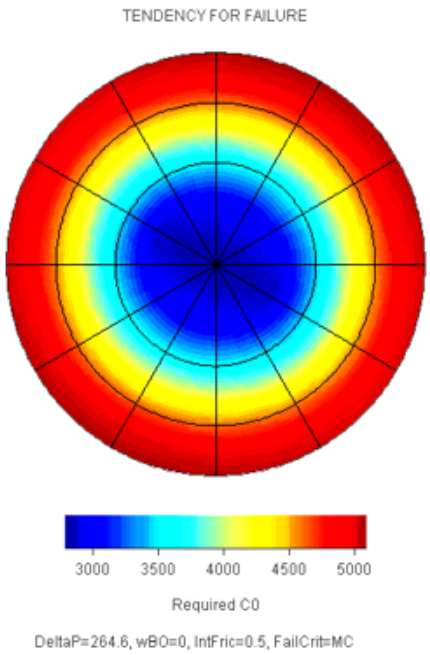

Figure 2. Wellbore tendency to failure under shear stresses (breakout formation)

Radius segments corresponds to possible wells orientations (15°) whereas circus corresponds to possible wells inclination (30°). The color scale corresponds to the rock strength (Co) required to inhibit failure by shear stress: (i) colors close to red represent cases when high Co is required; (ii) colors close to blue represents cases when lower Co is required (stable condition).

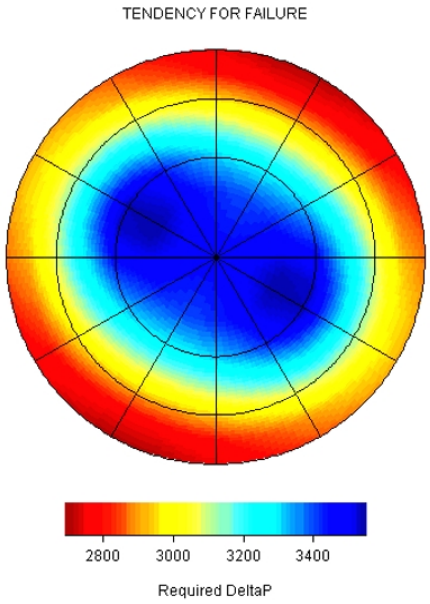

Figure 3. The wellbore tendency to failure under tensile stresses (hydraulic fracture formation).

DeltaP is the borehole fluid pressure less the pore pressure. The color scale corresponds to the differential mud weight at which tensile failure initiate: (i) colors close to red represent cases when very little differential pressure can initiate fractures; (ii) colors close to blue represents cases when appreciable differential borehole fluid pressure is required (stable condition).

Conclusion

Our results indicated that the studied oil field is submitted to a normal regime stress, in which the horizontal principal stresses are unequal (SHmax>Shmin; SHmax oriented to NNE-SSW). The simulations put into evidence how this information could be relevant in well design and, therefore, how important is to evaluate as accurately as possible the in-situ stress.

References Cited

AADNOY, B. S., 1988, Invertion Technique To determine the In-Situ Stress Field From Fracturing Data. SPE 18023: 55 - 67.

ASSUMPÇÃO, M., 1992, The Regional Intraplate Stress Field in South America. Journal of Geophysical Research, 97: 11,889-11,903.

ASSUMPÇÃO, M., 1997, Focal mechanisms of small events in SE Brazilian shield: a test for stress models of the South American plate. Geophys. J. Int., 133: 490-498.

ASSUMPÇÃO, M., 1998, Seismicity and stress in the Brazilian passive margin. Bull. Seism. Soc. Am., 88 (1): 160-169.

BELL, J. S., 1990, Investigating stress regimes in sedimentary basins using information from oil industry wireline logs and drilling records. In Geological applications of Wireline Logs Geological

Society Special Publication. Eds: A. Hurst, M. A. Lovell, and A. C. Morton, p. 305-325.

FEJERSKOV, M., & BRATLI, R., 1998, Can Dipmeter logs be used to identify In-situ Stress Directions in the North Sea? SPE/ISRM Eurock '98, SPE/ISRM 47237, p. 151-160.

LIMA, C. C., 1999, Expressions Topographiques et Structurales de L'Etat de Compression Generalisee au Sein de la Plaque Sud – Americaine. Tese de Doutorado, Université de Rennes 1, Rennes, 370 p.

LIMA, C. C., & NASCIMENTO, E. M., 1994, Determinação das direções de tensão máxima horizontal (SHmax) nas bacias sedimentares brasileiras através da análise de breakouts. Comunicação técnica SETEC 007/94, 33 p.

LIMA, C. C., NASCIMENTO, E., & ASSUMPÇÃO, M., 1997, Stress orientations in Brazilian sedimentary basins from breakouts analysis: implications for force models in the South American plate. Geophys. J. Int., 130: 112-124.

LIMA NETO, F.F. & BENEDUZI, C., 1998, Using leakoff tests and acoustic logging to estimate *in situ* stresses at deep waters - Campos Basin. AAPG International Conference, Rio de Janeiro, Nov. 8-11.

LIMA NETO, F. F., 1999, O Regime Atual de Tensões nas Bacias Sedimentares Brasileiras. Anais do VII SNET (Simpósio Nacional de Estudos Tectônicos) - Sessão 4, p. 25 - 28.

PLUMB, R. A., & HICKMANN, S. H., 1985, Stress-Induced Borehole Elongation: A Comparison Between the Four - Arm Dipmeter and the Borehole televiewer in the Auburn Geothermal Well. Journal of Geophysical Research, 90: 5513-5521.

SILVA, A. T., 2001, Um estudo da influência do estado de tensões *in-situ* sobre a estabilidade de poços. Tese de Mestrado, Universidade Federal do Rio de Janeiro, 105 p.

ZOBACK, M. L., 1992, First- and second-order patterns of stress in lithosphere: the World Stress Map Project. Journal of Geophysical Research, 97: 11,703 -11,728.

Intraplate Compression Across South America: a Key Element for Basement-involved Meso-Cenozoic Tectonics of Brazilian Marginal Basins

Cláudio Lima (*) , claudioc@cenpes.petrobras.com.b; Francisco F. Lima Neto (*); Cláudia Queiroz, TEKTOS/UERJ; Clayton Almeida, TEKTOS/UERJ; Amilson R. Rodrigues; Alex V.S. da Gama; Ricardo S.N. de Bragança (*)
(*) PETROBRAS/CENPES/TEGG

Abstract
Examples are briefly given of at least 2 events of post-rifting tectonic inversion in the Potiguar and in the Almada basins. The discussion of these examples within the frame of the Meso-Cenozoic tectonics of the South America plate leads to the conclusion that the paradigm following which post-rift deformation of the Brazilian margin basins are solely controlled by thin-skinned gravitational tectonics should be abandoned. As a corollary, it is proposed that basement-involved compressional tectonics should play an important role in the deformational history if these basins.

Introduction

Given the geometry of the breakup, the Atlantic Brazilian margins are considered to be developed under different tectonic regimes: extension along the Eastern margin; right-lateral wrench followed by extension along the Equatorial margin (Chang et. al, 1992; Zalan & Warme, 1985). Given these paradigms, wrench tectonics has been mostly recognized along the Equatorial margin, and seldom, if so, recognized along the Eastern Brazilian margin.

In this paper we briefly describe two examples of wrench tectonics found in the Potiguar and in the Almada basin that do not respect that paradigm and discuss some implications for the thinking concerning the deformational history of the Brazilian margins.

Potiguar Basin rift evolution

The Potiguar basin, NE Brazil, is part of the northeast Brazilian rift system whose Neocomian origin is associated with the opening of the South Atlantic (Matos, 1992).The basement is made up of Precambrian metamorphic rocks affected to different degrees by a Neoproterozoic (Brasiliano) event.

Following Mattos (1992), NE-SW-trending shear zones of the Brasiliano/Pan-African orogeny controlled the development of the intracrustal listric normal faults that form the basement framework of the basin. Moreover, the NE-trending rift evolution of the Potiguar was aborted in the late-Barremian (~120 m.y. B. P.) when major NW-trending rifting initiated at the Equatorial branch of the rift system. In these NW-trending rifts (e.g. offshore Potiguar and Ceará basins) a continued evolution into a passive margin following the main rift episode has occurred.

Post-rift evolution of the Potiguar basin and tectonic inversion

Since the early nineties, internal Petrobras reports have put into evidence that the post-rift evolution of the Potiguar basin can be described in terms of four main events (Lima et al., 1993): (1) Aptian to Santonian deposition and concomitant northwestward tilting of the Açu and Jandaíra Formations; (2) a probably Santonian-Campanian (~84 m.y. B.P.) episode of weak inversion, induced a N-S compression (documented in outcrops and seismics); (3) a post- Santonian northwestward tilting associated with continuous deposition offshore and with a Paleocene to Miocene hiatus followed by a continental sedimentation onshore; (4) a Tertiary/Neotectonic E-W to NW-trending compression. An Eocene to Oligocene magmatic event is also registered mainly offshore (Mizusaki, 1989).

In outcrops the Santonian-Campanian inversion is denoted by folds and strike-slip faults (fig. 2 and 3). The structures on the outcrops are consistent with a local N-S-trending compression in a context of wrench tectonics. In this context, NW-trending and NE-trending basement faults were prone to be reactivated as right-lateral and left-lateral respectively. The ENE-trending fold axis deduced from outcrops is parallel to the alignment of the buried oil producing anticlines of Alto do Rodrigues trend. These are transpressional features associated with a major (reactivated) rift fault. In some outcrops, the bedding is re-folded along N-S trending axis attributed to the E-W-trending Tertiary/Neotectonic compression (Lima, 1999).

In the offshore basin, the Santonian-Campanian event was responsible for the development of a 3 to 5 km-wide, right-lateral, WNW-ESE-trending wrench zone ("*Zona Transcorrente de Ubarana*"; Cremonini, 1994) affecting sediments underlying a regional meso-campanian unconformity. In the same area the N-S-trending fold axes attributed to the E-W-trending Tertiary affect sediments above and below the unconformity.

Figure 1. Anticlinal affecting limestones of the Jandaira Formation, Potiguar basin. Modified from Lima (1999)

Figure 2. Righ-lateral NW-trending strike-slip fault affecting limestones of the Jandaíra Fm, Potiguar basin. Modified from Lima (1999),.

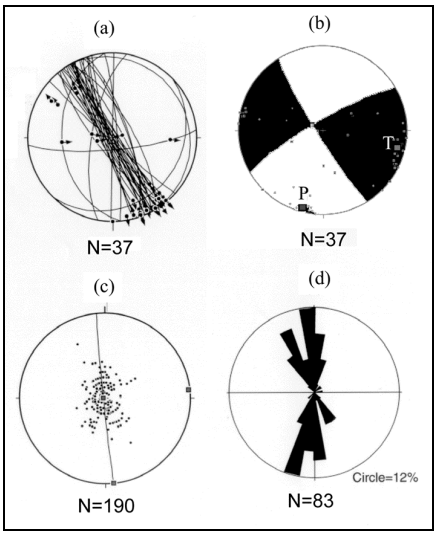

Figure 3. Outcrop analysis.

N is the number of measurements. a) Faults and striations. (b) Focal mechanism for the same faults using the Faultkin software (Marret & Allmendinguer, 1990), P and are the compression and extension axes. c) Girdle of bedding furnishing the fold mean fold axes (ENE-plunging). (d) circular diagram for the orientations extensional calcite veins (maximum concentration is N-S-trending).

Almada Basin

The Almada Basin (fig. 4) is located at the Eastern Brazilian margin, the one usually considered to be dominated by pure extensional tectonics. The basin includes an emerged preserved area of about 200km^2, and 1800m maximum thickness of sediments. Its offshore area goes up to 1300km2, with 6000m maximum thickness (Bruhn & Moraes, 1989). This basin has been developed over granulites of Transamazonian cycle (~2000 m.y), and alkaline intrusive rocks of Neoproterozoic age. The most important structure in the region, which represents the main borders of the Almada Basin, is the Itabuna-Itaju do Colônia Shear Zone (fig. 4), oriented N45^{o}E and with ductile-fragile to fragile character (Corrêa Gomes et al., 1998). According to these authors, this shear zone affected Archaean, Palaeoproterozoic and Neoproterozoic rocks, in a sinistral, then dextral-sinistral oscillation, and finally dextral sense.

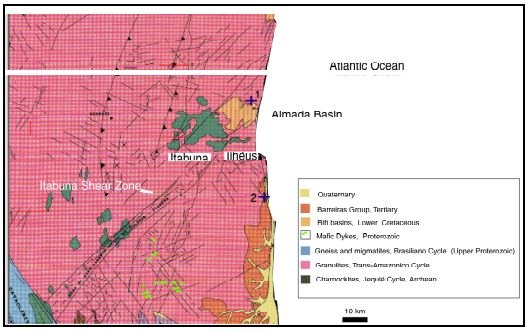

Figure 4. Regional context of the Almada Basin.

Modified from Lima (1993).

Here we briefly show signs of basin inversion found in two different outcrops of this basin. The first one is located at the northern border of the basin (fig. 4 and 5; #1). Fluvial-eolian sandstones of the Sergi Fomation, a Jurassic pre-rift rift unit, now strongly faulted and tilted towards SE outcrop (figs. 6 and 7). The Sergi Fm should be found at the base of the sedimentary stratigraphic column. In spite of that, this outcrop has some of the highest altitudes within the basin, defining its northern border. Maximum concentrations of faults are N82E/46NW and N40E/66NW, while joints are grouped about N45E/88NE and N60E/89NW. Secondary R and R' fault arrays and fault slip analysis indicate that the once NE-trending normal faults that form the northern border of the Almada rift basin have undergone at least 2 episodes of reactivation as strike-slip faults, one left-lateral, the other right lateral.

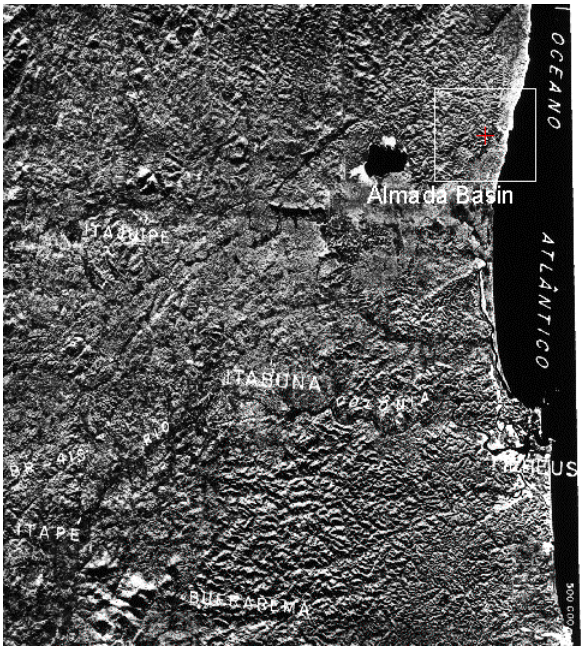

Figure 5. Radar image (RADAM-Brasil) showing the structural grain around the Almada basin.

See the how the northern border of the basin (red cross) is strongly affected by NE-trending faults (see also fig. 6).

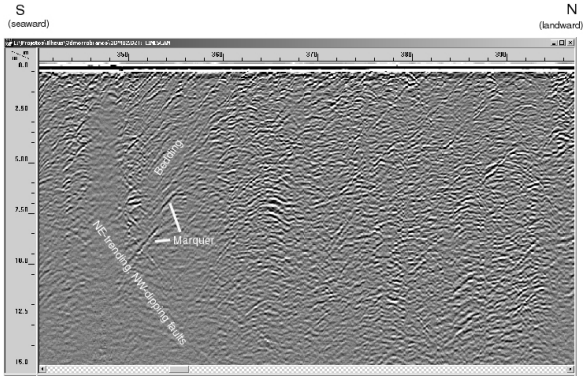

Figure 6. GPR image showing the faults and bedding

Strongly deformed, oil-saturated sandstones of Aptian age outcrop in a beach South of Ilhéus (fig. 7). The ex-sudation is known since the beginning of the last century and the observed deformation in this outcrop has been usually attributed to the intrusion of a mafic dike (Carvalho, 1965). Radiometric dating of this dike has furnished Proterozoic ages. On the basis of this result and of a structural analysis of the outcrop, Lima (1993) has proposed that the observed deformation was a result of wrench tectonics.

This interpretation has been confirmed in this present study. Actually a dozen of folds outcrop along a N-S trending beach for about 400 m (fig. 8)

Figure 1. NE-trending positive flower structure affecting the Sergi Fm at northern border of the Almada basin.

Figure 7. Dome-and-basin fold-interference pattern in Aptian oil-saturated sandstones, Almada basin.

Figure 8. Drag folds outcropping along a N-S-trending beach, Almada basin.

At the nuclei of the northernmost and the southernmost anticlines basement rocks have been pushed up forming positive flowers.

Detailed structural analysis have put into evidence that the observed deformation has been produced by at least 2 events of wrench, the first one responsible for ENE-trending folds, that were then refolded along N-S-trending axes by the second one. The structural relations between the folds and the underlying major basement faults remain unclear. Nevertheless, the observed interference pattern would be consistent with a post-Aptian NNW-SSE-trending compression, followed by a E-W-trending compression.

Discussion

The tectonics of the South American plate is dominated by the divergence with the African plate, by the frontal convergence with the Nazca plate and by oblique convergence with the other neighboring plates. The onset of this tectonic context probably happened during the Mid – Upper Cretaceous and has been definitely established in the Tertiary. This context could be analogous to a huge traffic accident, where a big truck travelling to the west frontally collides with another fast big truck traveling to the east, and is forced to pass by other small but strong and fast ones, also travelling to the east. In such a mechanic environment, it is reasonable to think that compressional deformation would prevail across our first big truck, probably locally concentrated along its favorably oriented mechanical discontinuities. Similarly, it is reasonable to infer that horizontal compression could have been dominating the intraplate basement-related deformation across South America plate since, at least, the Mid/Upper Cretaceous.

For the Present time, this inference is substantiated by *in-situ* stress data and by the active deformation, measured by spatial geodesy, since: (i) the basement beneath the Southeastern Margin Basins is in a thrust regime, while in the Northeastern Margin Basins, it is in a strike-slip regime; (ii) in a purely intraplate area, between Cachoeira Paulista (São Paulo State) and Kourou (French Guiana), the shortening measured by spatial geodesy is 7mm/year (Lima, 1999; 1997; Assumpção, 1997).

The examples of wrench tectonics that we briefly described here represent a paradox with respect to the paradigms that, first, the Eastern Brazilian margin would be "a classic passive margin" and, second, that wrench tectonics along the Brazilian Equatorial would be restricted to the timing and processes directly related to the Gondwana breakup. Given such examples and the rational concerning the Upper Cretaceous – Present tectonics of the South American plate, we believe that those paradigms should be abandoned. It seems to us more natural to think that wrench tectonics has dominated the deformational history of Brazilian marginal basins since, at least the Mid-Upper Cretaceous.

This proposition seems to be consistent with the observation that, broadly speaking, there is a timing match between the peaks of Andean orogenesis along the Pacific margin and the peaks of magmatism, the onset of unconformities and the intraplate deformation across South America, here including the Brazilian marginal basins (Lima, 1999; Pereira, 1994). Furthermore, the observed links between events of the so called "passive and active margins" reinforce the idea that plate tectonics is essentially a global phenomenon, meaning that a comprehensive approach is always mandatory in tectonic studies.

References

ASSUMPÇÃO, M., 1997. Focal mechanisms of small events in SE Brazilian shield: a test for stress models of the South American plate. Geophys. J. Int., 133, 490-498.

Bruhn, C. H. L. & Moraes, M. A. S. 1989. Turbiditos da Formação Urucutuca na Bacia de Almada, Bahia: Um Laboratório de Campo para Estudios de Reservatórios Canalizados. B. Geoci. PETROBRÁS, Rio de Janeiro, *3* (3): 235-267, jul./set.

Carvalho, K.W.B. 1965. Geologia da bacia Sedimentar do Rio Almada. Boletim Técnico da Petrobras, 8(1):5-56.

CHANG, H.K., KOWSMAN, R., FIGUEIREDO, A.M.F. *et al.*, 1992. Tectonics and stratigraphy of the east Brazil rift system: an overview. Tectonophysics, 213: 97-138.

Corrêa Gomes, L.C; Paiva de Oliveira, E.; Barbosa, J.F.S.; Fernandez da Silva, P.C. 1998. Tectônica associada à colocação de diques alcalinos félsicos a máficos neoproterozóicos da zona de cisalhamento de Itabuna- Itajú de Colônia, Bahia, Brasil. Revista Brasileira de Geociências, vol. 28, No 4, p 449-458.

CREMONINI, O. A., 1994. A zona trasncorrente de Ubarana, Bacia Potiguar, Brazil. Bol. Do 3º Simp. Sobre o Cretáceo do Brasil, 23-26. UNESP, Rio Claro.

LIMA, C.C., 1993. Controle das grandes descontinuidades do embasamento sobre o arcabouço estrutural das bacias do Jequitinhonha e de Almada e algumas analogias entre o 1-BAS-37 e o Embasamento Fraturado de Carmópolis. Relatório Interno PETROBRAS/CENPES/DIVEX/SETEX

LIMA, C.C., BENTZ, M.C., FONSECA, L., *et al.*, 1993. Correlações entre o campo de tensões neotectônicas, a topografia e estruturas geológicas na bacia Potiguar. PETROBRAS Int. Rep.

LIMA, C., 1999. Expressions topographiques et structurales de l'état de compression généralisée au sein de la plaque sud-américaine. Ph. D. thesis, Univ. Rennes I, Rennes, France, 370 p.

MATOS, R.M.D., 1992. The northeastern Brazilian rift system, Tectonics, 11(4): 766-791.

PEREIRA, M.J., 1994. Seqüências deposicionais de 2ª e 3ª ordens (50 a 2 Ma) e tectono-estratigrafia no Cretáceo de cinco bacias marginais do Brasil. Comparações com outras áreas do globo e implicações geodinâmicas. Thèse de Doctorat, présenté à l`Universidade Federal do Rio Grande do Sul (UFRGS), Brésil, 430 p.

ZALAN, P.V. & WARME, J.E., 1985. Tectonics and sedimentation of the Piauí-Camocim sub-basin, Ceará basin, offshore Northeastern Brazil. Ciência Técnica e Petróleo, Secção Exploração de Petróleo, 17, CENPES, PETROBRAS, 71 p.

Levantamento de Refração Sísmica Profunda no Setor Sudeste da Província Tocantins

*F. Perosi *, J. Berrocal, C. Fernandes, A. C. Medrado*
Instituto Astronômico e Geofísico – Universidade de São Paulo – Brasil (fabio@iag.usp.br**)**

Abstract

This work is inserted among the deep seismic refraction studies of the Thematic Project "Geophysical Studies and Tectonic Model of the Tocantins Province Central and Southeast Sectors, Central Brazil". Three refraction lines, of around 300 km long each, were deployed, two of them in the Central sector and the other in the SE sector, that is subject of the present work.

The main objective of this work is to obtain as a final product a seismic velocity model with the physical characteristics of the main discontinuities in the crust and upper mantle. The packages SAC, SU and SEIS were used to perform the data analysis and processing. To carry on the modelling were used the ray theory and the synthetic seismograms construction, belonging to the SEIS package

Data from the extreme and middle points of the seismic line were used to elaborate the final model, considering that due to technical problems signals from the other four explosions were not recorded. Apart from that, the recorded explosions did not present clear signals all along the extension of the line. Due to these facts, and considering also the geological units present in the studied region, are suggested three seismic velocity models.

The first model is referred to the direct shot (EX31), which is localised in the Southwest extreme of the line on the Parana Basin province. In this model we obtained the P wave velocity (V_P) of 2 km/sec at the surface, corresponding to the unconsolidated sediments and soil on the top of that basin. At a depth of 86 m we found V_P of 5,15 km/sec and at a depth of 350 m the velocity V_P of 4,6 km/sec, corresponding to the basalt and sand layers of the Parana Basin. Underlying them, at 650 m of depth we found the basement with V_P of 5,75 km/sec and finally at a depth of 4 km there is a layer with V_P of 6,07 km/sec, corresponding to a typical upper crust P wave velocity.

The second model corresponds to the reverse shot (EX34) that is localised in the middle point of the line on the granitoides of the Araxa Group. For this model we obtained V_P of 2 km/sec for the superficial layers, then at a depth of 60 m was obtained V_P of 5,69 km/sec and for a depth of 860 m the value of V_P is 6,25 km/sec.

Finally, the third model belongs to the whole line section (300 km) from the direct shot (EX31). This model was obtained by using the arrivals of secondary phases and the results of models proposed in other works. From the surface down to 4 km of depth this model is similar to the first one. At 20 km of depth there is a layer with V_P of 6,70 km/sec, corresponding to the lower crust, with Moho at a depth of 40 km with V_P of 8,00 km/sec.

Introdução

Este trabalho de refração sísmica profunda faz parte do Projeto Temático de Equipe "Estudos Geofísicos e Modelo Tectônico dos Setores Central e Sudeste da Província Tocantins, Brasil Central". Os levantamentos de refração sísmica profunda efetuados na Província Tectônica Tocantins como parte do Projeto Temático, são pioneiros no Brasil por utilizarem, de forma simultânea, mais de uma centena de sismógrafos com registro digital operando na componente vertical e explosões diretas e reversas com hora de origem controlada, programadas exclusivamente para este experimento.

Nessas pesquisas de refração sísmica profunda foram levantadas três linhas de aproximadamente 300km de extensão, duas no setor Central da Província Tocantins (linhas L1 e L2, na região norte do estado de Goiás) e uma no setor Sudeste (linha L3, na região do Triângulo Mineiro), sendo esta última o assunto de estudo deste trabalho. O objetivo previsto para este trabalho foi elaborar, como produto final, um modelo de velocidades sísmicas contendo as características físicas das principais descontinuidades na crosta terrestre e manto superior, existentes sob o setor. Sudeste da Província Tocantins.

Descrição da Linha e Procedimento

A linha de refração sísmica profunda deste trabalho atravessa o setor Sudeste da Província Tocantins (linha L3), se inicia na divisa entre os estados de São Paulo e Minas Gerais, segue no sentido SW-NE, passando pelas cidades de Uberaba, Patrocínio e Patos de Minas, terminando na proximidade do lugarejo conhecido como Varjão (Figura 1). Essa linha começa na porção NE da Bacia do Paraná, atravessa a Faixa de Dobramentos Brasília, e penetra no Cráton do São Francisco. Tem aproximadamente 300km de extensão e 120 pontos de registro, separados a cada 2,5km, distribuídos ao longo de estradas principais e secundárias. (Perosi, 2000).

Os procedimentos de campo deste trabalho foram descritos no VII Snet (Perosi et al., 1999). No presente trabalho são analisados os tiros: direto (EX31-EX34) e reverso (EX34-EX31) da Seção 1 e a Seção Total (EX31-EX37).

Para estudar a propagação das ondas elásticas em estruturas complexas podem ser utilizados métodos

analíticos de aproximação, tais como o método de propagação do raio sísmico. Nas aplicações sismológicas este método foi utilizado inicialmente para investigar principalmente a estrutura mais interna da Terra a partir das curvas de tempos de percurso das ondas de volume (P e S) e para calcular as trajetórias de raios e os tempos de percurso teóricos, em vários tipos de meio, para, finalmente, compará-los com os dados observados.

O processo de modelagem, utilizando o pacote SEIS88 (Cerveny, 1988), foi iniciado com dados relativos à Seção 1 (tiros direto e reverso). Os modelos utilizados para alimentar esse pacote foram os modelos preliminares obtidos com o programa TVEL. Neste processo foi possível delimitar melhor a interface relativa à Bacia do Paraná, considerando camadas inclinadas, e utilizou-se um gradiente de velocidade de 0.01 km/s, conforme recomendado por Mooney et al. (1983).

Interpretação dos Resultados

Seção 1

Os resultados obtidos para a Seção 1 (Figuras 2 e 3), de 150km de extensão, entre os tiros EX31 e EX34, não permitiram a elaboração de um modelo único representativo dessa seção. Isto foi devido à baixa qualidade dos sinais que não atingiram a extensão completa desta seção em ambos sentidos. Além disso, a presença da Bacia do Paraná num extremo desta seção dificultou o cálculo das profundidades devido à presença da camada de baixa velocidade sob a camada de basalto. Por este motivo o modelo final proposto para esta seção é apresentado, na Tabela 1, para os tiros direto e reverso.

A Bacia do Paraná é a feição tectônica dominante na região do tiro direto da Seção 1. Ela está presente nos primeiros 125km da porção superficial SW dessa seção. A seção da Figura 2 mostra uma curva (azul clara) correspondente a reflexão no topo da camada de baixa velocidade, porém esta fase não foi identificada nos sismogramas reais.

Na Figura 3 é apresentada a seção reduzida para o tiro reverso da Seção 1. Nesta seção observa-se a melhor qualidade dos sinais correspondentes a explosão EX34 que foi efetuada num poço perfurado numa rocha competente (granitóide do Grupo Araxá), apesar de ter sido utilizada uma carga de 500kg de explosivo, ou seja, a metade da carga utilizada na explosão EX31. Outro fator que pode ter influenciado na qualidade pobre dos sinais do tiro direto, além da falta de coesão no local do tiro, é a geologia da Bacia do Paraná que teria atenuado os sinais da carga de 1000kg da explosão EX31.

Seção Total

Para o modelo de 300km de extensão não foram elaboradas grades de velocidades específicas. Foi utilizada a grade da Seção 1, extrapolando a penúltima camada dessa grade e para as camadas mais profundas foram utilizados dados retirados de modelos existentes na literatura (Pereira, 1995). Foi possível observar algumas fases secundárias (prováveis reflexões) em torno dos 150km e dos 200km e outras mais que ajudaram a definir um modelo preliminar para a crosta sob a região de estudo.

Referências

Cerveny, V., Pacote SEIS88 e sua documentação, 1988, Março/2000, *Obtida via internet.* http://seis.karlov.mff.cuni.cz/software/seis/.

Mooney, W. D., Andrews, M. C., Ginzburg, A., Peters, D. A., Hamilton, R. M., 1983, Tectonophysics, v.94: 327-348.

Pereira,M. R. S., 1995, Perfil Sísmico na Região de Formiga-MG utilizando o Método de Refração Sísmica Profunda, Trabalho de Graduação, IAG / USP.

Perosi, F. A., Berrocal, J., Fernandes, C., Medrado, A. C., Anais do VII SNET, Volume único, Sessão 2, p.103, Maio/1999.

Perosi, F. A., 2000, Refração Sísmica Profunda no Setor Sudeste da Província Tocantins, Dissertação de Mestrado, IAG / USP.

Agradecimentos

À FAPESP pelo financiamento deste projeto. À colaboração do USGS (CA, USA) e do Program for the Array Seismic Studies of Continental Lithosphere (PASSCAL). Aos professores, técnicos e alunos do IAG/USP e do Observatório Sismológico/UnB.

Tabela 1 – Modelo final para a Seção 1 (150km)

	EX31-EX34		EX34-EX31	
Camadas	**Prof. (km)**	**V (km/s)**	**Prof. (km)**	**V (km/s)**
1	0	2,0	0	2,0
2	0,06	5,1	0,06	5,2
3	0,4	4,2	0,8	6,2
4	0,9	5,7	8,5	7,1
5	5,4	6,6		
6	9,8	7,2		

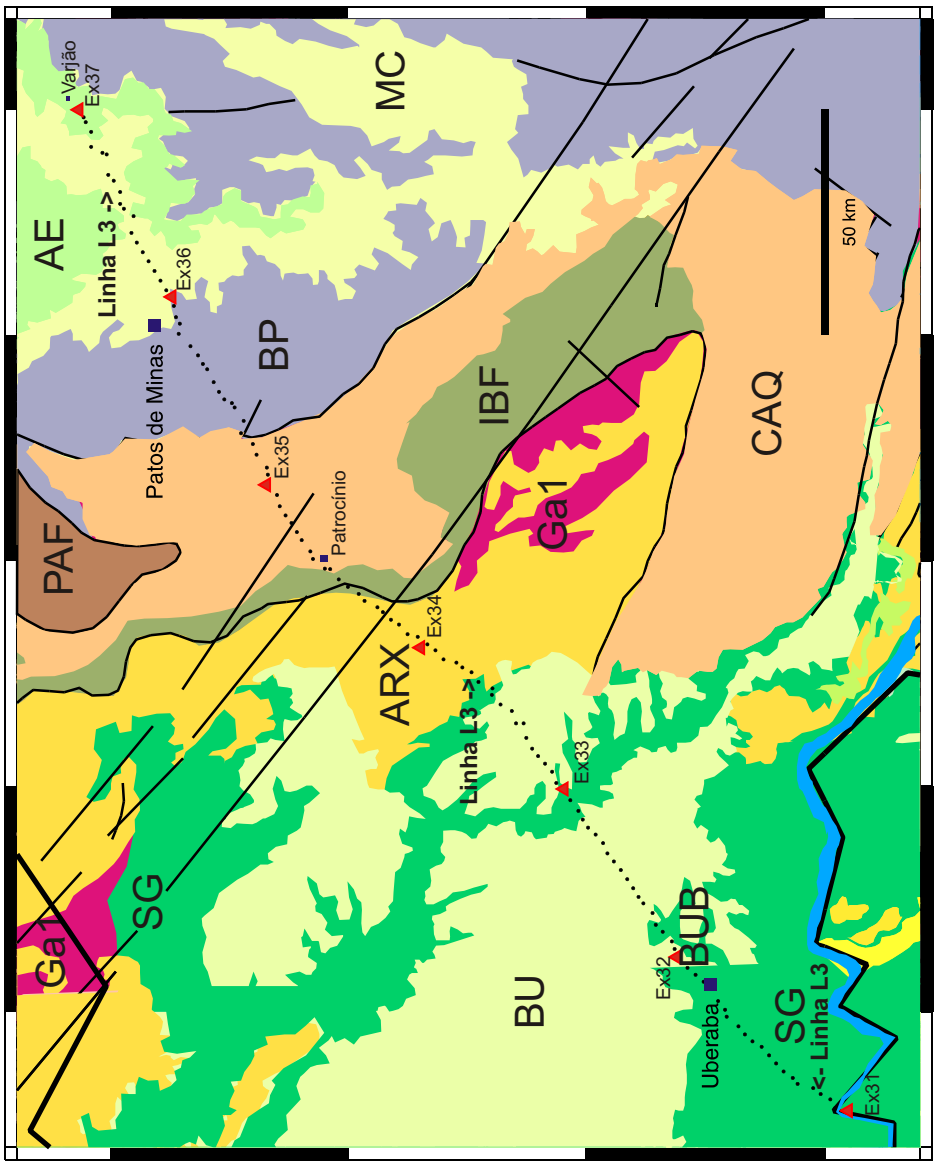

LEGENDA:
Bacia do Paraná:
SG - basaltos toleíticos com intercalações de arenito e diabásios (Formação Serra Geral, Grupo São Bento) Mesozóico.
BU - arenitos, arenitos calcíferos, conglomerados, calcários (Formação Marília, Grupo Bauru) Mesozóico.
BUB - arenitos, conglomerados e pelitos vulcanoclásticos (Formação Uberaba, Grupo Bauru) Mesozóico.
Faixa de Dobramento Brasília:
Ga1 granitos e granitóides Arqueano.
CAQ quartzitos e filitos (Grupo Canastra) Proterozóico Médio.
PAF quartzitos e filitos (Formação Paracatu) Proterozóico Médio.
ARX micaxistos, anfibolitos, quartzitos, gnaisses e formação ferrífera (Grupo Araxá) Proterozóico Superior.
IBF filitos (Formação Rio Verde, Grupo Ibiá) Proterozóico Superior.
Cráton do SãoFrancisco
BP - corresponde às rochas formadas por calcário, marga,

Figura 1 - Mapa geológico simplificado da região de estudo mostrando a Linha L3 de RSP, com a localização das explosões (▲).

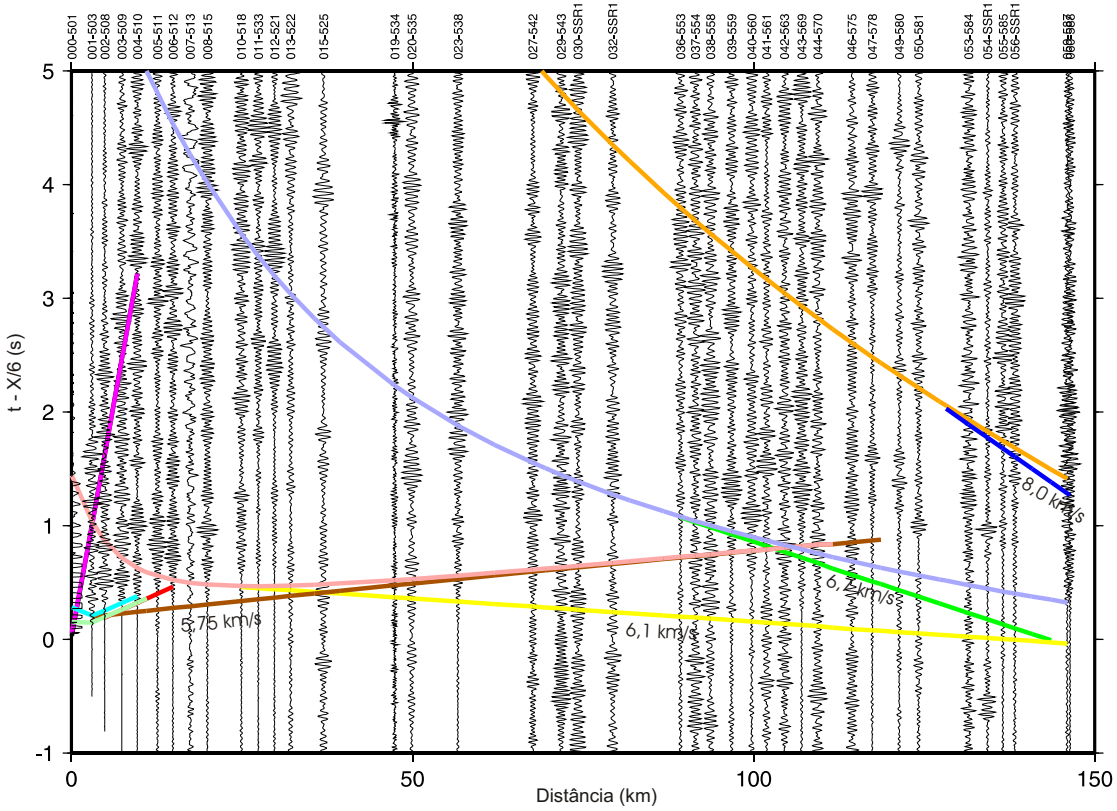

Figura 2 - Seção Sísmica, em tempo reduzido, referente ao tiro direto da Seção 1.

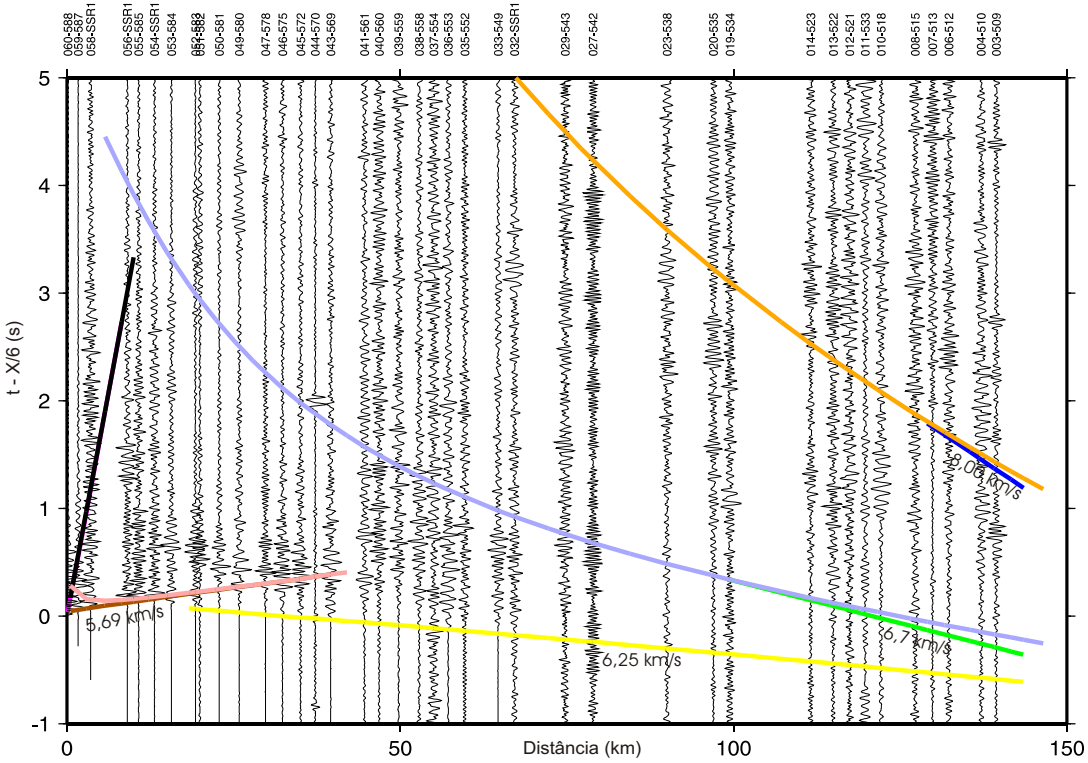

Figura 3 - Seção Sísmica, em tempo reduzido, referente ao tiro reverso da Seção 1.

Lithosphere Effective Elastic Thickness Pattern for the African Continent.

Wladimir Shukowsky, Instituto Astronômico e Geofísico - USP, wladimir@iag.usp.br
Marta S. M. Mantovani, Instituto Astronômico e Geofísico - USP, marta@iag.usp.br

Abstract

The effective elastic pattern for the African continent calculated by combining the gravity/topography coherence values with gravity tidal anomaly data is presented. Results are discussed and compared to the tectonic pattern of that continent.

Introduction

The rigidity parameter (D) or the equivalent effective elastic thickness (*Te*) provide information on the time-scale during which the lithosphere relaxes, reaching its isostatic equilibrium. While some authors prefer a short relaxation time (a few million years), others favor longer relaxation timescales (10 - 100 My) and still others advocate that the strength of the lithosphere depends both on the age of the loading and on the thermal structure of the lithosphere.

Recently, Shukowsky and Mantovani (1999) presented an alternative way to establish the degree of elasticity of a lithospheric segment, looking at its response to an external excitation. Assuming that the tidal response is mainly related to the Earth's viscoelastic properties, local deviations with respect to averaged global models are indicative of local variations of elastic properties.

Under these premises, and by combining the existing *Te* data obtained from the coherence analysis with those obtained in this work from the Earth tidal anomaly data set over Africa, we present the resultant *Te* pattern in correspondence with the topography. Only in its northernmost part Africa lacks of *Te* data, which are, here, constrained by *Te* values from tidal gravity anomaly in the surrounding areas.

Africa comprises a wide range of geological features providing an excellent field area to study the variation of the rigidity parameter (D) for different tectonic provinces (Figure 1).

A striking feature of the topography of Africa is its "basin and swell" architecture. The origin of this topography has been explained as that the basins and swells reflect differential heating of the lithosphere by one or more hotspots in the underlying mantle or that they are the consequence of the dynamic effects that act below the lithosphere such as mantle convection.

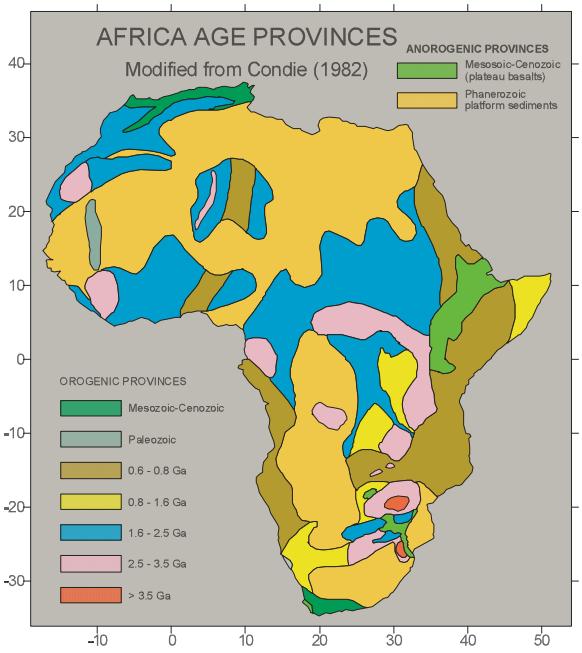

Figure 1 - Age provinces for Africa. Modified from Condie (1982).

Coherence data analysis

A common procedure to determine *Te* is to compare the observed amplitude of the Bouguer anomaly with its expected value for a locally compensated topography. Forsyth (1985) showed that if surface and subsurface loading are statistically independent, the coherence between the observed and expected gravity anomaly amplitudes will approach 1.0 at wavelengths that are long compared to the characteristic flexural wavelength, and will approach to 0.0 at wavelengths short enough for loads to be supported by stresses within the plate. The transition from the coherent to the incoherent topography and gravity will give a direct indication of the flexural rigidity of the plate, and hence of *Te*.

Tidal gravity analysis

Among the various tidal components, the semi-diurnal lunar wave (M2) can be determined more precisely than other components, and is thus preferred here over other components.

The tidal gravity anomaly (TGA) is a useful measure of the discrepancy between the observed and modeled tidal gravity, because it carries information on the Earth's internal structure not accounted for by the

model. The TGA is defined as the component in phase with the vector difference between observed tidal gravity corrected for the ocean loading and the model tidal gravity:

$$TGA = A\cos(\alpha) - L\cos\lambda - M \qquad (1)$$

where (A,α) are the amplitude and phase of the observed M2 component, (L,λ) are the amplitude and phase of the M2 ocean loading component and M is the reference viscoelastic tidal gravity amplitude given by:

$$M = 87.00\frac{r(\phi)}{a_E}\cos^2\phi\ \mu\text{Gal} \qquad (2)$$

where ϕ is the latitude of the measurement point, $r(\phi)$ is the distance to the center of mass of the Earth and a_E is the equatorial radius of the reference ellipsoid.

A statistical analysis between the variance of TGA and the latitude for the M2 lunar component performed with 277 tidal gravity stations, indicates that TGA data are spatially auto-correlated up to distances of 5° (~ 500 km). This suggests an association between the tidal gravity response and lithospheric-scale blocks (Shukowsky and Mantovani, 1999). Since the tidal response is mainly related to the Earth's viscoelastic properties, regional deviations relative to global reference models could indicate lateral variations of the elastic characteristics in the outer layers of the Earth. Experimental data suggests a regression model of the form

$$Te = a + b\frac{TGA}{\cos^2\phi} \qquad (3)$$

The analysis of 36 stations for which there exist both TGA and *Te* estimates allowed the determination of the model coefficients (Shukowsky & Mantovani, 1999):

$$\begin{cases} a = 70.58 \pm 2.72\ km \\ b = -15.11 \pm 3.35\ km/\mu Gal \end{cases} \qquad (4)$$

Tidal gravity data

Tidal gravity data for Africa were taken from the Trans World Tidal Gravity Profile (TWTGP) maintained by the International Center for Earth Tides (ICET). This is a data set of Earth tide data available worldwide (Ducarme & Melchior, 1978; Melchior, 1994). The location of the 34 tidal gravity stations used in this work in shown by filled circles in Figure 2.

Lithosphere effective elastic thickness data for the African Plate

Isostatic and thermomechanical *Te* estimates were taken from Bechtel et al. (1987), Docouré et al. (1996), Ebinger et al. (1989), Hartley et al. (1996) and Djomani et al. (1995).

The location of the 84 isostatic and thermomechanical *Te* estimates used in this work in shown by crosses in Figure 2.

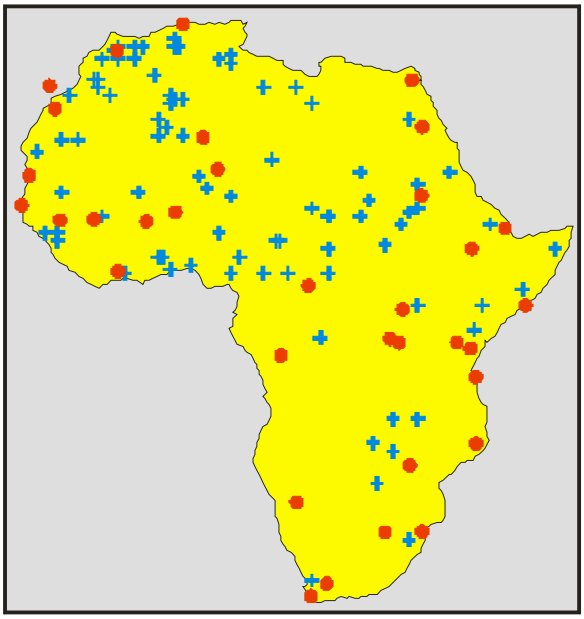

Figure 2 - Location of the tidal gravity stations (filled circles) and of the isostatic/thermomechanical *Te* estimates (crosses).

Data merging

The tidal anomaly values were converted to the effective elastic thickness scale by means of the regression model (3) and (4) and merged with the isostatic/thermomechanical *Te* estimates.

In order to assess the spatial correlation of the merged data set, it's experimental variogram, shown in Figure 3, is compared to experimental variogram for 277 TGA values from the global TWTGP data set shown in Figure 4.

The similarity of the variograms supports the use of the merged data set for regional *Te* pattern determination.

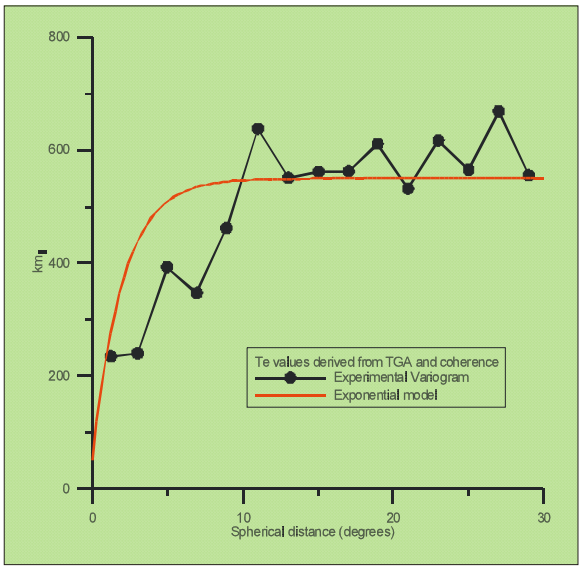

Figure 3 - Experimental variogram and exponential model (range 5°) for the merged data set.

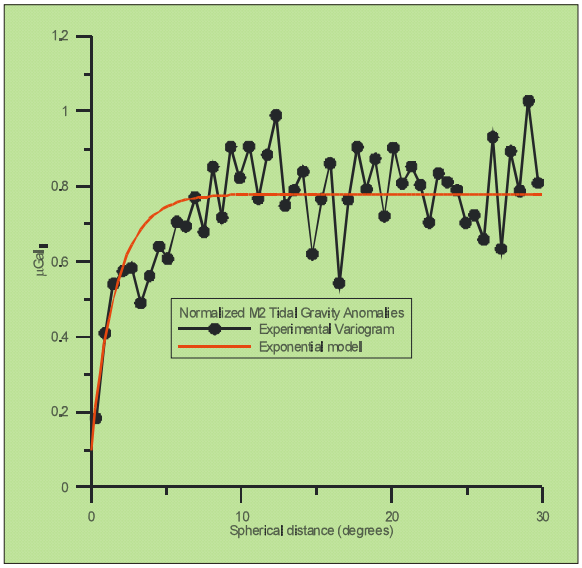

Figure 4 - Experimental variogram and exponential model (range 5°) for 277 TGA values from the TWTGP data set.

The Regional *Te* Pattern

The combined set of *Te* estimates for Africa was interpolated by kriging on a 0.5x0.5 degrees regular grid, using an exponential variogram model with range equal do 5 degrees. The resulting *Te* pattern is shown in Figure 5, in which the *Te* pattern is represented by a color scale.

Two main features are observed in the African *Te* pattern. Higher rigidity zones (colder and/or thicker lithosphere; *Te* > 72 km, blue in Fig. 5) are clearly distinguished from those of lower rigidity (hotter and/or thinner lithosphere; *Te* < 55 km, yellow, orange and red in Fig. 5). According to the scale and Africa tectonics the "blue zones" are associated with cratons (Congo, West Africa, Kaapvaal), Atlas Mts. and Proterozoic collision belts, while the "red zones" are associated with the East and Central Africa Rifts, the Saharan and other sedimentary basins. A common feature of the later structures is that magmatic activity has occurred in them since the Jurassic-Early Cretaceous. The transition (55 km < *Te* < 72 km) between high and low *Te* delineates the tectonic unit boundaries.

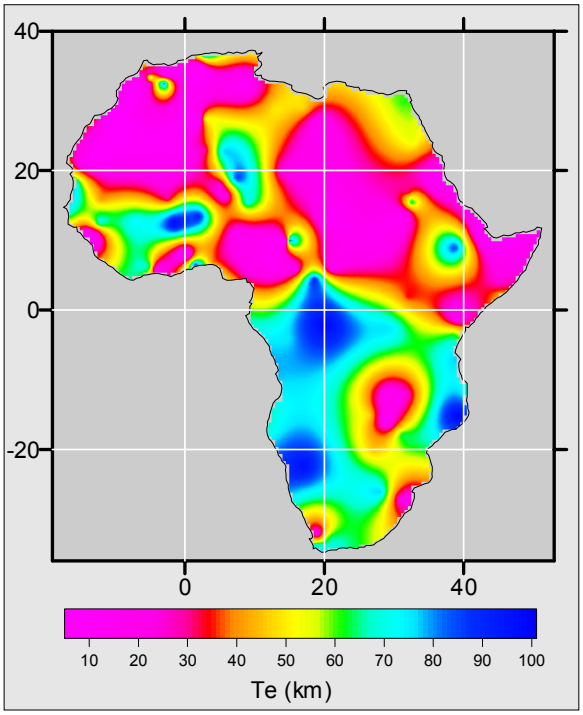

Figure 5 - Regional *Te* pattern for Africa derived from M2 tidal gravity anomalies and isostatic/ thermomechanic estimates.

References

Bechtel, T.D., Forsyth, D.W. and Swain, C.J., 1987. Mechanisms of isostatic compensation in the vicinity of the East African Rift, Kenya. Geophysical Journal of the Royal astronomical Society, 90: 445-465.

Condie, K.C., 1982. Plate Tectonics and Crustal Evolution. Pergamon, USA., 2nd edition, 310 pp.

Djomani Y.H.P., Nnange J.M., Diament M., Ebinger C.J., Fairhead J.D., 1995. Effective Elastic

thickness and crustal thickness variations in west central Africa inferred from gravity data. Journal of Geophysical Research, 100(B11): 22.047 - 22.070.

Docouré, C. M., de Wit M. J. and Mushyandebvu M.F., 1996. Effective elastic thickness of the continental lithosphere in South Africa. Journal of Geophysical Research, 101 (B5): 11.291 - 11.303

Ducarme,B and Melchior, P., 1978. A trans-world tidal gravity profile. Physics of the Earth and Planetary Interiors 16, 257-276.

Ebinger C. J., Bechtel T. D., Forsyth D. W. and Bowin C. O., 1989. Effective elastic plate thickness beneath the East African and Afar Plateaus and Dynamic compensation of the uplifts. Journal of Geophysical Research 94 (B3): 2883 - 2901.

Forsyth, D.W., 1985. Subsurface loading and estimates of the flexural rigidity of continental lithosphere. Journal of Geophysical Research, 90,12623-12632.

Hartley,.R., Watts, A .B., Fairhead, J.D., 1996. Isostasy of Africa. Earth Planet. Sci Lett., 137: 1-18.

Melchior, P., 1994. A new data bank for tidal gravity measurements (DB92). Physics of the Earth and Planetary Interiors 82, 125-155.

Shukowsky, W. & Mantovani, M.S.M., 1999. Spatial variability of tidal gravity anomalies and its correlation with the effective elastic thickness of the lithosphere. Phys. Earth Planet. Int., 114:81-90.

Acknowledgments

This work was financially supported by FAPESP, CNPq and CAPES.

O Estudo da Estrutura da Crosta na Faixa Ribeira, SE do Brasil, usando a Função do Receptor.

George Sand L. A. de França e Marcelo Assumpção

IAG/USP

Abstract

The Brazilian Lithosphere Seismic Project (BLSP), has been studying the crust in the SE region of Brazil. Assumpção et. al. (2001) obtained results for the thickness of the crust in the area. In this work, we concentrated the study on the Ribeira fold belt.

The study of the structure of the crust was accomplished in five stations using Receiver Function. For each station, the functions were stacked for a group of events acording to azimuths and distance. The wave converted from Moho (Ps) was easily identified. The thickness and the inversion for structure of the crust used an initial model obtained from the re-interpretation of a deep seismic refraction survey with average crustal velocity 6,3 km/s and Poisson ratio 0.25. The values obtained for crustal thickness range from 34 to 40 km. The results show a trend of crustal thinning towards the coast.

A waveform inversion, was carried out for the structure of the crust under the station Igaratá, where the Moho interface was found at approximately at 33 km depth.

Introdução

O estudo da estrutura da crosta é de fundamental importância para o conhecimento do processo de geração e evolução crustal de uma determinada região.

Em 1992, iniciou-se o projeto BLSP (*Brazilian Lithospheric Seismic Project*) com a participação da Universidade de São Paulo e o Instituto de Carnegie, onde foram instaladas várias estações de banda-larga no Sudeste do Brasil com sensores STS-2 e registradores RefTek com objetivo de estudar a litosfera. Com isso, Assumpção et. al. 2001 obtiveram resultados preliminares para espessura da crosta na região. Neste trabalho limitamos a estudar a Faixa de Dobramentos Ribeira que compreende o domínio que se estende pela região costeira da altura do paralelo 20° no Espírito Santo até o sul do Paraná.

O objetivo deste trabalho é mostrar as investigações para crosta na região da Faixa Ribeira usando a Função do Receptor e comparar com valores já obtidos na literatura.

Função do Receptor

A função do receptor é um dos métodos sismológico para o estudo da estrutura da crosta e é uma técnica recente, se comparada com outras técnicas. Este método pode fornecer um melhor detalhamento da estrutura da crosta, como por exemplo determinando até a espessura de camadas sedimentares de bacias. O método foi desenvolvido por Langston (1977,1979) para eliminar os efeitos da fonte, assim como dos instrumentos que influem nos sismogramas observados em um dado evento telessísmico.

Langston mostrou que a onda P de um sismo distante (telessismo) ao atingir a base da crosta, próximo à estação com um ângulo quase na vertical, parte da energia desta onda é convertida em S ao ser refratada na descontinuidade da Moho (denominada onda Ps) e também em reflexões múltiplas (ondas convertidas e reverberadas na crosta). Devido ao ângulo de incidência ser quase na vertical, a onda P direta será registrada com amplitude bem maior na componente vertical, ao passo que a onda Ps terá amplitude maior na componente horizontal. Portanto, através da deconvolução da componente horizontal com a vertical obtém-se a função do receptor, que normalmente tem a chegada da onda Ps aproximadamente 5 s após a onda direta (Langston, 1977, 1979, Owens et. al., 1984, 1987).

Embora sejam necessárias algumas informações adicionais (e.g., razão V_P/V_S, ou dispersão de ondas superficiais) para definir a espessura crustal, devido a uma certa ambigüidade na inversão da função do receptor para o perfil de velocidades (e.g. Ammon et. al., 1990, 1991), uma grande quantidade de dados de boa qualidade em uma única estação permitem definir a função do receptor com pouco ruído, uma boa estimativa na espessura da crosta, mesmo com poucas informações adicionais.

A informação adicional para faixa Ribeira foi um levantamento de refração sísmica profunda realizado por Bassini em 1986. O modelo de Bassini foi modificado por ter uma velocidade para crosta in-

1-V (km/s)	Z (km)	2-V (km/s)	Z (km)
$5,67 \pm 0,02$	0,0	$5,66 \pm 0,02$	0,0
$6,31 \pm 0,02$	7,6	$6,4 \pm 0,01$	8,0
$8,08 \pm 0,06$	36,3	$6,6 \pm 0,03$	25,0
-	-	$8,05 \pm 0,03$	38,2

Tabela 1: Parâmetros obtidos para o perfil Sorocaba/ITA por Bassini(1) e neste trabalho (2).

ferior muito baixa (6.31 km/s), já que, Assumpção et. al. 2001 chegaram a um valor idêntico para a profundidade da interface crosta-manto na região usando uma velocidade média Vp = 6,5 km/s na crosta. Para chegar a uma conclusão melhor para a região, decidimos reinterpretar o perfil obtido por Bassini.

Ajustamos a curva de tempo de percurso reduzido (t-x/7) versus distância epicentral, por tentativa e erro. A diferença principal da análise está em três chegadas interpretadas como chegadas primárias (Pg-onda P na crosta superior, P*-refratada na interface crosta superior/inferior e Pn-onda refratada na descontinuidade da Moho) que sofreram um nova interpretação de onda refletida, como por exemplo, PmP (corresponde a reflexão supercrítica em Moho). Na tabela 1 estão os valores encontrados para as velocidades e as espessuras com o erro para o ajuste de velocidade.

Análise do dados

A Fig. 1 mostra as cinco estações localizadas na Faixa Ribeira [SPB (Sorocaba-SP), JUQB (Juquiá-SP), IGAB (Igaratá-SP), PARB (Paraibuna-SP) e BRSB (Brasópolis-MG)] onde foram calculadas as funções do receptor. Duas estação já foram desativadas, que são a BRSB e PARB. As funções foram calculadas pela deconvolução da componente vertical das componentes radial e transversal, usando-se um filtro gaussiano $[\exp(-\omega^2/4\alpha^2)]$ com o parâmetro $\alpha = 2$, o que representa um filtro passa-baixo com freqüência de corte de 0,4 Hz. Para cada traço, o melhor valor de nível d'agua (usado para estabilizar a deconvolução) foi escolhido entre 0.01 e 0.001. O tamanho do registro também foi diferente para cada sismo, buscando-se a duração com melhor resultado em termos de ruído na função do receptor. As funções foram calculadas usando rotinas fornecida por Charles J. Ammon.

A Fig. 2 mostra as funções do receptor empilhadas para diferentes distâncias e azimutes para estação IGAB, com isso melhorando a razão sinal-ruído. A função do receptor na componente radial

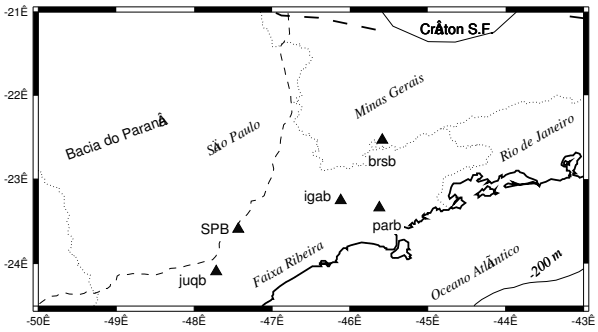

Figura 1: Estações sismográficas de banda-larga usadas no estudo (triângulos).

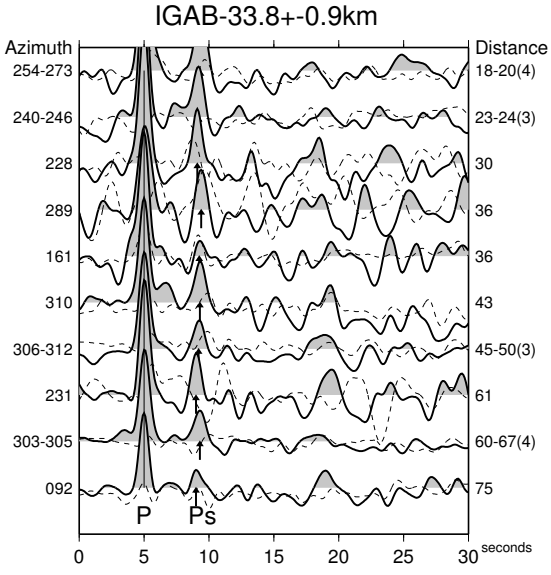

Figura 2: Exemplo de funções empilhadas para vários azimutes e distância para estação IGAB, Igaratá-SP. As linhas sólidas representam as funções radiais e as tracejadas as transversais. A seta marca o tempo da chegada Ps. O número de traços usados no empilhamento está indicando em parêntese, ao lado do intervalo de distância. Os empilhamentos foram ordenados por vagareza média. P é onda direta e Ps é onda convertida da Moho.

é representada por um traço contínuo e na componente transversal por um tracejado. O número de traços usado nos empilhamentos está indicado entre parêntese, ao lado do intervalo de distância. A seta na Fig. 2 indica a leitura da chegada da onda Ps (conversão de P para S na Moho). A componente transversal indica o grau de variabilidade lateral pois se a estrutura fosse constituida de camadas horizontais perfeitamente homogêneas, a componente

transversal seria nula.

A identificação da fase Ps é feita tanto pela sua amplitude (é um dos maiores picos, depois da onda direta) como pela *move-out* (NMO), i.e., pela diminuição da diferença de tempo com a onda direta (tempo "Ps-P") com aumento da distância epicentral. As funções do receptor mostradas na Fig. 2 podem ser todas corrigidas por NMO, para simular uma incidência vertical, alinhando todas as fases Ps. A Fig. 3 mostra o resultado, para cada estação, do empilhamento de todas as funções após a correção NMO. Observa-se a diferença Ps-P menor para estações mais próxima a costa, com exceção de JUQB.

Com o modelo de velocidade obtido na reinterpretação do levantamento refração sísmica profunda, podemos adotar um modelo de velocidades crustais médias (V_p e V_S), para calcular a espessura da crosta sob cada estação. O modelo tinha duas camadas de mesma espessura para crosta com a velocidade da onda P para a camada superior de 6.08 km/s e para inferior de 6.51 km/s. A Tab. 2 mostra os resultados obtidos para estas espessuras. Nesta tabela o tempo $(Ps-P)_\circ$ é o tempo Ps-P para incidência normal. Este tempo é obtido pela correção *move-out* de cada empilhamento simulando um incidência vertical. Os seja, $(Ps-P)_\circ$ é diferença de tempo entre as ondas P e S num percurso vertical por toda crosta, o que é uma informação útil para determinação da estrutura crustal.

A Tab. 2 mostra que as estações de Igaratá e Paraibuna têm espessuras crustais menores (34 e 35 km) do que as demais (38 a 40 km). As duas estações de crosta mais fina estão mais próximas da

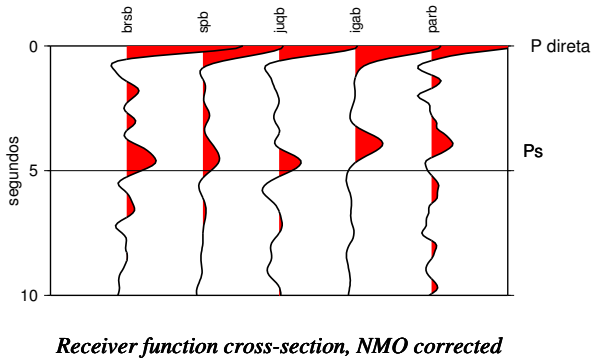

Figura 3: Seção com correção *move-out* das funções do receptor. Cada função foi empilhada após correção do *move-out* da conversão da P-para-S para uma incidência vertical. Note que a fase Ps chega mais tarde para estações mais distantes da costa (exceto JUQB).

estação	período	sismos	crosta *(km)*	$(Ps-P)_\circ$ *(s)*
JUQB	1999-00	9	40	4,6
BRSB	1998-99	-	40	4,6
IGAB	1999-00	20	34	3,9
PARB	1993-94	-	34	3,9
SPB	1996-97	14	38	4,4

Tabela 2: Dados das análises de Função do Receptor. "Crosta" é a espessura da crosta e "sismos" é o número de sismos.

costa, o que é consistente com o afinamento crustal devido a passagem da crosta continental/oceânica.

Com as funções bem definidas, partimos para fase da inversão dos dados, inicialmente para a estação IGAB, com as rotinas de C.Ammom (*Saint Louis University*). A metodologia da inversão usada nos programas é o algoritmo chamado "*jumping*" que foi desenvolvido por Parker, 1977 e permite a solução para o modelo de velocidade em cada iteração e não o vetor de correção do modelo de velocidade. Desta forma o vínculo mínimo de aspereza é diretamente aplicada ao modelo de velocidade.

Para fazer a inversão usamos o modelo de velocidade inicial obtido para região através da reintepretação do perfil Sorocaba/ITA. De acordo com Ammon, o procedimento de inversão inclui três diferentes passos de inversão. Primeiro, uma inversão simples é realizada para estimar o número de iterações necessárias para convergência. Depois um conjunto de inversões com várias asperezas, com objetivo de determinar o valor do peso da aspereza no cálculo final da inversão. Finalizando, a dependência do modelo inicial é explorada usando o número de iterações obtido inicialmente, e o peso da suavidade obtida na segunda etapa. Cada um dos três passos utiliza differentes programas de inversão (*http://www.eas.slu.edu/People/CJAmmon* de C. Ammon).

Inicialmente exploramos a primeira etapa, usando o empilhamento que tem azimute NW a uma distância epicentral média de 64 km e vagareza de 0,059 s/km. Após correr o programa foi observado que com cinco iterações já era possível chegar uma convergência aceitável. A Fig. 4 apresenta o dado real com o traço azul e o resultado da inversão. Ao lado do traço está o modelo correspondente à Função do Receptor e o modelo inicial usado na inversão. O pico Ps está bem ajustado e podemos chegar à conclusão que a interface crosta-manto sob a estação IGAB está a uma profundidade de 33 km aproximadamente.

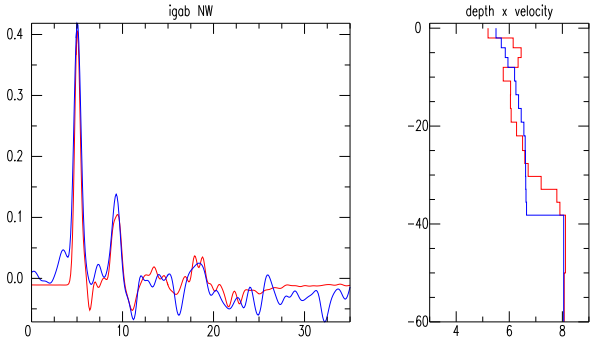

Figura 4: Inversão sob a estação IGAB, azimute NW. O traço azul é dado real e vermelho o sintético.

Comentários

O nosso objetivo é chegar a um modelo de velocidade sob as estações na Faixa Ribeira e obtemos inicialmente a profundidade da Moho sob as estações. Podemos observar o afinamento crustal na Fig. 5 onde as estações próximas à costa têm espessura mais finas comparadas às demais, exceto a estação em Juquiá e também podemos observar o gradiente positivo de anomalia bouguer em direção à costa. Provavelmente o modelo de velocidades sob Juquiá não tenha o mesmo padrão das demais estações.

Quanto à inversão estamos na fase inicial e notamos que com somente um empilhamento em uma estação chegamos a um resultado plausível, ao já obtido por Ps-P, com relação à interface crosta-manto ($\approx 33km$) sob a estação. O modelo de velocidade para crosta sob IGAB ainda é um trabalho inicial, mas podemos observar a semelhança do sintético com o dado real.

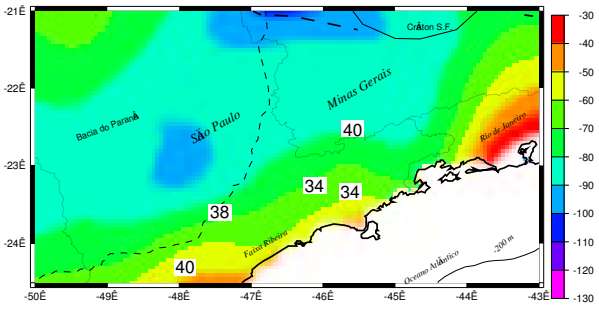

Figura 5: Espessura crustais (km) obtida por função do receptor para região de estudo em conjunto com anomalia Bouguer (mGal).

Agradecimentos

George Sand e Marcelo Assumpção agradecem ao CNPq e à Fapesp pelo apoio financeiro, ao técnico José Roberto Barbosa (IAG) pelo apoio de campo, a Charles Ammon pelo programas. Os mapas foram feitos usando GMT (Wessel and Smith, 1991).

Referências

[1] Ammom, C. J., G. E. Randall & G. Zandt, 1990, On the nonuniqueness of receiver functions inversions: J. Geophys. Res., **95**, 15303–15318.

[2] Ammom, C. J., 1991, The isolation effects from teleseismic P Waveforms: Bull. Seism. Soc. Am., **81**, 2504–2510.

[3] Assumpção, M., D. James & J. A. Snoke, revised version janeiro-2001, Crustal Thicknesses in SE Brazilian Shield with receiver function: Implications for Isostatic Compesation.Submitted to J. Geophys. Res.

[4] Bassini, A. M. 1986, Levantamento sismográficos na região sudeste do Brasil: Dissertação de Mestrado, Instituto Astrônomico e Geofísico/USP.

[5] Langston, C. A., 1977, The effect of planar dipping structure source and receiver responses for constant ray parameter: Bull. Seism. Soc. Am., **67** , 1029–1050.

[6] Langston, C. A., 1979, Structure under Mount Rainier, Washington, inferred from teleseismic body waves: J. Geophys. Res., **85**, 4749–4762.

[7] Owens, T. J., G. Zandt and S. R. Taylor, 1984, Seismic evidence for an ancient rift beneath the Cumberland plateau, Tenneesses: a detailed analysis of broadband teleseismic P waveforms: J. Geophys. Res., **89**, 7783–7795.

[8] Owens, T. J., S. R. Taylor and G. Zandt, 1984, Crustal structure at regional seismic test network stations determined from inversion of broadband teleseismic P waveforms: Bull. Seism. Soc. Am., , **77**, 631–662.

[9] Parker, R. L.,1977, Understanding inverse theory: Ann. Rev. Earth Planet Sci., **5**, 35–64.

[10] Wessel, P and W. H. F. Smith, 1991. Free software helps maps and displays data: Eos Trans. AGU, **72**(441), 445–446.

Paraguay Seismicity during 2000

L. Barros, V. Marza, C. Chimpliganond and D. Caixeta
Seismological Observatory , University of Brasilia, Brazil

Abstract

The work presents and analyses the recent earthquake activity in Paraguay, as detected by the Itaipu Binacional Seismograph Network during the year 2000. The discussion of Paraguay seismicity during 2000 is placed in the wider frame of the available historical seismicity of Paraguay based on all available data from various sources, as well. The main outcome of the presentation is to call attention on the April 28, 2000 event, m_R = 3.9 (Marza et al. 2000) and the subsequent smaller events occurring in the areas of Yacyreta and Ypacarai reservoirs. We find pretty compelling evidence that the events of the year 2000 associated with the Yacyreta reservoir were possibly triggered earthquakes, while the event close to Ypacarai natural lake, is associated with usual tectonic activity.

Introduction

The Itaipu Binacional Seismograph Network (ISN), composed by six remote stations, operating by radio telemetry has contributed to the monitoring of Paraguay seismicity, since its implantation, in 1981. The ISN was for a while (1981-1994) the sole current seismic system for regional monitoring of Paraguay detecting Paraguayan earthquakes with magnitudes between 2,5 and 5,6 m_b (Veloso et al., 1994). Recently, a seismograph station (CPUP) was installed in Paraguay, part of the GTSN (Global Telemetered Seismograph Network) Project, entered in operation only seven years ago (1994).

In April 28, 2000 an earthquake of magnitude 3.9 m_b was detected, having its epicenter relatively close to Yacyreta Reservoir, on the Paraná River, located in Paraguay-Argentina border region. This earthquake, reached an intensity of VI (MM), in the Itapuá and Misones districts, frightening the local population. With that occasion, the Seismological Observatory (SIS) of the University of Brasilia (UnB), having working in the region for 22 years, in agreement with Itaipu Binacional company for monitoring the Itaipu Binacional reservoir, issued, a special report, where the event was analyzed (Marza et al., 2000). Later, in December 2000, other three smaller earthquakes were detected in the region, with magnitudes ranging between 2.5 and 2.8 m_D.

This work presents the basic source parameters of the four recent events that occurred during 2000 and of the previous seismicity based on data available in the Seismic Data Base of SIS-UnB.

Itaipu Binacional Seismograph Network (ISN)

The ISN is composed of six remote stations, three of them situated in Brazil and other three in Paraguay. Figure 1 shows the Itaipu Binacional reservoir map, indicating the location of the stations composing the ISN. The analog signals of these stations are sent by radio to a central station, located in the structure of the dam, elevation 214 m, where they are digitized and recorded. Time signals of a GPS clock together with a tri-axial accelerometer signals are recorded in the same acquisition and data recording system (Fig. 2).

Fig. 1 - Itaipu Binacional Reservoir Local Seismographic Network.

Two seismic data acquisition, detection and analysis systems work in parallel, one operates with 24 bits resolution under a Windows operating system (ViSeis System) while the other operates within 12 bits resolution under a DOS operating System (PCQuake System).

The SIS/UnB can access this system, from Brasilia headquarters, using dial up line or Internet, for remote control or data retrieval. Figure 2 shows the block diagram of the reception and the Central Recording Station.

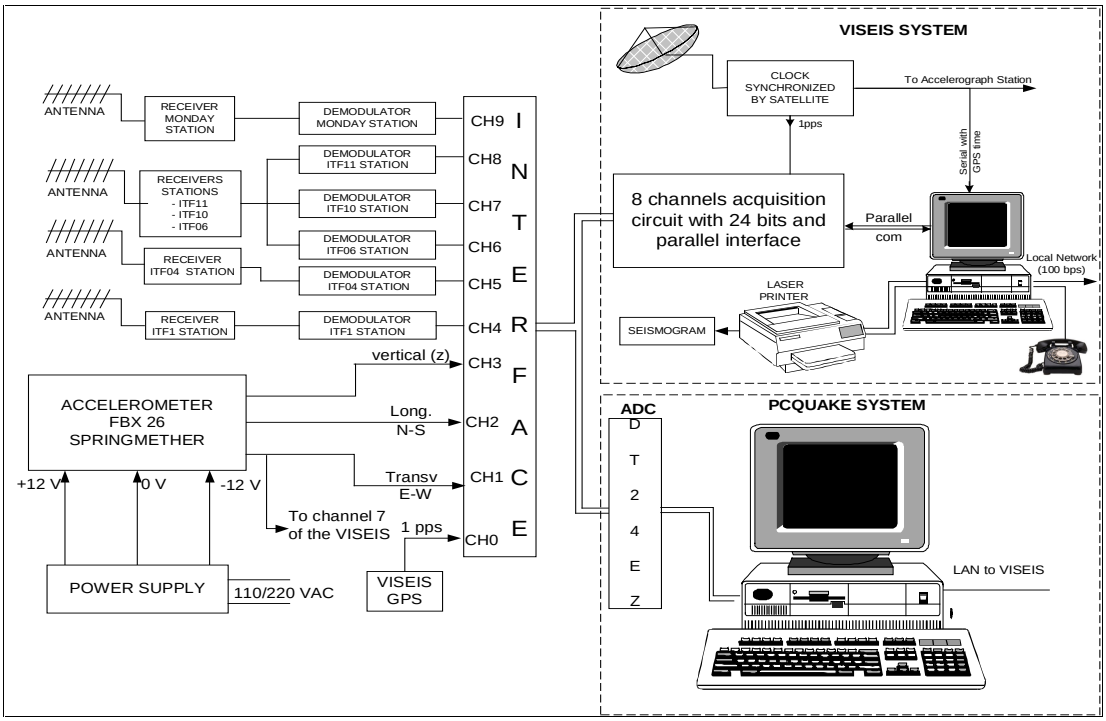

Figure 2 - Block diagram of the reception, acquisition and data recording systems (ViSeis and PCQuake) in the Central Station. Note the accelerometer signals being recorded together with the seismic signals.

Historical Seismicity of Paraguay

Paraguay, located in the central part of the South American Plate, between the Andean orogen and the Paraná Basin in South Brazil, is a region with very low seismicity compared with the Andean countries and related literature is very scarce (Velázquez, 2000).

The local instrumental monitoring of the Paraguay begun with the installation of the first station (ITA1) of the ISN, in January, 1979, and it was gradually upgraded with the deployment of the ISN network and GTSN/IMS station (CPUP). Table 1 summarizes the evolution of the completeness thresholds in Paraguay.

Table 1 - Detection threshold for Paraguay from 1950 to 1994 (updated after Assumpção, 1998)

Year	Magnitude	Commentary
1950	6.0	Summary of the International Seismological
1962	5.0	Deployment of the WWSSN Network
1968	4.0	Start operation of the SAAS (South American Array System) in Brasilia
1975	3.5	Start local seismographic Network of USP and UnB.
1979	2.5	Start of ITA1 Seismographic Station in Itaipu
1994	2.0	GTSN Station in Paraguay (CPUP)

Table 2 and the map in Fig. 3 show all Paraguay events present in the SIS-UnB and NEIS Database. As one can see, they are situated in two different regions divided by the Paraguay River: one in the western part in the Paraguay-Argentina boundary, whose seismicity in great part is associated with the Nazca plate subduction and another region in the central and southern part of the country with shallow earthquake as suggested by Assumpção (1992); Berrocal and Fernandes (1996).

Paraguay Seismicity (during 2000) as detected by ISN

The Itaipu Binacional Seismograph Network detected in the year of 2000, four regional events with epicenters in Paraguay, whose source parameters are listed in Table 2 and their epicenters are indicated in Fig. 3. The largest magnitude event (3.9 m_b), occurred in 2000/04/28, was located by the ISN and wide band three component GTSN station (CPUP). Figures 4 and 5 show the waveforms registered. Inherently, the instrumental locations of all earthquakes during 2000 are poor and certainly they are strongly scattered from their true locations, however the microseismic data can help to better place their origin close to Yacyreta reservoir or Ypacarai lake (cf. Velázquez J.C., 2001, personal communication).

Ypacarai is a smaller lake, located some 30 km east of Asuncion City, and crossed by a known tectonic active fault.

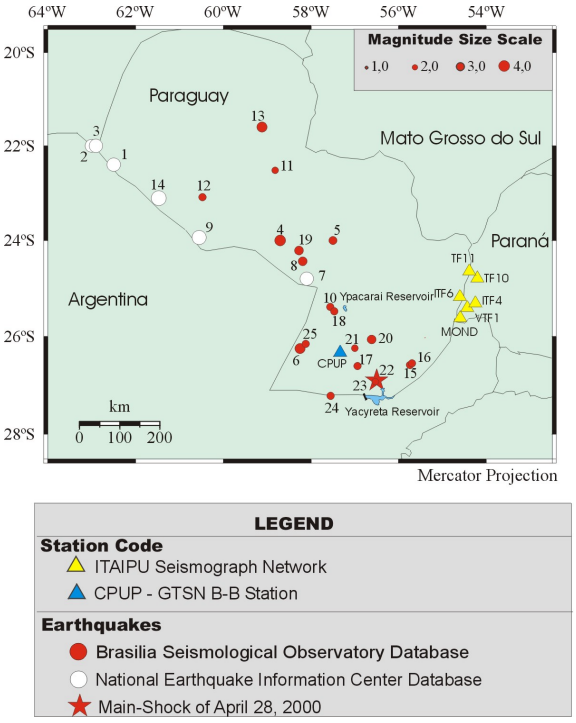

Fig. 3 - Map of Paraguay Seismicity according to Table 1. Events 22 to 25 belong to the seismicity of the year 2000.

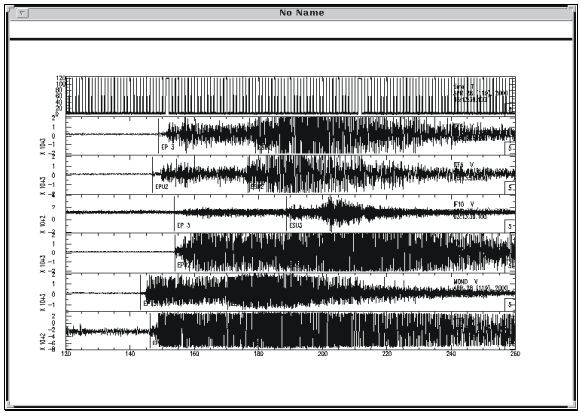

Figure 4 - Waveforms (vertical component) of the April, 28, 2000 Paraguay earthquake, registered by stations of ISN (Channel 1 - time code(IRIG); channel 2 - ITF4 Station; channel 3 - ITF6 Station; channel 4 - ITF10 Station; channel 5 - ITF11 Station; channel 6 - Monday Station and channel 7 - VTF1 Station).

Macroseismic data based on newspapers information (Noticias del Paraguay and ABC, editions of 2000/04/29), indicate the boundary of Paraguay-Argentina as the area of biggest intensity. The event was probably also felt in Argentina, however, no information was available in the Paraguay newspapers.

The probable RIS of the Yacyreta Reservoir

The Yacyreta Reservoir is a bi-national Paraguay-Argentina enterprise located in the boundary of these two countries, with a capacity of generating 3,200 MW of energy. The first turbine, of 160 MW, entered in operation in September, 02, 1994 and the last (twentieth) in July, 02, 1998. The barrage has a height of 83 m flooding an area of 1,600 km^2 with a volume of 21 x 10^9 m^3 (Yacyreta Bi-National Company, Online).

During December 2000 in the areas of both reservoirs was reported felt microearthquake activity (Velázquez J.C., 2001, personal communication). This is an indirect evidence that, in the ranges of location errors, the events #22,23 and #25 (in Table 2) occurred probably close to Yacyreta and Ypacarai reservoirs, respectively, the last one, however considered as natural manifestation of the tectonic activity of the area.

On the other hand, we must highlight, however, the low seismicity of the Paraná Basin, especially in its central part, considered one of Brazil's most aseismic areas. The Itaipu Binacional Reservoir with more than 22 years of uninterrupted Seismographic monitoring has never presented induced seismicity.

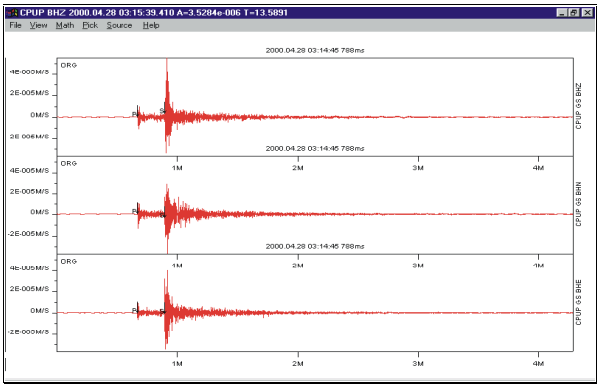

Figure 5 - Waveform registered by CPUP Station (GTSN), of the April, 28, 2000 Paraguay earthquake. The movement components (from up to bottom) are: vertical (Z), horizontal (N-S) and horizontal (E-W) with a high filter of 2 Hz and 4 polo. Phases P and S are marked in the seismograms. The vertical axis of the seismogram represents the ground velocity in m/s of each component and the horizontal axis indicates the time in minutes.

Table 2 - Source parameters of the events in Paraguay

	Data yyyy/mm/dd	Origin Time (UTC) hh:mm:ss			Depth (km)		
1	1947/08/31	06:17:29	-22.40º	-62.50º	223	5.2 m_b	NEIC-USGS
2	1959/05/30	03:07:03	-22.00º	-63.00º	500	4.9 m_b	NEIC-USGS
3	1961/04/28	08:40:26	-22.00º	-62.90º	82	5.1 m_b	NEIC-USGS
4	1979/01/16	05:38:24	-24.00º	-58.70º		4.0 m_b	SIS-UnB
5	1979/07/20	07:00:37	-24.00º	-57.50º		3.0 m_b	SIS-UnB
6	1980/11/20	22:29:07	-26.25º	-58.25º		3.8 m_R	SIS-UnB
7	1982/04/08	05:58:52	-24.80º	-58.10º	33	5.1 m_b	SIS-UnB/NEIC-USGS
8	1984/03/07	03:18:50	-24.44º	-58.19º		3.3 m_b	SIS-UnB
9	1985/04/12	14:34:54	-23.94º	-60.55º	24	5.3 m_b	SIS-UnB/NEIC-USGS
10	1986/12/11	05:27:10	-25.39º	-57.56º		2.8 m_R	SIS-UnB
11	1988/10/15	07:18:57	-22.52º	-58.82º		2.6 m_R	SIS-UnB
12	1988/10/17	06:27:47	-23.09º	-60.47º		2.8 m_R	SIS-UnB
13	1988/10/17	07:51:28	-21.60º	-59.12º		3.9 m_R	SIS-UnB
14	1989/02/28	13:01:58	-23.11º	-61.47º	569	5.6 m_b	SIS-UnB/NEIC-USGS
15	1989/09/21	02:59:19	-26.59º	-55.74º		2.7 m_R	SIS-UnB
16	1989/10/20	22:58:54	-26.55º	-55.70º		2.8 m_R	SIS-UnB
17	1990/09/20	20:54:27	-26.61º	-56.94º		2.8 m_R	SIS-UnB
18	1990/11/13	08:42:41	-25.48º	-57.47º		2.9 m_R	SIS-UnB
19	1994/02/09	12:14:05	-24.21º	-58.27º		3.4 m_R	SIS-UnB
20	1995/10/04	18:43:12	-26.06º	-56.62º		3.4 m_R	SIS-UnB
21	1998/05/06	04:27:41	-26.24º	-57.00º		2.6 m_R	SIS-UnB
22	2000/04/28	03:15:49	-26.90º	-56.50º	5	3.9 m_R	SIS-UnB
23	2000/12/01	00:28:42	-26.93º	-56.53º		2.5 m_D	SIS-UnB
24	2000/12/18	01:31:40	-27.22º	-57.55º		2.8 m_D	SIS-UnB
25	2000/12/21	04:43:34	-26.15º	-58.12º		2.8 m_D	SIS-UnB

Source: National Earthquake Information Center, USGC, and SISBRA Database, SIS/UnB.

Conclusions

The local seismographic monitoring of Paraguay begun after the deployment of the first station (ITA1) ISN, in 1979. Since then earthquake with magnitude above 2,5 has being detected in Paraguay. Before then only earthquake with magnitude over 5,0 m_b were detected by the Worldwide Seismographic Network.

The Paraguay seismicity clearly presents two seismogenic zones: one in the western and other in the eastern, both divided by the Paraguay River, as defined by Assumpção (1992) and Berrocal & Fernandes (1994).

In the year 2000 four regional events were detected by ISN, three of them probably could be associated with induced seismicity in the Yacyreta Reservoir, located in the Paraguay-Argentina boundary. To validate the case of RIS at Yacyreta, at least one seismographic station should be installed in the reservoir area.

References

Assumpção, M. Seismicity and stresses in the Brazilian Passive Margin. *Bull. Seism. Soc. Am.*, **88,** 160-169, 1998.

Assumpção, M. The regional intraplate stress field in South America, *J. Geophys. Res*. **97**, 11,889-11,903, 1992.

Berrocal, L. Fernandes C. Seismicity in Paraguay and Neighboring Regions, Alkaline Magmatism in Central-Eastern Paraguay. São Paulo, 1996.

Jornal Notícias del Paraguay, edition of 29/04/2000.

Jornal ABC del Paraguay, edition of 29/04/2000.

SIS-UnB Database of the Seismological Observatory University of Brasilia.

SIS/UnB - Reports (nºs 18- 23, 30-35, 40, 46, 50, 54, 55, 64, 68, 72, 74, 85, 95) Agreement FUB/Itaipu Binacional.

Marza, V. Barros, L. Soares, J. The Paraguayan earthquake of 2000/04/28, Special Report, Seism. Obs., Univ. of Brasilia, 12 pp., 2000 (in Port.).

Velázquez, R. J. F. - Earthquakes in Paraguay - An Appraisal, *Bull. Int. Inst. Seism. Earthq. Eng.* **34**, p. 75-77, 2000.

Veloso, J. A. V., Soares, J. E. P. & Velasquez, J. C. - Earthquake in Paraguay: An appraisal, Regional Seism. Ass. in South America, Brasilia, 1994.

Yacyreta Bi-National Comp. (La Entidad Binacional Yacyreta) (Online) http://www.eby.org.ar/html.

Acknowledgements

The authors which to express their sincere thanks to all the people who contributed direct or indirectly to the accomplishment of this work, in particular to, Eng. Evangelista C. Porto (Itaipu Binacional), Dr. J.C. Velázquez (University of Asuncion) and Mr. Pedro F. de Andrade (SIS-UnB).

Parámetros geológicos de la deformación superficial cosísmica asociada al terremoto de Mendoza de 1861 (Ms: 7.0), Argentina

Francisco A. Mingorance, U.N.Cuyo, Argentina

Abstract

Surface primary faulting accompanying the great Mendoza Earthquake of 1861 in western Argentina, produced a section of fault scarps 3.5 km long. The 1861 multiple fold scarp formed entirely along an older prehistoric scarp, and the amount of maximum coseismic displacement was 1.60 m. The mechanics of surface and near-surface deformation is dominated by fault propagation folding. Geomorphic, morphometric and stratigraphic information suggests that the La Cal fault repeated the same slip pattern during both, the 1861 earthquake and the most recent prehistoric event.

Introducción

El conocimiento sobre la deformación cosísmica asociada a terremotos históricos, proviene de observaciones directas o de correlaciones (mucho tiempo después del terremoto) de los rasgos geológicos superficiales con eventos específicos. En ambientes tectónicos compresivos, la deformación superficial cosísmica involucra cambios horizontales y verticales, por lo tanto, los parámetros geológicos resultantes presentan variaciones significativas, aún para una misma fuente sismogénica.

La mecánica de la deformación superficial asociada a fallas compresivas es compleja e involucra no sólo a fallamiento puro, sino también a combinaciones de fallamiento y plegamiento cercano a la superficie. Debido a ello, existe una amplia variedad de geoformas características en este tipo de ambiente tectónico.

La falla activa La Cal fue estudiada por métodos paleosísmicos y morfométricos con el objeto de aportar información científica sobre el carácter y tamaño de la deformación cosísmica asociada al terremoto de 1861, y sobre su mecanismo de deformación superficial.

Falla Activa La Cal

La falla sismogénica La Cal es una estructura compresiva (Thrust Fault) de 30.7 km de longitud (Figura 2), que deforma y desplaza superficies geomórficas aluviales de edades Pleistocena Superior y Holocena, generando geoformas que evidencian la recurrencia del fallamiento superficial (Escarpa de falla compuesta). La densidad del fallamiento es mayor en la parte norte, y la cantidad de desplazamiento vertical varía a lo largo del rumbo (hasta un máximo de 6 m).

La información proveniente de las secciones sísmicas realizadas por la industria petrolera, indica que este sobrecorrimiento migrando al E, despega en las calizas paleozoicas, las cuales afloran en el borde oriental del Cerro La Cal (Bettini, 1980).

Un estudio reciente sobre la geometría de la zona de falla La Cal, indica que su Extremo Norte se comportaría como un concentrador de esfuerzos e iniciaría la ruptura sísmica que se propagaría hacia el SE, para terminar en la parte mecánicamente más débil y simple del trazo de falla, su Extremo Sur (Mingorance, 2000).

Deformación Cosísmica Histórica

El terremoto de Mendoza de 1861 (Ms: 7.0) fue el evento sísmico más severo ocurrido en esta provincia de Argentina occidental (Figura 1) en los pasados 219 años. Este evento se caracterizó por la violencia del sacudimiento sísmico del terreno, el cual tuvo una dirección predominante NO – SE (Forbes, 1861). La reinterpretación de la abundante información histórica existente, indica que la distancia focal se habría localizado entre 20 y 40 km de la ciudad de Mendoza (Inpres, 1986).

A pesar de los tres informes geológicos posteriores al terremoto (Cirvini, 1989), la deformación superficial cosísmica no fue específicamente reportada como tal. La utilización errónea del término *Agrietamiento Superficial*, ligada a inspecciones de campo posiblemente insuficientes, serían algunas de las causas de esta falta de descripción detallada. Agrietamiento superficial del terreno (dirección N – S), sin especificar su génesis, fue reportado desde el extremo NO del área estudiada (Figura 2) hasta prácticamente el sector central del trazo de falla La Cal (Verdaguer, 1932).

Uno de los estudios iniciales sobre la tectónica de la Precordillera postula que el sobrecorrimiento Salagasta (Falla La Cal), que se extiende hasta la parte sur de la ciudad de Mendoza, es un testimonio inequívoco de movimientos tectónicos muy modernos (Keidel, 1907).

El único antecedente previo es el aportado por Bastías et al. (1993), quienes indican la existencia de fallamiento superficial histórico (Longitud: 8 – 10 km, Desplazamiento Máximo: 1.20 m) en el tramo central de la falla La Cal, pero sin asociarlo a ningún terremoto específico. Estos autores no caracterizan al tipo de evento, ni proponen un mecanismo de deformación superficial para esta fuente sismogénica.

El mapeo fotogeológico detallado (1:5.000) del fallamiento reciente, la utilización de fotografías de Bajo Ángulo de Inclinación Solar, y la medición de perfiles topográficos de detalle (análisis microgeomorfológico) a través de la escarpa de falla principal; hicieron posible la identificación precisa del tramo de falla que experimentó deformación

cosísmica primaria en 1861 (Figura 2). Por otro lado, las herramientas de la geomorfología tectónica y los principios básicos de la morfometría de escarpas de falla compuestas, fueron de vital importancia para diferenciar y cuantificar a los eventos histórico y prehistórico almacenados en el registro geomorfológico de la escarpa de falla La Cal (Figura 3).

La tabla I resume los parámetros geológicos de la deformación cosísmica asociada al terremoto de 1861, e incluye parámetros dimensionales relativos a la actividad tectónica prehistórica.

La manifestación superficial de deformación cosísmica primaria está representada por una Escarpa de Pliegue (Fold Scarp) Múltiple que reactivó a la escarpa principal preexistente (Figura 3). En este sitio, la deformación vertical histórica (A – B) alcanzó un valor de 1.25 – 1.30 m, mientras que el desplazamiento prehistórico máximo es de aproximadamente 1.50 m.

La escarpa histórica es interpretada como el resultado de la propagación hacia la superficie de la falla causal, con un ángulo moderado a bajo. Al momento de producirse el plegamiento superficial de estratos, parte del bloque levantado colapsa sobre el bloque hundido, produciendo una *Cara Libre* (cambios de pendiente) y una *Pendiente de Detritos* compuesta por remanentes del bloque levantado (Figura 3).

PARÁMETROS	DATOS
REACTIVACIÓN HISTÓRICA (1861)	
Longitud de ruptura superficial (Primaria)	3.5 km
Longitud de ruptura subsuperficial	5.5 km ?
Longitud total de ruptura (Superficial + Subsuperficial)	9 km
Desplazamiento superficial cosísmico	
Promedio	1.34 m
Máximo	1.60 m
Mecanismo de deformación superficial propuesto	Pliegue de propagación de falla
Tipo de evento	Múltiple
Geoforma resultante	Escarpa de pliegue (Fold Scarp)
DEFORMACIÓN PREHISTÓRICA	
Desplazamiento pre - terremoto de 1861	
Promedio (Area histórica)	1.33 m (Datos morfométricos)
Máximo (Area histórica)	1.55 m (Datos morfométricos)

Tabla I - Parámetros dimensionales de la deformación superficial cosísmica asociada al terremoto de Mendoza de 1861

Mecánica de la Deformación Superficial

Detallada información sobre la estructura interna de la escarpa de falla y sobre la mecánica de la deformación superficial, fue proporcionada por una trinchera exploratoria excavada a través del trazo de falla La Cal (Figura 4). El mecanismo de deformación superficial está controlado totalmente por Plegamiento de Propagación de Falla (Figura 5), el cual se resuelve internamente por fallamiento primario y secundario simultáneo (Evento Múltiple). El plano de falla **A** representa a la Falla Principal (Figura 4), y es responsable del 57% de la deformación vertical total (A + B + C : **1.50 m**). Si bien las evidencias y datos morfométricos (Figura 3 – Tabla I) y estratigráficos (Trinchera – Figura 4) documentan actividad tectónica prehistórica comparable a la deformación cosísmica máxima de 1861 (**1.60 m**); no se puede afirmar que aquella (Prehistórica) corresponda a un mismo evento. Estudios actualmente en ejecución arrojarán luz en este aspecto.

Figura 1 – Localización de la provincia de Mendoza.

Conclusiones

El tramo Norte de la falla La Cal se habría reactivado en 1861 (9 Km) produciendo deformación cosísmica primaria por unos 3.5 km, con un rechazo vertical máximo de 1.60 m. La mecánica de la deformación superficial influyó notablemente en la morfología y estructura interna de las escarpas histórica y prehistórica más reciente.

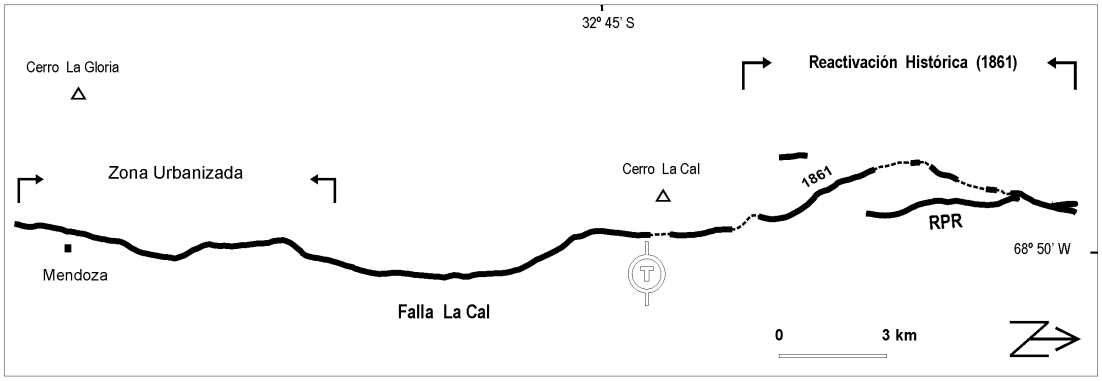

Figura 2 – Geometría, dimensión y posición del trazo de la falla activa La Cal. La fecha adjunta (1861) indica el tramo de falla que experimentó deformación superficial cosísmica primaria asociada al terremoto de Mendoza del 20 de Marzo de 1861. **RPR**: Ramal de falla Punta de Rieles. **T**: Localización de la trinchera exploratoria Minetti 1. El extremo Sur de la falla estudiada se prolonga por unos 10 km dentro del populoso Gran Mendoza.

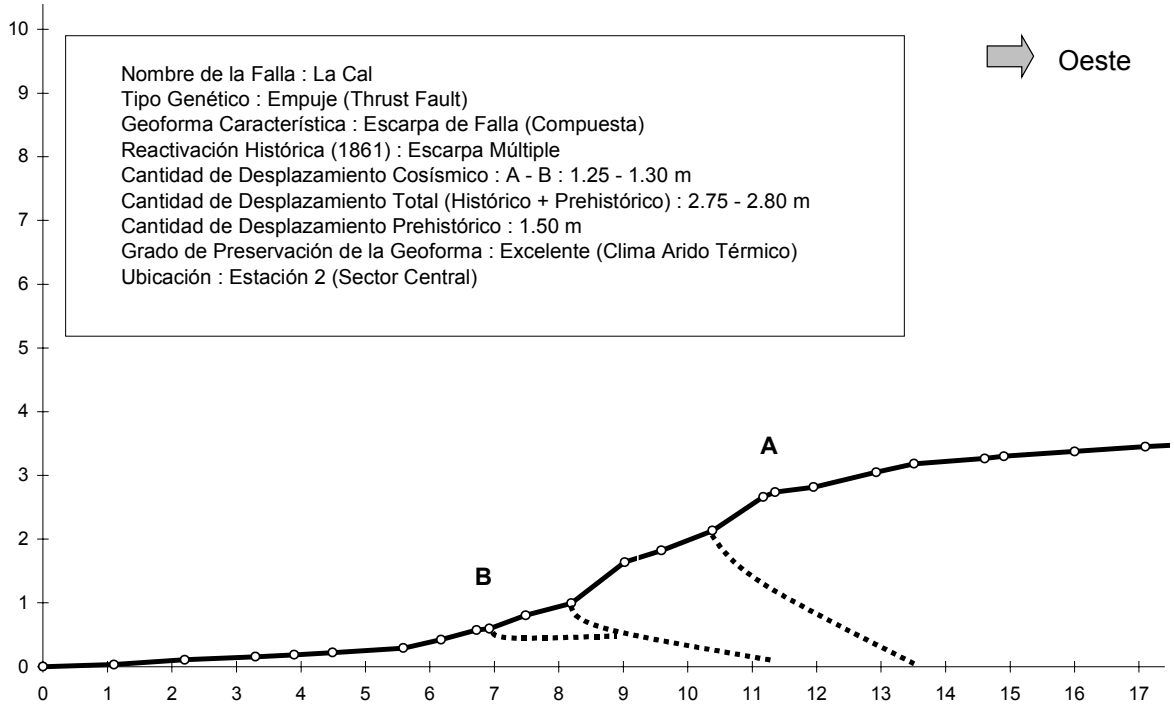

Figura 3 - Perfil topográfico de detalle medido a través de la escarpa de falla principal, evidenciando la reactivación histórica de 1861 (cambios de pendiente). La manifestación superficial de deformación cosísmica está representada por una Escarpa de Pliegue (Fold Scarp) Múltiple. El rechazo vertical total A – B (1861), determinado en base a un detallado análisis morfométrico de la escarpa de falla compuesta, incluye al desplazamiento superficial simultáneo de la falla principal y del fallamiento secundario asociado. El sitio analizado (Estación 2) se localiza en el sector Sur del tramo de falla que experimentó deformación cosísmica.

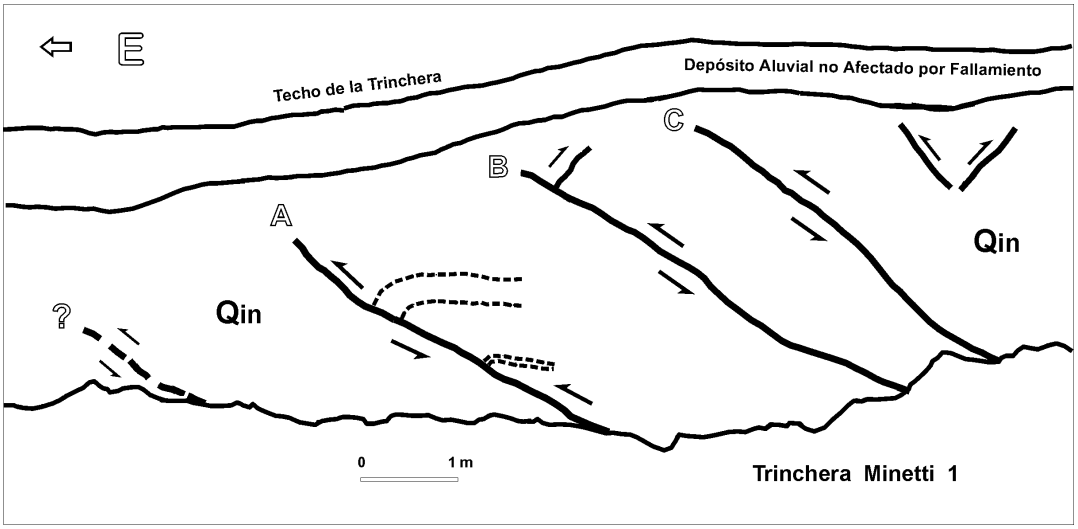

Figura 4 – Diagrama esquemático de la trinchera exploratoria Minetti 1 excavada a través del trazo de la falla La Cal. **A** : Falla Principal (16º - 25º O), **B** y **C** : Fallas Secundarias (30º O y 35º O). El evento prehistórico más reciente involucró a las tres fallas simultáneamente, produciendo un rechazo estratigráfico múltiple de 1.50 m. La mecánica de la deformación superficial es controlada totalmente por Plegamiento de Propagación de Falla. Este tramo de la falla La Cal no experimentó deformación cosísmica en 1861. Qin: Cuaternario Indiferenciado.

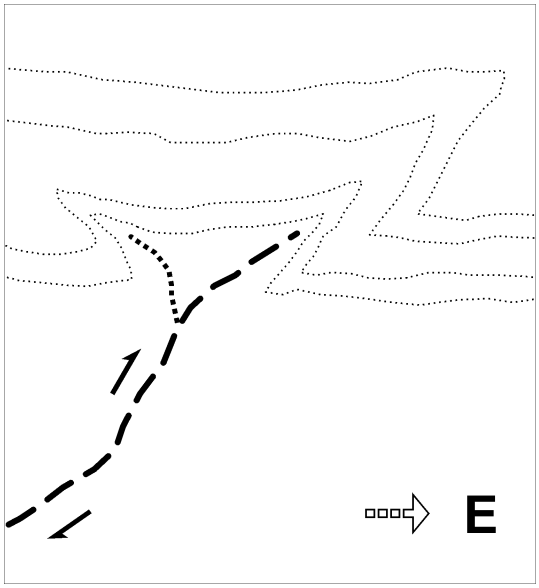

Figura 5 – Diagrama esquemático mostrando el plegamiento superficial de estratos de gravas gruesas, como resultado de la propagación hacia el Este de la falla secundaria **B** (trinchera). Cuando la superficie del terreno es deformada por este mecanismo se forma una Escarpa de Pliegue (Fold Scarp).

Referencias

Bastías, H., Tello, G., Perucca, L y Paredes, J., **1993**. Peligro sísmico y neotectónica. XII Congreso Geológico Argentino, V. Ramos (Ed.), Relatorio, VI (1): 645-658.

Bettini, F., **1980**. Nuevos conceptos tectónicos del centro y borde occidental de la Cuenca Cuyana. Revista de la Asociación Geológica Argentina, XXXV (4): 579-581.

Cirvini, S., **1989**. Los geólogos y el terremoto (1861-1862). La estructura profesional y técnica en la construcción de Mendoza (Capítulo II). IAIHAU, Mendoza: 61-78.

Forbes, D., **1861**. Informe sobre el terremoto de Mendoza del 20 de marzo de 1961. *In* Revista de la Junta de Estudios Históricos de Mendoza (1938), Tomo X: 111-120.

Inpres., **1986**. Gran Mendoza: El núcleo urbano expuesto al mayor nivel de riesgo sísmico en la República Argentina. Instituto Nacional de Prevención Sísmica, Publicación Técnica Nº 10, 57 p.

Keidel, H., **1907**. Sobre la estructura tectónica de los Andes argentinos. Sitzungsberichte der Akademie der Wissenschaften in Wien, Mathem. Naturn. Klasse. Tomo CXVI, Parte I: 649-674.

Mingorance, F., **2000**. Caracterización de la geometría de la zona de fallamiento activo La Cal, Mendoza, Argentina. IX Congreso Geológico Chileno, Actas, Vol. 1, Sesión Temática Nº 5: 800-804.

Verdaguer, J., **1932**. Historia eclesiástica de Cuyo. Tomo II, Capítulo XVI: 1361 p.

Receiver function in stratified sedimentary structure: Paraná basin

Iván Zevallos, Marcelo Assumpção**

Abstract

Receiver function technique is usually applied to studies of crustal and upper mantle estructures. We propose here to use in a shallow stratified medium of a sedimentary basin, using data from the seismografic stations deployed on the Paraná basin (BLSP Project) that recorded teleseismic signal of earthquakes in the west side of South America. Signal is processed to obtain the receiver function, then stacked to reduce noise. We applied an inversion technique to obtain a model of seismic velocities in the Paraná basin. As preliminary results, we found three main layers: a near surface ~400 m thick layer corresponding to Serra Geral basalts, under this the Botucatu sandstones with ~ 1.5 km thick, and below the rest of crust until the Moho at 39 km depth.

Introduction

In seismic exploration in the Paraná basin it is usually difficult to obtain good results because of the presence of a very strong reflector, volcanic rocks of Serra Geral formation with near 2 km thickness. A source of seismic energy are the earthquakes. Selecting some of these having a small incidence angle at the basement below the sedimentary pack (epicentral distance 15° to 20°), we avoid the attenuation from basaltic layer. The technique of receiver function uses the conversion of P to S waves at the interfaces of strata. The responses of radial and vertical components are different, being possible to isolate the conversions and reverberations by means of a deconvolution of both signals.

Data Processing

A seismographic station CAPB near Capivara reservoir (Paraná state) recorded four earthquakes with epicentral parameters show in Table 1. Receiver function analysis was applied to signal of each earthquake, then stacked, obtaining the pseudo-seismogram of Fig. 1 (solid line).

The peaks following the first P wave are reverberations in the sedimentary package (between 5 to 8 seconds in receiver function record). Our goal is to make a model of seismic velocities representing the structure of Paraná basin under CAPB station. We use initial depth constraints taken from MT surveys and borehole logs (Stanley et al., 1985). We invert for the S velocity in each layer keeping the depth to interfaces fixed.

Inversion of receiver function data is done using software of C. Ammon from S. Louis University (Ammon, 1991). Results are shown in Fig. 1. Solid line is the observed RF and dashed line is the theoretical curve. The model with the best fitting is in Figs. 2 and 3.

Preliminary results

The model obtained from the inversion shows three main features under CAPB station. Near the surface a thin layer, about 400 m, with V_s ~ 2.3-2.4 km/s, corresponding to a basaltic layer (Serra Geral formation). Below this we find a low-velocity layer with V_s down to 2.0 km/s about 1.5 km thick, maybe sandstones of Botucatu formation. Following in depth, seismic velocities return to a normal gradient and the next strong interface is the Moho at 39 km depth.

Conclusions

RF method can be applied to study the structure of sedimentary basins. P to S conversions within the sedimentary basin cause high amplitude peaks in the receiver function. Modelling receiver functions can thus provide good constraints on velocity profiles of sedimentary basins.

Bibliography

Ammon,C. (1991). *The isolation of receiver effects from teleseismic P waveforms.* Bulletin of the Seismological Society of America, 81, 2504-2510.

Stanley, W. et al. (1985). *Regional geotechnical surveys in hydrocarbon exploration, Paraná basin, Brazil* . The American association of Petroleum Geologists Bulletin,69, 346-360

*Universidade de São Paulo - Instituto Astronômico e Geofísico

Table 1: Epicentral parameters of earthquakes used in receiver function

Year	J. day	hh mm ss.ss	lat	long	depth km	m_b	dist. (°)	azimuth (angle)	slowness (s/°)
1995	160	05 35 49.3	-21.66	-68.03	131	5.2	15.7	270	12.3
1995	067	07 10 35.5	-22.14	-68.37	113	4.9	16.0	269	12.3
1995	045	15 53 56.9	-23.29	-67.70	155	5.7	15.3	265	12.3
1995	041	20 27 03.4	-19.77	-68.54	163	5.4	16.6	277	11.0

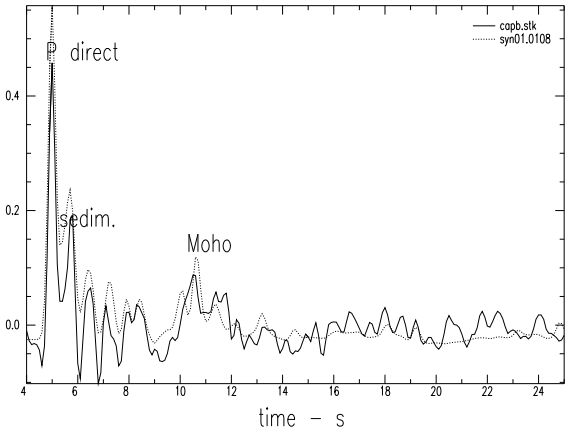

Figure 1: Receiver function stacked (solid line); inversion curve (dashed line). CAPB station.

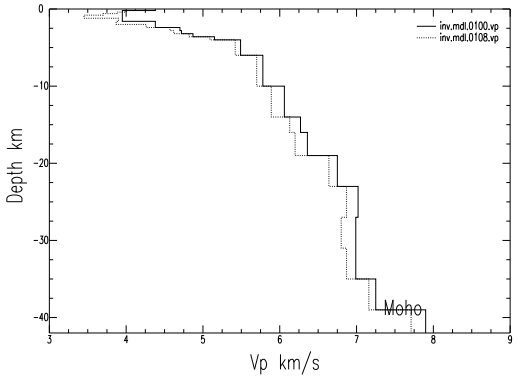

Figure 2: Model of best fitting inversion results. Solid line is starting model taken from a first inversion run, then used in the second inversion: dashed line is final model after 8 iterations. V_p/V_s ratio is 1.71; V_p is plotted in the x axis

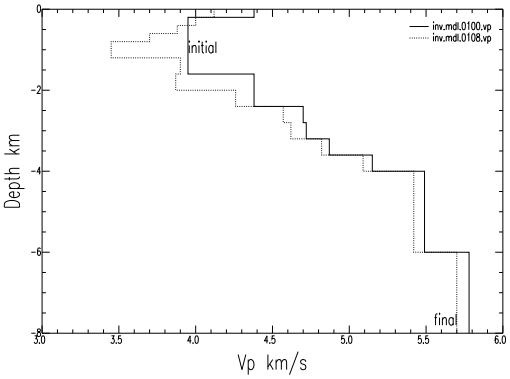

Figure 3: Inversion results of the upper layers. It is possible to see the negative gradiente of velocity corresponding to the basalt-sandstone transition.

Seismic Sequence in Porto dos Gaúchos/MT - Brazil After March/1998 Mainshock: Preliminary results

Lucas Vieira Barros, Vasile I. Marza, Daniel F. Caxeta, Juraci M. Carvalho

Seismological Observatory University of Brasilia - Brazil

Abstract

A 5.1 (m_b) magnitude earthquake happened on 1998/03/10, 23h32m (UTC), in the center-north part of Mato Grosso (MT) State, Brazil. This event was the second largest earthquake registered in the area and the largest one of the twelve already registered in Brazil. It was detected by stations located up to 150° away, affecting an area of approximately 220.000 km^2 with a maximum intensity of VI (MM). Three days after its occurrence, the Seismological Observatory of the University of Brasilia (SIS/UnB) installed the first seismographic station, especially setup to monitor events in that area – JUAB Station, belonging to a research project named AmazonScope, partially financed by FINEP according to PADCT/MCT (Program to Support Scientific and Technological Development of the Ministry of Science and Technology). Along the last three years a continuous seismic activity has been detected by a local seismographic network gradually deployed in the area.

The event of 1998/03/10 happened about 100 km to the northeast of the epicenter of the largest earthquake already registered in Brazil, 6.6 m_b, on 31/01/55 (Berrocal et.al., 1984). This earthquake was located by stations of the world wide network, located at teleseismic distances, therefore, an 100 km location error could occur and, in that way, the epicenter could be located in the same place as the event of 10/03/98 is, or, on the other hand, aligned along the same fault.

This work will present the first results, up to now disclosed in two reports emitted by SIS/UnB (Barros and Marza, 1998, Marza et al. 1999) with the purpose of informing the City Halls of the affected area and the National Civil Defenses and of the State of Mato Grosso about the evolution of the seismicity that has been monitored by SIS/UnB through a mixed local network, with analog seismographs of short period and vertical component, and three components digital seismographs.

Introduction

The municipal district of Porto dos Gaúchos, located in the center - north of the state of Mato Grosso, it is the Brazilian area that presents the most expressive seismicity in terms of magnitude and also, probably, in terms of seismic frequency. In this area, 1955/01/31 happened the largest earthquake ever registered in Brazil presenting a magnitude of 6.6 m_b and an inferred maximum intensity of IX (MM)(Berrocal at al. 1984).

Recently, on 1998/03/10, at 23h32m (UTC), the second largest earthquake of the area was detected, with a magnitude 5.1 m_b and a maximum intensity of VI (MM). With this earthquake SIS/UnB started monitoring the seismic activity in the area, installing, in 1998/03/16 a broad band permanent seismographic station (JUAB), Fig.1, belonging to the AmazonScope Project (Veloso, 1996). Later on, other five stations were installed, that due to instrumental (Q4120 - Quanterra) and operational problems presented operational flaws. In January of 2001, five new stations using Orion Dataloggers and seismometers (CMG-40T – Guralp) and (S3000 Sprengnether) were installed in substitution to those that were disabled. Now this network is operating satisfactorily. This work presents the preliminary results of the data analysis generated by this seismographic network in the last three years.

Brief historical of the area's seismicity

The Porto dos Gaúchos/MT area, in spite of being the most important Brazilian seismic area in terms of observed maximum magnitude, has been very little studied in terms of seismic history and, consequently, is not very well-known. The first earthquake registered in the area, that was also the largest magnitude observed in Brazil ($6.6m_b$), happened on 1955/01/31 and was not registered by any station in Brazil. At that time, only one seismographic station was operating in Brazil at the National Observatory of Rio de Janeiro, which did not register that earthquake. Therefore, the only data available were teleseismic records from the world seismograph network. It was detected also by a Richard type gravity barograph installed in the Observatório Dom Bosco of Cuiabá (Bombled, 1970), about 450 km to the south of the epicenter. The event was located, then, using the data from about 100 seismographic stations, in the Mountain of Tombador - MT (Lat.12.42ºS Long 57.30ºW), Berrocal et al. (1984) inferred for this earthquake a maximum intensity of IX (MM).

In agreement with the Northeast Explorer Matogrossense, in its report no. 54, of February of 1959, a strong earthquake was felt, on 59/02/05 in Gleba Arinos (Marza et al. 1999), an area where today is the city of Porto of Gaúchos, about 70 km to

the west of the epicenter of the earthquake of 10/03/98. The effects of the 1959 event in Porto dos Gaúchos, described in the referred report, is a little less than those produced by the earthquake of 98/03/10; therefore, it is reasonable to infer a magnitude around 5.0 for the event of 1959. The earthquake was followed by aftershock activity; in the same day were felt other three events, that according to descriptions, they reached intensities III-IV (MM).

Between January of 1957 and February 1959 any report of the Colonizadora Arinos make any mention to the event occurrence, except the report no. 54. Before 1957 the closest city, (Diamantino-MT), was in a distance of 350 km, to southeast of Porto dos Gaúchos. So, an earthquake with magnitude below 5.0 could not be felt in that region.

Only in the 80's the seismographic monitoring of the Amazônia region began, with the installation of seismograph stations at dams belonging to ELETRONORTE company, when they start to detect events with epicenters in Porto dos Gaúchos, with magnitudes over 3,3.

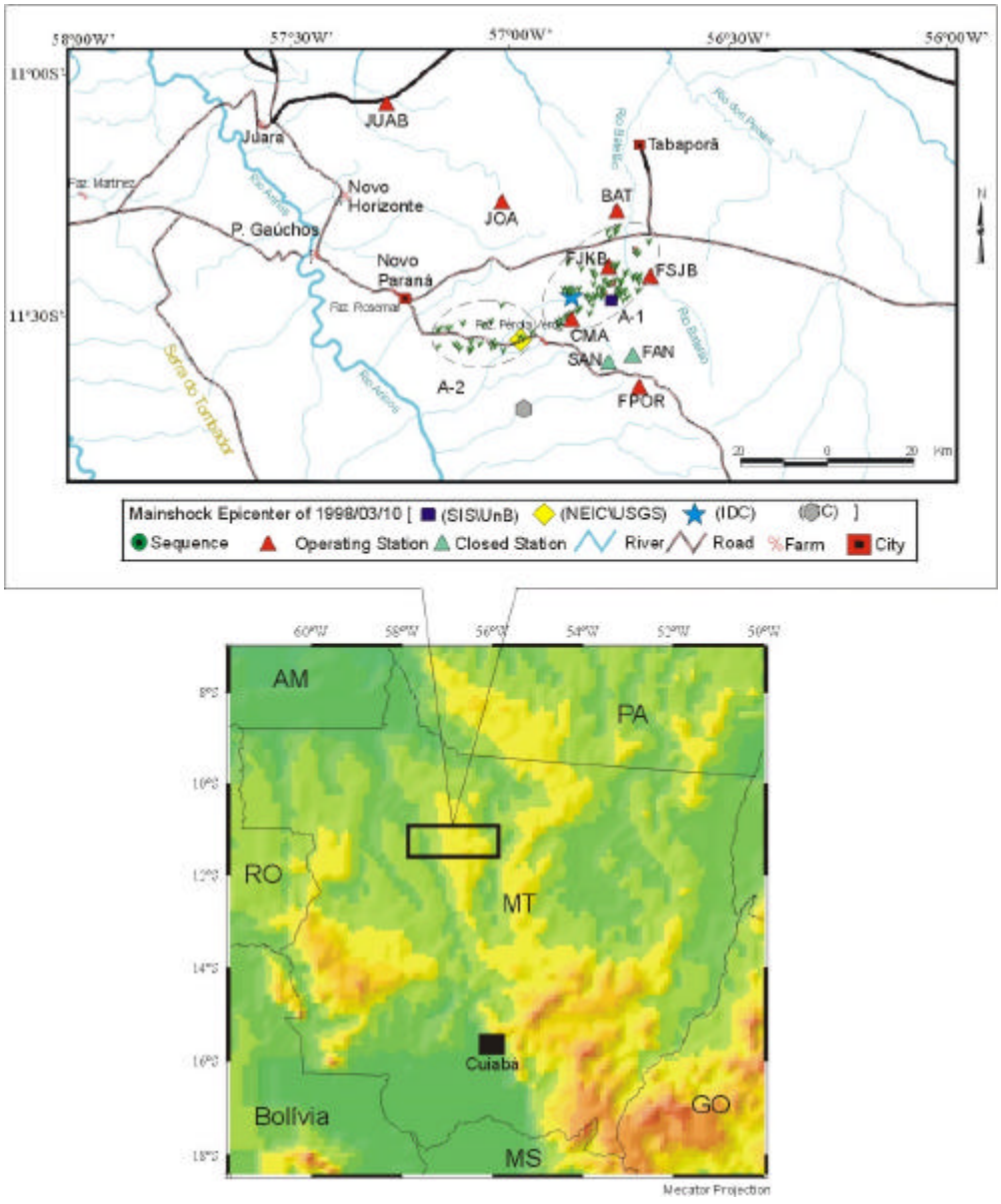

Fig. 1 - Map of the epicentral location of the seismic sequence of Porto dos Gaúchos area, between 1998/03 and 2001/03. Are also shown the locations of the seismographic stations .

Table 1 – Source parameters of the larger (m_b = 3.8) earthquakes registered in Porto dos Gaúchos/MT since 1955/01/31.

N.	Data yyyymm/dd	Origin Time h:mm:ss	Latitude	Longitude	Epicentral Region	Magnitude m_b	Fonte
1	1955/01/31	02:03:07	12.42ºS	57.30ºW	Serra do Tombador/MT	6.6	Berrocal, 1984
2	1959/02/05	---	11.53ºS	56.86ºW	Porto dos Gaúchos/MT	4.8	Historic
3	1981/03/09	17:27:40	11.71ºS	57.64ºW	Porto dos Gaúchos/MT	3.8	SIS\UnB
4	1987/10/15	06:01:41	11.60ºS	56.90ºW	Porto dos Gaúchos/MT	3.9	SIS\UnB
5	1988/08/11	05:06:16	11.71ºS	57.15ºW	Porto dos Gaúchos/MT	3.9	SIS\UnB
6	1988/08/11	08:07:00	11.70ºS	57.14ºW	Porto dos Gaúchos/MT	3.8	SIS\UnB
7	1993/05/10	15:17:00	11.60ºS	56.76ºW	Porto dos Gaúchos/MT	3.8	SIS\UnB
8	1993/10/05	15:17:17	11.72ºS	57.03ºW	Porto dos Gaúchos/MT	3.8	SIS\UnB
9	1996/11/26	04:14:21	11.27ºS	56.80ºW	Porto dos Gaúchos/MT	4.4	SIS\UnB
10	1998/03/10	23:32:44 23:32:43 23:32:44 23:32:43	11.53ºS 11.59ºS 11.67ºS 11.74ºS	56.86ºW 56.88ºW 57.00ºW 56.96ºW	Porto dos Gaúchos/MT	5.0 4.8 5.2 5.3	SIS\UnB IDC NEIC\USGS ISC
11	1998/03/22	05:26:50	11.60ºS	56.80ºW	Porto dos Gaúchos/MT	3.8	SIS\UnB
12	1998/07/19	00:32:59	11.62ºS	56.78ºW	Porto dos Gaúchos/MT	3.8	SIS\UnB
13	1998/07/21	22:22:59	11.62ºS	56.78ºW	Porto dos Gaúchos/MT	4.1	SIS\UnB

Source Parameters of the 1998/03/10 Mainshock

The earthquake of 1998/03/10 was sufficiently strong to be detected at teleseismic distances (it was registered by stations up to 150º away). Consequently, it was also located by the seismological international agencies, particularly by International Data Center (IDC), Washington, Virginia, USA, National Earthquake Information Center (NEIC) of USGS, in Golden, Colorado and by ISC (International Seismological Center), in Newbury, Berks, UK.

It was also registered by many the Brazilian seismograph stations. SIS/UnB used, for location data of its own seismograph network, together with

the data supplied by stations of the seismograph network of the Institute of Astronomy and Geophysics (IAG) of the University of São Paulo (USP), generously supplied by Prof. Dr. Marcelo Assumpção, adding up to 24 registering stations. Table 1 lists source parameters reported by the four agencies and the locations are indicated in Fig. 1.

To characterize the size of the 1998/03/10 earthquake we find that mean magnitude of the individual values of the reporting agencies could be adopted as a more reliable size quantificator, hence we adopt a magnitude m_b=5.1.

Seismic activity during the 1998-2001 period

During the last three years of continuous seismic monitoring in the area of Porto dos Gaúchos, 1322 events were detected, of which three with magnitudes larger or equal to 3,8 m_R, are include in Table 1 and Fig. 2. As well.

In spite of continuous monitoring, the stations operation was very irregular, of the total detected events, only 116 were located.

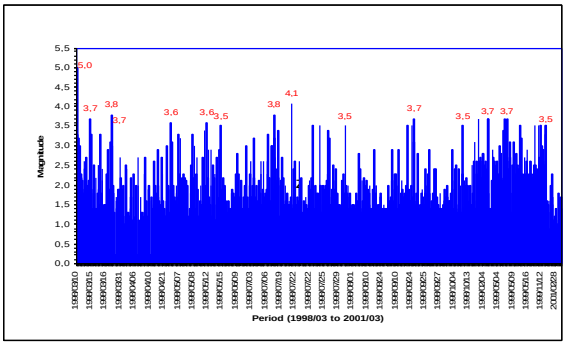

Fig. 2 - Temporal distribution of the Porto dos Gaúchos – MT seismicity in the period of 1998/03 to 2001/03.

For epicentral location of the events a crustal speed model presented in Table 2 was used. That model presented satisfactory results for most of the 116 events, located with data of three or more stations (up to six). The residues where inferior to 0.6 for the events inserted in the area A-1 of the Fig. 1. Figure 3 shows the distribution of the depth with the longitude. The most reliable depths are those for the events placed in area A-1 of Fig. 1, corresponding to the area between longitudes 56.91ºW and 56.70ºW, because the respective events produced data of good quality, being registered by at least three and up to six three components digital stations.

Table 2 – Crustal velocity model adopted.

Layer Depth (km)	Vp (km/s)	Vs (km/s)	Vp/Vs
0.00	4.50	2.60	1.731
2.00	5.80	3.35	1.731
15.00	6.78	3.92	1.730
40.00	8.22	4.75	1.730

The hypocenters, in their great majority, are located to a depth between 1 and 6 km with a maximum depth of 10 km.

The area A2, indicated in Fig 1 refers to events for which it do not have a reliable location.

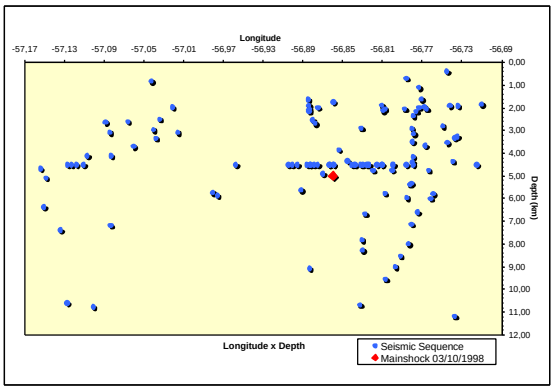

Fig.3 - Distribution of the focal depths with the longitude.

Discussion and Conclusion

1. The seismicity of Porto dos Gauchos area was continuous in the last three years, when 1.322 events were detected, of the which 28 events with magnitude larger than 3,5m_R;

2. Of the total events detected in Porto dos Gaúchos, only 116 were located. Of these only the ones with a more precise location are indicated in Fig 1, area A-1. In the location of those events of Area -1 data from at least three and up to six stations were used. The depth on the events are between 1 and 6 km, presenting a concentration around 5 km, that is the depth of the mainshock of 1998/03/10.

3. It was still not possible to present the results of studies of focal mechanism. For this new seismographic network installed in January 2001 can generate data of good quality and help in the definition of the orientation of the local stress that act upon area. The current seismographic stations network will have one more station and will operate for a long time.

4. The results presented here are preliminary, and could be changed with the refinement of the readings and analysis and the inclusion of the data of 1999 FSJ station, that still remain unread.

References

Barros, L.V., Marza, V.I., *As Ações do SIS/UnB face ao evento de Mato Grosso do dia 10 de março de 1998*, - Special Report, Nº 1, 28pp, Brasilia, April, 1998 (in Portuguese).

Berrocal J., Assumpção M., R. Antezana., C. M. Dias Neto., R. Ortega., H. França., J. A. V. Veloso - Sismicidade do Brasil, IAG/USP e Comissão Nacional de Energia Nuclear, 1984;

Bombled, J.,- *Meio Século de Meteorologia* F.U.F.M.T, 3º Vol., 12º fascículo, pp.37-41, 1970.

Colonizadora Nordeste Matogrossense Arinos - Report Nº 54, Fev/1959.

Marza, V. I., Barros, L.V. & Carvalho, J. M., *As Ações do SIS/UnB face ao evento de Mato Grosso do dia 10 de março de 1999*, - Special Report, Nº 2, 34 pp, Brasilia, April 1999 (in Portuguese).

Veloso, J.A.V. - *Projeto AmazonScope*, novembro de 1996, 20 pp.

Acknowledgments:

The authors express their most sincere gratefulness to all those people that especially contributed to the accomplishment of that work, especially those that contributed with the installation (Darlan Fontele and Isau Gomes) and operation of the seismographic stations network of Porto dos Gaúchos, to the operators of the stations of JOA (Oscar de Almeda), JUAB (Afonso Vasele) station FSJ (the brothers Jose Aparecido and Leandro); to the farmers: Mr. José Chaviquiole (JFK Station), Mr. Selso Rosato (CMA Station), Mr. Otavio Molina (FPOR Station), Mr. Noel Pagottto (BAT Station) and FINEP which financed part of the AmazonScope project Agreement number 65950362000.

Seismic Tomography of the Upper Mantle Beneath SE Brazil

Christian Escalante, Martin Schimmel, Marcelo Assumpç ̃ao

Instituto de Astronômia, Geofísica e Ciências Atmosféricas, University of São Paulo, São Paulo, Brazil

Abstract

We present preliminary results from teleseismic travel time inversions for P-wave data mainly recorded at portable broadband stations deployed at 47 sites along SE Brazil encompassing an area of 1500 x 1700 km during the years 1992 - 2001. More than 5000 relative P-wave arrival times were obtained from the waveforms using a new coherence functional. These P phase times are independently inverted for slowness perturbations, earthquake relocations, and station corrections. The models obtained represent the least amount of structure required to explain the residuals within a defined standard error. The robust and consistent features in the P wave velocity anomaly models are interpreted and their resolution is tested with synthetic case inversions. These results confirm the existence of a cylindrical low-velocity anomaly beneath the Parana Basin, which has been interpreted by VanDecar et al. (1995) as a fossil conduit of the Tristan da Cunha plume. We show that this low-velocity structure is confined to the upper mantle. The results also permit a more detailed separation of geological structures and velocity perturbations because of a larger amount of data that permit us to improve the resolution of the anomalies beneath SE Brazil.

Introduction

"Tomography" means a technique used to obtain an image of a selected plane section of a solid object, and comes from the Greek word *tomos* meaning a cutting or slice. One could refer to a reflection seismic section or a resistivity or chargeability pseudo-section as a tomogram. However, the term is normally reserved for imaging problems. The idea is to use observed values of some quantity which is related via a line integral to the physical parameter we wish to infer. Tomography is widely applied in medicine and geophysics for determining unknown structures. In seismic tomography one can use waveforms or travel times of seismic waves to image velocity perturbations, applying techniques of the Inversion Theory. These velocity perturbations reflect the different compositions and temperatures in the Earth's interior. We use this tool and invert teleseismic travel times to image the P-wave velocity perturbations beneath SE Brazil.

The study of the Brazilian upper mantle structure is important for the determination of tectonic regimes, the thermal and geological evolution of the South American continent, and to understand the regional convection style and forces. This study at scales of cratons and fold belts is motivated by the presence of the major structural units of Western Gondwana, younger mobile fold belts and relics of the opening of the South Atlantic ocean such as continental fold basalts and dyke swarms. The upper mantle structure is expected to correlate to these surface tectonic environments and reveal hidden anomalies and limits of structural units that are controversial due to the presence of cover rocks.

This study is a continuation of two researches carried out by VanDecar et al. (1995) and Schimmel et al. (2001). They reveal the existence of a cylindrical structure of low-velocity in the upper mantle under the Parana Basin. This cylindrical anomaly was interpreted as the fossil conduit through which the initial Tristan da Cunha plume head traveled to generate the Parana flood basalts. The São Francisco craton appears as a body seismically visible until 200 km depth. Also the subduction of the Nazca plate under South America is shown; however the resolution is not enough to decide if the Nazca plate subducts beneath Brazil as a continuous body or in two separated segments. The increased aperture of the seismic network with more station sites and a larger data set, permit a more detailed separation of geological structures such as the São Francisco craton and an extension of the study to larger depths. The larger resolution at depth is important for determining if the Nazca plate that subducts beneath Brazil is segmented or continuous, which has impact in the determination of geodynamic forces.

Stations, Event Selection, and Data Processing

The database is constructed from seismic waveforms recorded at stations deployed at more than 47 sites within an area of 1500 x 1700 km during the years 1992 - 2001. Up to 15 stations were in

operation at any time and almost all stations were equipped with three-component broadband seismometers. Most stations are from a joint project (BLSP92) of the Carnegie Institution of Washington and the University of São Paulo (USP) and from a continuation of this project by the USP (BLSP95). Figure 1 shows a map with the station locations that provide the data for our tomographic inversions. The colored marks are the stations that are actually in operation. Red marks show the new stations and the blue marks show stations that already provided data in the previous analyses. With the data from the new stations, we increase the study area and the resolution, specially at the margins of the previous results.

We selected P phases from events at angular distances between 30^o and 95^o with body wave magnitude (m_b) larger than 4.6. For the selected distance range, the P waves turn in the lower mantle, which means that we avoid difficulties with the upper mantle triplications and the non-linearity of the ray path which otherwise turns where the heterogeneities are stronger. In addition, we picked events ($m_b \geq 5.4$) that permit an unambiguous detection of the core phases PKPdf by their slowness and travel times. These core phases propagate to the stations along steep paths.

Our observations are relative arrival times of P-waves simultaneously recorded at 4 or more stations. The data we use in the inversions are relative residuals to decrease the possible biases from outside the target volume. A "multi-channel cross-correlation" (MCCC) technique by VanDecar and Crosson (1990) which exploits the waveform coherence over the network has been adapted for the determination of relative arrival times. This MCCC technique uses all possible pairs of waveforms and solves in the least square sense for the best set of relative arrival times for all stations. We also incorporated a new cross-correlation function (Schimmel, 1999) into the MCCC technique and call this modified derivative "Multi-channel phase cross-correlation" (MCPCC). The backbone of the phase cross-correlation (PCC) is the instantaneous phase of the analytic traces. PCC determines waveform similarity by the greatest number of coherent samples rather than the largest sum of cross products. As a consequence, the large amplitude portions in the correlation window do not bias the coherence measure.

The waveforms of short period instruments have been transformed to mimic broadband records and used together with the vertical broadband data at frequency bands around 1 Hz. The picking is performed at a high frequency band since a high frequency approximation (ray theory) of wave propagation is applied in the inversion procedure. The most common frequencies used for the P arrivals range between 0.8 Hz and 2.5 Hz. The corresponding seismic wavelengths in the upper mantle are smaller than 12 km.

We determined the relative arrival times for more than 5000 P and PKP arrivals. The standard deviation for the P-wave data is 0.4 seconds.

Travel Time Inversion

The inversion follows the approach described by VanDecar et al. (1995).

The model perturbations beneath the stations are parameterized by splines under tension (Neele et al., 1993) which are pinned at a series of regular knots. This interpolation scheme allows for a smooth slowness distribution and accurate ray tracing.

It is expected that the seismic energy travels on a ray path to the station. The problem has been linearized based on the assumption of weak perturbations. This means it is expected that the true rays and earthquake locations are linearly close to the initial guess. Further, it is assumed that data bias from structure outside the target volume is negligible given our use of relative residuals or absorbed by the station terms and low-resolution areas.

The P-wave relative phase times are independently inverted. Earthquake relocations and stations corrections are simultaneously inverted with the model perturbations. The linear problem is partly under-determined which means that inversion is non-unique. Occam's razor is followed to search for the model with the least amount of structure to explain the relative time residuals within a defined standard error. Because of noise in the data one should not try to make the misfit function as small as possible, which would likely map noise into structure. Numerically, the conjugate gradient method is employed for the inversion. Several inversions are iteratively performed. Except for the first iteration, equations for residuals larger than 1.5 standard deviation are systematically down-weighted. This approach leads to a robust solution with L2 residual minimization for data within 1.5 residual standard deviations and L1 minimization of the equations with larger residuals.

Discussion of Preliminary Results

The increased aperture of the seismic network and the larger data density allowed us to image, with a higher resolution, the seismic velocity anomalies in an enlarged volume of the mantle underneath SE Brazil. The images obtained were computed for various inversion settings and only the robust features will be discussed. We also carried out several synthetic inversion tests to support our interpretations; that is, to see what we can expect to resolve.

Figure 2 shows, as preliminary result, the horizontal cross-section at 150 km depth. White squares and yellow circles denote station sites and Late-Cretaceous alkaline intrusions (age range from 90 - 55 Ma), respectively. The warm and cold colors mark slower and faster than average velocities for that depth. In general low-velocity anomalies can be interpreted as higher than average temperatures. Areas with ray density less than 20 rays/$(100\text{km})^3$ are darkened in the images. In Figure 2 we can appreciate low-velocity anomalies in the Brasilia and Ribeira belts which correlate with the locations of the Late-Cretaceous alkaline intrusions (yellow circles). Besides, the São Francisco craton is visible as a fast-velocity anomaly. From the vertical sections we can see the roots of the São Francisco craton down to about 200 km depth. The fossil plume head (VanDecar et al, 1995) ranges from about 200 to 800 km depth. At the top of the lower mantle North-South orientated fast anomalies are detected. These anomalies are caused by the subduction of the Nazca plate underneath Brazil.

During the presentation we will show and discuss new images of the seismic anomalies down to about 1000 km depth.

Acknowlegments

The data are from GTSN, GEOSCOPE, UnB, and BLSP stations and we are very grateful to all the researchers and technicians who somehow contributed to these data. This work is supported by the FAPESP (Fundação de Amparo à Pesquisa do Estado de São Paulo) grants 01/01867-0 and 97/03640-4.

References

Neele, F., J. C. VanDecar, and R. Snieder, The use of P-wave amplitude data in joint inversion with travel times for upper mantle velocity structure, J. Geophys. Res., 98, 12033 - 12054, 1993.

Schimmel, M., Phase cross-correlations: design, comparisons and applications, Bull. Seismol. Soc. Am., 89, 1366 - 1378, 1999.

Schimmel, M., M. Assumpção, J. C. VanDecar, Seismic velocity anomalies beneath SE Brazil from P- and S-wave travel time inversions, accepted for publication in J. Geophys. Res., 2001.

VanDecar, J. C., and R. S. Crosson, Determination of teleseismic relative phase arrival times using multi-channel cross-correlation and least squares, Bull. Seismol. Soc. Am., 80, 150 - 169, 1990.

VanDecar, J. C., D. E. James, and M. Assumpção, Seismic evidence for fossil plume beneath South America and implications for plate driving forces, Nature, 378, 25 - 31, 1995.

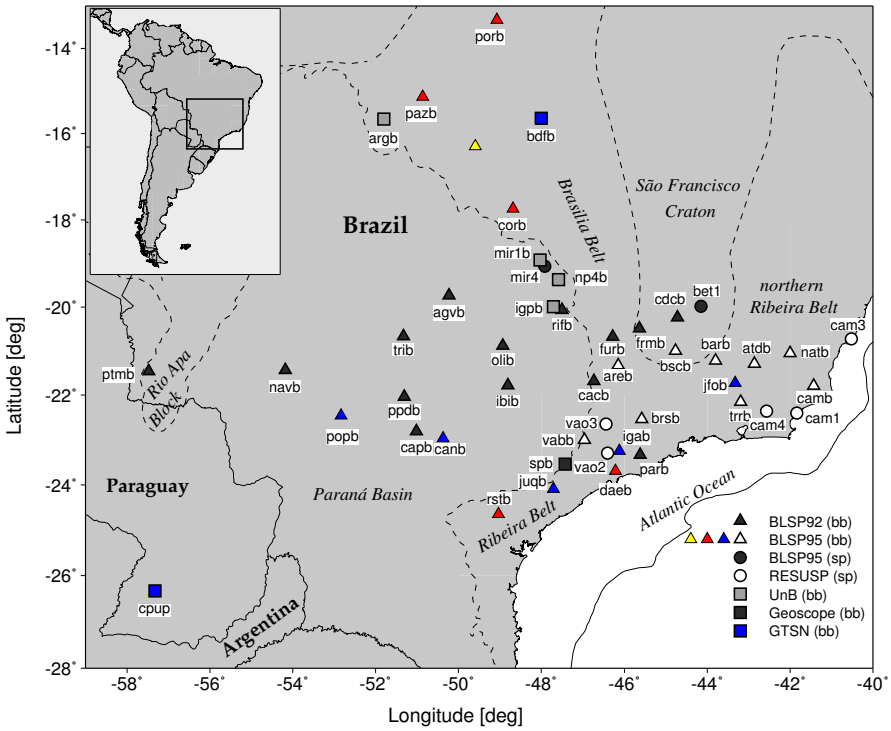

Figure 1: Map with seismic stations used for the relative arrival time data set and gross geological provinces.

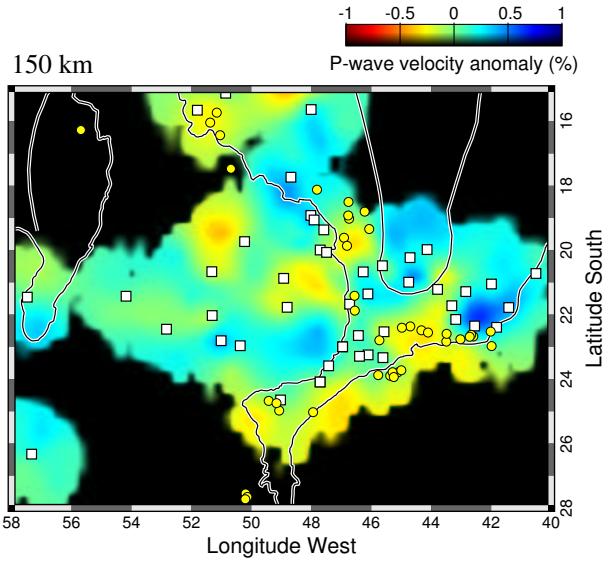

Figure 2: Horizontal cross-section through a preliminary P-velocity perturbation model at 150 km depth. Squares mark the stations used and the black areas indicate the regions with poor resolution, with ray density lower than 20 rays per $(100\ \mathrm{km})^3$.

Sismicidad de San Luis, Argentina

Mario A. Araujo, Marcelo H. Millán, Angel M. Pérez,
Instituto Nacional de Prevención Sísmica y Universidad Nacional de San Juan, Argentina

Abstract

In this paper the most significant seismicity of the San Luis province, Argentina, is analized, in order to asóciate it to different seimogenic sources in the region. It is showed that shallow seimic activity is related to the western zone of the Sierras Pampeanas Centrale, where others authors have identified a numbers of faults presenting some of them Quaternary activity. The intermediate seimic activity is related to the subdution of the Nazca Plate beneath the Souh America Plate. Both shallow eartquakes of M > 5.0 which occurred in this province could have been generated from the San Luis province comparing their locations with the fault trace, even though it must be pointed out that there is not surface rupture for both events. When seismic activity for earthquake M < 5.0 is analized , it can be observed that the relation between the hypocenter and the fault trace is not so accurate. This relation will be improved when the number of seismological stations in the north and center part of the province is increased which will conduct to more accurate locations.

Introducción

La provincia de San Luis está ubicada en la región central de la República Argentina y su sismicidad superficial está asociada a fuentes sismogénicas (fallas activas) de la porción occidental de las Sierras Pampeanas Centrales. Otra fuente sismogénica de menor importancia es la zona de subducción de la placa de Nazca debajo de la Sudamericana. La sismicidad de esta provincia es considerada moderada si se considera el número de sismos ocurridos en la historia sísmica de esta región como así también el tamaño de los mismos. Sin embargo, se ha observado que esta región tiene un alto nivel de microsismicidad que seguramente esta relacionada con fuentes sismogénicas reconocidas o no identificadas de la región. El evento más importante ocurrido en esta provincia es el terremoto del 22 de mayo de 1936, que tuvo características destructivas aunque no produjo víctimas y estuvo localizado en el norte de las Sierras de San Luis en la zona de San Francisco del Monte de Oro. Otro evento importante fue un sismo de menor tamaño que el anterior, que ocurrió el 28 de julio de 1996 y que se ubicó en la región central de la provincia, en la zona de la falla de San Luis.

Sismicidad de la provincia de San Luis

La principal actividad sísmica de esta provincia se ubica en la parte norte y central de la misma, diminuyendo hacia el sur debido a que las estructuras correspondientes al sistema de Sierras Pampeanas son poco significativas ya que en dicha zona finaliza este sistema (figura 1).

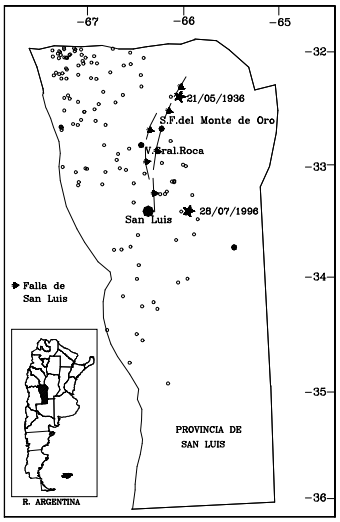

Figura 1 – Sismicidad de la provincia de San Luis

La sismicidad que se muestra en esta figura incluye los dos eventos más importantes de la provincia que tuvieron magnitudes mayores que 5.0 grados y que serán descriptos posteriormente y todos los eventos con magnitudes comprendidas entre 3.0 y 5.0 grados y que han sido localizados por el Servicio Geológico de los Estados Unidos de América y el INPRES.

Terremoto de San Luis del 21 de mayo de 1936

Este terremoto ocurrió en la noche del 21 de mayo de 1936 y produjo daños de importancia en todas las poblaciones del norte de la Provincia de San Luis y fue percibido en una amplia región del país, hasta una distancia de 800 km desde el epicentro (figura 2).

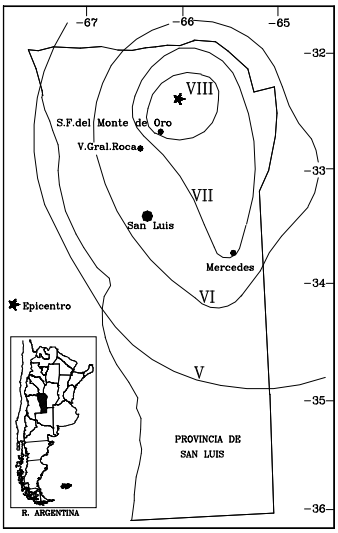

Figura 2 – Isosistas del terremoto del 21 de mayo de 1936.

Este evento tuvo una magnitud de 6.5 grados en la escala de Richter y alcanzó una intensidad máxima epicentral de VIII grados en la escala Mercalli Modificada. Las principales ciudades de la provincia son las ciudades de San Luis y Villa Mercedes y en éstas el sismo alcanzó intesidades de V-VI y de VI-VII grados, respectivamente. El área donde se produjo la mayor destrucción abarcó a un grupo de pequeñas poblaciones, entre las cuales podemos mencionar a San Martín; San Francisco del Monte de Oro; Quines; Villa Fraga y Las Chacras. Los daños característicos en esta zona consistieron en agrietamientos múltiples en las casas de adobe, derrumbamiento de techos y paredes y en menos escala, colapso completo de casas muy viejas. En el mapa de isosistas éstas localidades han quedado incluidas dentro del grado VIII de la escala Mercalli Modificada. En las sierras de Rialito, ubicadas en la parte central de la isosista VIII, "las casas y cercas quedaron totalmente destruidas, notándose agrietamiento del suelo". Esta descripción podría estar indicando la zona de mayor destrucción, donde posiblemente la intensidad haya alcanzado el grado IX Mercalli Modificada. Además, "se observaron grandes desmoronamientos en las sierras ubicadas a tres kilómetros de San Francisco del Monte de Oro".Este terremoto también ocasionó daños en Villa Mercedes, Provincia de San Luis, donde "el temblor fue de una intensidad y duración sin precedentes, ocasionando perjuicios considerables en los edificios que en más de un 70% han resultado con desperfectos". En Río Cuarto, Provincia de Córdoba, "se agrietaron las paredes en algunos edificios", mientras que en la Ciudad de Córdoba "fue fácilmente advertible, pues el sacudimiento, si bien resultó brevísimo, se percibió en forma general". Asimismo el temblor fue sentido en Mendoza "con mediana intensidad y escasa duración", en San Juan donde "apenas fue perceptible", en la Capital Federal donde "en algunas casas de familia causó cierta alarma" y en Rosario "su intensidad fue sentida en forma más acentuada por personas ubicadas en edificios altos". Es interesante destacar que en la localidad de Almafuerte, "la población se lanzó a las calles, presa de pánico. El fenómeno no produjo daños materiales". Esto indicaría para este punto una intensidad entre V y VI grados de la escala Mercalli Modificada. Por otra parte, el terremoto fue seguido de una gran cantidad de réplicas. Hasta el día 27 de mayo "en San Francisco del Monte de Oro se sintieron no menos de 150 remezones". El día 28 se produjo una réplica muy fuerte seguida de una nueva serie de temblores, y según el informe antes mencionado "los sismos del día 28 no fueron sentidos en Córdoba, no obstante haber sido tan fuertes y destructores en la región del epicentro como el del día 21". Otra réplica fuerte hubo el día 8 de junio en que "numerosas viviendas se derrumbaron en Las Chacras y San Francisco, aquellas que ya estaban agrietadas desde el fuerte temblor del 21 de mayo".

Sismo de San Luis del 28 de julio de1996

A las 21 horas y cinco minutos (hora local) del día 28 de julio de 1996, los habitantes de distintas ciudades de la provincia de San Luis, fueron sorprendidos por un sismo de moderada intensidad y corta duración, con percepción de ruidos subterráneos (figura 3). El evento causó alarma en gran parte de la ciudad de San Luis (Capital) y en Villa Mercedes, incluidas otras poblaciones menores de esta provincia. El sismo alcanzó una intensidad máxima epicentral de V grados en la escala Mercalli Modificada, IV grados en las ciudades de San Luis (Capital) y Villa Mercedes y III grados en la ciudad de Mendoza. Este evento fue registrado en más de 20 estaciones de la Red Sismológica Nacional del Instituto Nacional de Prevención Sísmica (INPRES).Los parámetros focales de este sismo son los siguientes :
Latitud: 33° 23' 56"
Longitud: 65° 56' 17"
Hora ocurrencia: 21: 04: 40.9
Profundidad: 32 km
Magnitud: 5.1 (Richter)
Intensidad Máxima Epicentral.: V (M.M.)

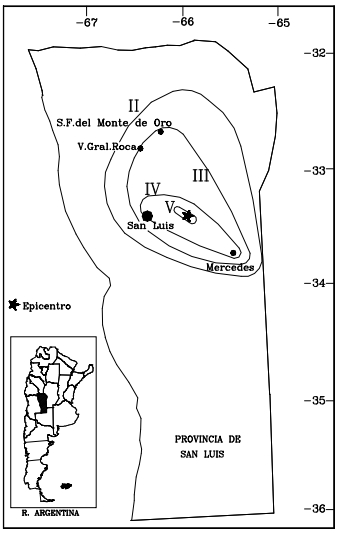

Figura 3 – Isosistas del sismo del 28 de julio de 1996

Después de ocurrido el evento principal fueron registradas más de diez réplicas en la Red Nacional de Estaciones Sismológicas, de las cuales la mayor tuvo una magnitud de 4.1 grados en la escala de Richter. De éstas, sólo tres fueron percibidas por la población de la ciudad de San Luis, con una intensidad de II grados en la escala Mercalli Modificada y sus epicentros se ubicaron en las cercanías del evento principal.

Fuentes sismogénicas de las Sierras de San Luis

Algunas fuentes sismogénicas de las Sierras de San Luis están representadas por fallas activas, las cuales han sido clasificadas en tres categorías: (i) falla con actividad cuaternaria comprobada; (ii) falla con actividad cuaternaria probable; (iii) falla inferida, debiéndose destacar que estas fallas sólo han sido reconocidas pero no están cuantificadas. Estas fallas están estrechamente asociadas con la actividad sísmica superficial que se manifiesta en estas sierras. Por ejemplo los sismos de 1936 y de 1996 estarían probablemente asociados a la falla de San Luis o algún fallamiento activo que no presenta manifestación superficial.

Discusión y recomendaciones

De acuerdo a lo expresado, la provincia de San Luis ha sido afectada por terremotos locales de pequeña y mediana magnitud como así también por otros de mayor tamaño ocurridos en provincias vecinas. La actividad sísmica de San Luis está estrechamente relacionada con fuentes sismogénicas , previamente descriptas , que son las generadoras de ésta en líneas generales. Todavía queda por relacionar con mayor precisión la sismicidad y el fallamiento activo con manifestación superficial. Esta limitación puede mejorarse con la instalación de nuevas estaciones sismológicas, preferentemente en las regiones norte y centro de la provincia con el objeto de optimizar la localización de los eventos, y de este modo asociar a estructuras conocidas o estructuras que pueden no tener manifestación superficial.

Referencias

Archivo de sismos históricos del INPRES.

Castano, J.C., 1977, Zonificación Sísmica de la Republica Argentina, Publicación Técnica N°5, INPRES.

Costa, C., Ortiz Suarez, A., Gardini, C., Chiesa, J., Ojeda, G., Strasser, E., Carugno, A., Rivarola, D. y Morla, P., 1997, Hoja Geológica 3366-I, San Francisco, Informe Inédito, 106p., SEGEMAR.

Costa, C., Gardini, C., Ortiz Suarez, A., Chiesa, J., Ojeda, G., Rivarola, D., Tognelli, G. y Sales,D., 1998, Hoja Geológica 3366-III, San Luis, Informe Inédito, 98p., SEGEMAR.

Criado Roque, P., Mombru, C., y Ramos, V., 1980, Estructura e Interpretación Tectónica, Geología de la Provincia de San Luis, VIII Congreso Geológico Argentino, 152-155.

Agradecimientos

Los autores desean agradecer los valiosos comentarios del Doctor Carlos Costa de la Universidad Nacional de San Luis, Argentina y al Ing. Fernando Forconesi y Técnicos Mario Figueroa y Carlos Rufino, del Departamento Investigaciones Sismológicas del INPRES, por la colaboración prestada para la realización del presente trabajo.

Sismicidade na Margem Continental do Sudeste do Brasil

Marcelo B. Bianchi, Jesus Berrocal e Celia Fernandes.
Instituto de Astronomia, Geofísica e Ciências Atmosféricas (IAG/USP), São Paulo, Brasil.
mbianchi@iag.usp.br, berrocal@iag.usp.br, celia@iag.usp.br

Abstract

In this paper we analyze the seismic activity that occurs in the continental margin of Southeastern region of Brazil. In 1975 these events started to be detected when the first seismographic station was installed in that region. Before that only events with m_b larger than 4,5 were observed. The activity that occurred after that includes only small events with m_b smaller than 4,5. The larger part of these events is located in the continental platform mainly at the slope.

Introdução

A região de estudo deste trabalho está localizada entre as coordenadas 18^o - 30^o S e 30^o – 50^o W, constituída pela porção oceânica em frente à porção continental da região Sudeste do Brasil.

Do ponto de vista sismológico, essa região, e todo o território brasileiro, estão localizados em uma região tectonicamente estável, onde o índice de atividade sísmica é relativamente baixo (Assumpção et al., 1980; Berrocal et al., 1996), o que é típico de regiões intraplaca.

A auscultação instrumental no Brasil começou na década de 1960 e na região SE no final da década seguinte. Dados sobre sismos ocorridos antes disso foram recuperados a partir de descrições macrossísmicas compiladas por Berrocal et al. (1984), exceto alguns eventos de maior magnitude cujos epicentros foram determinados com dados da rede sismográfica internacional. Por esse motivo, a atividade sísmica na Margem Continental somente começou a ser conhecida apropriadamente a partir da década de 1970.

O objetivo do presente trabalho é apresentar o nível atual de conhecimento sobre a atividade sísmica que ocorre na Margem Continental localizada em frente à região SE do Brasil, em função da evolução da rede sismográfica existente nesta região.

Aspectos geológicos

A região Sudeste do Brasil abrange porções das províncias estruturais da Mantiqueira, São Francisco, Tocantins, Paraná e Margem Continental (Almeida et al., 1977). As três primeiras províncias são constituídas de rochas pré-cambrianas e as outras de rochas sedimentares e vulcânicas não deformadas da cobertura fanerozóica da Plataforma Sul-Americana.

A Margem Continental apresenta as seguintes zonas fisiográficas: plataforma, talude e sopé continental. A estruturação destas províncias está relacionada aos grandes processos tectônicos-orogenéticos de formação do arcabouço da própria Margem Continental e as progradações sedimentares mais volumosas que ocorrem nessa província. As estruturas mais destacadas nelas são as depressões e altos. Nas bacias de Campos e de Santos, desenvolvidas durante o Mesozóico e Terciário, ocorrem falhamentos cenozóicos gravitacionais, que teriam originado as serras do Mar e Mantiqueira (Asmus e Ferrari, 1978).

Feições batimétricas, como o Platô de São Paulo ou a cadeia Vitória-Trindade, as ocorrências de rochas alcalinas em áreas emersas e as direções leste-oeste de alguns rios importantes, sugerem a continuidade de fraturas oceânicas para o interior do continente. à porção continental da região Sudeste do Brasil.

O embasamento das bacias de Campos e de Santos, de acordo com Cordani (1984), é composto por rochas que foram retrabalhadas no período Brasiliano, e está constituido por rochas migmatíticas de afinidade granulítica e gnaises cortadas por inúmeras intrusões graníticas. Recobrindo o embasamento foram depositados sedimentos clasticos grosseiros a finos, e coquinas tipicamente de origem alúvio-lacustre (de Figueira, 1985). Esses sedimentos são recobertos por rochas clásticas e evaporitos aptianos cuja possança aumenta para leste-nordeste. Depois que a plataforma foi submergida ocorreu uma deposição de calcilutitos, margas e folhelhos contendo reservatórios arenosos turbidíticos e seus equivalentes de águas rasa.

Dados sismológicos

Os dados sismológicos para o presente estudo, foram extraídos de Berrocal et al.(l984), cujo catálogo compreende o intervalo 1560-1981, e do Boletim Sísmico Brasileiro, que é publicado regularmente na Revista Brasileira de Geofísica, contando com dados correspondentes ao intervalo 1982-2000.

A grande maioria dos dados apresentados no catálogo de Berrocal et al. (l984), correspondentes a eventos ocorridos antes da década de 1970, são provenientes de informações macrossísmicas, contidas principalmente em notícias de jornais ou em resenhas históricas em nível regional ou nacional. Até então,

poucos são os sismos com epicentros localizados na Margem Continental, somente os de magnitude significativa, que foram registrados pela rede internacional de sismógrafos, No mapa da Fig. 1 apresentam-se os epicentros dos sismos ocorridos na região SE até 1975.

A partir de meados da década de 1970, foram instaladas as primeiras estações sismográficas na região SE, principalmente pelos grupos do IAG/USP, IPT/CESP e do SIS/UnB. Atualmente, esta região conta com cerca de quinze estações sismográficas, que permitem determinar os epicentros de sismos ocorridos na região SE, inclusive quando eles não são sentidos pela população.

No mapa da Fig. 2 são mostrados os epicentros de sismos ocorridos na região SE, incluindo a Margem Continental, desde 1976 até dezembro de 2000.

A rede sismográfica da região SE

As redes e estações sismográficas que operam na região SE com registro em tempo real, são:

Rede Sismográfica da USP (RESUSP), com as seguintes estações: Valinhos, SP (VAO), com três componentes de período curto; Socorro, SP (VAO3) e Serra do Gil, SP (VAO2), com uma componente vertical de período curto; e

Rede Sismográfica da Bacia de Campos (RSBC), com as seguintes estações: Campos, RJ (CMBB) sistema triaxial de banda larga; Macaé, RJ (CAM1), Pico da Caledônia, RJ (CAM4) e Guarapari, ES (CAM3), com uma componente vertical de período curto;

Estação Sismográfica de São Paulo (SPB), pertencente ao programa francês GEOSCOPE, composta por um sistema triaxial de banda ultra-larga.

Os dados da RESUSP são transmitidos via rádio-telemetria, para o prédio do IAG/USP no campus da Cidade Universitária. Os dados das estações de período curto da RSBC são transmitidos por telefone para esse prédio. Todos esses dados são demodulados e convertidos ao formato digital antes de serem registrados de forma contínua em um PC exclusivo para esta função. Os dados da estação CMBB são digitalizados na própria estação e transmitido via rádio transiver/telefone ate o IAG/USP onde são continuamente registrados em outro PC.

Os dados da estação SPB são registrados em um PC na própria estação localizada na Mina Santa Helena , da Votorantim, próxima de Sorocaba, SP. Esses dado atualmente podem ser recuperados de GEOSCOPE, com um pouco de atraso, porém estamos terminando as gestações com Votorantim para ter acesso a essa estação via Internet, com o qual esses dados estarão também disponívei em tempo quase real.

Além dessas redes, operam na região SE outras estações portáteis de duração menos longa em um determinado local, que são implantadas para estudos sismotectônicos específicos, em vários lugares desta região, pertencentes ao projeto *Brazilian Lithosphere Seismic Project* (BLSP) (Assumpção et al., 1998).

Fora dessas estações operadas ou administradas pelo IAG/USP, existem outras estações sismográficas e redes administradas por outras instituições, que operam na região SE ou em regiões vizinhas, com as quais existe um intercambio irrestrito de dados. Essas instituições são o IPT/CESP, que opera em torno de dez estações em locais associados as hidroelétricas da CESP no Estado de São Paulo, e o SIS/UnB que opera várias redes principalmente nos estados de Goiás e Minas Gerais, também em torno de reservatórios hidrelétricos desses estados.

No mapa da Fig. 3 apresentam-se as estações sismográficas que operaram durante o intervalo 1970-2000.

Análise de dados

Os registros digitais obtidos no IAG/USP são pre-processados diariamente para verificar a ocorrência de eventos sísmicos. São criados arquivos contendo os prováveis sismos os quais são transmitidos para o Laboratório de Processamento Sismológico (LABPS).

No LABPS é utilizado o programa SAC (New Seismic Analysis Code 7/12/1999, Copyright 1995 Regents of the University of California) desenvolvido na Universidade da Califórnia, para a leitura dos sismogramas. Este programa possibilita a visualização dos registros, aplicação de filtros passa alta, baixa e passa banda, e a leitura do tempo de chegada das fases gerando um arquivo no formato desejado para o cálculo dos hipocentros com o programa HYPO71.

O programa HYPO71 (Lee & Lahr,1975) permite a determinação dos parâmetros hipocentrais calculando os resíduos em tempo para cada uma das estações, que servem como parâmetro de qualidade para a determinação hipocentral. Esse programa também calcula os erros na determinação do epicentro (erh) e na profundidade (erz), além de outros parâmetros que servem para qualificar a qualidade da determinação hipocentral.

Análise da sismicidade da Margem Continental

A ocorrência de sismos na Margem Continental está representada nos mapas das Figs. 1 e 2. No primeiro mapa podemos observar que poucos sismos foram determinados com seus epicentros na porção oceânica, utilizando dados da rede internacional de sismógrafos, por ter suas magnitudes relativamente grandes. Esses sismos são:

-28.06.1939	em frente ao litoral de SC	m_b=5,5
-18.07.1946	em frente a Cananeia, SP	m_b=4,6
-28.02.1966	em frente a Vitória, ES	m_b=6,3
-24.10.1972	em frente ao litoral N, RJ	mb=4,8

Fora desses sismos ocorreu em 01.08.1767 outro sismo que foi sentido em Vitória, ES, com intensidade maior que a sentida durante o sismo de 1955, chegan-do a destruir uma igreja e ter sido provavelmente sentido em Salvador, BA, o que sugire para o sismo de 1767 uma magnitude superior a m_b 6,3.

Da mesma forma existem informações sobre outro sismo com m_b 4,5, ocorrido em 05.05.1917, cujo epicentro foi determinado na cidade de Campos, RJ utilizando dados macrossímicos, que poderia ter ocurrido no mesmo local que o sismo de 1972

Depois da instalação dos primeiros sismógrafos na região SE, por volta de 1975, começam a ser registrados os sismos de pequena magnitude ocorridos na Margem Continental e não sentidos na porção continental. Os epicentros desses simos estão mostrados no mapa da Fig. 2. Neste mapa podemos observar um estado mais realístico do nível de sismicidade que ocorre na Margem Continental em frente à região SE.

O nível de atividade sísmica na porção oceânica é compatível com o da sismicidade da porção continental. Por outro lado comparando os dois mapas de epicentros, podemos ver que os sismos ocorridos antes de 1975, foram de magnitude maior que m_b 4,5 alcançando magnitudes, provavelmente, maiores que m_b 6.3.

Discussão e conclusões

No presente trabalho se analisa as atividades sísmicas que ocorrem na Margem Continental do Sudeste. Esses fenômenos começaram a ser detectados a partir de 1975 quando as primeiras estações sismográficas foram instaladas nessa região. Antes disso foram observados somente sismos de magnitudes maiores que m_b 4,5. A atividade sísmica que ocorreu a partir de 1975 esta constituída de pequenos sismos com m_b menor que 4,5. A maior parte desses eventos acontece na plataforma continental principalmente na região do talude.

Agradecimentos

Os autores deste trabalho ficam muito gratos com a Companhia Hidro Elétrica do São Francisco (CHESF) por financiar os trabalhos de auscultação sismográfica nos seus reservatórios do rio São Francisco. Agradecem também ao CNPq pela bolsa PIBIC do aluno Marcelo B.de Bianchi.

Bibliografia

Assumpção, M.; Dias Neto, C.M.:Berrocal, J.; Antezana, R.; França, H. & Ortega, R., 1980. Sismicidade do Sudeste do Brasil. Na. 31^o Congr. Brás. Geol., 2: 1075 – 1092.

Assumpção, M., 1998. Focal mechanisms of small earthquakes in SE Brazilian shield: a test of stress models of the South American plate. Goephys. J. Int., 133, 490-498

Berrocal, J., Fernandes, C., Bassini, A. & Barbosa, J. R., 1996. Earthquake hazard assessment in Southern Brazil, Geof. Intern, 35:257-272.

Berrocal, J; Assumpção, M.; Antezana, R; Dias Neto, C.M.; Ortega, R ; França, H. & Veloso, J.A.V., 1984. Sismicidade do Brasil. IAG/USP – CNEN, 320 p.

Lee, W.H.K. & Lahr, J.C.,1975. HYPO71 (Revised) a computer program for determinig hypocenter, magnitude and first motion pattern of local earthquakes. U.S. Geological Survey.

Almeida, F.F.M., Hasui, Y., Brito Neves, B.B. & Fuck, R.A.,1977. Províncias Estruturais Brasileiras. Atas 8o. Simp. Geol. Mord., p. 363-391. Campinas Grande.

Asmus, H.E. e Ferrari, A.L., (1978). Hipótese sobre a causa do tectonismo cenozoico na região Sudeste do Brasil - In: Brasil, Projeto REMAC, Aspectos Estruturais da Margem Continental Leste e Suseste do. Brasil. PETROBRÁS, Projeto REMAC, 4: 75-88. Rio de Janeiro.

Cordani, U. G., Estudo Preliminar de integração do Pré-Cambriano com os eventos tectônicos das Bacias Sedimentares Brasileiras. Rio de Janeiro, PETROBRÁs, CENPES. SINTEP, 1984.

de Figueiredo , A. M. F., 1985, Geologia das Bacias Brasileiras. Em Viro, E. J. editor, Avaliação de Formações no Brasil. Sociedade Comercial Brasileira de Pesquisas de Subsolo pelo Método Schlumberger Ltda.

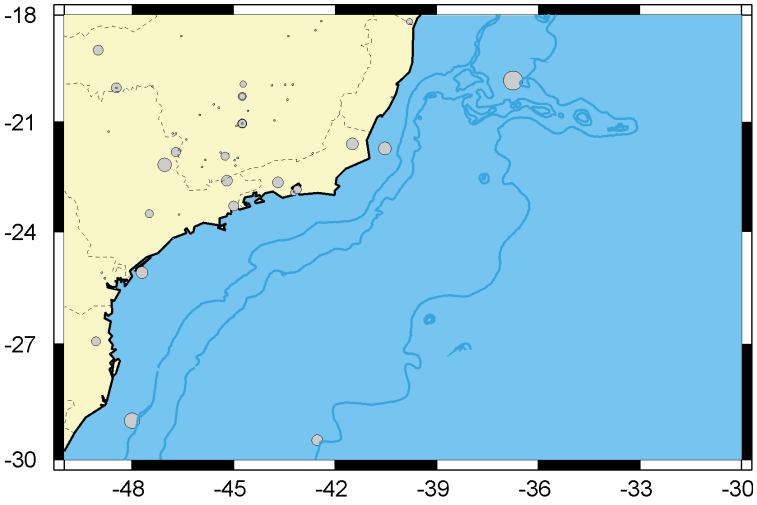

Figura 1: Atividade sísmica na Margem Continental antes de 1975.

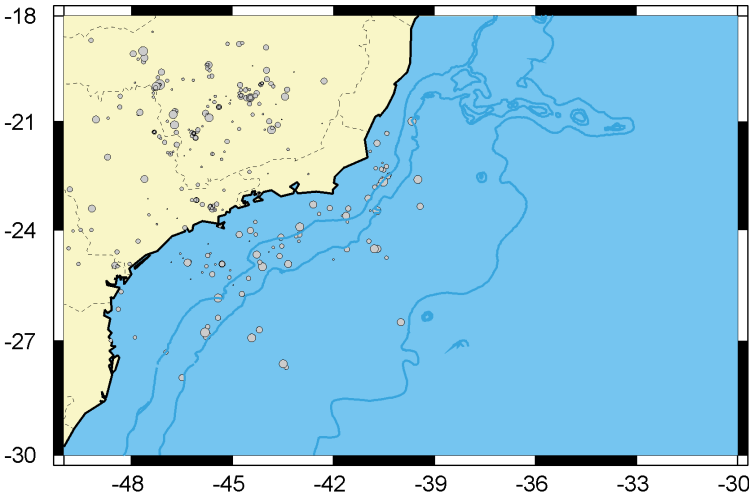

Figura 2: Atividade sísmica na Margem Continental a partir de 1975.

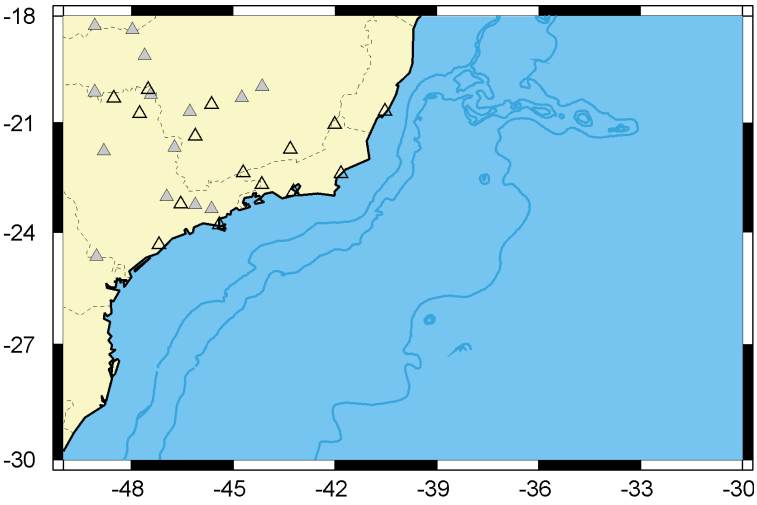

Figura 3: Rede sismográfica na região Sudeste. As estações vazadas são estações desativadas as preenchidas estão ativas.

Testing two methods for depth to magnetic basement estimation

Marta E. Ghidella, Instituto Antártico Argentino, mghidella@dna.gov.ar
Gustavo A. Rodríguez, Instituto Antártico Argentino, gusalrod@dna.gov.ar

Abstract

We consider two well-known methods of depth to magnetic basement estimation. Both of them are applied to magnetic profile data. Their numerical approaches are quite different: method 1 uses maximum entropy autocorrelation analysis and method 2 (Werner deconvolution) uses least square fits to the dike anomaly. We find that the published program for method 1 needs a correction in the autocorrelation estimation. If the correction is applied, the method is numerically consistent but then the results are not sensitive to the absolute depth. We use method 2 for comparison. It yields a wide dispersion of estimates that can be partly reduced by constraining susceptibility estimates. For the examples we use data from an airborne survey on the Argentine continental shelf.
Despite the remaining dispersion, method 2 still gives better results.

Introduction

One of the tools for magnetic survey interpretation is the estimation of depth and location of magnetic sources. We use profile analysis when the flight line density is not adequate to perform grid analysis. If this is the case, we need to take into account that profile analysis can be made under the assumption that the distribution of sources is perpendicular to the flight path. This condition is oftentimes accomplished when the aerosurvey is designed so that the flight paths are orthogonal to regional trends. Figure 1 displays the magnetic anomaly map resulting from a compilation of various data sets in the Argentine margin (Ghidella et al., 2000). All the offshore data intervening in this compilation belong to the ARGUS aerosurvey (Max et al., 1999). The straight black line plotted on the map is the location of the profile whose depth to source analysis we discuss in this paper. We used profile depth to basement estimation before for another survey and with good results (LaBrecque and Ghidella, 1997). The method used then was based on spectral Fourier analysis. As at this time we wanted to use a higher resolution technique, we resorted to Phillips (1978), and also to Werner deconvolution (Hartman et al., 1971) techniques. Regarding the former, we refer to it as ACME, a reminder of its keywords: *Autocorrelation* and *Maximum Entropy*.

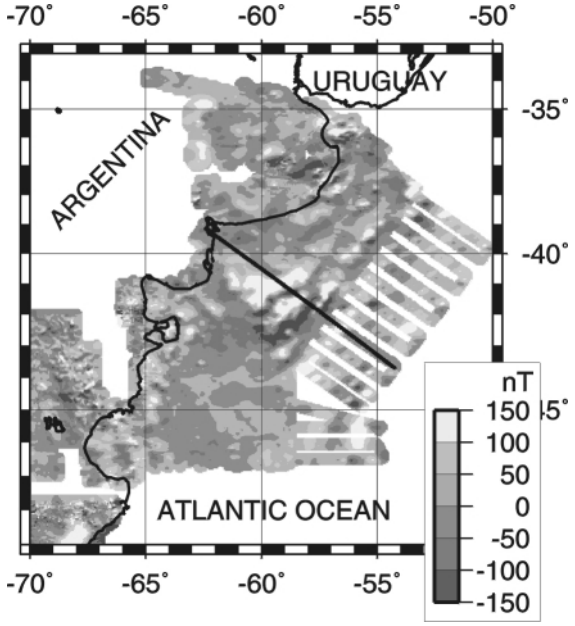

FIGURE 1: Magnetic anomaly map resulting from a compilation of various data sets in the Argentine margin. The straight black line plotted on the map is the location of the profile in figures 2 and 3.

ACME method

The physical assumptions for the ACME method are that the magnetic basement can be represented by a succession of semi-infinite dikes whose magnetization vector is constant in direction but randomly changing in magnitude. Under these assumptions an expression is found that relates the depth to the dikes' top with the autocorrelation function of the magnetic anomaly profile (Phillips, 1978). The autocorrelation function is estimated using Burg's maximum entropy method. In this way, successive autocorrelation lags are calculated recursively. The procedure is applied to a window that moves along the profile. For each position of the window four lags are calculated, thus obtaining four depth estimates. If the assumptions made hold exactly, the four estimates are identical. Normally this is not the case for real data, but then the successive estimates are used for testing the model's applicability at each window position. Values not meeting convergence criteria are rejected.
Figure 2(a) displays magnetic anomaly versus distance for the profile whose location appears in figure 1. In figure 2(b) we show the results of our application of the original ACME method to the profile. Only the first and fourth estimates are plotted, but no rejection criterion has been applied. We have also plotted bathymetry and acoustic basement, the latter

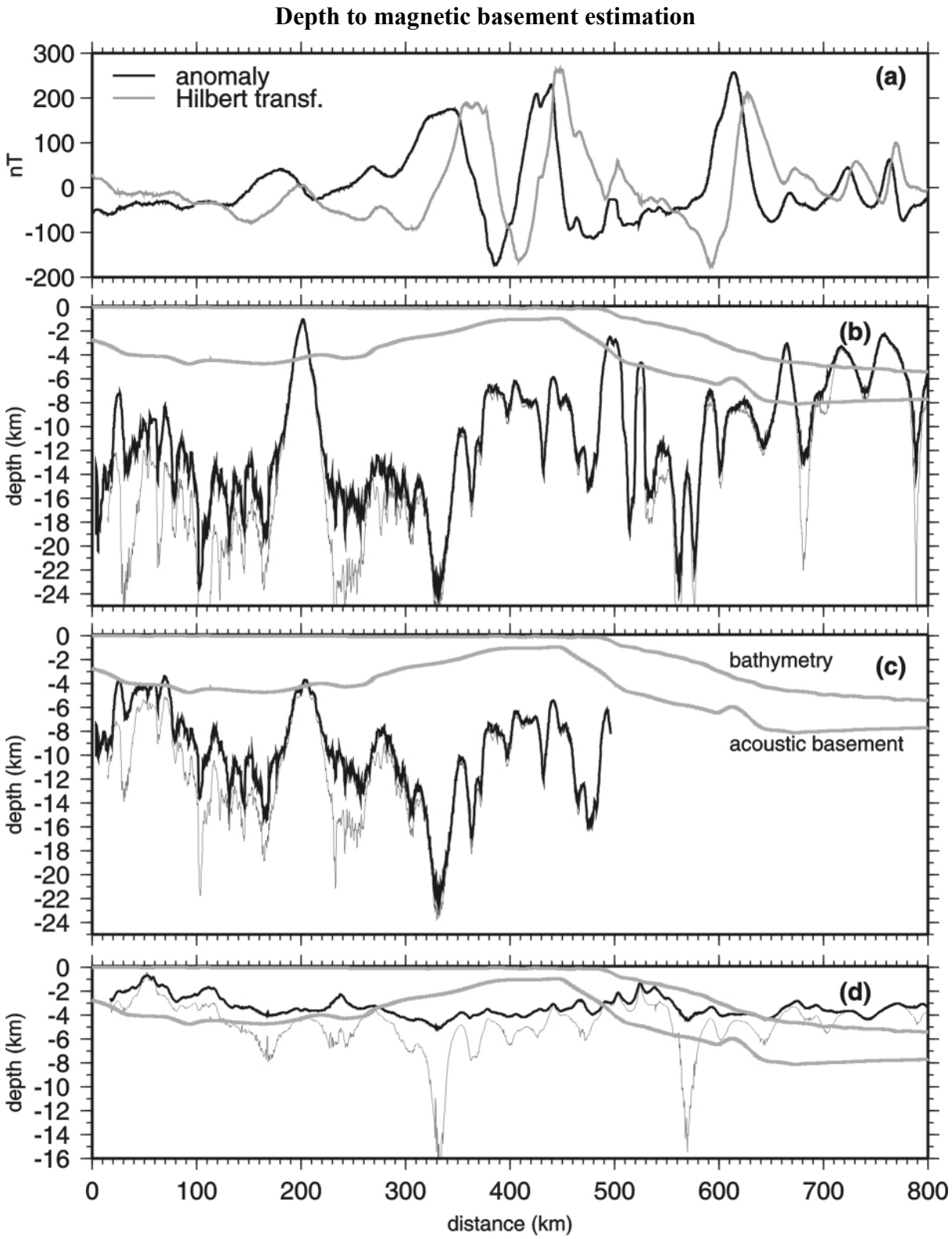

FIGURE 2: Three examples of ACME depth to magnetic basement for profile in (a). (b): with original method; (c): same as (a) but using a shorter shorter portion of the profile; (d): with corrected method. Examples display first estimate (thick line) and fourth estimate (thin line).

interpolated from a published map. The first 250 km of the profile traverse the Colorado Basin, where we would expect the sources to be deep. The anomaly profile is relatively flat there, and the map in figure 1 shows that the pattern is far from being two-dimensional. Therefore we could interpret that the divergence in successive estimates means that the model does not apply to this sector of the profile. But there is a peak at 200 km where the estimates converge and the result is not good. Furthermore, where the profile reaches the ocean, source depth is noticeably underestimated.

In figure 2(c) we show the results obtained if only the first 500 km of the profile are used. They look better, but they should be exactly the same as those in figure 2(b). We tried different sectors of different profiles and the results were dependent upon the length of the profile. This moved us to look at the program code carefully, and we found the reason for the discrepancy. In Burg's method the equations for recursive calculation of the autocorrelation are valid if the mean of the data series is zero. In the original ACME program the mean value is removed from the data but for the whole profile. Then the *backward* and *forward* vectors are calculated for all the profile, and subsets are used for each position of the window. As Burg's algorithm is applied to each window position, and the windowed data normally do not have a zero mean, the result may be strongly biased.

We modified the program, making sure that the mean is removed at every window position. The results of the corrected method are shown in figure 2(d). As we can see, although numerically consistent, they are not good. The estimates corresponding to the first lag generally give small depth values. We have used a wider moving window for this case, 30 km, whereas for the original ACME we had used 7.5 km. Larger windows give greater depth estimates, so in this way we forced the corrected ACME to yield deeper solutions.

Werner deconvolution

This method uses a completely different approach (Hartman et al., 1971). A moving window is run along the profile. The dike anomaly is adjusted to the anomaly itself as well as to its horizontal and vertical

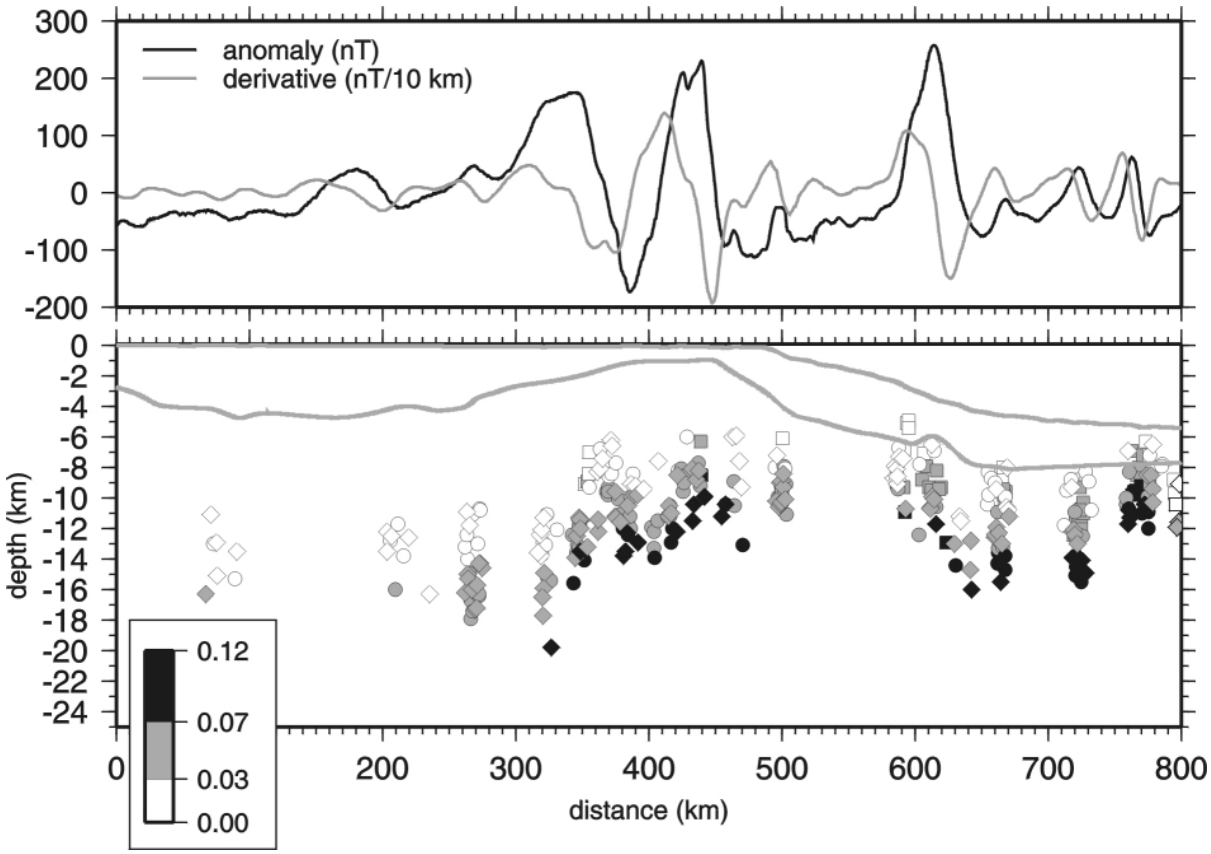

FIGURE 3: Magnetic anomaly profile and its horizontal derivative (top) and depth estimates using Werner deconvolution (bottom). Square symbols are estimates from the anomaly profile, circles are from the horizontal derivative and diamonds from the vertical derivative. Color bar is for estimated susceptibility in SI.

derivatives, the former being calculated from the data, and the latter inferred from the former considering that if they match the dike anomaly then they are Hilbert transform pairs. Three corresponding estimates are obtained. Acceptance - rejection criteria are applied, based on the quality of the adjustment. We have added a crude estimate of the susceptibility, which provides an additional constraint: the susceptibility has to be between specified bounds for the depth estimate to be accepted. In figure 3 we display our results for a 30 km moving window. In the first 300 km of the profile there are few accepted estimates. This is the zone in which the 2D approach is less valid, as mentioned above. Between 300 and 500 km the profile shows intense magnetic anomalies in a region where the 2D approximation is somewhat better. We observe dispersion in the accepted estimates, the deeper ones requiring higher susceptibility as is natural. What we find particularly interesting is that the area covered by the accepted estimates roughly delineates the shapes of the bodies that we used for forward 2D modeling of the anomalies. In the remaining sector of the profile the ocean - continent boundary is reached: the high amplitude anomaly at 600 km is anomaly G, and again, the accepted estimates somewhat delineate the magnetic model in Hinz et al. (1999) which is supported by the observation of a volcanic wedge inferred from seaward deeping seismic reflectors. The estimates farther offshore may be the sources of the Mesozoic anomalies.

Conclusions

The tests that we have performed and our previous experience tell us that for deep sources the semi infinite dike model fails (ACME method).
Werner deconvolution is a good approach to start depth to source analysis.

References

Ghidella, M.E., C. J. Chernicoff, C.M. Paterlini, J. C.Gianibelli, E. Suárez, I.R. Cabassi and J. Kostadinoff, 2000. Estudio de avance de la integración de levantamientos magnéticos marinos y continentales en la franja litoral entre las latitudes 35 y 47 S, Argentina. Proceedings of the IX Congreso Geológico Chileno, Vol. 2, Simposio Nacional No 5, 443-447.

Hartman, R.R., D.J. Teskey, J.L. Freidberg, 1971. A system for rapid digital aeromagnetic interpretation, Geophysics 36, 891-918.

Hinz, K., S. Neben, B. Schreckenberger, H. A. Roeser, M. Block, K. Goncalves de Souza and H. Meyer, 1999. The Argentine continental margin north of 48°S: sedimentary successions, volcanic activity during breakup. Marine and Petroleum Geology 16: 1-25.

LaBrecque, J.L., M.E. Ghidella, 1997. Bathymetry, depth to magnetic basement, and sediment thickness estimates from aerogeophysical data over the Western Weddell Basin, J. of Geoph. Res. 102, No B4, 7929-7946.

Max, M.D., M.E. Ghidella, L. Kovacs, M. Paterlini,, J.A. Valladares, 1999. Geology of the mainland Argentine continental shelf and margin from aeromagnetic survey. Marine and Petroleum Geology, 16, 41-64.

Phillips, J.D., 1978. ADEPT: a program to estimate depth to magnetic basement from sampled magnetic profiles. U.S. Geological Survey computer contribution. Reston, VA, p. 35.

The Cavalcante and Minaçu-Brasília deep seismic refraction lines: a travel time interpretation of crustal structure in Central Brazil

[1]SOARES, J.E.P., [2]BERROCAL, J. and [2]ANTUNES, J.A.
[1]Observatório Sismológico /IGD-UnB, Brasília-DF, Brazil,
[2]Instituto de Astronomia, Geofísica e Ciências Atmosféricas/USP, São Paulo-SP, Brazil:
emails: soares@unb.br, berrocal@iag.usp.br; juliana@iag.usp.br

Abstract

The travel time interpretation of two deep seismic refraction lines deployed in the northeast part of Tocantins Province, Central Brazil, lead to a crustal model characterized by a lateral discontinuity with an upper crust with Vp of 6,2 km/s and a lower crust with Vp of 7.1 km/s in Brasília Fold Belt and 6.9 km/s in São Francisco Craton. The Moho is around 40 km deep.

Introduction

This work presents the travel time analysis of the Cavalcante and Minaçu-Brasília deep refraction lines that crossed the Brasilia Fold Belt (BFB) and São Francisco Craton (SFC) in Central Brazil. The Minaçu-Brasília refraction line has an almost N-S direction and mapped, essentially, the BFB while the Cavalcante line has a NW-SE direction, crossing the limit between BFB and SFC.

Refraction/wide angle reflection analyses results of these experiments lead to a model having a smooth upper crust with a mean velocity of 6.2 km/s and a lower crust beginning at around 26 km of depth, with velocity varying from 6.9 km/s beneath SFC to 7.1 km/s beneath BFB. The Moho discontinuity is around 40 km deep with a relief that suggests an Airy isostatic compensation in Central Brazil.

These deep seismic refraction experiments are part of a major project, supported by FAPESP, that is studying the crustal structure of the Tocantins Province in Central Brazil.

Geological Setting and Gravimetric Data

The Tocantins Province was build up during the Brasiliano orogenic cycle and represents the inversion of an oceanic basin of passive margin, closed between the São Francisco and Amazon cratons (Fuck et al., 1993). This province may represent the most complete Proterozoic orogenic reminiscent in South America. It is formed, in the eastern side, by metasediments of the Brasilia Fold Belt and in the western side, by metasediments of the Araguaia Fold Belt, enclosing a complex terrain, the former Goiás massif, with continental and island arc features.

The refraction lines were performed, one in the eastern side of the Tocantins Province along BFB (Minaçu-Brasília profile) and the other almost perpendicular to the border BFB-SFC (Cavalcante profile), see Fig. 1. The BFB and SFC are, respectively, a Proterozoic platform and shield terrain.

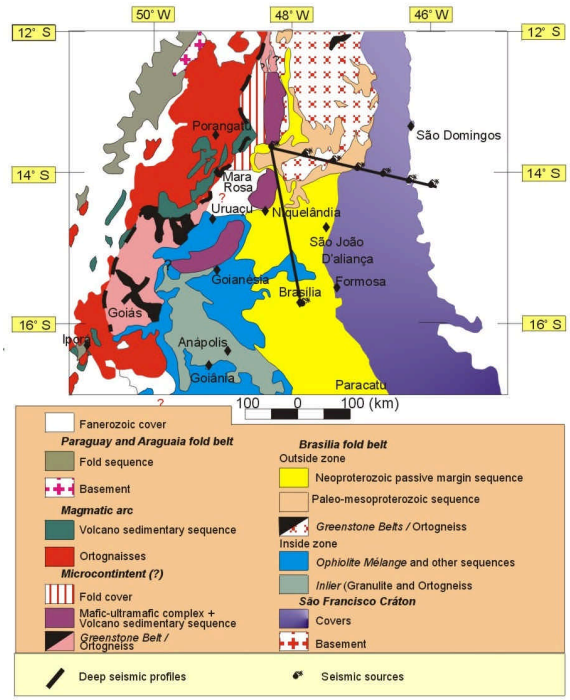

FIGURE 1 – Geologic sketch of the Tocantins Province showing the deep seismic refraction lines that were deployed in the northeastern side of the province.

Central Brazil has a good regional gravimetric coverage (Marangoni et al. 1999) that shows strong NW-SE gravimetric variation. The contrast between gravimetric anomalies marks the limit between major geological features of the Tocantins Province (Fig. 2). The gravimetric low, represented by anomalies smaller than -100 mGals, are representative of BFB and the easternmost gravimetric anomalies larger than that are related to SFC. In the Tocantins Province the topographic highs are well correlated with low gravimetric anomalies. Within the SFC this relation is less evident.

Field Parameters

The Minaçu-Brasília line was performed in November 1997, between Brasília, Distrito Federal, and Minaçu, Goiás. Initially it was considered as an

experimental line to test source charges for the main refraction experiment that was deployed in September 1998. This almost NS line had twenty digital recording points distributed in almost 260 km. Some of these stations belong to the Serra da Mesa and Brasília seismological arrays. Sources were 800 kg of explosives filled in 3 inches 10 m deep boreholes. The direct profile had its source in the Cimento Tocantins Mine (Brasília) and the reverse profile in the SAMA Mine (Minaçu). The reverse profile was enlarged by data recorded at the Serra da Mesa and Brasília arrays during the main refraction experiment performed in 1998. The direct profile of the Minaçu-Brasília line is shown in Fig. 3a. These records are of moderate quality but due to their direction and position they are important in the context of the Brasilia Fold Belt investigation.

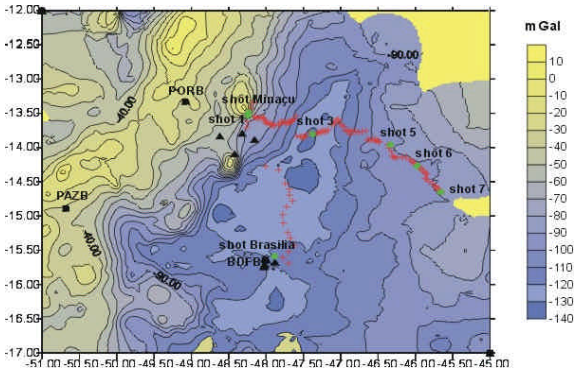

FIGURE 2 – Bouguer map of the northeast part of Tocantins Province with the Brasília-Minaçu (~N-S) and the Cavalcante (~NW-SW) deep refraction lines. Crosses are temporal recording points, triangles permanent network of Serra da Mesa (N) and Brasilia (S) arrays, stars the shot points and squares the receiver function stations.

The Cavalcante deep refraction line was about 300 km long in a NW-SE direction. It was deployed with around 120 recording points and explosions at every 50 km along the profile. The explosive used was IBEMUX emulsion filled in 6 inches bore holes 45 to 65 m deep. The explosive charges varied from 500 kg, in the center of the line, to 1000 kg in the extremes. They were detonated during the night to diminish the influence of cultural noise. These records are of good quality, shot 1 is shown in Fig. 3b, except for shots 6 and 7 that were fired in Cretaceous sandstone and had their energy strongly absorbed, weakening deep phases.

Both lines have the explosions at Minaçu as a common point, one directed to the south (Minaçu-Brasília line) and the other to the SE (Cavalcante line), as shown in figs. 1 and 2.

Considerations About Data Analysis

The Cavalcante line allowed to elaborate five profiles, one for each explosion, that were mounted by using the Seismic Unix (SU) package (Fig. 3a). This package permits to pick phases directly in the section, resulting in an improvement of the interpretation. On the other hand, the Minaçu-Brasília profiles were elaborated by using the Seismic Analysis Code (SAC) package (Fig. 3b) that mount sections but pick phases in individual traces. When the data quality is not high, the SAC package is recommendable because it allows a better detail of the seismic trace.

a) Shot Brasília profile

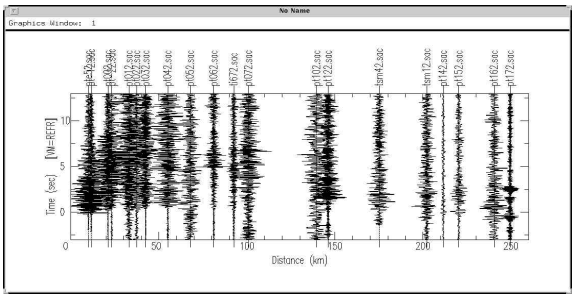

b) Shot 1 profile

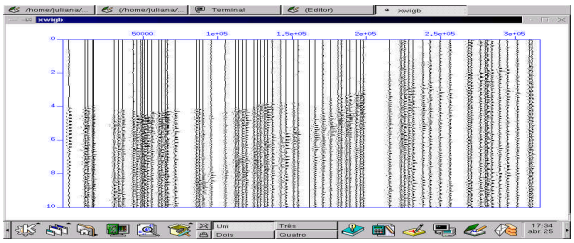

FIGURE 3 – Minaçu-Brasília and Cavalcante sections reduced with V_P=6.0 km/s. In the shot Brasília the time grows upward while in shot 1 the time grows downward.

The profiles were reduced with a P wave velocity (V_P) of 6.0 km/s and 8.0 km/s to pick phases. The set of first break time-distance curves for Cavalcante line reduced by a velocity of 8.0 km/s are shown in Fig. 4. Band pass filter of 1-10 Hz was used to pick the first breaks mentioned above and a band pass of 1-15 Hz to pick the Moho reflection phases. Once the apparent velocities and intercept times of the main refractors were determined, the reverse profiles were interpreted and an initial model was obtained by using the intercept time method (see Fig. 5). Flat layers are considered with V_P changing only with depth, although it presents a lateral discontinuity that cuts the entire crust. The lateral changes were determined by observing the differences in the results of the analysis of two by two direct/reverse profiles along the Cavalcante refraction line.

By using the refraction phases of the direct/reverse profiles 1-7 (~300 km) and 1-6 (~250 km), the Moho discontinuity could have been mapped if the signal on sections 6 and 7 were of better quality. The Moho

discontinuity has been defined in this work by using the reflection phases with the X^2-T^2 method.

While the Cavalcante refraction line crosses BFB and SFC, with its results reflecting their mean physical properties, the Minaçu-Brasília line follows only BFB and, in spite of the poor data quality, it is important for the determination of behavior of the lower crust and Moho discontinuities along the BFB.

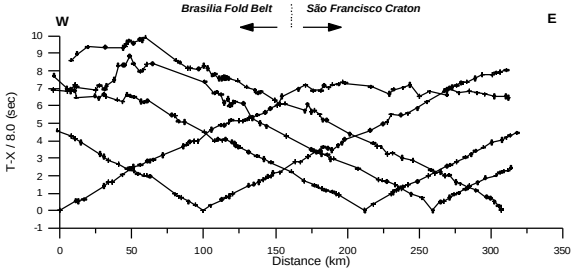

FIGURE 4 – Time-distance curves from Cavalcante profiles, shots 1, 3, 5, 6 and 7 respectively. The curves are presented with a reduction V_P=8.0 km/s.

Main Results

The initial model is displayed in Fig. 5. Near the surface, V_P for the BFB is 5.8 km/s close to shots 1 and 3 (Cavalcante line) and 5.5 km/s close to Brasília. To the east V_P changes to 5.7 km/s in shot 5 (Posse) and to 4.7 km/s in shots 6 and 7. The abrupt lateral change in surface velocity in the Cavalcante line represents the passage from the Neoproterozoic Bambuí Group to the Cretaceous sediments of the Urucuia Group in SFC. A few kilometers below the surface, V_P changes to 6.1 km/s and increases smoothly up to around 6.3 km/s at the depth of 26 km where it jumps to 7.1 km/s in BFB (platform terrain) and to 6.9 km/s in SFC (shield terrain), along the Cavalcante line. Close to Brasilia (Fig. 2) the transition to the lower crust is around 30 km deep and presents a velocity of 7.0 km/s. This sharp horizontal discontinuity marks the beginning of the lower crust in the region. Moho discontinuity is around 41.4 km to 42.4 km deep in the BFB and around 39.0 km in the western portion of SFC. The mantle V_P is 8.2 km/s.

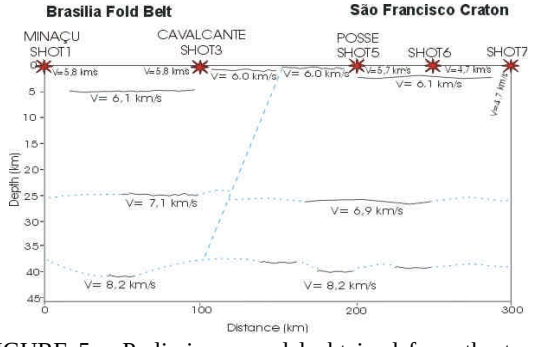

FIGURE 5 – Preliminary model obtained from the travel time analysis of deep seismic refraction lines deployed in the northern part of the Brasilia Fold Belt (platform terrain) and the western part of the São Francisco Craton (shield terrain). V is P wave velocity given in km/s. V values in the superficial layers of the western side of shot 6 vary from 5.8 to 5.7 km/s and are equal to 4.7 km/s in the eastern side of the shot.

This model is in agreement with the deep refraction results of Giese and Schutte (1980) for southeastern SFC and Pedreschi (1989) for northern SFC. Together these data allow to coarsely infer the SFC deep structure.

Moho discontinuity depths and crustal mean P wave velocities shown in Table 1 were determined from the analysis of wide-angle reflection phases. These values were roughly corrected by using the ray tracing modeling package SEIS88 (Cervený et al., 1977) for a two layer model with a crustal mean velocity of 6.42 km/s and a slight dipping Moho. The wide-angle reflection analysis for shot 7 from the Porangatu deep seismic refraction line (Berrocal et al., 2001) is also included in Table 1 for comparison. This line is the west continuity of the Cavalcante line and crosses the high gravimetric anomalies of the Tocantins Province, represented by Proterozoic island arc terrain.

Table 1- Moho depth and mean crustal velocity of the BFB and SFC.

Profile	Altitude (m)	Crust thickness (km)	Crustal mean velocity (km/s)
Cavalcante-shot 1	880	41.4	6.45
Cavalcante-shot 3	520	38.6	6.34
Cavalcante-shot 5	520	38.7	6.20
Cavalcante-shot 6	780	40.7	6.32
Cavalcante-shot 7	930	39.3	6.32
Shot Brasilia	1000	42.4	6.30
Porangatu-shot 7	680	36.1	6.25

In addition to the wide reflection data, receiver function solutions were presented by Assumpção (in Berrocal et al. 2001) for the BDFB station, that is coordinated by the Observatório Sismológico / Universidade de Brasília, and for the temporary stations of Porangatu, Araguapaz and Corumbá, that are part of the this same project (see Table 2).

The Porangatu crustal thickness from wide angle reflection is in agreement with the result of PORB station located near the Porangatu deep refraction line. Stations PAZB and CORB are located far from the refraction lines, sampling different points of Tocantins Province. In synthesis, the data suggest that the Moho discontinuity is deeper beneath the topographic highs, that are closely related to gravimetric lows.

Table 2- Receiver function solutions for the Tocantins Province (modified from Assumpção, in Berrocal et al. 2001)

Station	Altitude (m)	Crust thickness* (km)	Crustal mean velocity Vp (km/s)
BDFB	1095	40.7	6.46
PORB	365	36.7	6.38
PAZB	410	33.2	6.38
CORB	950	42.4	6.46

(*) Thickness calculated with a $V_P/Vs=1.732$ in the crust.

Discussion

The lateral discontinuity of the initial model shown in Fig. 5 represents the seismic limit in depth of BFB and SFC that, in general, coincides with the surface geological limit. The variation of velocity throughout the discontinuity, in the upper crust, is very smooth, denoting close similarities between the rocks of both blocks. Supported by geological studies, Cruz and Kuyumjian (1993), concluded that the basement in the Natividade/Dianópolis area, north of Cavalcante line, is similar to the basement of São Francisco Craton, matching the result above. In the lower crust, however, the lateral limit is more abrupt indicating different material on both sides. Considering that BFB is a platform terrain, formed by the stretching of the western border of the São Francisco Craton, this difference can be an evidence that the BFB lower crust is the reworked São Francisco Craton lower crust. Reworking probably took place during the opening of the former "Goiás Ocean".

The Moho depth and the crustal velocity from shots 3, 5, 6 and 7 (Table 1) are representative of the SFC while results from shot 1 and Brasilia shot are representative of BFB. These results provide a mean crustal velocity of 6.3 km/s and a crustal thickness of around 39.0 km for the SFC and a mean crustal velocity of 6.45 km/s and a crustal thickness of 41.4 km for the BFB, close to shot 1. In the Brasília area the BFB mean crustal velocity is 6.3 km/s and 42.4 km of crustal thickness, showing a southward variation of the BFB mean crustal properties.

Three important considerations must be emphasized: 1) shot 6 presents a Moho depth apparently discrepant from shots 3, 5 and 7 but the mean crustal velocity is concordant; 2) the Moho in Brasilia obtained from the Minaçu-Brasília profile is a little deeper than that determined by the receiver function method and the mean crustal velocity smaller than that used by Assumpção (in Berrocal et al. 2001); 3) the crustal mean velocities obtained from Moho reflections match very well with mean crustal velocities obtained from refraction phases, either in Cavalcante or in Minaçu-Brasília profiles.

Although some details are still open, in general the refraction and receive function results are very close. Seismic data together with the gravimetric map shows that the isostatic compensation in Central Brazil is preferentially controlled by variation in crustal thickness. In other words, the isostatic equilibrium in Tocantins Province is controlled by Airy mechanism (Assumpção in Berrocal et al. 2001) and it seems to be true also for a wider region, with SFC included.

Acknowledgements

The authors thank the FAPESP by the financial support.

Thanks, also, the Minaçu Mine, the Toniolo-Busnello Mine, the Tocantins Mine, the Pratudão Agropecuária and the farmers for the logistic and material help during the field works.

Special thanks to Prof. R. A. Fuck for his valuables comments and suggestions.

Reference

Berrocal, J., Assumpção, M., Côgo de Sá, N., Marangoni, Y., Fuck, R. A., Pimentel, M., D`el-Rey Silva, L.J.H., 2001, *Estudos Geofísicos e Modelo Tectônico dos Setores Central e Sudeste da Província Tocantins, Brasil Central*. Third Annual report of a thematic research project support by FAPESP.

Cervený, V., Molotkov, J. and Psencik, I., 1977, *Ray Methods in Seismology*. Charles University, Prague, 1977.

Cruz, E.L.C.C. and Kuyumjian, R.M., 1993, In: Domingues, J.M.L., Misi, A. (eds.). *O Cráton do São Francisco*. Salvador, SBG/SGM/CNPq, p. 302-304.

Fuck, R.A.; Jardim de Sá, E.F.; Pimentel, M.M.; Dardenne, M.A.; Pedrosa Soares, A.C., 1993, In: Domingues, J.M.L., Misi, A. (eds.). *O Cráton do São Francisco*. Salvador, SBG/SGM/CNPq, p. 161-185.

Giese, P. and Schutte, K.G., 1980. Resultados das medidas de sísmica de refração a leste da Serra do Espinhaço, M.G., Brasil. Unknown publication title, p. 44-50.

Marangoni, Y., Côgo de Sá, N. and Lobianco, M.C., 1999, *Mapa gravimétrico de Goiás*. Submitted to Rev. Bras. de Geofísica.

Pedreschi, E. S, 1989, *Modelo regional preliminar da estrutura crustal na região do reservatório de Sobradinho com dados de refração sísmica profunda*. Under graduation report. IAG-USP, São Paulo.

THE GEOMAGNETIC Dst INDEX: A STUDY

V.M.Silbergleit
Dep. de Física de la Facultad de Ingeniería. Universidad de Buenos Aires.
Av. Paseo Colón 850 – Piso 2. 1063 -Bs.As. Argentina.

ABSTRACT

Largest geomagnetic storms characterized by the Dst index, that happened from 1957 to 1989 are considered. Gumbel's first asymptotic distribution extreme values to predict the occurrence of storms is used. According to this, modal extreme values and return periods are estimated .
Times of repetition of 2 and 7 solar cycles are obtained for events with Dst peak of approximately -400 nT and -600 nT respectively.

INTRODUCTION

Geomagnetic storms are identified by the enhancement of the ring currents and quantified by the Dst index. The hourly Dst index registers with the greatest accurateness the occurrence of events for which it was projected. It is actually compiled by the World Data Center C2 for Geomagnetism in Kyoto, Japan.
The biggest storms generally beginning with a sudden commencement which is prior to the geomagnetic perturbation. These events are taken to be related to random processes.
The extreme values arranges a series in order of size, considering a chi-square function to test whether the data follows a normal distribution. In this way, it is possible to obtain maximum values and return periods (Gumbel,1967).
Prior geomagnetic prediction studies (Siscoe, 1976 and Gao, 1986) were done using the Gumbel's first asymptotic distribution applied to aa and Ap indices respectively.

PREDICTION MODEL

Extreme value statistics are deduced using the lowest or highest value of series.
$\Phi(M)$ and $[1-\Phi(M)]$ are the probabilities that a given observation of an extreme D in a solar cycle be less or greater than M respectively (where D is the absolute value of the Dst index magnitude). The theory of extremes provides the expression of $\Phi(M)$ (Gumbel,1967).
The first asymptotical function distribution of the extreme value of Gumbel is defined by:

$$\Phi(M) = \exp\{-\exp(-y)\} \quad \text{and} \quad y = \beta(M-m) \qquad (1)$$

where m (mode) and β are constants.
As $\Phi(M)$ is not known, the constants m and β must be found by fitting the observations using:
The return intervals T(M) between such extreme values are calculated by using the expression:

$$T(M) = [1-\Phi(M)]^{-1} \qquad (2)$$

where T(M) is the expected time required to have one event with the extreme equal to or exceeding M.
Fig. 2 shows the curve T(M), when the ordinate is equal to 2, the abscissa is equal to the median value. Extreme values of D of approximately 400 and 600 nT are obtained for the next 2 and 7 solar cycles respectively.

SELECTION OF STORMS

Temporal distribution of Dst minimum values associated to largest storms per solar cycle from 1957 to 1989 as published by Mayaud and Romañá (1977) and Sugiura and Kamei (1991) are studied.

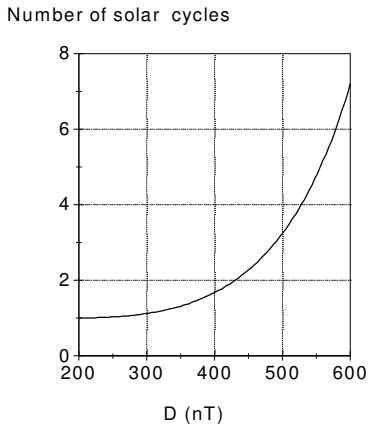

Fig. 2. *Number of solar cycles required to detect one cycle with extremes equal to or exceeding M.*

CONCLUSIONS

We studied the occurrence of geomagnetic storms by the method of extreme value statistics applied to Dst index. By considering this predictive method, a least squares straight line fit to the observations is performed and the statistical relationship is well satisfied.
Repetition times for events with modulus of Dst greater than 400 nT and 600 nT will be expected to occur within the next 2 and 7 solar cycles, respectively.
To improve the assurace of the results for largest storms, more solar cycles are needed.

ACKNOWLEDGMENTS

Geomagnetic and solar data were kindly supplied to us by T.Iyemori and T.Kamei and G. Heckman respectively. This research was supported in part by UBA and CONICET of Argentina.

REFERENCES

Gao,M.,A comparison of solar and geomagnetic activities from the 13th to 21th solar cycles.,in *Solar wind -magnetosphere coupling.* Ed. Y.Kamide and J.A.Slavin. Terra Scientific, Tokyo, pp. 149,1986.

Gringorten,I.I. A Plotting Rule for Extreme Probability Paper, *J. Geophys. Res. 68*, 813, 1963.

Gumbel,E.J. *Statistics of extremes*. Columbia Univ. Press, NY,pp. 375,1967.

Mayaud, P.N. and A. Romañá. *IAGA Bulletin n°39*, 112,1977.

Siscoe, G.L., On the Statistics of the Largest Geomagnetic Storms per Solar Cycle. *J. Geophys. Res., 81*, 4782, 1976.

Sugiura,M., and T. Kamei. *IAGA Bulletin nº 40*, 17,1991.

The gravity database of the Observatório Nacional and the current status of the Brazilian Fundamental Gravity Network

Walter Humberto Subiza Piña and Mauro Andrade de Sousa, OBSERVATÓRIO NACIONAL, Rua Gal. José Cristino, 77 – São Cristóvão, 20921-400 Rio de Janeiro, RJ, Brazil. E-mail: humberto@dge1.on.br *and* mauro@on.br

Abstract

A project was set up at Observatório Nacional-ON to establish a gravity database open to the national and international communities. This is an ongoing project aiming at recording the raw fieldwork information, performing the conventional data reduction and, when needed, the adjustment of the gravity intervals. An important by-product of this project is the adjustment of the Brazilian Fundamental Gravity Network to the absolute datum.

Introduction

For many decades the Observatório Nacional has been involved with the establishment of gravity standards in Brazil and their uses in geodetic, geophysical and metrological applications. Although gravity measurements had been sporadically taken in the mid XIX century (De Oliveira, 1851), systematic land gravity surveys initiated only in 1955 with a Worden gravimeter. After 1968 LaCoste & Romberg meters were adopted, and the effort to establish a national gravity network began in 1976 using LC&R G meters only. In 1986, an adjustment of this network to the IGSN71 datum was made, including 388 stations (Observatório Nacional, 1986). This dataset is known as the "Rede Gravimétrica Fundamental Brasileira – RGFB". Several absolute gravity stations were established in South America in 1989-91 by the Institut für Erdmessung-IfE in collaboration with national organizations (Torge *et alli*, 1994). A JILAG-3 absolute gravimeter was used and seven of these stations are in Brazil. Thus, a new gravity datum precise to a few $nm \cdot s^{-2}$ was made available, allowing the adjustment of the dataset collected with the LC&R 61 in the 1968-1975 period. This dataset, comprising 1483 stations, is referred to the absolute datum (De Sousa & Moreira, 1994). The Observatório Nacional established well over 6000 gravity stations in Brazil, many of them through collaborative work with other Brazilian institutions. A need was recognized to efficiently organize this data base, referring it to a single and well-defined datum and make it available to interested individuals, private and state institutions. A brief description of the effort done follows.

The gravity database of the Observatório Nacional

All gravity campaigns carried out by the ON since 1955 have been or are in the process of being archived in digital format. An excerpt of the datasets currently held are shown in Table 1.

Table 1 – Excerpt of the gravity information held at the ON database.

Meter	Number of stations	Number of observations	Period
W178	1649	7214	1955-1967
G061	1580	4172	1968-1975
RGFB	530	8051	1976-2000
Total	3759	19437	-

The database has been built using MS Access® due to the relative small amount of information and the wide format exchange possibilities offered by this software. All gravity information is organized in four different tables, each one using appropriate sorting keys:

Main Table – station identification, geographical coordinates, altitude, adjusted gravity value, gravity standard deviation, Free-air and Bouguer anomalies and terrain correction.

Description Table – station identification and description, photos and station location croquis;

Occupation Table – station identification, date and mean time of the reading, gravimeter type and serial number, mean reading and GMT zone;

Quality Table – station identification, sources and quality factors of the adjusted gravity values and geographic coordinates, meter and terrain correction types.

Tailored reports may be issued from different tables as shown in Figure 1.

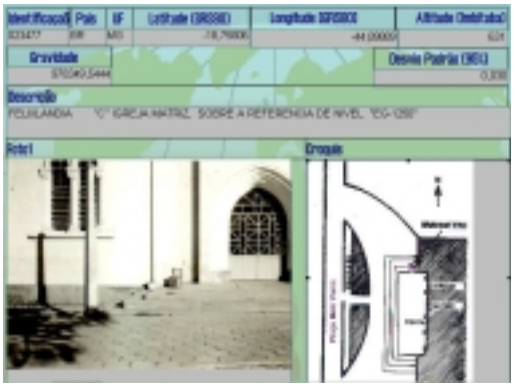

Figure 1 – Example report showing gravity station information.

An effective test of the usefulness and ease of use of the database was devised by recovering all information related to the RGFB. Since 1986 new stations have been added to this first-order gravity network and several ties to the absolute stations in Brazil and neighboring countries were made.

Adjustment of the Brazilian Fundamental Gravity Network (RGFB)

The RGFB established by Observatório Nacional was simultaneously adjusted to 9 absolute stations of the JILAG-3 datum by conventional least squares minimization (LSQ). Currently, the RGFB is made up of 521 gravity stations spanning a gravity range a little over than 1900 mGal and distributed over a 39.5° latitude range (Figure 2). This network is connected to Bolivia, Venezuela and Uruguay.

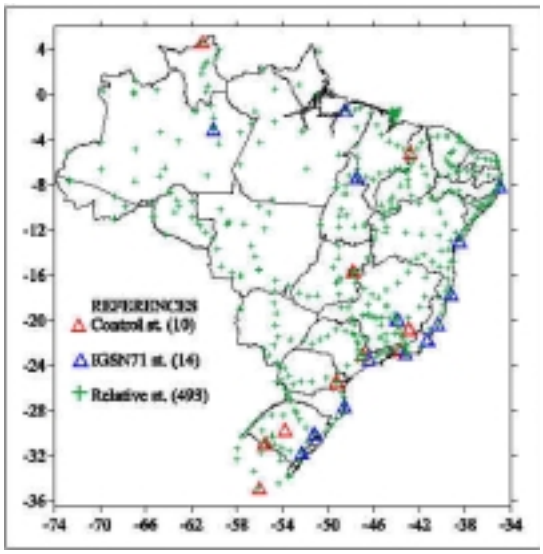

Figure 2 – The Brazilian Fundamental Gravity Network established by the Observatório Nacional.

Data processing started forming sets of observed gravity intervals between stations for each meter used in establishing the RGFB. Software GRR.FOR (De Sousa & Veiga, 2001) was employed in this phase, taking into account static and dynamic meter drifts. Tide corrections using Longman´s model (Longman, 1959) were adopted. This model does not consider oceanic tides and the loading effect and a comparison was made at selected stations and epochs with the Tayler, Cartwright and Eden model for 552 waves. Differences found did not exceed 1 μgal and were found irrelevant to the present study. As a result, mean gravity differences between stations were thus obtained for individual meters. Mean gravity differences were then scaled, according to the residual scale factors previously determined by De Sousa & Moreira (1994), Escobar *et alli* (1996) and Subiza *et alli* (1998). Scaled intervals were LSQ adjusted producing adjusted gravity intervals and *g* values for each station. Close examination of the skewness in the distribution of gravity residuals allowed for better estimates of the scale factors for LC&R meters 11, 13, 61, 454 and 703 (Table 2).

Table 2 – Statistics of gravity intervals and scale factors for LC&R gravimeters used in the RGFB.

LC&R meter	Observed Intervals	Valid	Dataset %	Rejected	Scale factor
G011	22	15	0.9	7	0.99995
G013	16	14	0.9	2	0.99860
G041	51	51	3.2	0	1.000761
G061	279	278	17.2	1	1.000000
G257	520	513	31.8	7	1.000317
G454	19	19	1.2	0	1.000000
G602	296	292	18.1	4	1.000471
G622	250	246	15.2	4	1.000448
G628	4	1	0.1	3	1.000460
G674	139	137	8.5	4	1.000476
G703	16	16	1.0	0	1.00065
Total	1612	1580	-	32	-
%	-	100	98.1	1.9	-

The weight matrix used in the adjustment procedure was derived from: **i** standard deviations already known for the absolute stations (Torge *et alli*, 1994) and the Montevideo station (Subiza Piña *et alli*, 1998), **ii** mean standard deviations of 20 μGal for ties between absolute stations and the RGFB, and **iii** mean standard deviations of 25 μGal for internal RGFB gravity differences. A reduced chi-square of 1.14 was found after the adjustment, further confirming the adequacy of the weight matrix.

Table 3 – Location and *g* uncertainty of the JILAG-3 and Montevideo stations employed in the adjustment of the RGFB.

Station Id.	Lat. (deg.)	Long. (deg.)	Height (m)	Absolute *g* (mGal)	Standard deviation (mGal)
IfE 040	+ 4.67	-61.07	93	977822.084	0.0027
IfE 112	- 5.08	-42.80	70	978016.343	0.0031
IfE 122	-15.67	-47.83	1100	978048.798	0.0005
IfE 132	-20.73	-42.88	653	978460.230	0.0035
IfE 142	-22.55	-43.65	400	978637.581	0.0019
IfE 152	-22.98	-47.00	850	978563.778	0.0032
IfE 162	-25.42	-49.27	910	978760.387	0.0021
IfE 173	-29.68	-53.80	85	979261.636	0.0022
IfE 212	-30.88	-55.53	213	979344.377	0.0014
250187	-34.85	-56.03	16	979732.397	0.0105

A summary of the statistics of this adjustment is shown in Table 4. This table also lists the statistics of the corrections applied to the preliminary absolute gravity values, to the residuals of the adjusted gravity intervals and to the standard deviations of the 521 stations. Figure 3 plots the residuals of Table 4 at 5 μGal interval.

Table 4 – Summary statistics for the adjustment of the RGFB.

Absolute Stations	9			
Relative Stations	512			
Absolute gravimeters	1			
Relative gravimeters	11			
Fixed control stations	0			
Station data records	521			
Gravity intervals	1580			
Adjustment unknowns	521			
Parameter (μGal)	**Mean**	**Max.**	**Min.**	**Std. Dev.**
Corrections	36.5	288.8	-240.8	55.8
Residuals	-0.63	106.01	-109.7	21.6
Std. Deviation of stations	27.5	48.8	0.5	-

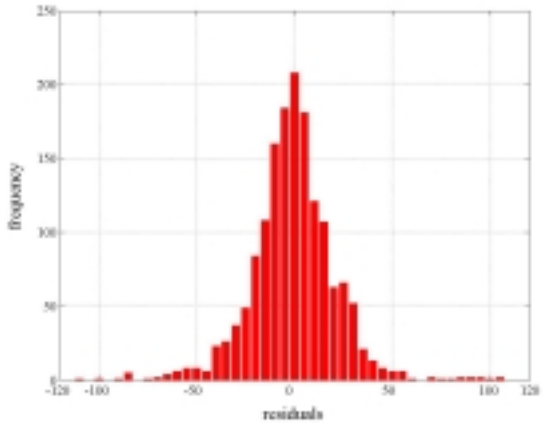

Figure 3 – Histogram of residuals (1580 samples).

Residual statistics for all gravimeters employed in establishing the RGFB are shown in Table 5, while Figures 4 to 7 exhibit histograms for meters G 61, G 257, G 602 and G 622.

Table 5 – Residual statistics for all gravimeters (in μGal).

Gravimeter	Mean	Max.	Min	Std. Dev.
G011	+2.6	89.9	- 82.7	53.5
G013	-1.9	35.6	- 26.7	19.9
G041	-2.5	30.9	- 39.9	20.3
G061	+1.4	106.0	-90.1	21.7
G257	-0.1	98.9	- 109.7	20.3
G454	-2.1	34.2	- 34.7	19.6
G602	-3.5	73.2	- 75.9	20.0
G622	+0.6	85.2	- 97.8	22.8
G674	-2.5	91.2	- 83.6	22.3
G703	-0.7	29.0	- 29.1	18.7

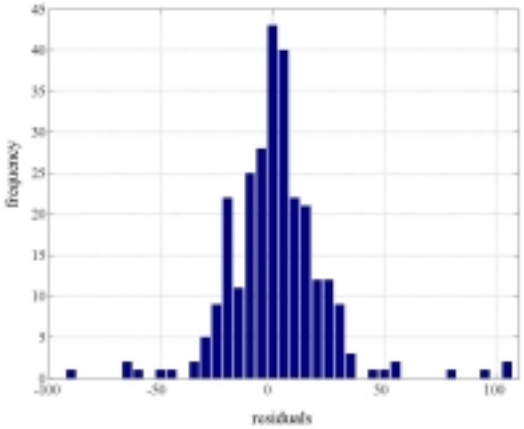

Figure 4 – Residuals for LC&R G 61.

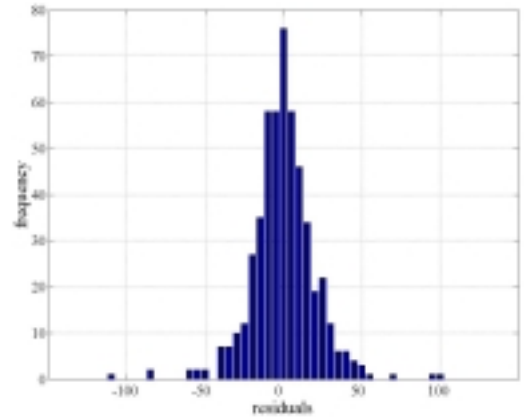

Figure 5 – Residuals for LC&R G 257.

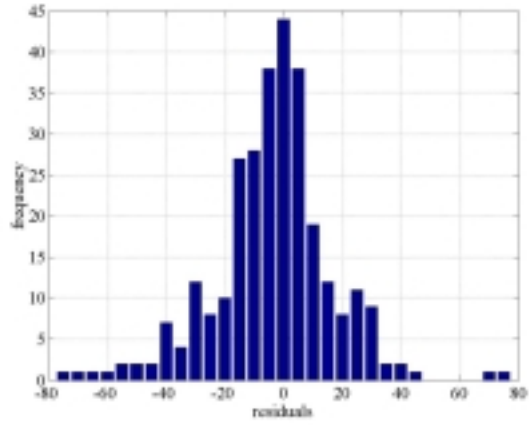

Figure 6 – Residuals for LC&R G 602.

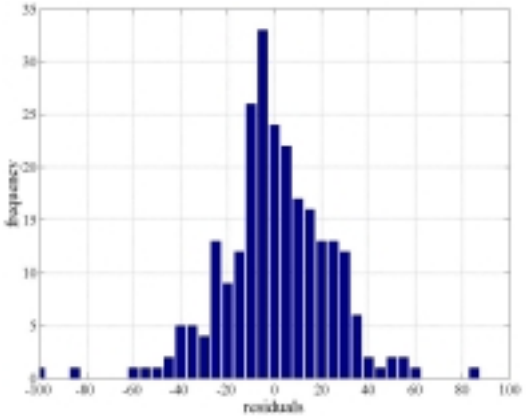

Figure 7 – Residuals for LC&R G 622.

Finally, results for the absolute stations are presented in Table 6 and Figure 8. A comparison of the adjusted *g* values with the IGSN71 gravity datum at selected stations are shown in Table 7. All the differences to the IGSN71 datum are less than or equal to the standard deviation of the adjusted network, showing very good agreement between both systems in South America.

Table 6 – Adjusted *g* values for the absolute and Montevideo stations (in mGal).

Station	Lat.	*g* adjusted	St. Dev.	Residuals	Ties
IfE 040	+ 4.67	977822.0844	0.0029	-0.0004	3
IfE 112	- 5.08	978016.3425	0.0033	+0.0005	2
IfE 122	-15.67	978048.7979	0.0005	+0.0001	3
IfE 132	-20.73	978460.2331	0.0034	-0.0031	10
IfE 142	-22.55	978637.5834	0.0022	-0.0024	14
IfE 152	-22.98	978563.7719	0.0032	+0.0061	14
IfE 162	-25.42	978760.3871	0.0022	-0.0001	27
IfE 173	-29.68	979261.6349	0.0023	+0.0011	24
IfE 212	-30.88	979344.3774	0.0015	-0.0004	3
250187	-34.85	979732.3982	0.0102	-0.0012	5

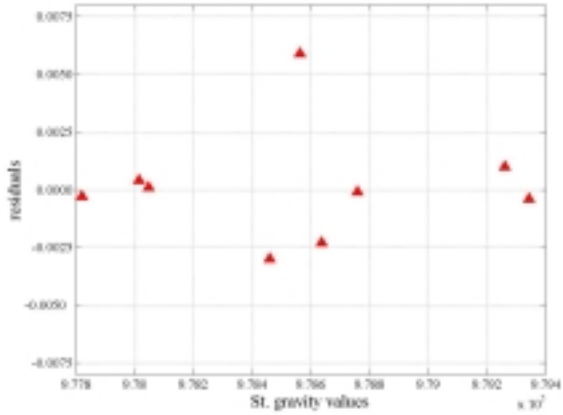

Figure 8 – Residuals found at absolute stations (in mGal).

Table 6 – Comparison of the Brazilian gravity datum – the RGFB – with the IGSN71 datum (in mGal).

IGSN71 Station	Lat. (deg.)	Adjusted g (mGal)	IGSN71 g (mGal)	IGSN71 St. Dev.	Differences
32918A	- 1.43	978022.2386	978022.24	0.039	-0.00
33039J	- 3.07	978006.1477	978006.16	0.052	-0.01
32838J	-3.72	978067.8238	978067.81	0.036	+0.01
32977J	-7 .32	978031.1671	978031.11	0.053	+0.06
32884J	- 8.08	978151.2508	978151.25	0.034	+0.00
36428B	-12.97	978311.3686	978311.31	0.042	+0.06
36479J	-17.63	978511.4733	978511.46	0.038	+0.01
36593J	-19.90	978385.5616	978385.50	0.043	+0.06
40100B	-20.30	978641.8122	978641.83	0.042	-0.02
40111J	-21.68	978717.4747	978717.49	0.035	-0.02
40123A	-22.88	978789.8630	978789.90	0.027	-0.04
40136J	-23.38	978627.2784	978627.29	0.036	-0.01
40178A	-27.58	979112.4395	979112.39	0.042	+0.05
43801B	-30.03	979304.9667	979305.00	0.041	-0.03
43812B	-31.75	979466.5978	979466.63	0.039	-0.03
43846K	-34.89	979731.4253	979731.56	0.043	-0.13

Conclusions

An effort undertaken at Observatório Nacional made available to the geosciences community all the gravity data gathered by the institution since the 1950's in Brazil. The establishment of a gravity database and the adjustment of the RGFB to the JILAG-3 datum have been completed.. CD-ROMs containing the adjustment results are available upon request to Observatório Nacional. Remaining datasets will be included in the database and progress will be reported.

References

De Sousa M.A., Veiga, C.H. (2001), Gravity reductions routines for fieldwork data (submitted), *Computers & Geosciences*.

De Oliveira, C.B. (1851), Notes des resultats obtenues dans les experiences faites à Rio de Janeiro, sur le mouvement du pendule, pendant le mois de septembre et les premiers jours d´octobre de 1851, à la latitude australe de 22° 50′, *Comptes Rendus*, **33**, 582.

De Sousa, M.A. e Moreira, E.M. (1994), Referring the old gravity network of the National Observatory to the IGSN71/Absolute datum. Part I: The LC&R 61 data set, *Bulletin d'Information Bureau Gravimetrique International*, **174**: 30-43.

Observatório Nacional (1986), Rede Gravimétrica Fundamental Brasileira 1976-1986, 16 pp.

Torge, W., Timmen, L., Röder, R.H. and Schmil, M. (1994), The IfE absolute gravity program "South America" 1998-1991, *Deustche Geodätische Kommision*, B299, Munchen.

Subiza Piña, W.H., Torge, W. and Timmen, L. (1998), The National Gravimetric Network of Uruguay, *Geodesy on the Move. Gravity, Geoid, Geodynamics and Antarctic International Association of Geodesy Symposia*, 119 pp.

Tremores de Terra Recentes no Povoado Alto da Lagoinha - Bahia

Joaquim X. Cerqueira Neto[†] *e Telésforo M. Marques*

CPGG-IGEO/UFBA

Abstract

In this article we describe the characteristics of seismic events in the region of Ubaira municipality, State of Bahia (Brazil) that occured during June and July 1999. We conclude that these microseismic events have intensitiy equal to $IV_{(MM)}$ and are very localized but probably related to reactivation of faults. We correlated these events with the seismicity observed around the area by the Seismological Laboratory of the University of Brasilia and IAG-USP during the last century. The epicentres of these seismic events in a radius of 100km form an alignment 300km long and 100km in width. We suggest that these events delineate part of a large neotectonic belt that may even include the Recôncavo-Tucano Graben.

Introduç˜ao

Eventos de sismicidade em área compreendida no raio de 100 km da sede do Mun. de Ubaíra-Bahia têm sido reportados no último século. Os mais recentes ocorreram entre os dias 19 de Junho e 12 Julho de 1999, no povoado Alto da Lagoinha (coordenadas: Lat. 13^o 10' S; Long. 39^o 35' W), Município de Ubaíra, distante 20,6 km da sede. Datas e hor´arios desses eventos encontram-se no Quadro-1, na forma como foram reportados pelos moradores.

Q u a d r o - 1

DATAS E HORA DOS TREMORES

Data	*Hora local*	*Intensidade(*)*	*Obs.:*
19-06-1999	*9:00*	*fraco*	
25-06-1999	*23:00*	*médio*	
07-07-1999	*9:00*	*médio*	
10-07-1999	*23:30*	*fraco*	
10-07-1999	*23:32*	*médio*	
10-07-1999	*23:35*	*muito forte*	*p^anico*
12-07-1999	*10:00*	*fraco*	

* *na forma descrita pelas pessoas*

Os trabalhos de campo foram realizados nas datas de 17 e 18/07/1999 juntamente com o Prefeito daquele Município, quando foram entrevistados muitos moradores dã regiao, desde a cidade de Mutuipe até Ubaíra, principalmente, das localidades de Alto da Lagoinha, Baixa da Areia e Serra Negra. Seguiu-se a investigação geológica concentrada nos locais onde os tremores foram mais intensos.

Resultados das Entrevistas

Moradores de localidades mais distantes, como por exemplo, na cidade de Mutuipe, ñao ouviram ou sentiram qualquer estrondo ou tremores nas datas acima. Já nas localidades situadas no raio de 6 km (Baixinha, a noroeste e Lagoa Grande, a sudeste) do possível epicentro (Alto da Lagoinha) v´arias pessoas informaram que ouviram um forte estrondo, `as 23:30h do dia 10 de julho/1999, mas que ñao sentiram nenhum tremor.

Constatou-se uma unanimidade, por parte dos entrevistados, no que se refere ao forte estrondo e aos tremores do dia 10 de julho/1999 `as 23:30h, atingindo os lugarejos de Baixa da Areia e Serra Negra, respectivamente a SW e NW do foco provável, e o povoado Alto da Lagoinha (Fig.2).

A inspeção realizada nas casas mais atingidas mostra que esses tremorês nao ocasionaram maiores danos materiais, apenas leves fissuras ou aumento de abertura de fendas preexistentes em paredes, induzidos por vibrações da ordem de 8 a 10 gals nas casas mais afetadas (valores estimados com base na experiˆencia de um dos autores com ensaios sismográficos e medição dos níveis de vibrações e seus efeitos em diferentes tipos de construções, produzidas por detonações, eg. (Cerqueira Neto et al., 1997). Objetos e mesmo os telhados estremeceram e móveis se deslocaram durante o tremor mais forte. Após esse estrondo as pessoas saíram das casas, estabelecendo-se em seguida o pânico geral com o "black out" de energia, em virtude de queda de árvore sobre a linha de transmissão.

Verificou-se que uma pedreira distante aproximadamente 8 km^2 do local dos tremores, encontrava-se desativada. E, também, que ñao existem barragens nas imediações que possam justificar sobrecarga no macico ou induzir pressões hidrostáticas em falhas ou fraturas.

Aspectos Geologicos da Área

A área em apreço é constituída de rochas ígneas, plutˆonicas, graníticas, metamorfizadas na fácies granulito, pertencentes ao cratõn do Sao Francisco,

[†]Research Center for Geophysics and Geology/Federal University of Bahia (CPGG/UFBA), Campus Univ. da Federação, Salvador, BA, Brazil, 40170-290.

localizadas no domínio do Bloco Jequié (Barbosa, 1986).

Tais rochas formaram a crosta há mais de 2 bilhões de anos (2,7 Ga) e, provalvelmente, foram retrabalhadas depois, há 2,0 Ga, quando adquiriram estabilidade geológica.

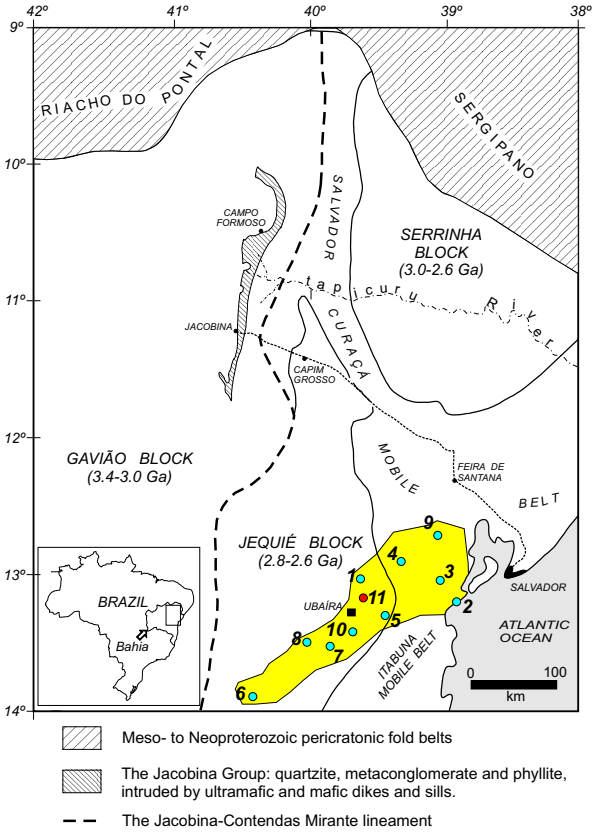

Figura 1: Esbôço Geotectônico da Região (Teixeira et all, 2000). O círculo 1 (em azul) refere-se ao sismo de 1899 em Amargosa e o de número 11 (vermelho) ao de Ubaíra, em 1999 (v. a seqüência no Quadro-2).

A investigação geológica de superfície, realizada nos arredores do povoado Alto da Lagoinha, mostra que há um forte controle estrutural das rochas, bem evidenciado por uma zona de falha de direção NW-SE e largura mínima de 200m. Localmente, identifica-se a rocha granítica fortemente gnaissificada, minerais fortemente estirados, rotacionados e foliação caracterizada pela orientação dos minerais máficos planares na direção predominante N 25^o W, subverticais (Fig. 3). As falhas regionais têm direções $\approx$ N 25^o W a N 40^o W, e N 60^o E.

Além do controle da drenagem, observam-se outros aspectos morfológicos como topos arredondados de elevações e desníveis da ordem de 50 a 60m para um vale encaixado na zona de falha. No vale ocorrem afloramentos da rocha e vertentes possuindo densa cobertura de solo residual (regolito), com espessura provável superior a 30m (Fig. 4).

É importante registrar que os locais onde os tremores foram percebidos com maior intensidade (Baixa da Areia, Alto da Lagoinha e Serra Negra) também estão situados no alinhamento NW-SE.

Histórico de Microssismos na Região

Dados do Observatório Sismológico da Universidade de Brasília (OBSIS) e do IAG-USP revelam que a região possui história de sismicidade caracterizada por eventos de pequena magnitude ou intensidade, situados na faixa dos microtremores, $< 3.7 m_R$, (Barros, 1999); e que tremores mais próximos do povoado Alto da Lagoinha (raio $\simeq$ 25km) ocorreram nos anos de 1899, 1984 e, talvez, em 1994.

Quanto aos tremores em análise (constantes do Quadro-1), os mesmos não foram detectados pela rede sismográfica do observatório da UnB (Barros, 1999), evidenciando que se trata de evento localizado superficial, cuja intensidade I em unidades da escala Mercalli modificada (MM) pode ser inferida, por exemplo, com o emprego da fórmula de Rosenblueth (Dinis da Gama, 1979):

$$I = \frac{14\ v}{\log\ 2},$$

onde v é a velocidade máxima de partícula do terreno em cm/s. O cálculo indica intensidade máxima I = 4, isto é (IV), na referida escala.

Os epicentros dados no Quadro-2 estão indicados no esboço geotectônico (Fig. 1) com orientação preferencial N 58^o E (média das direções dos epicentros exatos referidas ao c7), sugerindo a possibilidade de existência de uma grande zona de atividade tectônica nesse lineamento e que transcende unidades litológicas antigas e de características diferentes, a exemplo do Bloco Jequié e do cinturão móvel Salvador-Curaçá. Em que pese a incerteza de alguns epicentros, a sua distribuição abrange uma área com extensão de 300km e largura máxima de 100km, que dificilmente seria controlada apenas por uma falha.

Note-se, ainda, uma forte correlação da orientação com a zona tectônica que deu origem à Bacia sedimentar do Recôncavo-Tucano, delimitada pelos sistemas de falhas de Salvador e Maragogipe.

Análise das Causas e Conclusões

A análise dos dados mostra que: i) - os tremores situam-se em região de rochas cristalinas tectonicamente estáveis e tiveram intensidade máxima de IV (MM), ficando restritos a uma área estreita (aproximadamente 1,5 km de comprimento); ii) - não ocasionaram maiores danos materiais nas estruturas das casas (geralmente construídas em alvenaria de blocos cerâmicos); e iii) - não foram detectados pela estação sismográfica de Brasília.

Esses dados evidenciam que os tremores de terra do Alto da Lagoinha se caracterizam como um fenômeno localizado e de pequena energia, aparentemente associado à reativação da falha geológica próxima, esquematizada na Fig. 2 Não se espera alguma relação dessa neotectônica com falhas de idade Pré-Cambriana, pois estas seriam partes reminiscentes profundas, soldadas (raiz de falha), portanto, muito estáveis, mas sim, com falhas menos antigas. Assim, uma possível explicação é a correlação da zona de distribuição de epicentros, destacada na Fig. 1, com a zona tectônica que deu origem à Bacia sedimentar do Recôncavo-Tucano. Uma outra hipótese é baseada no neotectonismo da região costeira (Bittencourt e all, 1999), cujo modelo flexural indica influências até distâncias de 100 km da linha de costa, podendo tal influência traduzir-se em reativações de antigas falhas ou no surgimento de novas. Note-se que a falha geológica do Alto da Lagoinha dista aproximadamente 70 km da linha de costa. Finalmente, não se pode descartar a hipótese de estar ocorrendo a liberação de energia, devida ao surgimento de juntas de alívio de tensões na área indicada. Também, é importante observar que tais hipóteses não são excludentes.

Conclui-se que seria da maior relevância para o conhecimento científico desse fenômeno a determinação dos hipocentros desses eventos, o que somente seria possível com uma rede sismográfica mais próxima em operação, a exemplo da RPC Pedra do Cavalo, atualmente desativada.

Agradecimentos

Os autores agradecem aos professores Dr. Olivar L. Lima e Dr. João Batista Teixeira pelas valiosas discussões e à Prefeitura Municipal de Ubaíra pelo apoio durante os trabalhos de campo.

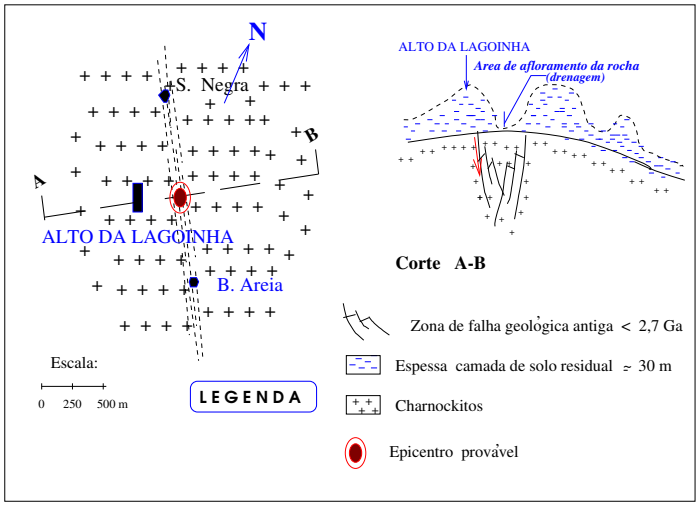

Figura 2: Planta e Seção Geológica Esquemáticas

Referências

Barbosa J. S. F., 1986, Constitution lithologique et metamorphique de la région granulitique du Sud de Bahia, Brésil: Tese de Doutoramento, Université PARIS-IV, France.

Barros, L. V., 1999, Comunicação pessoal.

Bittencourt, et al., 1999, Flexure as a Tectonic on Large Scale Geomorphic Characteristics of the Eastern Brazil Coastal Zone: Journal of Coastal Research, v. 15 **02**, 505-519.

Cerqueira Neto, J. X.; Couto, L. S. e Marques, M. P., 1997, Ensaio de Vibrações Induzidas em Paredes de Alvenaria de Tijolos Cerâmicos: 5^o CISBGf, Res. Exp., v. 1 434-37.

Dinis da Gama, C. A. J. V., 1979, Tratamento Matemático de Dados Sismológicos. **In** Anais do Simpósio sobre Sismicidade Natural e Induzida, 151-175.

Teixeira, J. B. G.; Mascarenhas, J. F.; Souza, S. L.; Conceição Filho, V. M, 2000, Archean and Paleoproterozoic Terranes and the Gold Deposits of Central-North Bahia State, Northeastern Brazil. Post-Congress Field Trip 31^{st} International Geological Congress, 47 p.

Figura 3: Afloramento horizontal no fundo do vale. Rocha granítica fortemente gnaissificada, minerais fortemente estirados, rotacionados desenvolvendo formas sigmoides predominantemente sinistrógiras, foliação caracterizada pela orientação dos minerais máficos planares, direção predominante N 25^{o}W, subvertical. Localidade: Alto da Lagoinha

Figura 4: Padrão morfológico nos arredores do povoado Alto da Lagoinha, apresentando morros arredondados com desníveis da ordem de 50 a 60m e espessa cobertura de solo argilo-arenoso acima de 30m. A falha principal, está localizada neste vale.

Q u a d r o - 2

SISMICIDADE NA REGIÃO DE UBAÍRA[1] ($< 3.7m_R$)

Data	Hora local	$\phi(S)$	$\lambda(W)$	Localidade	Dist. (km)	Obs.:
-12-1899		13,03^o	39,60^o ($\pm 0km$)	Amargosa	31.	Fig.1, circ. c1
18-04-1912		13,20^o	38,89^o ($\pm 0km$)	BR. Jequiriçá	91.	
19-04-1912	05:00	13,20^o	38,89^o ($\pm 0km$)	"	91.	" c2
19-04-1912	10:00	13,20^o	38,89^o ($\pm 0km$)	"	91.	
12-06-1916	10:00	13,04^o	39,01^o ($\pm 0km$)	Nazaré	82.	" c3
28-06-1983	17:10:15	12,90^o	39,30^o ($\pm 50km$)	S. A. Jesus	63.	" c4
12-08-1984	01:45:19	13,30^o	39,42^o ($\pm 5km$)	Valença	34.	" c5
11-06-1986	22:43:49	13,90^o	40,40^o ($\pm 50km$)	Jequié	100.	" c6
25-04-1987	12:00	13,50^o	40,00^o ($\pm 50km$)	Apuarema	38.	
26-04-1987		13,50^o	40,00^o ($\pm 0km$)	"	38.	" c7
09-06-1992	07:27:55	13,53^o	39,83^o ($\pm 20km$)	Jaguaquara	32.	" c8
25-08-1992	14:26:26	12,73^o	39,03^o ($\pm 50km$)	Recôncavo	94.	" c9
23-09-1994	01:05:17	13,42^o	39,66^o ($\pm 40km$)	Jaguaquara	17.	" c10

(*) FONTE: IAG-UNB [1] (Barbosa, 1986)

Upper Mantle Anisotropy in SE and Central Brazil from SKS Splitting

M. Assumpção[*], *M. Heintz*[†], *A. Vauchez*[‡], *M. Egydio Silva*[*], *J.R. Barbosa*[*], *and T. Benevides*[*]

Abstract

We present a compilation of upper mantle anisotropy derived from measurements of SKS and SKKS splitting in SE and Central Brazil. The fast polarization direction shows consistent orientation over hundreds of kilometers and is generally parallel to the structural trend of the last major orogeny. In the Brasilia fold belt, SW of the São Francisco craton, the fast polarization direction has a NW-SE trend, parallel to the Goiânia flexure, consistent with a final collision between a cratonic block beneath the Paraná basin and the São Francisco craton. In the Ribeira belt the anisotropy direction is remarkably parallel to the WSW-ENE trend of the shear belt, specially in the southern Ribeira belt where transcurrent shear zones predominate. This pattern is interpreted as due to escape tectonics during the Brasiliano collision with a cold, thick São Francisco craton. In some sites the amount of anisotropy reaches a total splitting delay of 2.4s which is one of the largest delays worldwide. In the northern part of the Ribeira belt, the anisotropy pattern is more complex, which is probably related to the transition between vertical shear deformation in the south to a more E-W compressional tectonism in the north where N-S trending reverse faulting and nappes predominate. In the central part of the Paraná basin, the anisotropy direction tends to be E-W oriented. Although the reason is not yet clear, this direction is consistent with possible E-W extension in the Paleozoic. In the Tocantins province, Goiás, a trend of SW-NE orientation is observed, roughly parallel to the Transbrasiliano lineament.

Introduction

SKS and SKKS phases are S waves converted to P at the core-mantle boundary and converted back to S when leaving the core on their way up to the surface, arriving at the station at nearly vertical incidence. Because of the P-to-S convertion at the core-mantle boundary, they should be polarized along the radial direction if the mantle were isotropic. Quite often, however, SK(K)S waves exhibit some energy on the recorded transverse component which is best explained as the result of shear-wave splitting during propagation in some anisotropic layer beneath the station. The splitting is usually of the order of 1 sec, although up to 2.5 s has been observed (e.g., Silver, 1996). Anisotropy of normal crustal rocks cannot contribute more than 0.1 or 0.2 s to the observed SK(K)S splitting (e.g., Barruol & Mainprice, 1993). The reduced contribution from the crust, and other seismological considerations, indicate that most of the observed SK(K)S splitting originates at the upper mantle, above 400 km depth. Seismic anisotropy in the upper mantle results from preferential mineral orientation (specially olivine) which can be caused by deformation and flow of mantle rocks during past and present orogenic activity (e.g., Silver & Chan, 1991; Vinnik et al., 1992; Mainprice & Silver, 1993; Silver, 1996). For this reason SKS splitting is a useful tool to investigate strain processes in the mantle and its correlation with tectonic crustal deformation observed at the surface (e.g., Vauchez et al., 2000)

In intraplate areas, far from present plate margins, Vinnik et al.(1992) attributed most of the observed SKS anisotropy as being caused mainly by flow in the asthenosphere due to the present absolute plate motions. However, the measured fast polarization direction often correlates well with the structural trends observed in the upper crust due to the last major orogeny which indicates an alternative explanation: paleo orogenic processes that affected the crust could also leave the lithospheric upper mantle with a preferred mineral orientation still observable today (fossil anisotropy e.g. Silver, 1996). Growing observational evidence suggests that frozen anisotropy in the lithosphere (such as observed in SE Brazil by Assumpção, 1996) is probably more important than present asthenospheric flow. This indicates that orogenic mechanical processes affect the entire lithosphere and can be preserved over geological time. For this reason, measurements of upper mantle anisotropy from SKS splitting can be used to assess different models of orogenic processes, such as done for continental rifting by Vauchez et al.(2000).

[†]Univ. of São Paulo, Brazil; marcelo@iag.usp.br
[‡]Univ. of Montpellier, France

SKS anisotropy observations in Brazil

Following the initial results of James & Assumpção (1996) seismic anisotropy in the upper mantle beneath SE Brazil has been investigated with an extensive cooperation program between the University of São Paulo, Brazil, and the University of Montpellier, France, since 1996. Results from portable broad-band stations (both Brazilian and French) have been deployed in more than 20 sites in SE Brazil, specially in the coastal Ribeira fold belt.

The analysis of the SK(K)S splitting was carried out with the method of Silver & Chan (1991) and an example is shown in Figs. 1 to 3 for the station *pazb*. Fig. 1 shows the radial and transverse components of the SKS phase as recorded at the station (top two traces). The signal observed in the transverse component ("T-obs.") is a result of splitting which causes the fast and slow components to arrive at the station out of phase making the particle motion eliptical instead of linear (Fig. 2). The fast polarization azimuth (Az) and the lag time between fast and slow components (dt) are determined with a grid search by correcting the observed components from the anisotropy effect so as to minimize the energy in the transverse component (Fig. 3). The two bottom traces in Fig. 1 are the radial and transverse components corrected from the effect of anisotropy. Note that the anisotropy parameters (Az= 60°, and dt= 1.65 sec, Fig. 3) which best corrects the SKS phase also reduces the transverse energy of the SKKS phase (Fig. 1, "T-corr."). Results from SKS and SKKS measurements are usually consistent.

Table 1 shows the anisotropy results from the stations in the Tocantins Province (Goiás), the central part of the Paraná basin (SP), and the Ribeira belt (SP, MG, RJ). In Fig. 4 we plot the data from Table 1 including the previous results of James & Assumpção (1996). The data for the permanent Brasilia station (BDF) is a preliminary average of the values determined by Russo & Silver (1994) and Vinnik et al.(1992): Az=53° and 40°, respectively.

Discussion

In the Brasilia fold belt, SW of the São Francisco craton, the fast polarization direction has a NW-SE trend, parallel to the Goiânia flexure, and the general structural trend, consistent with a final collision between a cratonic block beneath the Paraná basin and the São Francisco craton.

In the Ribeira belt the anisotropy direction is remarkably parallel to the WSW-ENE trend of the shear belt, specially in the southern Ribeira belt where transcurrent shear zones predominate. This pattern is interpreted as due to escape tectonics during the Brasiliano collision with a cold, thick São Francisco craton (Vauchez et al., 1994). In some sites the amount of anisotropy reaches a total splitting delay of 2.4s (Igarata', SP) which is one of the largest delays observed worldwide. In the northern part of the Ribeira belt, the anisotropy pattern is more complex, which is probably related to the transition between vertical shear deformation in the south to a more E-W compressional tectonism in the north where N-S trending reverse faulting and nappes predominate. In this transition zone, some stations (*natb* and *barb*) seem to suggest different anisotropy directions for SKS waves arriving from the south compared to waves arriving from the north (see Table 1); further work on this problem is necessary, however.

In the central part of the Paraná basin, the anisotropy direction tends to be E-W oriented. Quintas (1995) and Quintas et al.(1999) analysed subsidence rates in the central part of the Paraná basin to estimate crustal stretching factors during the basin evolution. Although stretching factors are not large, the area of maximum stretching for the two main events in the Paleozoic (at 440 Ma and 296 Ma) trend roughly in the N-S direction. Maybe these results indicate that the lithosphere was extended in the E-W direction causing the E-W oriented anisotropy. However, it is not clear why this anisotropy was not destroyed during the Mesozoic flood basalt volcanism around 140-130 Ma. Interestingly, in the Ribeira belt, the WSW-ENE direction of the anisotropy, parallel to the Brasiliano structural trend of the fold belt, does not seem to have been much affected by the extensional deformation during the Mesozoic Atlantic rifting.

In the Tocantins province, state of Goiás, the few available measurements indicates a fast anisotropy direction roughly SW-NE, parallel to the Transbrasiliano Lineaments. Although structural patterns observed in the upper crust are rather complex, a general SSW-NNE direction would mark the final suture between the Amazon and São Francisco cratons. In southern Goiás, a station at Corumbá (*corb*) has a well defined E-W anisotropy direction, somewhat intermediate between the patterns of northern Goiás and the Brasilia belt.

Acknowledgments

We thank Andrea Tommasi and Guilhem Barruol for help during field work. Work supported by grants FAPESP 96/01566-0, 97/03640-6; CNPq 30.0227/79-5, 52.0078/00-4; CAPES-COFECUB and CNRS.

references

Barruol, G. & D. Mainprice, 1993. A quantitative evaluation of crustal rocks to the shear-wave splitting of teleseismic SKS waves. *Phys. Earth Planet. Int., 78*, 281-300.

James, D.E. & M. Assumpção, 1996. Tectonic implications of S-wave anisotropy beneath SE Brazil. *Geophys.J.Int., 126*, 1-10.

Mainprice, D. & P.G. Silver, 1993. Interpretation of SKS waves using samples form the subcontinental lithosphere. *Phys. Earth Planet. Int., 78*, 257-280.

Quintas, M., 1995. O embasamento da Bacia do Paraná: reconstrução geofisica de seu arcabouço. *Ph.D. thesis*, IAG-Univ. of São Paulo.

Quintas, M., M. Mantovani & P. Zalan, 1999. Contribuição ao estudo da evolução mecânica da Bacia do Paraná. *Rev. Bras. Geoc., 29*, 217-226.

Russo, R.M. & P.G. Silver, 1994. Trench-parallel flow beneath the Nazca plate from seismic anisotropy. *Science, 263*, 1105-1111.

Silver, P.G., 1996. Seismic anisotropy beneath the continents: probing the depths of geology. *Annu. Rev. Earth Planet. Sci., 24*, 385-432.

Silver, P.G. & W.W. Chan, 1991. Shear wave splitting and subcontinental mantle deformation. *J. Geophys. Res., 96*, 16429-16454.

Vauchez, A. & A. Nicolas, 1991. Mountain building: strike-parallel motion and mantle anisotropy. *Tectonophys., 185*, 183-201.

Vauchez, A., A. Tommasi & M.E. Silva, 1994. Self-indentation of heterogeneous continental lithosphere. *Geology, 22*, 967-970.

Vauchez, A., A. Tommasi, G. Barruol & J. Maumus, 2000. Upper mantle deformation and seismic anisotropy in continental rifts. *Phys.Chem.Earth(A), 25*, 111-117.

Vinnik, L.P., L.I. Makeyeva, A. Milev & A. Y. Usenko, 1992. Global patterns of azimuthal anisotropy and deformation in the continental mantle. *Geophys. J. Int., 111*, 433-447.

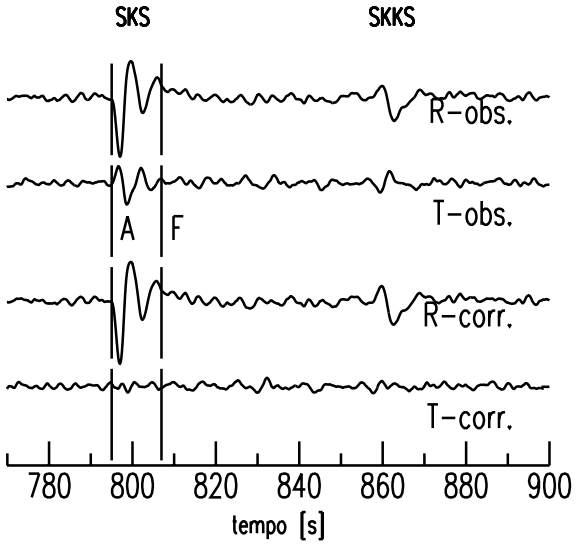

Figure 1: Example of SKS and SKKS at station *pazb*. Observed and corrected radial and transverse components; A-F is the window used to minimize the transverse component; origin of time scale is arbitrary.

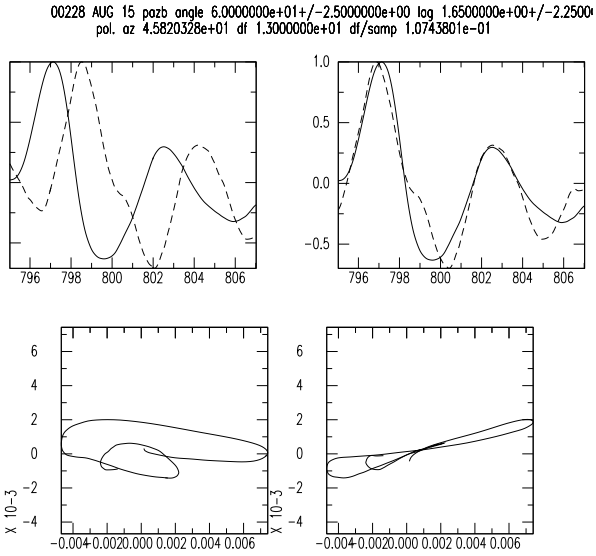

Figure 2: Analysis of the SKS phase of Fig. 1. Clockwise from top left: normalized fast and slow components with the estimated splitting delay, same components corrected for the delay, observed elliptical particle motion, linear particle motion after removing the effect of the splitting delay.

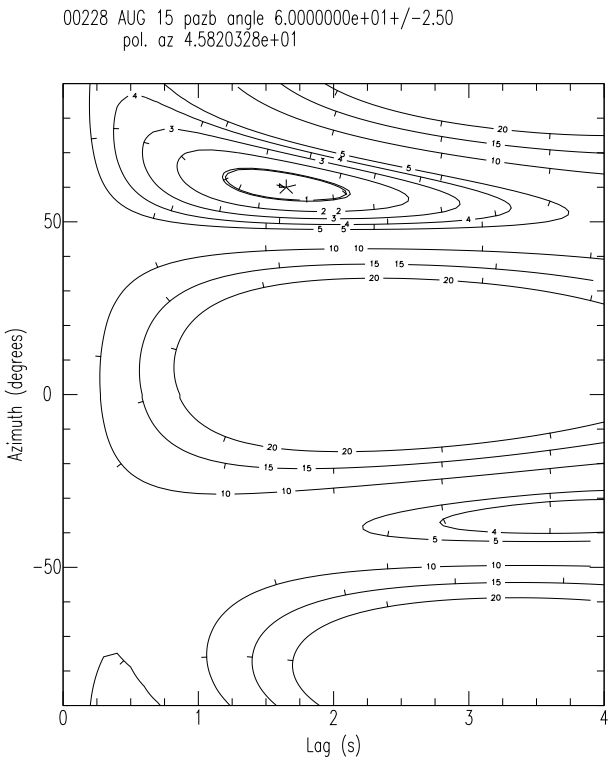

Figure 3: Contours of the transverse energy to find the best azimuth of the fast anisotropy polarization and the delay (lag time) between fast and slow components.

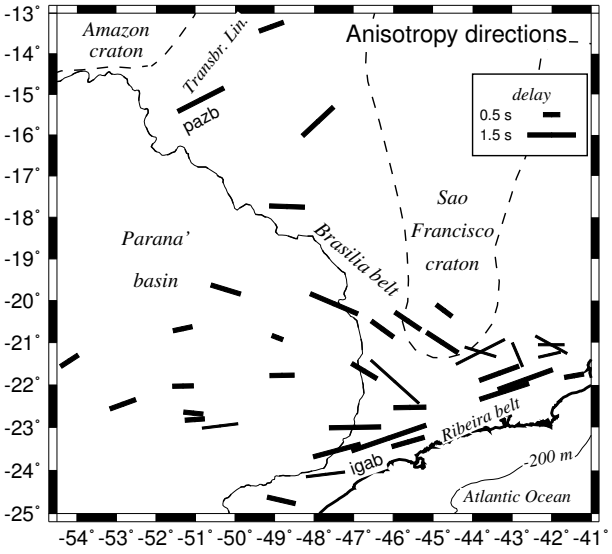

Figure 4: Anisotropy directions in Central and SE Brazil. Bar length denotes delay time between fast and slow components; thin bars are less reliable measurements based on few events.

sta.	lat.	long.	Az.	dt	comments
Ribeira belt					
bscb	-20.998	-44.763	-57	1.1	Bom Sucesso, MG
natb	-21.055	-42.004	90	0.8	Natividade, RJ. SW
natb	-	-	-61	1.1	back azimuth North
barb	-21.222	-43.801	63	1.7	Barbacena, SE+SW
barb	-	-	-73	1.0	back azim. NE+NW
LJM	-21.286	-42.053	77	0.7	Lage do Muriaé, MG
atdb	-21.290	-42.861	-23	0.8	Astolfo Dutra, MG
jfob	-21.728	-43.326	70	1.3	Juiz de Fora, MG
camb	-21.784	-41.429	80	0.6	Campos, RJ
ALP	-21.880	-42.664	70	1.8	Além Paraiba, RJ
SJM	-21.931	-45.962	-48	2.0	S. João da Mata
trrb	-22.154	-43.195	72	1.6	Três Rios, MG/RJ
brsb	-22.535	-45.585	89	1.0	Brasópolis, MG
vabb	-23.002	-46.966	89	1.6	Valinhos, SP
igab	-23.252	-46.116	71	2.4	Igaratá, SP
SPB	-23.540	-47.430	75	1.5	Geoscope, SP
juqb	-24.093	-47.716	83	1.2	Juquiá, SP
rstb	-24.697	-48.828	-77	0.9	Tijuco Alto, SP
Paraná basin					
popb	-22.456	-52.837	70	0.8	P. Primavera, SP
canb	-22.961	-50.378	83	1.1	Canoas, SP
Tocantins Province					
porb	-13.330	-49.079	70	0.8	Porangatu, GO
pazb	-15.137	-50.863	63	1.6	Araguapaz, GO
BDF	-15.664	-47.903	47	1.3	Brasilia, DF
corb	-17.743	-48.689	-88	1.1	Corumbá, GO

Table 1: New SK(K)S splitting results for SE and Central Brazil. "Az" is the direction of the fast polarization; uncertainties are usually around 5° to 10°. "dt" is the splitting delay time; its uncertainty is usually about 0.2 to 0.4 sec.

Utilização do pacote GIANT na análise de um conjunto de sismos ocorridos em 1987 em João Câmara-RN

Michele D. Martins & Jesus Berrocal

Instituto de Astronomia, Geofísica e Ciências Atmosféricas / USP

Abstract

In this work, we used the software package GIANT that was developed for data analysis of large seismological experiments. Several functions that are executed in this kind of experiments normally are realized by different groups, where some actions can be duplicated. This disadvantage is eliminated by using GIANT package, because it integrates different programs in a interactive sequence. To test the functionallity of this package it is necessary to use a large quantity of data recorded by a convenient number of stations. For this reason, we used the João Câmara-RN seismic data recorded in a nine stations network. This was the major earthquake sequence occurred and registered in Brazil, with more than 65,000 events (1986-2000) with magnitudes up to $m_b = 5.1$. In this work were analysed 175 earthquakes, by reading their seismic phases, determining the hypocenters and velocity model from simultaneous inversion and solving focal mechanisms.

Introdução

O objetivo deste trabalho foi experimentar o pacote de programas GIANT (**G**raphical **I**nteractive **A**ftershock **N**etwork **T**oolbox), que foi desenvolvido para auxiliar um trabalho de levantamentos sismográficos que envolva um grande número heterogêneo ou não de eventos e estações. Para a utilização deste pacote, trabalhamos com um pequeno conjunto de réplicas da maior seqüência de sismos ocorrida no Brasil, localizada em João Câmara-RN (ciclo iniciado em 1986). Apesar destes dados serem antigos e já bastante estudados por outros autores, a rede de João Câmara é até o momento a maior em número de estações e eventos registrados no Brasil, portanto sendo a única capaz de testar a funcionalidade do pacote GIANT.

O pacote GIANT

Em 1998 o IAG recebeu através do projeto "Estudos sismológicos nas Regiões Sudeste e Nordeste do Brasil", apoiado pelo programa CAPES/DAAD (PROBAL) o pacote GIANT elaborado por Rietbrock & Scherbaum (1998).

O pacote GIANT foi projetado inicialmente para a análise de experimentos portáteis de grande escala em sismologia, onde o tamanho dos dados ultrapassa rapidamente a ordem de Megabytes, ou casos em que seja necessário analisar dados coletados por diversos grupos, ou seja, diferentes instrumentos. Mas pode também ser utilizado para a análise de redes de trabalho permanentes, visando integrar todos os processos de análises sismológicas. Este pacote é compatível com sistemas SunOS, Solaris e Linux.

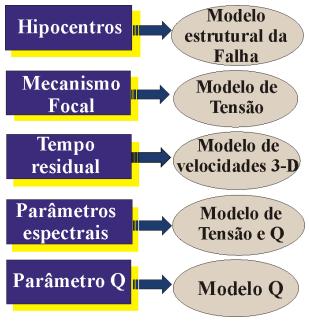

Figura 1: Visualização das análises realizadas num processamento de dados sismológicos e os modelos resultantes obtidos.

Observando a Fig. 1, podemos ver no lado esquerdo os tipos de determinações que são freqüentemente extraídos de um conjunto de dados. No lado direito temos os tipos de modelos que são usualmente obtidos dos dados, como estrutura da falha, modelo de tensão, de velocidades e de atenuação. Estas análises são geralmente realizadas separadamente e muitas vezes por diversas pessoas, o que pode tornar a análise como um todo bastante dispersa e demorada, já que grupos que tenham realizado as determinações hipocentrais iniciais novamente terão que refazê-las quando um outro grupo determinar o modelo de velocidades da região. Quando se tem uma grande quantidade de eventos, onde há estas dependências, o processamento pode ficar comprometido, podendo a chegar em resultados não tão consistentes como desejado para a região de estudo.

O pacote GIANT é formado por uma série de

ferramentas e programas, tais como:

- PITSA - visualização dos dados em forma de onda e análise interativa.
- HYPO71 - determinação hipocentral para modelo unidimensional de velocidades.
- FPFIT - cálculo do mecanismo focal utilizando as polaridades da onda P.
- FOCMEC - cálculo do mecanismo focal utilizando as polaridades da onda P, SV e SH.
- SIMUL - estimação simultânea de parâmetros hipocentrais e modelo 3-D de velocidades.

Os dados de João Câmara

O ciclo de atividade sísmica que ocorreu em João Câmara-RN a partir do segundo semestre de 1986, cujo evento mais importante foi o de magnitude $m_b = 5{,}1$ e intensidade VII MM ocorrido em 30 de novembro de 1986, foi a seqüência de maior número de eventos sísmicos ocorrida no Brasil e que teve o maior número de sismos registrados instrumentalmente, Takeya et al. (1989).

Na aplicação do pacote GIANT utilizamos 174 eventos registrados pela rede local de João Câmara, ocorridos no intervalo de 11-09 a 19-09 de 1987. Uma vez que o GIANT esteja devidamente instalado é necessário criar um banco de dados, que pode ser facilmente realizado através de um roteiro.

Após a importação dos arquivos para o banco de dados, ao iniciarmos o pacote, ele reconhece esse banco, e num gráfico de estações versus tempo, ele mostra todos os eventos importados com seus respectivos horários de ocorrência. Esta janela de visualização é muito útil quando se tem um número muito grande de estações, ficando extremamente fácil escolher uma determinada estação e um evento.

A partir dessa janela selecionamos o evento cujas leituras de chegada das ondas nas estações desejadas serão realizadas. Os dados selecionados (com o auxílio do mouse) são transferidos para o programa PITSA (Programmable Interactive Toolbox for Seismological Analysis) desenvolvido por Scherbaum (1993), onde é possível realizar as leituras das fases sísmicas, envolvendo vários processos como filtros, análise espectral, convolução e deconvolução, cálculo de magnitudes (Fig. 2). O programa utilizado para determinação hipocentral é o HYPO71 obtido por Lee & Lahr (1975), que está implementado dentro do PITSA.

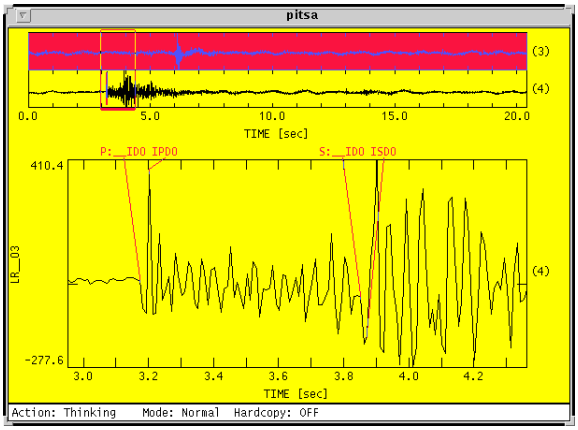

Figura 2: Visualização do arquivo em forma de onda utilizando o programa PITSA.

A cada determinação hipocentral, o PITSA demonstra no arquivo em forma de onda, o tempo lido e o tempo calculado pelo HYPO71.

A cada determinação hipocentral os sismos são automaticamente plotados através do programa Station Geometry (Fig. 3), juntamente com as estações. Essa rápida visualização nos permite realizar melhores leituras e compreender a sismicidade da região à medida que o trabalho se desenvolve.

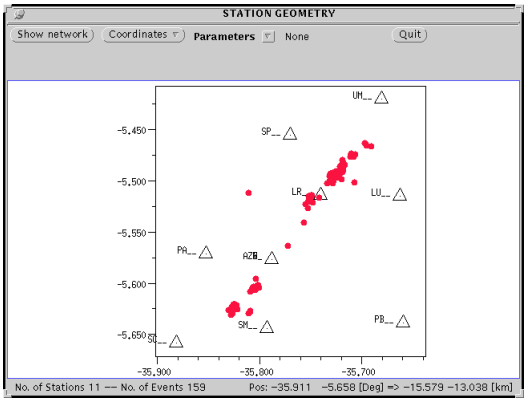

Figura 3: Visualização dos epicentros e estações através do programa Station Geometry.

Após a leitura de todos os eventos, selecionamos os hipocentros convenientemente distribuídos e mais confiáveis, com base no número de estações registradas e nos menores resíduos, para a estimativa de um modelo de velocidades representativo da região em estudo através de um programa de inversão simultânea de hipocentros.

Dessa forma obtivemos 97 sismos selecionados para a obtenção do modelo. O modelo preliminar conseguido neste trabalho esta mostrado na Fig.4a e foi conseguido depois de 100 iterações e várias aproximações, como se mostra na Fig.4b.

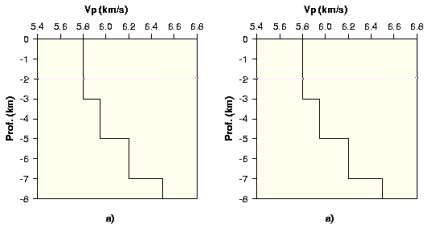

Figura 4: a)Modelo obtido através do processo de inversão simultânea e b)iterações realizadas.

No mapa sismotectônico da Fig. 5 são mostrados os eventos selecionados (vermelho) e não selecionados (azul). Nesse mapa podemos observar ao norte uma extensa área de calcário e dolomitos fossilíferos (rosa), onde a parte sedimentar (Bacia Potiguar) é composta por arenitos, conglomerados e argilitos (amarelo). Mais ao sul, encontram-se alguns afloramentos de granitos do Proterozóico (verde escuro)e uma área de biotitas e hornblendas-gnaisses quartzo-feldspáticos, que compõem o embasamento pré-cambriano (demais cores). A região apresenta um complexo sistema de falhas cisalhantes.

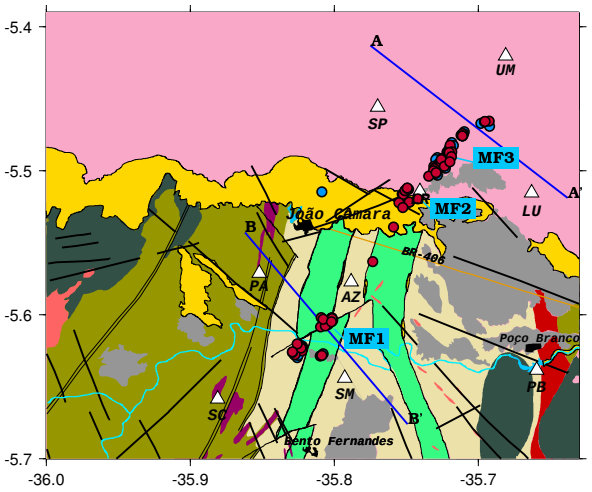

Figura 5: Mapa sismotectônico da região de João Câmara.

No mapa da Fig. 5, são mostrados alguns eventos (MF) para os quais determinamos o mecanismo focal.Estes resultados concordam com a direção das falhas apresentada no mapa geológico, e sugerem que provavelmente esses sismos ocorreram pela reativação de falhas antigas e não por uma única falha, como foi sugerido por alguns autores.

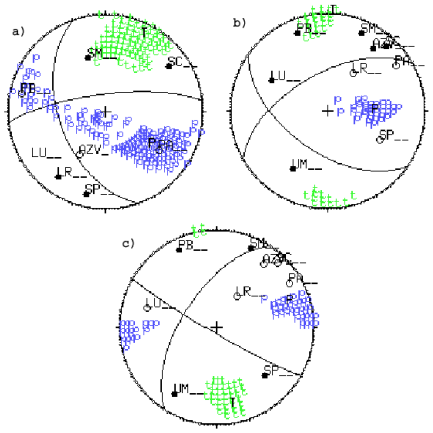

Figura 6: Soluções do Mecanismo Focal a)MF1, b)MF2 e c)MF3.

Podemos observar um alinhamento N30E de epicentros na parte da Bacia Potiguar e outro alinhamento N50E na porção cristalina, que permitiram realizar duas seções verticais (A-A' e B-B') perpendiculares a esses alinhamentos respectivamente. Para uma falha retilínea com um mergulho constante em toda a sua extensão, os eventos projetados deveriam estar alinhados com um ângulo de mergulho próximo ao mergulho da falha.

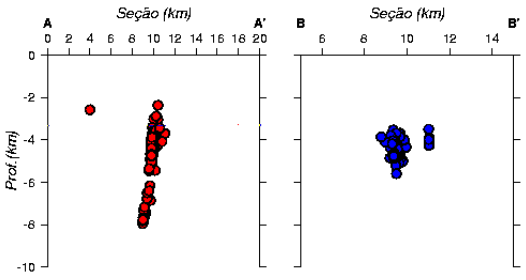

Figura 7: Seção vertical utilizando todos os eventos estudados.

As seções da Fig. 7 foram projetadas com todos os sismos estudados neste trabalho. Nas seções da Fig. 8 utilizamos somente os eventos selecionados. A seção A-A'da Fig. 7 nos mostra que os eventos apresentam um alinhamento coerente, exceto de alguns poucos eventos. No entanto, a seção B-B' apresenta uma projeção bastante diferente da seção

A-A', o que nos indica que esses sismos não correspondem a uma mesma falha. Também é possível notar que não há um alinhamento principal, podendo então estes sismos estar relacionados com mais de uma falha. Quando utilizamos somente os eventos selecionados, a seção A-A'fica ainda mais clara, o que não ocorre com a B-B', reforçando nossa hipótese de que os sismos da parte sul não pertencem a mesma falha que os sismos da parte norte.

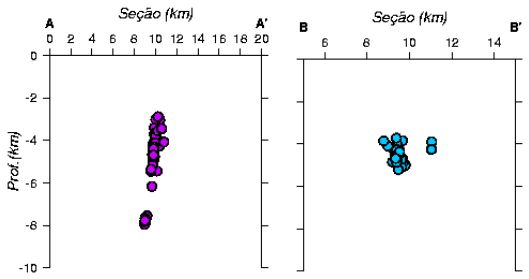

Figura 8: Seção vertical utilizando os sismos selecionados.

Conclusões

Neste trabalho foi possível testar as capacidades do pacote de programas GIANT. No entanto, não foi possível explorá-lo mais a fundo devido ao pequeno número de estaçoes e eventos registrados, já que esse pacote foi formulado para grandes projetos. Mas mesmo com essas limitações, podemos dizer que o trabalho com GIANT torna-se mais compreensível e dinâmico, o que nos permitiu obter resultados bastante confiáveis.

Agradecimentos

Agradecemos a M. Takeya pelo fornecimento dos dados que utilizamos neste trabalho, a C.M. Fernandes por viabilizar a utilização dos mesmos e pela ajuda prestada em todas as etapas deste trabalho e a J. Wassermann e F. Scherbaum pela instalação do GIANT e pela disposição em resolver nossas dúvidas. Além disso agradecemos ao CNPq/PIBIC pela Bolsa de Iniciação Científica e ao Departamento de Geofísica do IAG-USP pelo estágio concedido.

Referências

Lee, W. & Lahr, J., 1975. HYPO71 (REVISED): A computer program for determining hypocenter, magnitude, and first motion pattern of local earthquakes, U.S. Geol. Surv., Open File Report, 75-311.

Rietbrock, A. & Scherbaum, F., 1998. Short introduction to the software package GIANT 1.1. Institut für Allgemeine und Angewandte Geophysik.

Scherbaum, F. & Johnson, J., 1993. PITSA, Programmable Interactive Toolbox for Seismological Analysis: IASPEI Software Library, Vol. 5.

Takeya, M., Ferreira, J.M, Pearce, R.G., Assumpção, M., Costa, J.M. & Sofia, C.M., 1989. The 1986-1988 intraplate earthquake sequence near João Câmara, Northest Brazil - evolution of seismicity: Tectonophysics, **167**, 117–131.

Variação Secular no Brasil de 1900 a 2000: uma comparação com o modelo ELEMAG

[1]*Katia Jasbinschek Pinheiro &* [2] *Luiz C.C. Benyosef*
[1]*Bolsista CAPES. Curso de Pós-graduação em geofísica/ Observatório Nacional.*
[2] *Departamento de Geofísica/Observatório Nacional.*

Abstract

Values of the geomagnetic total field (F) obtained at repeat stations in Brazil for the period 1900 to 2000 were analyzed. These data were compared with that obtained through the theoretical model ELEMAG, prepared at the Observatório Nacional. The comparison indicates that the model provides a good fit to geomagnetic variation at repeat stations, important to the study of the secular variation. In some stations the discrepancy between the real and the theoretical data is higher than the average deviation. These stations were analyzed taking into account their geological characteristics and this has allowed the identification of the presence of crustal anomalies. For the anomaly stations on South and Southeast Brazil it has been possible to identify relationships with the Mesozoic flood volcanism of the Paraná Basin.

1. Introdução

A variação secular engloba variações de origem predominantemente interna (*Bloxham & Gubbins, 1985*), com períodos de um ano à milhões de anos (*Merrill et al., 1998*). Estas variações são descritas pelo modelo do IGRF (International Geomagnetic Reference Field), que basicamente é uma representação teórica de um somatório de harmônicos esféricos, cujos coeficientes são determinados periodicamente pela Associação Internacional de Geomagnetismo e Aeronomia (*Campbell, 1997*). Entretanto existem outros métodos regionais para modelagem do campo principal, sendo usual a utilização de polinômios de Taylor com grau variável na latitude, longitude e tempo (do 1º ao 4º grau), para a elaboração de cartas magnéticas localizadas (*Wienert, 1970*). Neste contexto foi desenvolvido no Observatório Nacional o modelo ELEMAG (*Mota, com. pess.*), caracterizado por um polinômio de 4º grau em latitude e longitude e 2º grau em tempo, gerado para o modelamento do campo geomagnético somente no Brasil.

Tanto o IGRF quanto o ELEMAG, são equivalentes nas suas representações dentro do território brasileiro, podendo assim ser igualmente utilizados para auxiliar como referência nas pesquisas em geomagnetismo.

Normalmente, em áreas onde existe pouca informação do campo geomagnético ocorrem as maiores discrepâncias entre os dados medidos e os modelos, que podem atingir valores superiores a 250 nT em relação ao campo total (*Milson, 1989*). Entretanto no Brasil existe uma ampla rede geomagnética, atualmente com 128 estações de repetição (*Lima & Carvalho, 2001*) que são reocupadas periodicamente, de modo que as discrepâncias encontradas na maior parte das estações não podem ser relacionadas a ausência de dados.

Trabalhos comparando valores das componentes do campo geomagnético com intensidades calculadas através de modelos teóricos, são comumente relatados para várias regiões, como é o caso da África (Vassal, 1987) e México (*Urrutia-Fucugauchi & Campos-Enriquez, 1993*).

Neste trabalho foi utilizado o ELEMAG para o período de 1900 até 2000, objetivando comparar os valores teóricos do campo geomagnético total (F) com os valores medidos nas estações de repetição do Brasil.

2. Estações de Repetição

As estações de repetição constituem-se, de modo geral, como um complemento do trabalho dos observatórios magnéticos com a finalidade de estudar o campo geomagnético principal, abrangendo grandes áreas (*Barreto, 1992*). Além das variações relacionadas ao interior da Terra, também pode-se constatar a presença de anomalias crustais através de constantes discrepâncias entre valores do campo geomagnético medido e teóricos, ao longo dos anos.

Este trabalho engloba todas as estações de repetição do Brasil (128), com relação ao campo geomagnético total. A figura 01 mostra a distribuição espacial das estações de repetição do Brasil, entretanto só foram analisadas graficamente aquelas que apresentaram ocupações superiores a duas vezes.

3. Metodologia

Com a utilização do ELEMAG, foram obtidos valores teóricos para cada um dos dados das estações de repetição. As diferenças entre os valores medidos e os teóricos foram calculadas e foi obtida uma média destes desvios para cada estação. A partir destes valores, foi calculada uma média total englobando todas as estações, com objetivo de encontrar quais destas apresentam desvios superiores à média total.

O desvio médio calculado foi de 95,1 nT, que corresponde a cerca de 0,35% do campo geomagnético total.

4. Resultados e Discussão

As estações de repetição com desvios acima da média total apresentam-se na tabela I, com suas respectivas coordenadas geográficas, número de reocupações e média do desvio. A figura 2 mostra gráficos representativos de algumas estações de repetição com discrepâncias entre os dados reais e o modelo utilizado.

A distribuição destas estações é mostrada na figura 1, onde nota-se que há uma maior concentração na região sul e sudeste do Brasil. Grande parte destas regiões localiza-se dentro da Bacia do Paraná, que é uma província estrutural da América do Sul que contém o maior depósito vulcânico continental na superfície terrestre (*Sousa, 1998*). Os derrames vulcânicos ocupam considerável área na Bacia do Paraná sendo da ordem de 1.200.000 km², e estando distribuídos parcialmente nos estados de Minas Gerais, São Paulo, Paraná, Santa Catarina e Rio Grande do Sul (*Salamuni et al., 1999*), onde localizam-se 60% das estações geomagnéticas anômalas estudadas.

Desta forma, o derrame vulcânico existente na região pode explicar as discrepâncias encontradas, já que rochas basalticas apresentam forte magnetização, com altos valores de susceptibilidade magnética com média de 6 x 10^9 emu (*Sharma, 1986*). Esta característica indica a presença de anomalias magnéticas crustais, que não são previstas pelo ELEMAG, já que este modelo calcula somente variações do campo geomagnético principal.

5. Conclusão

Observa-se que a média da discrepância entre os valores do campo geomagnético total (F) medidos e calculados através do ELEMAG, correspondem a cerca de 0,35% do campo geomagnético (F). Isto mostra que o modelo ELEMAG, gerado a partir de séries de Taylor, representa de forma satisfatória os valores do campo geomagnético total (F) das estações de repetição do Brasil.

Entretanto nota-se que algumas estações apresentam maiores desvios (superiores a média) com relação ao modelo utilizado. Considerando o modelo ELEMAG como um bom representante para a área estudada, provavelmente estas constantes diferenças podem indicar a presença de anomalias crustais ocorrentes principalmente nas regiões sudeste e sul do Brasil, que sofrem influência do basalto existente na Bacia do Paraná.

6. Referências Bibliográficas

Barreto, L. M., 1992. Introdução às Cartas Magnéticas. Publicação do IPGH. 93 p., n°1.Universidad Nacional Autónoma de México, 52 p.

Bloxham, J & Gubbins, D., 1985. The Secular Variation of Earth's magnetic field. Nature, vol. 317 (777- 781).

Campbell, W. H., 1997. Introduction to Geomagnetic Fields. Cambridge University Press. 290 p.

Lima, E. C. & Carvalho, R. M., 2001. Rede Geomagnética Brasileira- Descrição das Estações. Publicação do Observatório Nacional, n°3.

Merrill, R, T, McElhinny, M. W., McFadden, P. L., 1998. The Magnetic Field of the Earth-Paleomagnetism, the Core, and the Deep Mantle. International Geophysics Series, v. 63.

Milson, J., 1989. Field Geophysics. Geological Society of London handbook.

Sousa, N., 1998. The Geology of Basaltic Rocks, and the Biblical Flood. Trabalhos Técnicos do Centro de Pesquisa da História da Terra.

Salamuni, R., Salamuni, E., Rocha, L. A., Rocha, A. L., 1999. Sítios Geológicos e Paleontológicos do Brasil - O Parque Nacional do Iguaçu. Publicação da Comissão Brasileira de Sítios Geológicos e Paleobiológicos, n°11.

Sharma, P. V., 1986. Geophysical methods in geology. Elsevier Science Publishing Co., Inc.

Urrutia-Fucugauchi, J. & Campos-Enriquez, J. O., 1993. Geomagnetic Secular Variation in Central Mexico since 1923 AD and Comparison with 1945-1990 IGRF Models. J. Geomag. Geoelectr. 45, (243-249).

Vassal, J., 1987. Secular Change in the Geomagnetic Field in West Africa for Thirty Years: Comparison with Fourth Generation IGRF Models. J. Geomag. Geoelectr., 39, (699-707).

Wienert, K. A., 1970. Notes on geomagnetic observatory and survey practice. Unesco.

7. Agradecimentos

Ao Prof. Luiz Muniz Barreto pelas valiosas sugestões. Aos prezados colegas Ronaldo M. Carvalho, Elizabeth C. Lima e Constantino M. Mota pelo fornecimento dos dados e ao apoio durante a execução do projeto. Também queremos agradecer à FAPERJ pelo suporte deste trabalho.

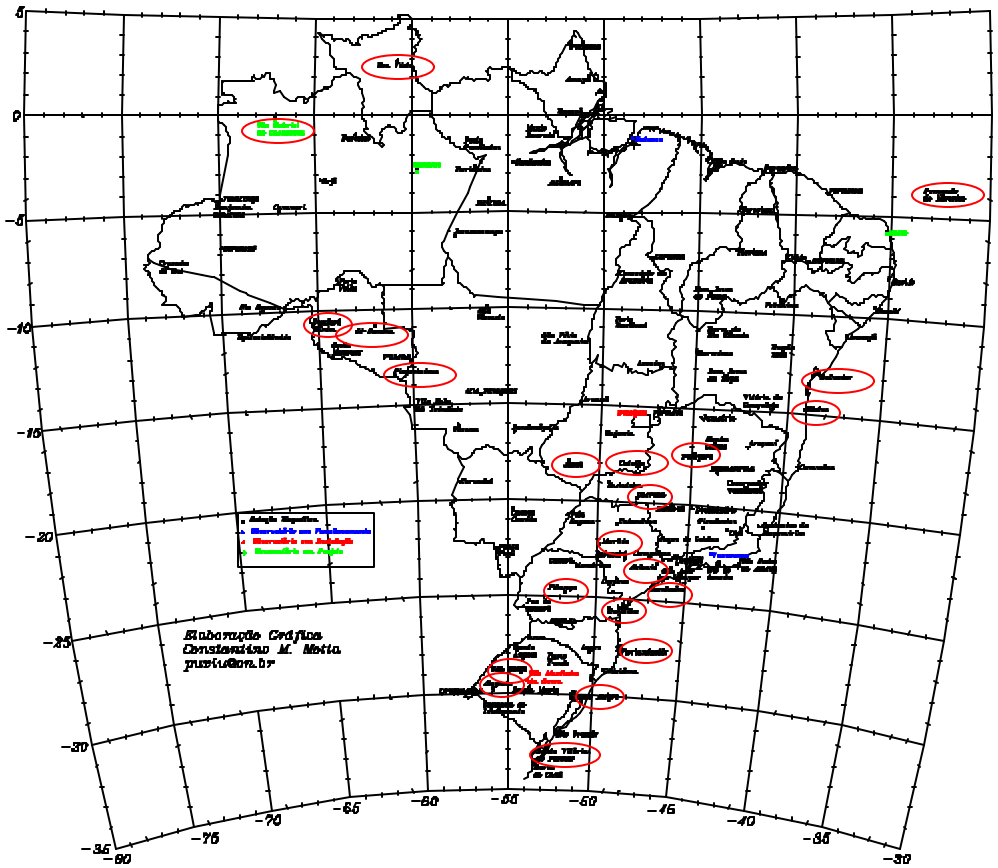

Figura 01: Mapa da localização das estações de repetição geomagnéticas do Brasil. Os contornos em vermelho indicam as estações com desvios superiores ao desvio médio (média da diferença entre o modelo teórico e os dados observados de todas as estações).

Tabela I: Estações de repetição geomagnéticas anômalas, com suas coordenadas geográficas, número de reocupações e média do desvio.

NOME DA ESTAÇÃO	Estado	Latitude	Longitude	N° de reocupações	Média do desvio
ALEGRETE	RS	29 48.869 S	55 53.584 W	3	560,9
ATIBAIA	SP	23 07.853 S	46 34.515 W	1	170,8
BOA VISTA	RR	02 51.000 N	60 41.000 W	11	246,6
CATALÃO	GO	18 98.800 S	47 55.600 W	12	138,8
CURITIBA	PR	25 31.482 S	49 10.926 W	11	119,0
FERNANDO DE NORONHA	PE	03 51.000 S	32 25.000 W	6	147,7
FLORIANÓPOLIS	SC	27 39.853 S	48 32.971 W	9	152,4
GUAJARÁ-MIRIM	RO	10 47.300 S	65 16.900 W	1	156,7
ILHÉUS	BA	14 48.800 S	39 02.000 W	8	175,1
ITANHAÉM	SP	24 09.900 S	46 47.100 W	3	106,9
ITAPEVA	SP	23 58.000 S	48 51.800 W	9	187,2
JATAÍ	GO	17 52.600 S	51 43.800 W	7	109,3
JI-PARANÁ	RO	10 52.000 S	61 57.000 W	3	442,9
JUAZEIRO	SC	27 46.908 S	50 16.835 W	6	104,2
MARÍLIA	SP	22 11.900 S	49 55.705 W	12	93,1
PASSO FUNDO	RS	28 15.020 S	52 31.035 W	6	93,4
PIMENTEIRAS	MT	13 28.900 S	61 02.800 W	1	190,3
PIRAPORA	MG	17 18.771 S	44 51.454 W	9	176,1
PITANGA	PR	24 45.135 S	51 46.327 W	2	610,6
PORTO ALEGRE	RS	29 59.548 S	51 09.801 W	17	126,7
SALVADOR	BA	12 55.200 S	38 19.100 W	21	212,2
SANTA VITÓRIA DO PALMAR	RS	33 30.100 S	53 20.600 W	3	192,2
SÃO BORJA	RS	28 39.033 S	56 01.702 W	3	245,0
SÃO GABRIEL DA CACHOEIRA	AM	00 08.000 S	67 06.000 W	4	387,9
UBERABA	MG	19 46.600 S	47 56.600 W	18	140,7

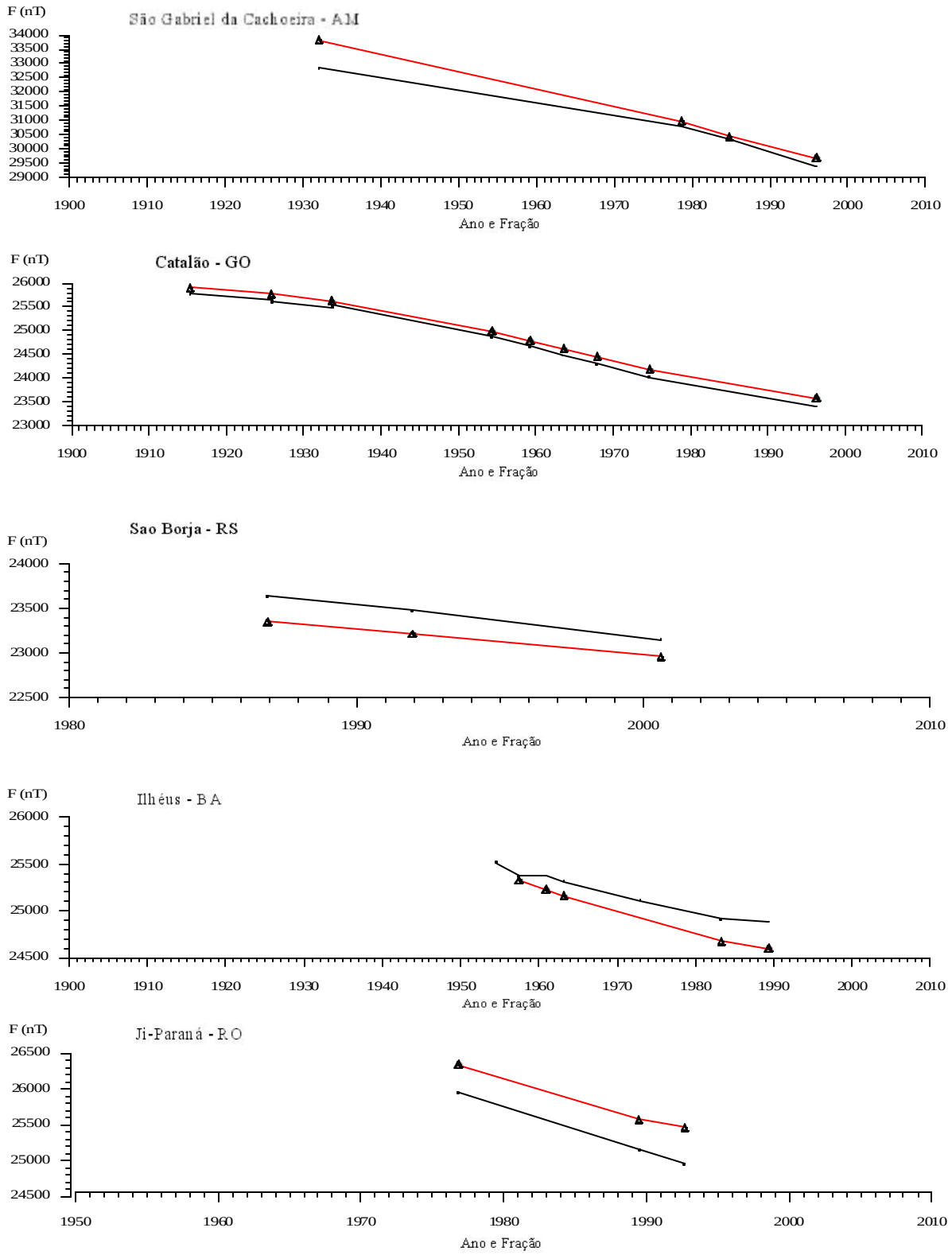

Figura 02: Representação gráfica de alguns exemplos das estações de repetição geomagnéticas que apresentam anomalias crustais, segundo comparações com o modelo ELEMAG. A linha preta representa os dados observados e a linha vermelha (com triângulos) representa os valores teóricos calculados pelo modelo ELEMAG do Observatório Nacional.